STRUCTURE AND BONDING 128

Series Editor D. M. P. Mingos
Volume Editor T. Kato

Liquid Crystalline Functional Assemblies and Their Supramolecular Structures

Springer

128
Structure and Bonding

Series Editor: D. M. P. Mingos

Structure and Bonding
Series Editor: D. M. P. Mingos

Recently Published and Forthcoming Volumes

Contemporary Metal Boron Chemistry
Volume Editors: Marder, T. B., Lin, Z.
Vol. 130, 2008

Recognition of Anions
Volume Editor: Vilar, R.
Vol. 129, 2008

Liquid Crystalline Functional Assemblies and Their Supramolecular Structures
Volume Editor: Kato, T.
Vol. 128, 2008

Organometallic and Coordination Chemistry of the Actinides
Volume Editor: Albrecht-Schmitt, T. E.
Vol. 127, 2008

Halogen Bonding
Fundamentals and Applications
Volume Editors: Metrangolo, P., Resnati, G.
Vol. 126, 2008

High Energy Density Materials
Volume Editor: Klapötke, T. H.
Vol. 125, 2007

Ferro- and Antiferroelectricity
Volume Editors: Dalal, N. S., Bussmann-Holder, A.
Vol. 124, 2007

Photofunctional Transition Metal Complexes
Volume Editor: V. W. W. Yam
Vol. 123, 2007

Single-Molecule Magnets and Related Phenomena
Volume Editor: Winpenny, R.
Vol. 122, 2006

Non-Covalent Multi-Porphyrin Assemblies
Synthesis and Properties
Volume Editor: Alessio, E.
Vol. 121, 2006

Recent Developments in Mercury Sience
Volume Editor: Atwood, David A.
Vol. 120, 2006

Layered Double Hydroxides
Volume Editors: Duan, X., Evans, D. G.
Vol. 119, 2005

Semiconductor Nanocrystals and Silicate Nanoparticles
Volume Editors: Peng, X., Mingos, D. M. P.
Vol. 118, 2005

Magnetic Functions Beyond the Spin-Hamiltonian
Volume Editor: Mingos, D. M. P.
Vol. 117, 2005

Intermolecular Forces and Clusters II
Volume Editor: Wales, D. J.
Vol. 116, 2005

Intermolecular Forces and Clusters I
Volume Editor: Wales, D. J.
Vol. 115, 2005

Superconductivity in Complex Systems
Volume Editors: Müller, K. A., Bussmann-Holder, A.
Vol. 114, 2005

Principles and Applications of Density Functional Theory in Inorganic Chemistry II
Volume Editors:
Kaltsoyannis, N., McGrady, J. E.
Vol. 113, 2004

Liquid Crystalline Functional Assemblies and Their Supramolecular Structures

Volume Editor: Takashi Kato

With contributions by

J. E. Bara · M. Funahashi · D. L. Gin · J. W. Goodby · T. Kato
R. L. Kerr · H. Kikuchi · M. Lee · P. T. Mather · C. S. Pecinovsky
S. J. Rowan · J.-H. Ryu · I. M. Saez · H. Shimura · M. Yoshio

Springer

The series *Structure and Bonding* publishes critical reviews on topics of research concerned with chemical structure and bonding. The scope of the series spans the entire Periodic Table. It focuses attention on new and developing areas of modern structural and theoretical chemistry such as nanostructures, molecular electronics, designed molecular solids, surfaces, metal clusters and supramolecular structures. Physical and spectroscopic techniques used to determine, examine and model structures fall within the purview of Structure and Bonding to the extent that the focus is on the scientific results obtained and not on specialist information concerning the techniques themselves. Issues associated with the development of bonding models and generalizations that illuminate the reactivity pathways and rates of chemical processes are also relevant.
As a rule, contributions are specially commissioned. The editors and publishers will, however, always be pleased to receive suggestions and supplementary information. Papers are accepted for *Structure and Bonding* in English.
In references *Structure and Bonding* is abbeviated *Struct Bond* and is cited as a journal.

Springer WWW home page: springer.com
Visit the Struct Bond content at springerlink.com

ISBN 978-3-540-77866-0 e-ISBN 978-3-540-77867-7
DOI 10.1007/978-3-540-77867-7

Structure and Bonding ISSN 0081-5993

Library of Congress Control Number: 2008921239

Cover design: WMXDesign GmbH, Heidelberg
Typesetting and Production: LE-TEX Jelonek, Schmidt & Vöckler GbR, Leipzig

Printed on acid-free paper

9 8 7 6 5 4 3 2 1 0

springer.com

Series Editor

Prof. D. Michael P. Mingos

Principal
St. Edmund Hall
Oxford OX1 4AR, UK
michael.mingos@st-edmund-hall.oxford.ac.uk

Volume Editor

Prof. Takashi Kato

Department of Chemistry/Biotechnology
School of Engineering
The University of Tokyo
7-3-1 Hongo, Bunkyo-ku
113-8656 Tokyo, Japan
kato@chiral.t.u-tokyo.ac.jp

Editorial Board

Structure and Bonding
Also Available Electronically

For all customers who have a standing order to Structure and Bonding, we offer the electronic version via SpringerLink free of charge. Please contact your librarian who can receive a password or free access to the full articles by registering at:

springerlink.com

If you do not have a subscription, you can still view the tables of contents of the volumes and the abstract of each article by going to the SpringerLink Homepage, clicking on "Browse by Online Libraries", then "Chemical Sciences", and finally choose Structure and Bonding.

You will find information about the

- Editorial Board
- Aims and Scope
- Instructions for Authors
- Sample Contribution

at springer.com using the search function.

Color figures are published in full color within the electronic version on SpringerLink.

Preface

Liquid crystals are a soft material formed through molecular assembly. The liquid crystalline state is unique because it combines molecular order and dynamic properties. Nematic liquid crystals have been widely used in display devices because of their anisotropic nature and responsiveness to electric fields. Generally, nematic liquid crystals consist of rod-like molecules and they form no nano-segregated structures. Recently, intensive studies have focused on liquid crystals forming nano-segregated structures such as smectic, columnar, and cubic phases to develop new functional materials. These nanostructured liquid crystals are expected to show enhanced or anisotropic properties in the following applications: electrooptics, photonics, transportation of electrons, ions, or molecules, sensory, catalysis, and bioactivity properties. To induce these functions in nanostructured liquid crystals, control of the nano-segregated structures of the molecular assemblies as well as the design of the structure of each molecule is of great importance.

A number of fundamental aspects of liquid crystals were presented in volumes 94 and 95 of *Structure and Bonding*, published in 1999 and edited by Prof. Mingos. The present volume reflects recent aspects in the development of functional liquid crystals which form nano-segregated structures. The editor has intended to provide readers with the most up-to-date information on the design of liquid crystalline materials. In conventional liquid crystalline compounds, the shapes of the mesogens were basically rod-like or disk-like molecules with covalent bonds. On the basis of their molecular weights, the materials were classified simply into low molecular weight liquid crystals and polymer liquid crystals. The polymer liquid crystals were categorized as main-chain and side-chain types. The design of new molecular architectures based on liquid crystals involves the syntheses of polymers with well-defined structures such as dendrimers and molecules with block structures. Moreover, supramolecular architectures based on liquid crystals have been intensively studied. Supramolecular liquid crystals form well-defined structures through non-covalent bonding including hydrogen bonding and ionic interactions. The present volume covers these new aspects of design and functionalization of liquid crystals.

In Chapter 1, Saez and Goodby describe unconventional liquid crystals having "supermolecular" structures that are more complex than those of conven-

tional liquid crystals. They focus on dendritic liquid crystals with monodispersed and discrete molecular structures. These materials can incorporate functional moieties in the self-organized states. In Chapter 2, Lee reports on the self-assembly of rod–coil molecules consisting of a rod-like mesogenic part and flexible coils. They have block structures inducing a variety of liquid crystalline phases that form the nano-segregated structures.

Chirality is also an important aspect of liquid crystals. The introduction of chiral moieties into the chiral smectic phases induces functions such as ferroelectricity and antiferroelectricity. A few of the unconventional chiral liquid crystals are described in Chapter 1. The blue phase is one of the exotic chiral liquid crystalline phases. In Chapter 3, Kikuchi introduces the basic aspects and recent progress in research of the blue phase. Recently, the materials exhibiting the blue phases have attracted attention because significant photonic and electro-optic functions are expected from the materials.

In Chapters 1, 2, and 3 unconventional liquid crystalline molecules with complex structures based on covalent bonding are described. In Chapter 4, Rowan and Mather demonstrate that non-covalent bonding such as hydrogen bonds may be used for the design and construction of liquid crystalline materials.

Polymeric materials have advantages because of their stability and structure-forming properties. Electron- and ion-active organic polymeric materials have attracted attention for new devices. In Chapter 5, Kato and co-workers focus on polymeric liquid crystalline materials that are used for the development of functional materials transporting ions and electrons. The nanostructures such as smectic and columnar phases exhibited by side-chain, main-chain, dendritic, and network polymers may exhibit one- and two-dimensional transportation properties.

Thermotropic liquid crystals and also lyotropic liquid crystals generate functional molecular assemblies. Lyotropic liquid crystalline phases are exhibited by amphiphilic molecules in appropriate solvents. They form nano-segregated structures because the molecular structures consist of hydrophilic and hydrophobic components. In Chapter 6, Gin and co-workers describe how lyotropic liquid crystals may be used to form functional materials. Lyotropic liquid crystals can act as templates for inorganic materials, ion conductors, catalysts, drug delivery systems, and nanofilters.

I hope the present volume will be very informative and inspiring for scientists and engineers who are interested in developing new functional materials based on the molecular order formed in liquid crystals and their nanostructures.

Tokyo, January 2008 Takashi Kato

Contents

Struct Bond (2008) 128: 1–62
DOI 10.1007/430_2007_077

Published online: 7 February 2008

Supermolecular Liquid Crystals

Isabel M. Saez · John W. Goodby (✉)

The Department of Chemistry, The University of York, York YO10 5DD, UK
iss500@york.ac.uk

Abstract In this article we review recent work on the development and study of the properties of self-organizing, supermolecular materials which have discrete structures that are comparable in size to small proteins. We take the concept of the creation of dendritic liquid crystals and apply it to the creation of new materials with single identifiable entities so that they are monodisperse or are single compounds. We show how functionality can be in-built into such materials so that self-organizing functional systems can be created with designer physical properties.

Keywords Antiferroelectricity · Chirality · Ferroelectricity · Nanostructured liquid crystals · Self-organizing and self-assembling systems · Supermolecular materials · Thermochromism

1 Introduction

The materials of living systems are based on supermolecular and supramolecular self-organizing and self-assembling systems of discrete structure

and topology where the term supermolecular describes a giant molecule made up of covalently bound smaller identifiable components. Supramolecular in this context means a system made up of multiple components that are not covalently bound together. For example, proteins, although polymers of amino acids, have defined and reproducible primary compositions, specified α-helical and β-pleated secondary constructions, and gross topological tertiary structures. Moreover, highly specific functionality, and thereby the ability to perform selective chemical processing, is in-built in such molecular machines which are organized on mesoscale lengths. Concomitantly, the study of materials that self-assemble into supramolecular structures with desirable functionality and physical properties at nano- and meso-scopic length scales is currently an exciting area of intense research, and provides a "bottom-up" approach to the design and synthesis of functional materials [1–5].

Until recently, most thermotropic liquid crystals were designed to be either low molar weight for displays or high molecular weight for prototypical high yield strength polymers [6]. Supermolecular liquid crystals, on the other hand, combine the unique traits of the self-organization of discrete low-molecular-weight materials with those of polymers in their ability to form secondary and tertiary structures. Furthermore, super- and supra-molecular liquid crystals [7–13] exhibit a variety of physical properties, which make them attractive for applications in the fields of nanoscience, materials, and biology. They offer a very elegant and effective way of adding functionalization together with an exquisite and unprecedented level of control of the precise nature and location of specific functionalities and hierarchical molecular architectures, as in proteins. As a consequence, the initial interest in super- and supra-molecular liquid crystal synthesis has shifted towards functional dendrimers because of the latter's rich supramolecular chemistry and self-assembling properties [14–24]. The very properties of precise control of functionality and molecular architecture are also essential ingredients in the molecular engineering of liquid crystals for controlling and fine-tuning the physical properties that ultimately define the self-organizing process that leads to mesophase formation [6]. Thus, super- and supra-molecular liquid crystals provide unique materials for the study of the structures and properties of self-organizing and self-assembling processes [7–27].

1.1 Defining the Structures of Supermolecules

In the fledgling field of super- and supra-molecular liquid crystals, many different terms have been introduced which describe some of the same structures. Figure 1 shows some classical molecular architectures that can be used to describe the gross structures of super- and supra-molecular liquid crystals. For example, two mesogenic units, i.e., molecular entities that can be deployed in material design in order to induce mesophase formation, can

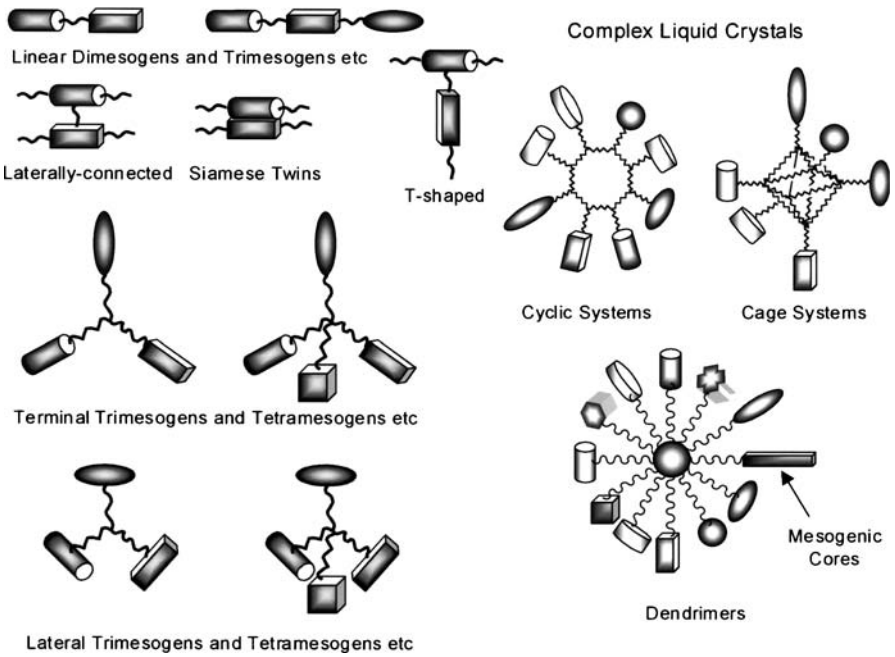

Fig. 1 Templates for the design of liquid-crystalline supermolecular materials. The mesogenic units are shown as various shapes, however, the materials may be constructed with mesogenic units of the same type. In this case, many of the constructions shown are essentially dendritic

be tied end to end to give linear supermolecular materials. If the mesogenic groups are the same, then they are called *dimers or bimesogens*, but if they are different, they are referred to as *dimesogens*. The mesogenic units may also be tied together laterally, rather than end to end, or they may have terminal units tied to lateral units to give *T-shaped dimers* or *T-shaped dimesogens*, as shown in Fig. 1 [25].

Figure 2 shows some examples of liquid-crystalline dimers where the liquid crystal units are identical [28–30]. In the first example, the cyanobiphenyl mesogenic moieties are joined together with a simple aliphatic chain. These materials exhibit unusual odd-even effects for the clearing point transition temperatures where the liquid crystal phases melt to the amorphous liquid. Generally, for such systems, the homologues that have connecting spacer chains with an even number of methylene units have much higher clearing points in comparison to the systems with an odd number of methylene units. This is because the odd members tend to have bent conformational structures which induce disorder into the mesophase structure, whereas the even members tend to have linear structures that support mesophase formation.

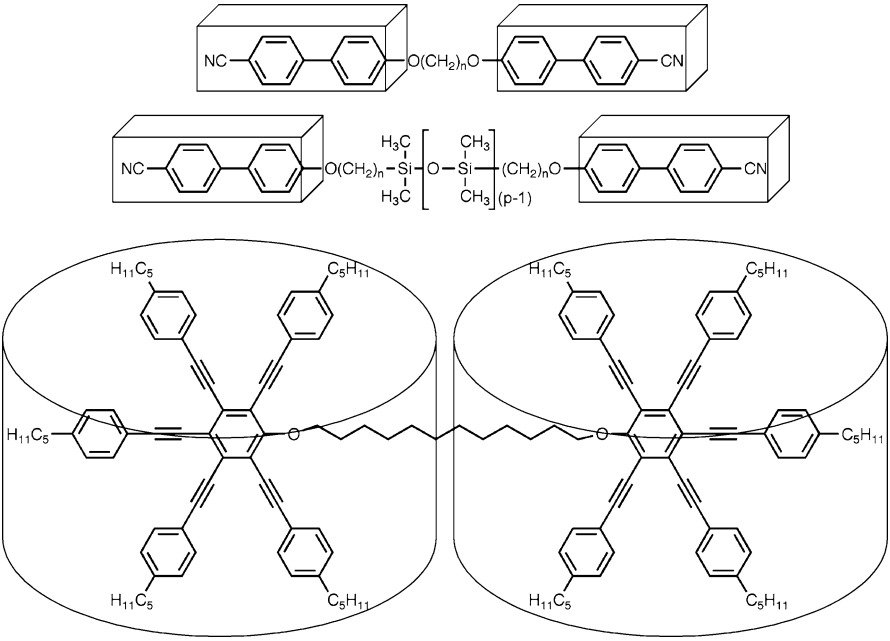

Fig. 2 Examples of typical dimeric liquid crystals, where the mesogenic groups in each example are the same [28–30]

The type of spacer chain can be varied without change to the mesogenic units. For example, the second structure in Fig. 2 has a short dimethylsiloxane spacer included in the aliphatic linking chain. The inclusion of such groups can affect the overall packing of the molecules leading to reductions in melting points and the stabilization of lamellar smectic phases over nematic phases.

Not only are there examples of dimers based on mesogens with rod-like structures, there are also examples reported of dimers composed of disc-like mesogens, see bottom structure in Fig. 2. Generally for these types of material the pattern of mesomorphic behavior follows that of the analogous monomers.

Di-, tri-, tetra-mesogens, etc., can have very subtle differences in structure. For example, the first dimesogen shown in Fig. 3, has two different mesogenic units, i.e. a steroidal moiety and a Schiff's base unit, where one is chiral and the other is not [31]. Thus the properties of this material are roughly averaged between the two mesogenic groups. The trimesogen shown however has a central biphenyl unit with two attached external cyanobiphenyl units [32]. Although the mesogenic moieties are similar, the polar cyanobiphenyl units will impart very different properties in comparison to the central biphenyl entity. Lastly the tetramesogen [33] in Fig. 3 has four identical aromatic units, however, the external two possess flexible aliphatic chains whereas the in-

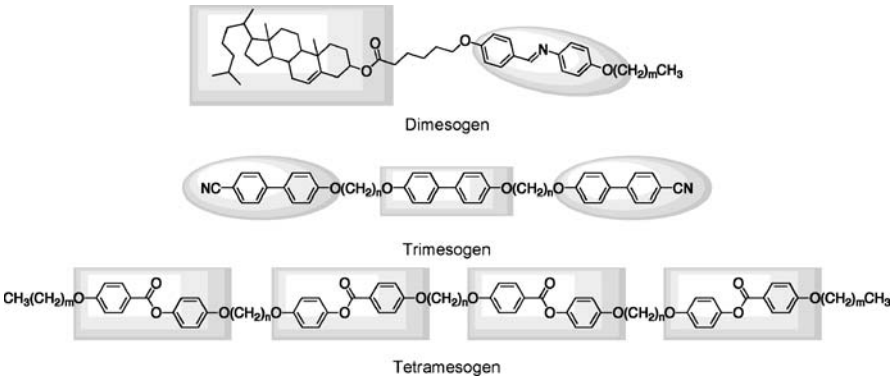

Fig. 3 Examples of typical di-, tri-, and tetra-mesogenic liquid crystals

terior two have aliphatic chains that are tethered, and therefore these two mesogenic units have different properties from the exterior groups.

In a systematic study led by Nishiyama into dimeric and trimeric liquid crystals [34–45] investigations were made firstly on deploying the same mesogens in dimeric systems but with accompanying variation of the linking group, and secondly on incorporating non-mesogenic units into supermolecular architectures, but with the result that mesomorphic materials were still obtained.

The first set of four materials, shown in Fig. 4, all possessed the benzoyloxybiphenyl unit commonly deployed to support the formation of antiferroelectric properties in liquid crystal systems. All of the materials were designed to be chiral via the incorporation of 2-octyl moieties with both *RR* and *SS* variants being available for the resulting bimesogens. With a simple dimethyleneoxy-linking unit between the mesogens, a phase sequence of ferroelectric-ferrielectric-antiferroelectric, e.g., **1**, as a function of temperature was found [36, 37]. When the linking group was changed to a dithioether [43] unit ferroelectric and ferrielectric properties were suppressed in favor of antiferroelectric phase formation, see **2**. It is known from other investigations that the incorporation of sulphur in place of oxygen in aliphatic chains tends to favor the formation of more ordered phases such as the crystal B phase over the hexatic smectic B phase [46, 47]. Through the incorporation of a biphenylyl unit in the bridging chain, thereby creating a trimesogen, higher ordered antiferroelectric phases, such as the smectic I_A^* phase, are found, see compound **3** [45]. Lastly for this family of materials, the linking group was substituted with a silyloxy unit [41]. Silyloxy substitution has the effect of lowering melting point and, because an odd number of atoms substituted into an even number of atoms in the methylene chain, antiferroelectric phases are stabilized. For the last compound, **4**, this is the case with a melting point of only 34.1 °C and the other supermolecular materials having melting points above 101.5 °C. As the number of atoms located in the chain between

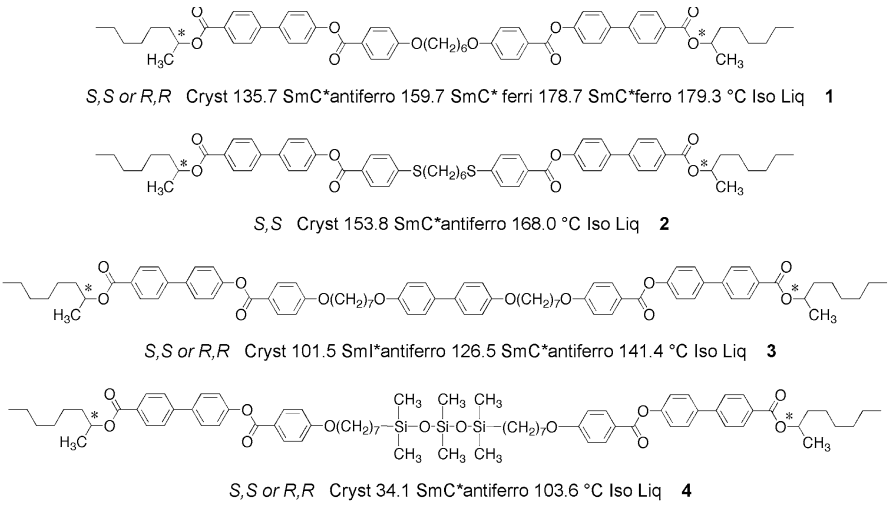

Fig. 4 Systematic study of the change in linking groups in dimeric and trimeric liquid crystals

the two mesogenic units is odd, the overall structure is bent, and therefore antiferroelectric phases are stabilized.

Further studies by Nishiyama et al. [34–45] showed that when taken in isolation, only one of the aromatic units within a supermolecular system has a propensity to exhibit liquid crystal phases, then the supermolecular material itself could be mesomorphic, see Fig. 5. For example, for the top molecular structure, **5** [45], in Fig. 5, only the biphenyl unit at the center of the structure supports mesophase formation, whereas the benzoate units are too isolated from the biphenyl moiety in order to affect mesomorphic behavior. The second material, **6** [45] has terminal phenyl units, which are only connected by aliphatic chains to the benzoate units. Thus in this case, the material has four aromatic units out of six which are not in positions that can enhance mesophase formation. However, the second material has similar transition temperatures and phase sequences to the first, i.e., both materials exhibit an unidentified smectic phase and a synclinic ferroelectric smectic C* phase. If the third material, **7** [38], is examined, it can be seen that the mesogenic unit at the center of the supermolecule is an azobenzene unit which is more strongly supportive of mesophase behavior than the simple biphenyl moiety. Thus the clearing point is higher for this material in comparison to the other two. The attachment of the terminal phenyl unit is by a methylene spacer of odd parity, and as a consequence the smectic C phase has an anticlinic structure rather than synclinic.

These studies demonstrate that for supermolecular materials it is not necessary to have all of the aromatic/rigid units being supportive of mesophase formation for a supermolecular material to be mesomorphic. Odd par-

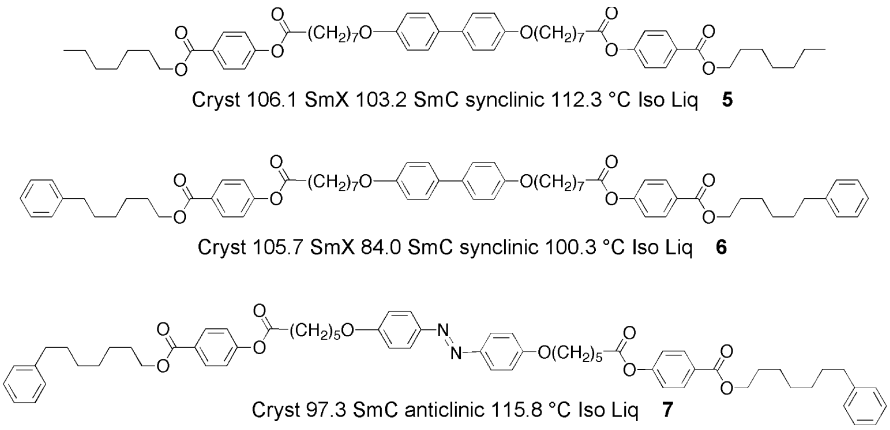

Fig. 5 Supermolecular liquid-crystalline materials consisting of only one unit that has mesogenic tendencies

ity spacer units tend to support anticlinic properties, whereas even parity spacers support synclinic properties.

There have also been a number of examples reported of supermolecular materials composed of different mesogenic units. For example, Yelamaggad et al. [48, 49] reported a supermolecular material, **8**, that was composed of three different mesogenic groups linked together in a linear fashion, see Fig. 6. This material possesses a chiral steroidal unit, a linear biphenyl moiety and a photoactive azobenzene unit, and remarkably it exhibits unusual frustrated chiral mesophases.

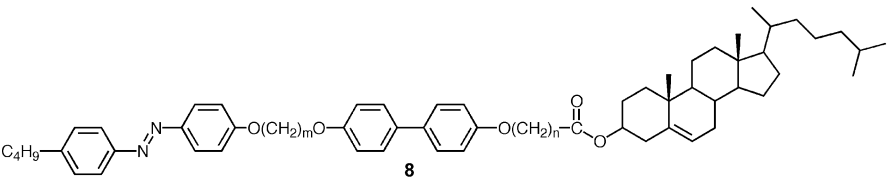

Fig. 6 A trimesogen that possesses three different mesogenic units, and which exhibits frustrated liquid crystal phases

Laterally appended mesogens have been investigated for a number of systems. For example Fig. 7 shows a comparative family of laterally appended dimeric systems which were investigated systematically by Mehl et al. [50–53]. A three-ring (A) and a four-ring (B) monomer were synthesized with the potential to be linked together through a silyloxy uniting moiety. The synthetic programme yielded the symmetrical **9** (AA) and **10** (BB) bimesogens, and the **11** (AB) dimesogen. For completion, the silyloxy terminated, laterally-substituted monomers were also prepared, **12** and **13**. The AA and

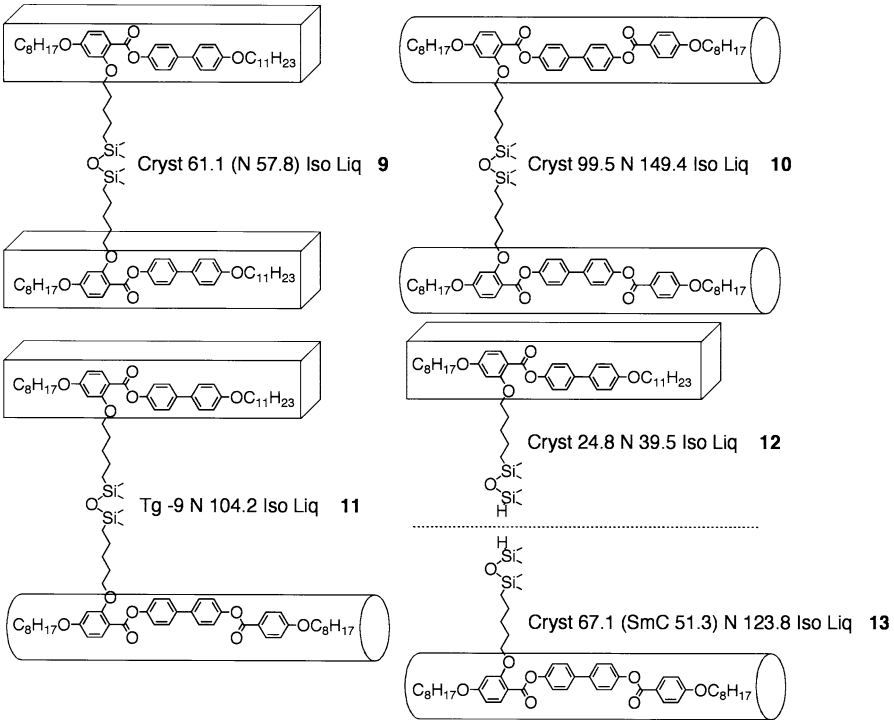

Fig. 7 Comparison of laterally appended bimesogens and dimesogens with the parent monomers

BB bimesogens, **9** and **10** were found to exhibit higher clearing points than the parent monomers, and the AB dimesogen, **11**, was found to form a glass at low temperature rather than recrystallize. This is a very interesting result as it demonstrates that by introducing dissymmetry into molecular architecture a material can be effectively prevented from recrystallizing. In addition, in all cases laterally appending the mesogens to the linking group results in the formation of nematic phases in preference to any other mesophase. This result holds true for many other systems, including dendritic liquid crystals and side-chain liquid crystal polymers (SCLCPs).

With trimeric supermolecular materials the situation becomes more complicated because not only are there linearly and laterally linked possible structures, but also there are structures where the mesogenic units could be linked to a central point, creating a "molecular knot". In a similar way, tetra-, penta-, etc., substituted supermolecules can be created.

Typically tri-, tetra-, penta-, etc., substituted supermolecules are used as dendrons in the formation of dendritic liquid crystals. Figure 8 shows an example of a dendron that was created to attach to a scaffold in order to prepare a dendromesogen [25]. In this case, three cyanobiphenyl mesogens

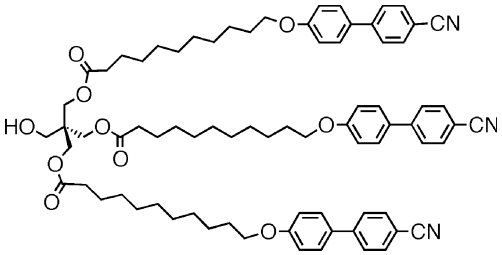

Crystal 26.2 Smectic C 43.5 Smectic A 96.2 °C Iso Liq **14**

Fig. 8 Trimeric dendron composed of cyanobiphenyl mesogenic moieties

were attached to a pentaerythritol unit leaving one hydroxyl group free for attachment to a scaffold. The trimeric dendron, **14**, so formed was also found to exhibit liquid crystal phases, as shown in Fig. 8. Remarkably this material was found to exhibit smectic A and smectic C phases, but not a nematic phase. The 4-*n*-decyloxy-4′-cyanobiphenyl parent system exhibits nematic and smectic A phases. The suppression of the nematic phase is not surprising because the ester groups will promote smectic A formation over that of the nematic phase. However, the formation of a smectic C phase is interesting. Molecular simulations show that, at least in the gas phase at 0 K, the mesogenic moieties interact strongly together and bunch up to form a cylindrical cluster of biphenyl groups, see Fig. 9. Thus the overall structure of the mesophase is rod-like. The tight packing of the mesogenic units together does not allow for any overlap of the mesogenic units, thereby preventing the formation of bilayer structures. Alkoxy cyanobiphenyls form bilayer smectic A_d phases with layer spacings 1.4× the molecular length. The close packing of the mesogens in the dendron ensures that the prevention of interdigitation between the layers results in the formation of a monolayer smectic A_1 phase, see Fig. 10. The tight packing also has the effect of introducing the formation of smectic C phase, which is caused by the limited overlapping of only the nitrile units.

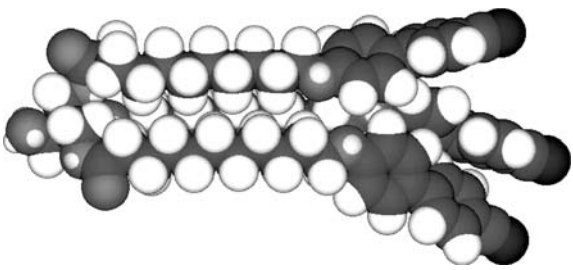

Fig. 9 Molecular simulation of a trimeric dendron, **14**, composed of cyanobiphenyl mesogenic moieties

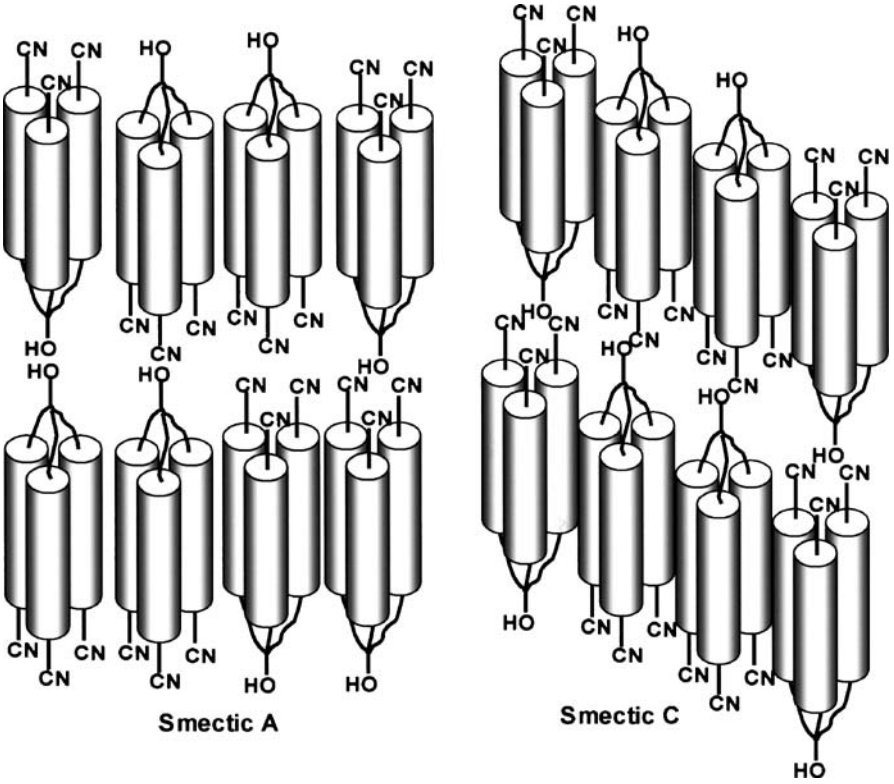

Fig. 10 Schematic of the molecular packing arrangement in the smectic A and smectic C phases of a dendron, **14**, based on the 4-alkoxy-4′-cyanbiphenyl moiety

As noted above, increased numbers of mesogenic units attached to a central point can be created by introducing a central scaffold upon which to build the supermolecular structures. Thus cyclic, caged, or hyperbranched scaffolds can be utilized, as shown in Fig. 1. Such supermolecular materials can be thought of as dendritic structures when the mesogenic units are all of the same type. Figure 11 depicts the general structure of a dendrimer where repeating branched units are linked together one shell on top of another to create various generations of the dendrimer. Typically identical mesogenic units are located at the surface to the dendritic scaffold, thereby creating a dendritic liquid crystal, or a polypedal (an object having many feet which are the same) supermolecule. Alternatively, if the mesogenic units are mostly different with respect to one another, then the supermolecule will have many different feet, and thus could be termed a multipedal supermolecule. There is a clear distinction between these two types of supermolecular system; the polypedal supermolecule, like a polymer, can be subject to polydispersity, whereas the multipedal supermolecular material is not; it can be similar in

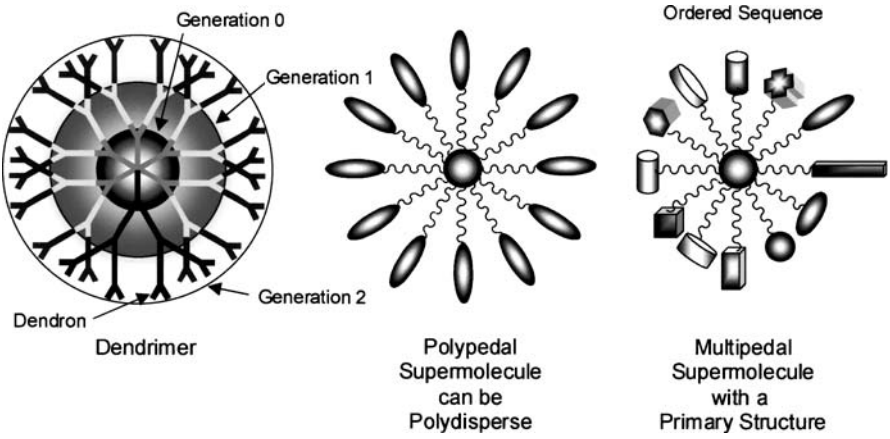

Fig. 11 A dendritic scaffold, polypedal (many feet the same) supermolecule which can be subject to polydispersity, and a multipedal (many different feet) supermolecule which is not necessarily subject to polydispersity

constitution to a protein and have a primary structure. In fact, Newkome et al. make the observation that *"on the preparation of dendritic macromolecules, the continued inability to ascertain the absolute homogeneity of the resultant structures has led many to claim monodisperse character of their products"* [54].

There is of course a further distinction between a supermolecule and a supramolecular system. A supermolecule is a giant molecular entity that is made up of covalently bonded identifiable molecular units, thus it is similar in constitution to that of a tertiary structure of a protein. A supramolecular system, on the other hand, is a self-assembled, non-covalently bonded entity where complete molecular units are brought together through non-covalent forces to create a complex structure similar in constitution to that of a quaternary structure of a protein. Figure 12 shows both of the supermolecular and supramolecular constructions. Thus a supermolecule has a clearly defined chemical constitution, whereas for the supramolecular system it is possible to have variations in the constitution depending on how many molecular units are required to create the self-assembling, and hence self-organizing, complex system.

Through the incorporation of chemically or physically active moieties into the structures of super- and supra-molecular systems, "functional" or "smart" self-organizing materials can be created. Such material systems are related to proteins in that they can be designed to have specific structures and properties. For example, Fig. 13 shows a template for a supermolecular system where two functional units **A** and **B** are incorporated into its structure. **A** and **B** may interact with each other or with other chemical entities introduced to the supermolecular system. The design of such "smart" func-

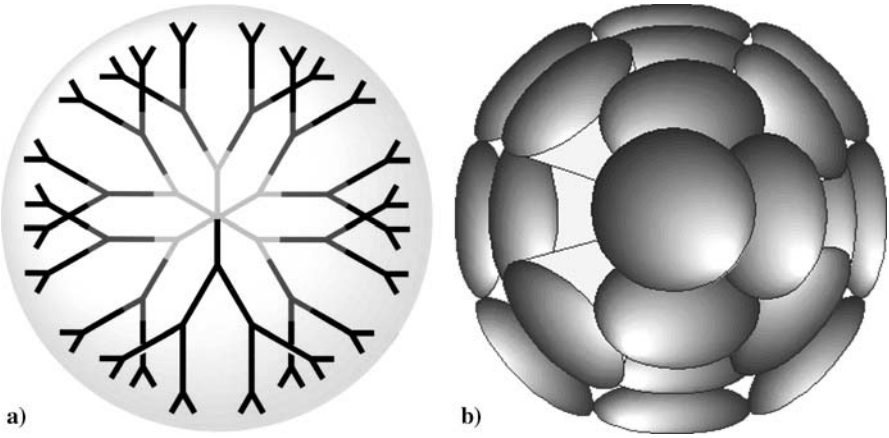

Fig. 12 **a** The architecture of a supermolecule, and **b** the complex self-organized structure of a supramolecular entity

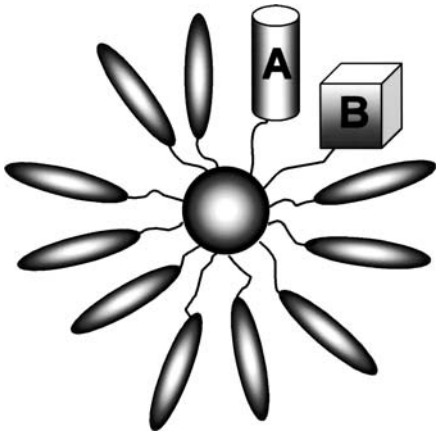

Fig. 13 Template structure of a smart or functional supermolecular material

tional supermolecular materials is expected to have a strong impact on the future development of materials science, as this area of research offers a powerful alternative for managing the awkward gap in the length scale that exists between top-down miniaturization and bottom-up nanofabrication.

1.2 The Self-Organization Process

The way in which supermolecules can self-organize is dependent to a large degree on simple structural features, such as the density of the mesogenic units attached to the periphery of the central scaffold, their orientation of at-

tachment, and the degree to which they are decoupled from the scaffold. For example, the density of mesogenic groups attached to the periphery can effectively change the overall gross shape of the structure of the supermolecule from being rod-like, to disc-like, to spherulitic. Thus, the structure of the systems at a molecular level can be considered as being deformable, where each type of molecular shape will support different types of self-organized mesophase structure. Thus, for supermolecular materials, rod-like systems will support the formation of calamitic mesophases (including the various possibilities of smectic polymorphism), disc-like systems tend to support columnar mesophases, and spherulitic systems form cubic phases, as shown in Fig. 14.

Similar structure-self-organizing properties are also found for supramolecular systems, and indeed in some cases far more complex polymorphism and a richer variety of mesophase types are found [55–57]. Although there have not been extensive research studies into the effects that the type (rod-like, disc-like or spherulitic) of mesogenic group attached to the central scaffold has on mesophase formation, it is clear for rod-like shaped mesogenic groups that the orientation of the attachment can markedly influence the type of mesophase formed and polymorphism of any smectic phases formed. As with side-chain liquid crystal polymers (SCLCPs), lateral attachment (side-on) of the mesogenic units often leads to supermolecular systems exhibiting

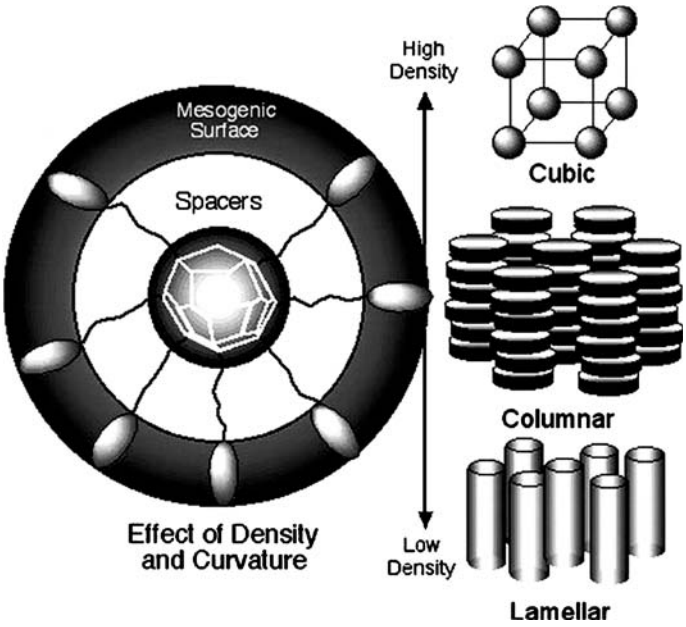

Fig. 14 Effect of the number density of mesogens on the surface of the supermolecular structure on the formation of various mesophases

nematic phases, whereas for terminal attachment (end-on) smectic phases appear to predominate, as shown in Fig. 15.

In addition to number density and orientation of attachment, the degree to which the mesogenic units are decoupled from the central structure is important. The shorter the linking unit, the more likely the material will act as a single supermolecular entity, whereas the longer the spacer the more likely it is that the properties of the individual mesogenic groups will dominate the overall properties of the material.

Apart from these coarse property-structure–activity relationships, a secondary level of structure needs to be considered in defining the finer points of such relationships. For example, the central scaffolds might be considered to be soft (flexible) or hard (rigid), there might be blocks of mesogenic groups of one type or another, there could be microphase segregating units incorporated into the periphery or the scaffold of the material, mesogenic units might be incorporated into the scaffold as well as the periphery, it is also possible to incorporate metallomesogenic units as well as conventional organic mesogenic moieties, and chirality might be introduced into any part of the structure. Figure 16 shows some examples of templates for supermolecular

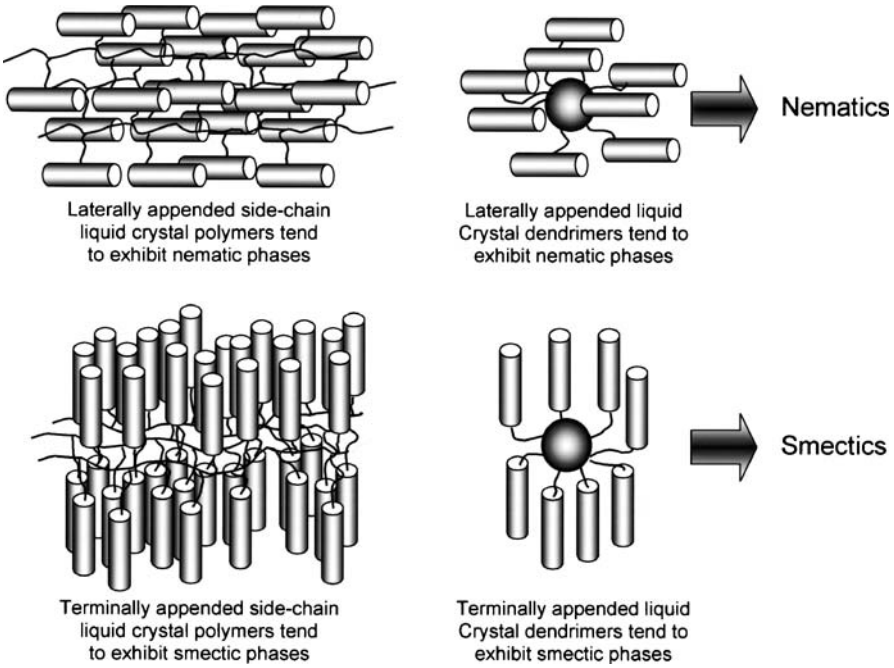

Fig. 15 Orientation of attachment of rod-like mesogenic groups to a central scaffold and mesophases formed for supermolecular systems, shown in comparison to the structures of side-chain liquid crystal polymers

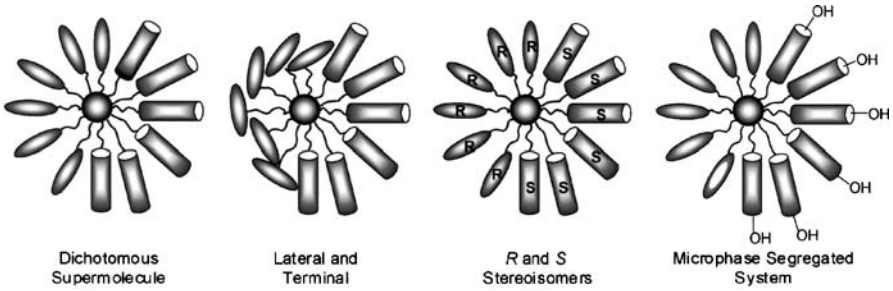

Fig. 16 Templates for supermolecular materials bearing A–B blocks of mesogenic units, some of which are functionalized

materials bearing blocks of mesogenic units, some of which are functionalized. The variety of templates available is thus very large, indicating the potential for the development of novel materials with designer properties.

Through self-assembly and self-organization processes, liquid-crystalline phases have opened up new perspectives in materials science towards the design and engineering of supramolecular materials [58–61]. The self-organization in two- and three-dimensional space offered by the liquid-crystalline medium is an ideal vehicle to explore and control the organization of matter on the nanometer to the micrometer scale, which are key to the emerging development of nanotechnology.

In the following sections we describe the structures of novel polypedal, multipedal and functional supermolecular materials.

2
Liquid-Crystalline Polypedes – Dendrimers

As noted above, various morphologies have been documented for dendritic and hyperbranched liquid crystal polymers, and this topic has recently received intense interest [14–27, 62–70]. Although the exhaustive revision of this area is outside the scope of this article, several types can be easily identified:

(i) hyperbranched polymers and liquid crystal dendrimers in which the mesogenic groups form part of each branching unit;
(ii) dendrimers without mesogenic groups that form liquid crystal phases, where the formation of the mesophases is due to self-assembly process of the constituent dendrons, aided by microphase segregation, and
(iii) liquid crystal dendrimers formed by attachment of liquid crystal moieties to the periphery of a suitable core dendrimer, where the mesogenic units are located on the surface of the dendritic core.

The first thermotropic liquid-crystalline dendrimer, **15**, shown in Fig. 17, was reported by Percec and Kawasumi for a hyperbranched polyether structure that consisted of an AB_2 monomer, with a mesogenic unit based on confor-

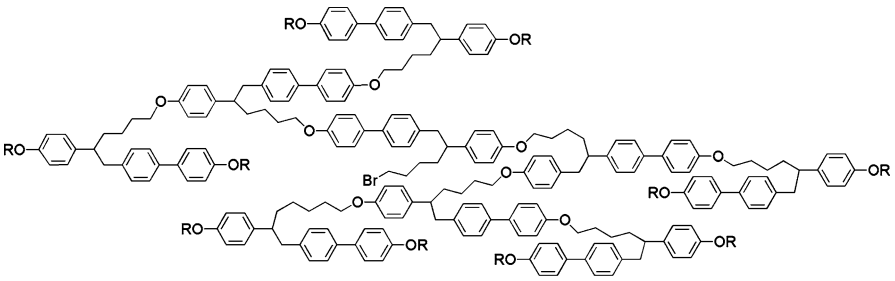

Fig. 17 A nematic supermolecular material which forms a rod-like conformation

mational isomerism. Different end-groups were used to terminate the polymer, and the *gauche* conformation was found to favor the dendritic geometry in the solid state; however, the *anti* conformation was obtained at higher temperatures, and this was found to stabilize the formation of the nematic phase [71].

Lattermann et al. reported the first metallomesogenic dendrimer when they described results on trigonal bipyramidal metal complexes of ethyleneimine dendrimers of the first and second generation, based on derivatives of tris(2-aminoethyl)amine. Complexes of cobalt, nickel, copper, and zinc were prepared and found to exhibit relatively low temperature mesophases, which generally possessed hexagonal columnar structures. These materials therefore provided the first examples of metallomesogenic dendrimers [72, 73].

The groups of Shivaev and Frey reported (at a similar time) the first examples of materials that are classed as conventional liquid crystal dendrimers. In these reports they described the synthesis of liquid-crystalline carbosilane dendrimers, which differ from the above dendritic liquid crystals in that the mesogenic groups are located only at the surface [74, 75]. Thus the materials combine a flexible, dendritic carbosilane inner core which is functionalized on the surface with cyanobiphenyl groups or cholesteryl groups, attached by flexible spacers via either classical hydrosilylation reactions or through esterifications, see Fig. 18 for example. This material, **16**, has 36 mesogenic moieties attached to its periphery, however, the flexibility of the central scaffold allows the supermolecule to deform its shape to give a rod-like overall form, thereby supporting the formation of calamitic mesophases. Remarkably, although the individual mesogenic groups would normally support the formation of nematic phases at temperatures above room temperature, the supermolecule exhibits a wider temperature range for the mesomorphic state, with a glassy phase being formed well below room temperature. In this series of materials up to 124 mesogens have been attached to the periphery, and at higher number densities of mesogens, i.e., for higher generations of the dendritic scaffold, columnar phases start to appear. However, the introduction of columnar phases at higher generations is

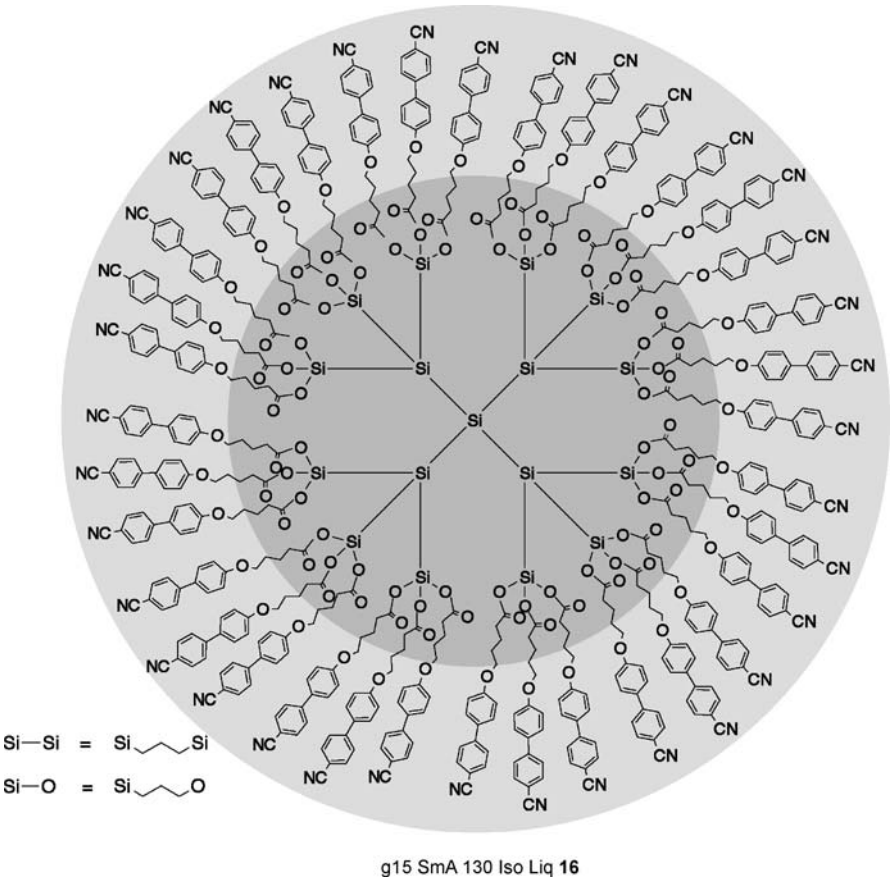

Fig. 18 Example of a typical liquid crystal dendrimer with its mesogenic units covalently attached to the outer surface of a flexible scaffold

indicative of the flexibility of the scaffold, which allows for a wide variety of conformers to be present in the lower generations that support the formation of rod-like gross shapes of the supermolecule (see Donnio and Guillon for a very detailed review of liquid-crystalline dendrimers and polypedes [76]).

2.1 Effect of Density of Mesogens and Number Generation

The reports by Elsäßer et al. concerning the formation of carbosilazane-based multipedal systems provides for one systematic study where material design and preparation was taken from a simple bimesogen to trimesogen and through to dendrimer. In addition, the soft-centered core was changed in generation number from 0 to 2, where mesogens were appended laterally to the

scaffold, thereby providing for a more complete study. The synthetic pathway to the various carbosilazane scaffolds is shown in Fig. 19. Derivatization of the double bonds with hydrosiloxane derivatized mesogens results in the formation of multipedal and dendritic liquid crystals [50–53].

Figure 20 shows a list of the transition temperatures for the various polypedes and dendrimers that were prepared. It is interesting that the systems bearing four aromatic rings, **22** to **26** exhibited polymorphism, whereas the three-ring systems, **17** to **21**, did not. All of the materials, however, exhibited the nematic phase, in keeping with the earlier description of lateral versus terminal appendages of the mesogens to the central scaffold. The four-ring systems also exhibited crystalline phases whereas the three-ring systems essentially formed glassy states at low temperature. This effect is probably related to the fact that the systems with four-ring mesogens are behaving as though they are a collection of individual mesogens, ie, the system is being dominated by the liquid crystal units because the length to breath ratio is quite high. The three-ring systems on the other hand have greater flexibility due to the lower length to breath ratios, and the relative dynamics will ensure that these materials will only exhibit nematic phases. Overall it is also very interesting that the three-ring systems are in their nematic phases at room temperature down to temperatures well below 0 °C!

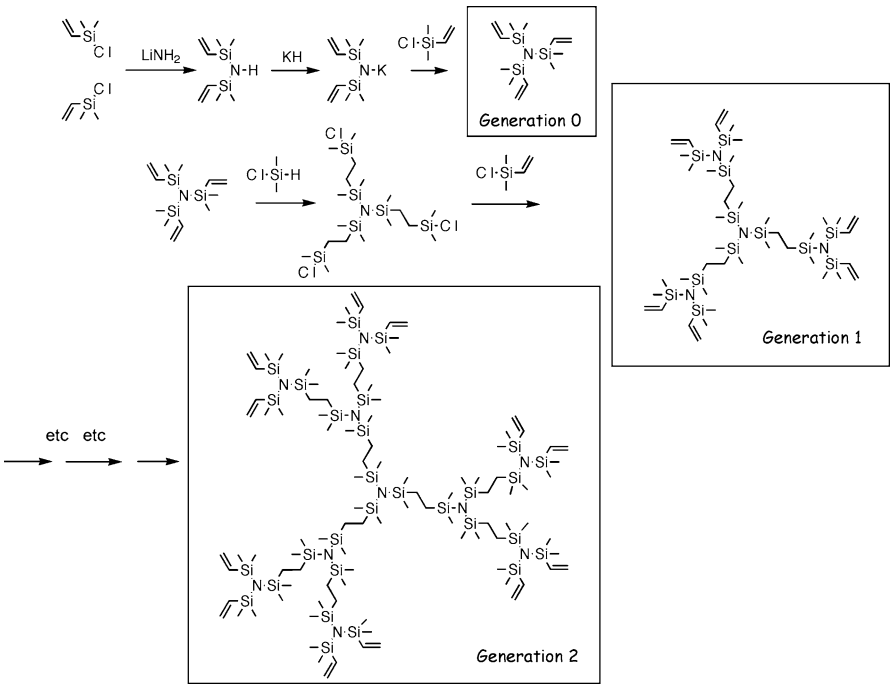

Fig. 19 Synthetic scheme to prepare carbosilazane-based dendritic scaffolds

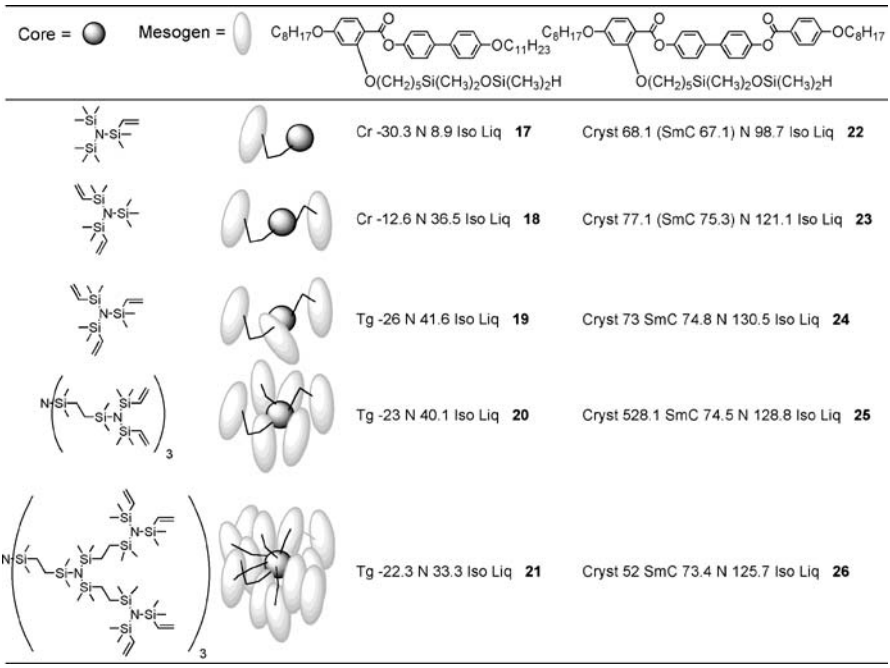

Fig. 20 Effect of density of mesogens and number generation in multipedal and dendritic carbosilazanes

2.2 Effect of Spacer Length

The effect of the length of the linking chain between the mesogenic units and the scaffold were investigated using simple model tetrahedral systems with cubic symmetry that were created by reacting *tetrakis*-(dimethylsiloxy)silane with a variety of alkenyloxy-cyanobiphenyls [77, 78], thereby generating a set of tetrahedrally substituted mesogenic supermolecules, see Fig. 21 where four mesogenic units are tethered to a central point. The figure shows that the tetramers exhibit smectic A liquid crystal phases which are preferred over the nematic phase exhibited by the mesogenic monomers themselves. In this sense, these supermolecules are similar in mesophase behavior to conventional side-chain liquid crystal polysiloxanes which have cyanobiphenyl moieties as the mesogenic side group.

In general, the smectic A phase has a structure where rod-like molecules pack in diffuse layers where there is no positional ordering of the molecules in the plane and out of the plane of the layers [79]. The only way in which the tetramers can form such a phase is by molecular distortion away from a spherical shape to give a rod-like conformational structuring. Molecular

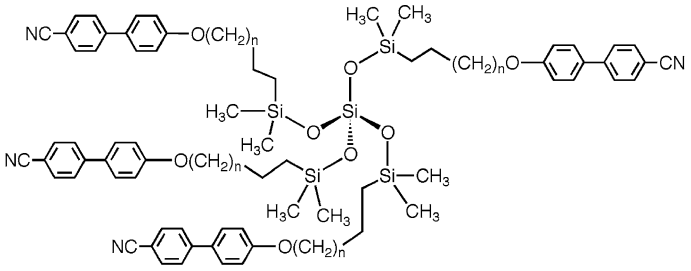

Spacer (n)	Tg (°C)	SmX - SmA	SmA - Iso Liq (°C)
4	- 9.6	-	88.7
6	-14.7	-	118.7
11	-6.3	38.7	129.7

Fig. 21 Transition temperatures (°C) for the tetramers of alkenyloxy-cyanobiphenyls substituted *tetrakis*-(dimethylsiloxy)silane

modelling studies reveal that even in the gas phase at absolute zero, the conformation where the mesogenic side-chains are aligned is the more energetically favored conformation (see Fig. 22), thereby allowing the supermolecules to achieve rod-like molecular shapes.

The materials with C_4 and C_6 spacers exhibited only a smectic A phase, whereas the tetramer with a C_{11} spacer shows, upon heating, a transition to an additional unidentified phase at 38.7 °C. When the number of methylene units is increased, the isotropization temperatures increase accordingly. The material with the C_6 spacer has the lowest solidification temperature (–14.7 °C). Thus these symmetrically substituted systems show low melting

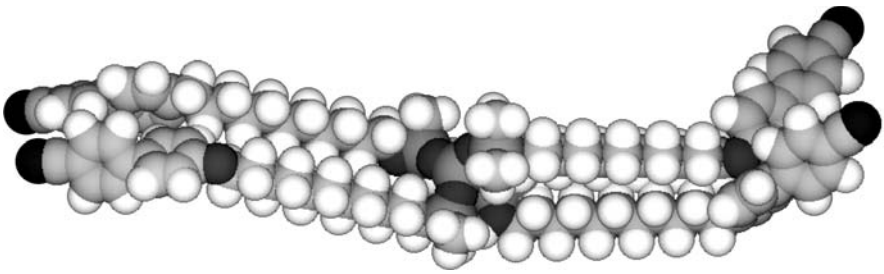

Fig. 22 The molecular shape of tetramer with a C_{11} spacer unit shows the minimized structure in the gas phase at absolute zero using a Silicon Graphics system operating with Quanta and CHARMm software

behavior and primarily glass formation on cooling. This effectively widens the relative temperature ranges of the liquid crystal mesophases.

X-ray diffraction shows that the trichotomous nature of the tetramers allows for different packing characteristics to exist for the molecules in the smectic A phase. Thus, the separate interactions of the mesogenic units, the alkyl spacers and the silicon cores have to be considered in the formation of the A phase. For the shorter methylene spacer lengths, internal phase separation leads to the smectic A phase being described as a smectic A_d phase with respect to the mesogens and a monolayer smectic A_1 phase with respect to the silicon cores, see Fig. 23. In the smectic A_d phase, the mesogenic units are partially interdigitated giving a layer spacing d, where $1 \times l < d < 2 \times l$, and l is the molecular length. The smectic A_1 phase is a disordered layered phase where the layer spacing is approximately equal to the molecular length. For the longer methylene spacer lengths, the co-existence of smectic A_d and smectic A_2 phases is probable (the smectic A_2 phase is a bilayer system where the layer periodicity is twice the molecular length). The occurrence of these structures can be explained by the presence of biphasic or incommensurate smectic A phases, or even a smectic A anti-phase.

Thus for the tetramers there is adequate free volume for the cyanobiphenyl "mesogenic arms" to rotate so as to give a distorted rod-like molecular shape. Increasing the number of mesogenic units attached to the central point, however, has the effect of reducing the free volume for the packing of the mesogenic groups, which in turn reduces their freedom of movement and suppresses the ability of the supermolecular system to generate a rod-like conformational form. Increasing the number of mesogens attached to a central point is difficult to achieve without moving in the direction of dendrimer formation, but the substitution of polyhedral core units with mesogenic groups can provide an alternative route to packing a larger number of mesogenic units about a central focal point. The use of various polyhe-

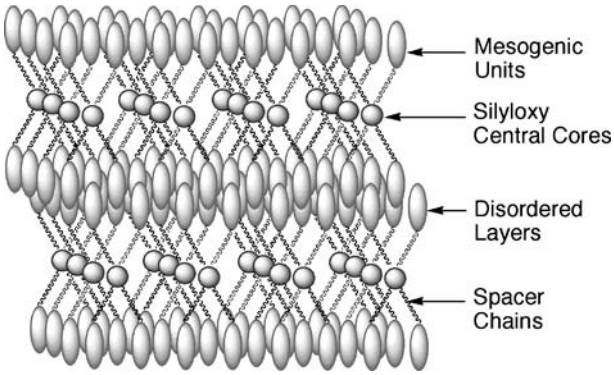

Fig. 23 The proposed structure of the smectic A phase of the tetramers

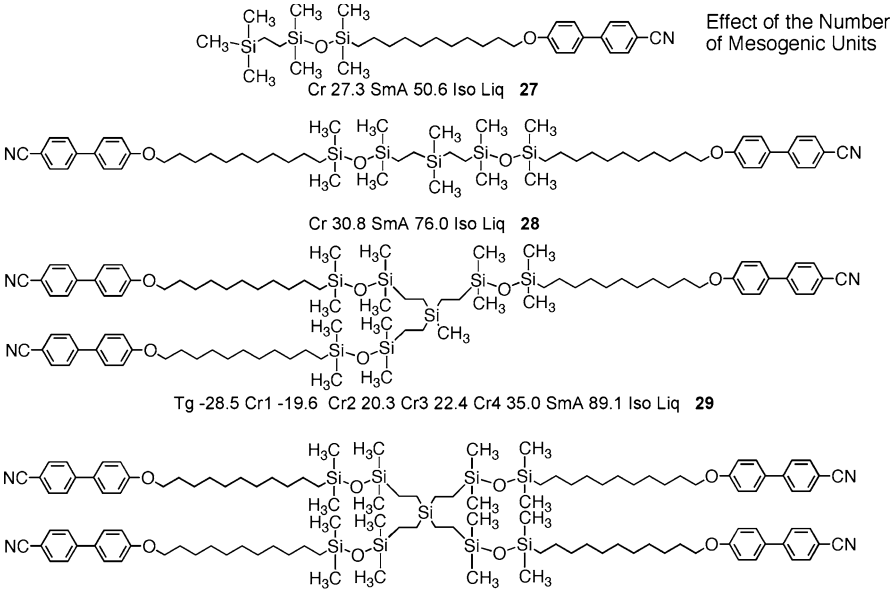

Fig. 24 The change in transition temperatures (°C) as the number of mesogenic groups increases

dral siloxane-substituted systems, as the central cores of the supermolecular systems, allows for meaningful comparisons to be made as the free volume available to the mesogens is reduced as the degree of substitution about the polyhedral core is increased [80, 81], see Fig. 24.

2.3 Effect of Incompletion of Outer Shell or Generation

Often dendritic liquid crystals are assembled through the preparation of dendrons, and then the dendrons are attached to a central scaffold of a suitable generation number. This technique allows for the dendrons to be prepared on a large scale and then the attachments to the scaffold are done in smaller number than if the mesogens are directly attached. However, one problem that is sometimes encountered in this synthetic approach is that the scaffold becomes progressively crowded as the dendrons are attached, and sometimes this can lead to incomplete derivatization. In the following section, complete and incomplete substitutions are investigated and compared.

Firstly, however, we can compare the attachment of dendron carrying either terminally or laterally appended mesogens. Although the scaffold in this example is a first-generation system based on pentaerythritol, the dendrimer was in fact prepared from dendrons based on pentaerythritol, which were

then attached to pentaerythritol itself, via formation of the propanoic acid derivative.

In the materials discussed in the next section, the mesogenic groups have four aromatic rings, in order to promote mesomorphic behavior. In all of the examples a chiral unit was included into the structure of the mesogens, and in the first of the materials, dendrimer **31**, see Fig. 25, a chiral 2-methylbutyl group was appended laterally to the long axes of the mesogens. As expected, the terminally appended material exhibited a smectic phase, in this case chiral smectic C*, but in addition, a chiral nematic phase was also exhibited. The local structure of the smectic C phase is shown in Fig. 26, where the mesogens are constrained into a cylindrical conformation. The mesogens are located towards the layer interfaces and the aliphatic spacers or linking groups are towards the interiors of the layers. The mesogens are also tilted with respect to the layer plains, but this does not indicate that the cylindrical structures are tilted, rather just that the mesogens are at an angle to the layers. The material

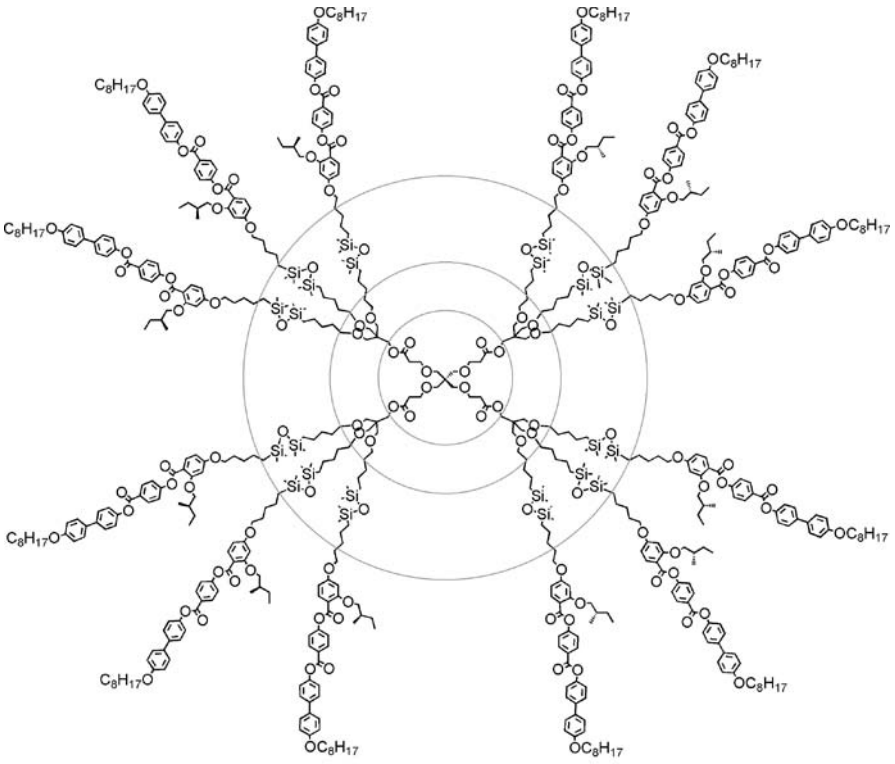

Fig. 25 Dendrimer **31** with terminally appended mesogens which themselves have laterally appended chiral groups

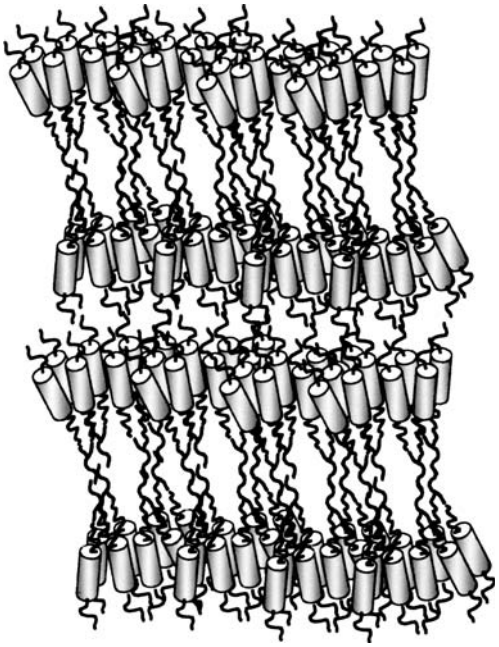

Fig. 26 Local structure of the chiral smectic C* phase

showed a crystalline solid at lower temperatures. As the chiral group chosen was 2-methylbutyl, the chiral nematic phase was not iridescent, because the pitch of the chiral phase was too long. In addition, the smectic C* phase is expected to be ferroelectric, however, the polarization would be expected to be relatively small because of the weak dipole at the stereogenic center.

The laterally appended dendrimer, **32**, shown in Fig. 27, as expected exhibits a chiral nematic phase, with smectic mesophase formation being suppressed. The clearing point is almost 50 °C lower, whereas the melting point is only 25 °C lower in comparison to the terminally appended system. This demonstrates that lateral appendages of the mesogens causes disruption to the intermolecular packing, thereby destabilizing mesophase formation. The local structure of the chiral nematic phase is thus shown in Fig. 28.

In the synthesis of the dendrimers it is more difficult to attach the dendrons with laterally appended mesogens to the scaffold than it is to attach the dendrons with terminally appended mesogens. This may be associated with the effects of a higher degree of crowding produced by the laterally attached mesogens. This forces the issue of dispersity, but in a controlled way, it is possible to prepare a dendrimer with only three dendrons rather than the four that are possible, as shown in Fig. 29. The three-armed product, **33**, possesses a nematic phase with a similar structure to that shown in Fig. 28 for the four-armed dendrimer. Remarkably, the melting points and clearing points of the

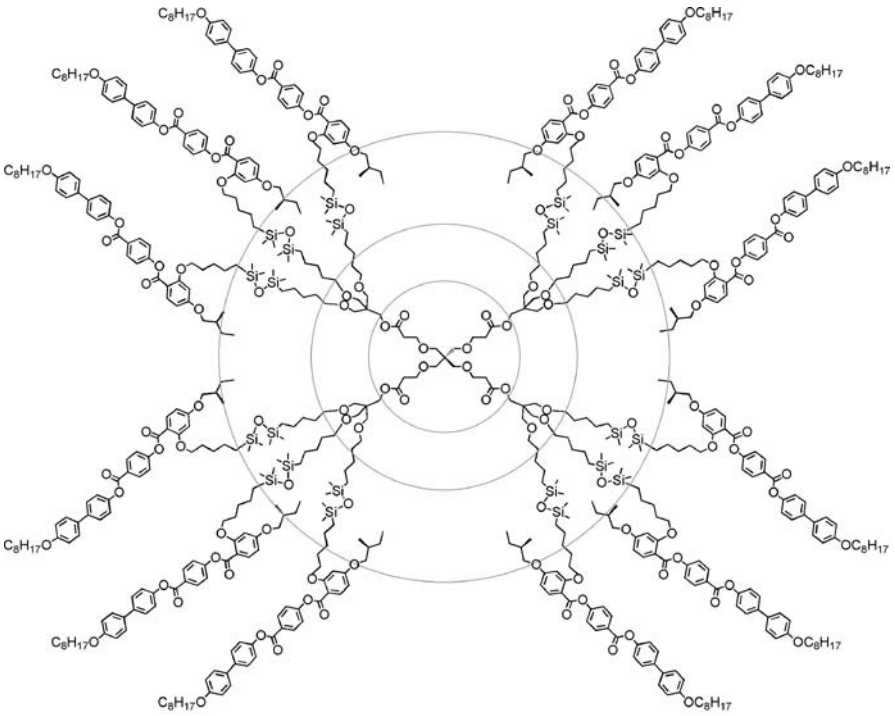

Cryst 50.9 N* 70.1 °C Iso Liq **32**

Fig. 27 Dendrimer **32** with laterally appended mesogens

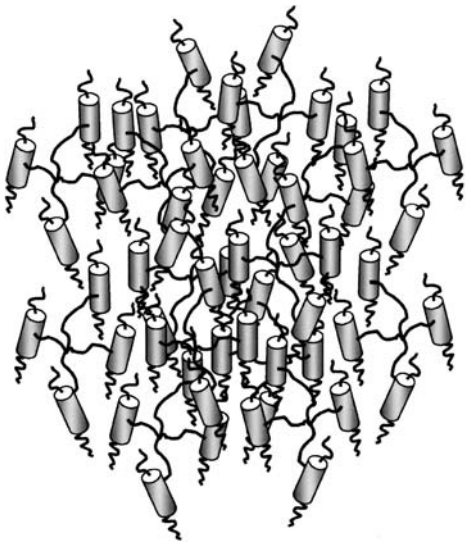

Fig. 28 Local structure of the chiral nematic phase

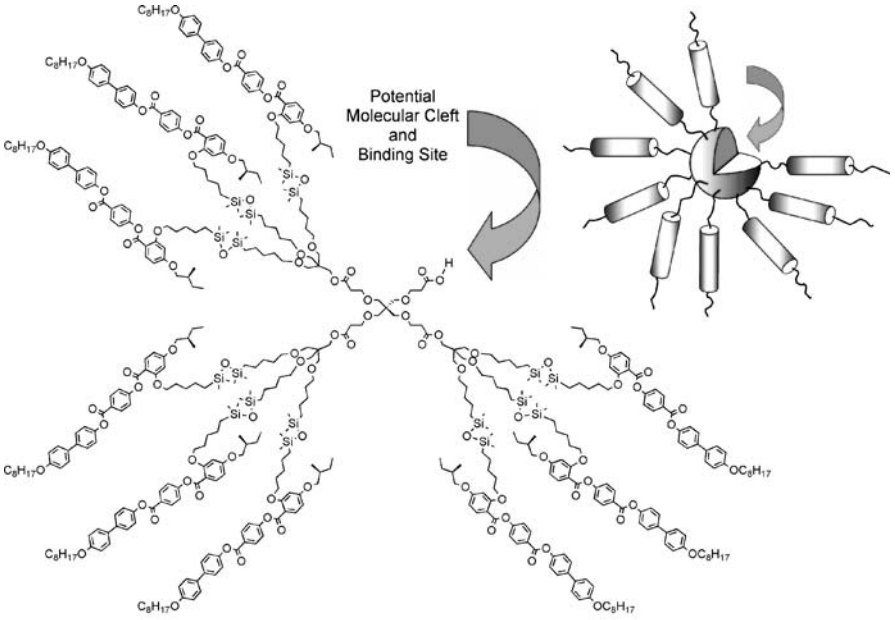

Fig. 29 A three-armed dendrimer with a potential binding site at the fourth unsubstituted location

two are almost identical. This result demonstrates that in this system the liquid crystal properties are dominated by the properties of the dendrons. Thus it does not matter to the giant molecular system whether three or four arms are present, the system simply does not know the difference.

One of the more interesting features about the three-armed system is that the fourth unsubstituted site still has an acid moiety associated with it. Thus, this location can act as a binding site, and potentially a catalytic site, and the system has the potential to act somewhat like a protein, with a binding cleft in its structure, see Fig. 29.

2.4
Effect of Chirality on Physical Properties

As noted earlier, the incorporation of chiral groups in the liquid crystal moieties can have the effect of inducing non-linear properties, which include thermochromism, ferroelectricity, antiferroelectricity, electrostriction, and flexoelectricity. In a now classical study, Hult [82] demonstrated that it was possible for supermolecular material **34** to exhibit two-state ferroelectric switching. The remarkable material he investigated, shown in Fig. 30, was found to exhibit two hitherto unclassified mesophases between the smectic

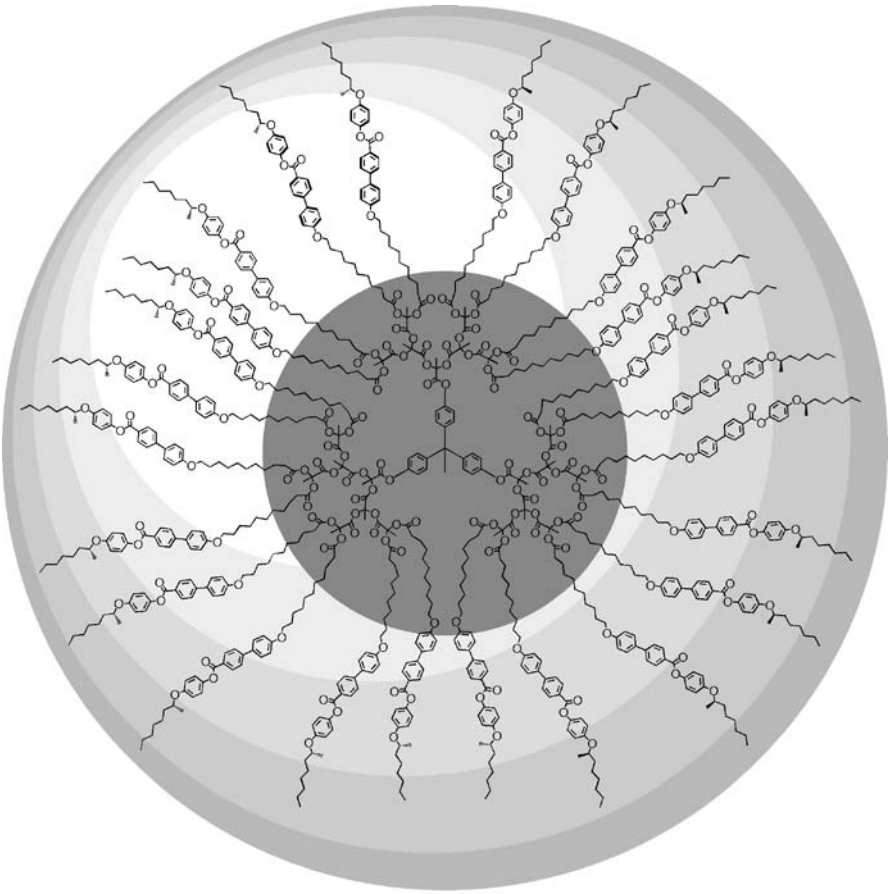

Cryst 80 SmC* 105 Sm1 125 Sm2 132 Sm A* 148 °C Iso Liq θmax 26° at 105 °C **34**

Fig. 30 Ferroelectric supermolecular material, **34**

A* phase and the smectic C* phase. At a temperature of 105 °C, just in the smectic C* phase, ferroelectric switching was achieved with a tilt angle of 26°. The mesogenic units were based upon the famous MHPOBC ferroelectric material which had a switch angle of approximately 25°. Thus this result demonstrated that the dendrimer is really acting as a collection of low-molar-mass liquid crystals.

2.5
Effect of Hard Core Scaffolds – Silsesquioxanes

Within the now conventional group of liquid crystal dendrimers, a group of liquid-crystalline dendrimers based on the hexa- and octa-silsesquioxane

core has been reported, which provide six or eight primary (radial) branches for derivatization, allowing an increased packing of the mesogens around the dendritic core at earlier generations; moreover, the rigid framework of the silsesquioxane cores offer the possibility of a contrasting comparison with dendrimers derived from entirely flexible scaffolds. The structures of the hexa- and octa-silsesquioxanes are shown together in Fig. 31.

A_1 example, **35**, of a nematogenic supermolecule possessing an octasilsesquioxane central core is shown in Fig. 32 [83]. The material, by virtue of possessing laterally appended mesogenic units, is nematic, where the nematic phase is enantiotropic by two to three degrees. On heating from the solid state it exhibits a crystal to nematic phase transition, but on cooling back to the solid it forms a glass, which is usually the case for supermolecules with laterally appended mesogens.

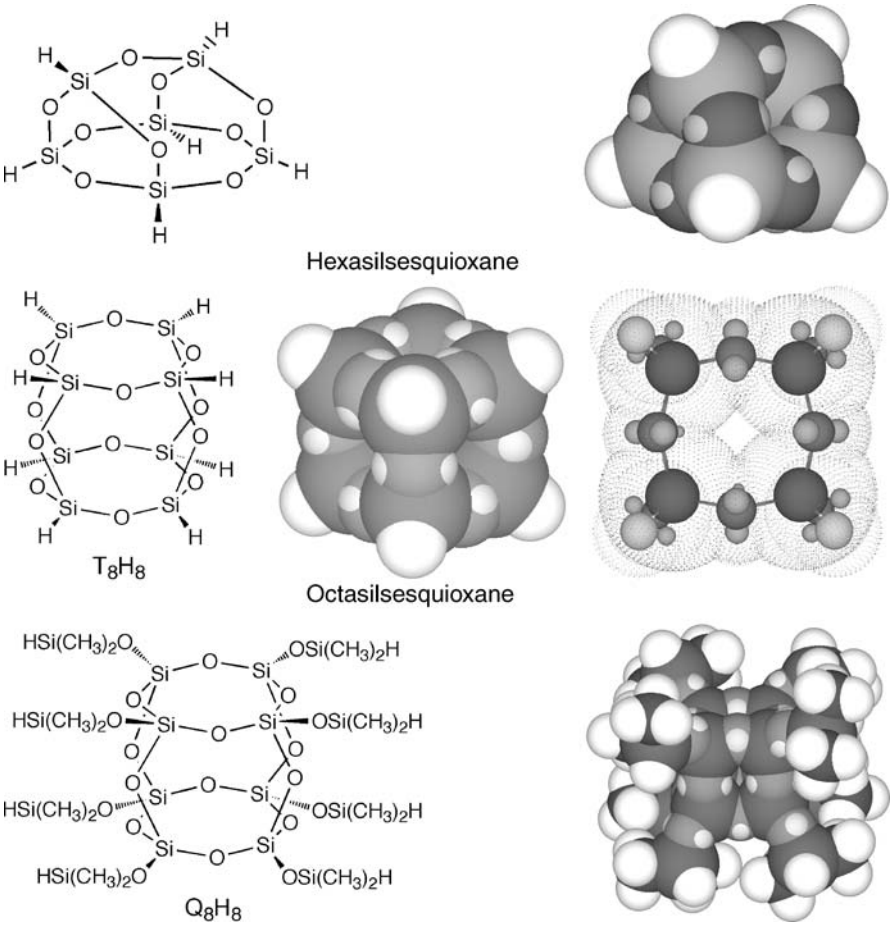

Fig. 31 The structures of the hexa- and octa-silsesquioxanes cores for use as scaffolds

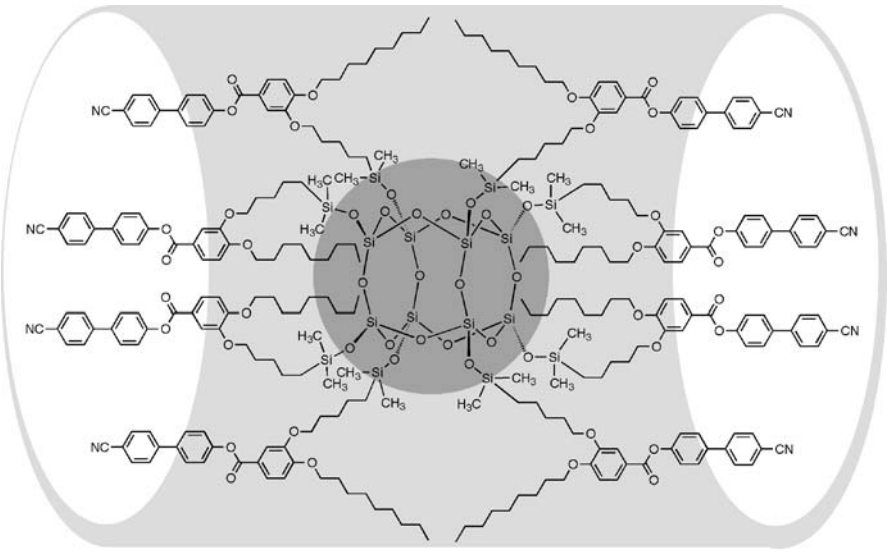

g -25 Cryst 48.9 N 51.8 Iso Liq **35**

Fig. 32 A nematogenic supermolecular octasilsesquioxane, **35**, with laterally appended mesogenic groups

The structure of the nematic phase is proposed to be one where the central cores are surrounded by the mesogenic groups, with the long axes of the mesogens pointing in roughly the same direction, as shown in Fig. 33.

Terminally appended systems on the other hand tend to have more pronounced stability of the smectic phases, and indeed in some cases polymorphism is also observed. For example, the substitution of silsesquioxanes with mesogenic groups that are conducive to smectic mesophase formation, yields supermolecular materials that as expected exhibit smectic phases. For the many materials studied, the formation of smectic phases and mesophase temperature ranges are considerably enhanced for the supermolecular material over those of the individual mesogenic parents. In the case of substitution of the hexasilsesquioxane scaffold with the 4′-(2-methyl butylbenzoylxoy)biphenyl-4-carboxylate mesogenic unit, **36**, see Fig. 34, [81] which favors the formation of orthogonal smectic A and tilted smectics C, I, and F phases, the supermolecule exhibits only the tilted smectic C phase. Smectic polymorphism is suppressed, which is important for uses of such materials in various applications. For compound **36** the smectic C phase is present from 11.5 to 191.5 °C, i.e., a temperature range of over 180 °C, whereas it is only present over a temperature range of 22–23 °C for the mesogenic monomer unit. The coupling of the potential stability of the smectic C phase with chirality built into the mesogenic units allows for the possibility of synthesizing supermolecular ferroelectric materials, which may have inter-

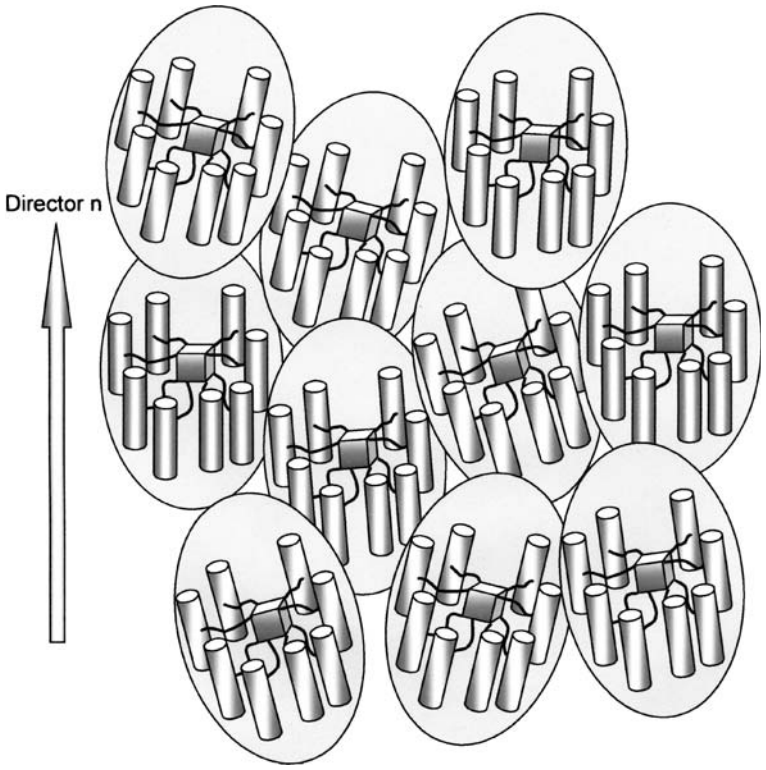

Fig. 33 Local structure of the nematic phase of an octasilsesquioxane dendrimer, **35**, possessing laterally appended mesogens

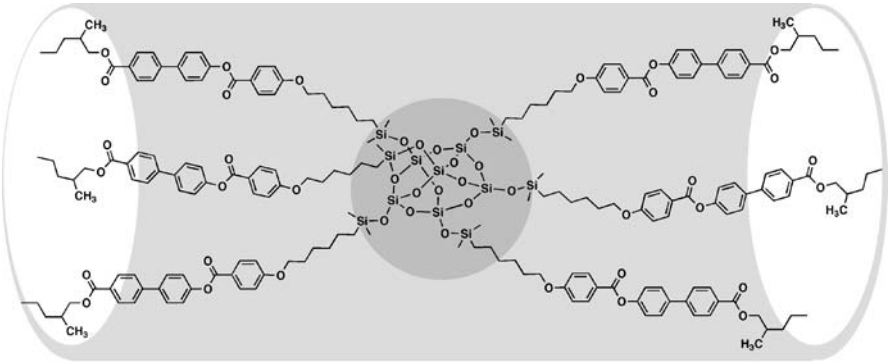

g 11.5 SmC 191.5 °C Iso Liq **36**

Fig. 34 A terminally appended hexasilsesquioxane, **36**

esting non-linear physical properties, e.g., antiferroelectric, pyroelectric, and piezoelectric properties.

The next family of materials, which are to be discussed all possess cyanobiphenyl moieties as the mesogenic units. The systematic studies of the liquid crystal properties are described in terms of spacer length and peripheral number density. The first material, **37**, shown in Fig. 35, is an octamer based on the octasilsesquioxane core unit [86]. This material was prepared and purified in such a way that by HPLC and ^{29}Si NMR spectroscopy it was shown to be a single compound without dispersity. The material was found to exhibit smectic polymorphism with SmC and SmA phases being formed. The incorporation of cyanobiphenyl mesogenic moieties means that the material has interesting

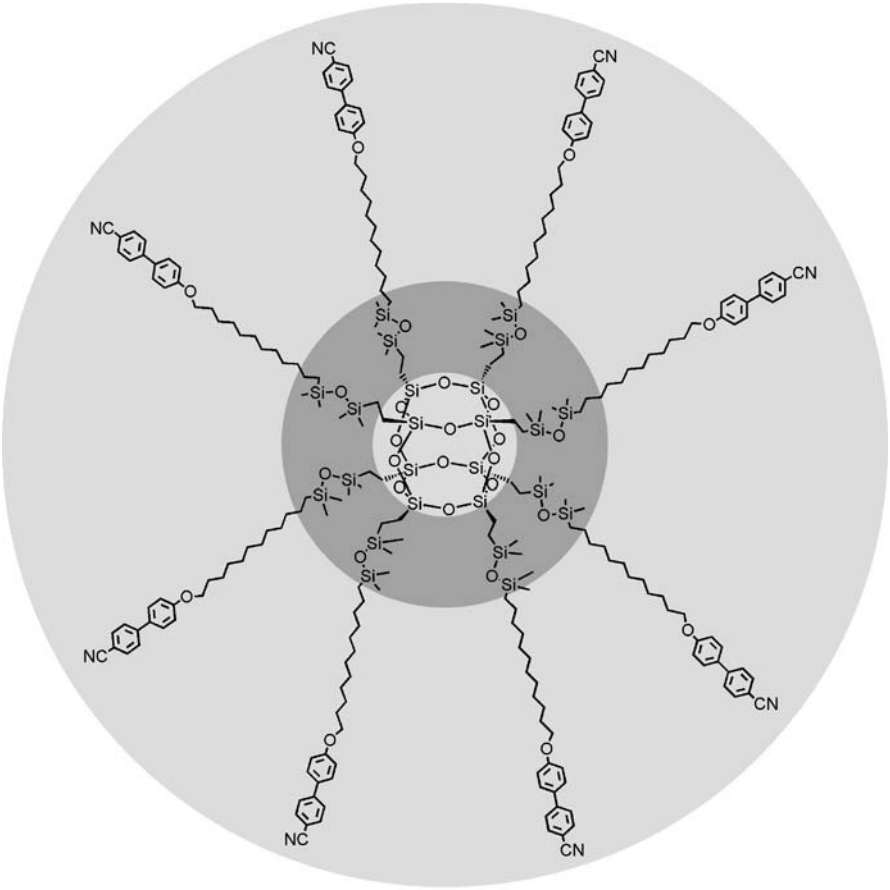

g –12.8 $Cryst_1$ 4.7 $Cryst_2$ 39.0 SmC 74.2 SmA 102.9 °C Iso Liq **37**

Fig. 35 Octamer of octasilsesquioxane, **37**, bearing cyanobiphenyl moieties

dielectric properties, and the presence of the smectic C phase indicates that with the introduction of chirality the material would also be ferroelectric and pyroelectric. The mesophase sequence of g –12.8 $Cryst_1$ 4.7 $Cryst_2$ 39.0 SmC 74.2 SmA 102.9 °C Iso Liq, demonstrates that the dendritic structure of the supermolecule is constrained to being rod-like, see Fig. 36, and that the rod-like conformers tilt over at the smectic A to smectic C phase transition, as shown in Fig. 37. Thus, the structures of both the smectic A and the smectic C phases have alternating organic and inorganic and layers. As the inorganic and organic layers have differing refractive indices, the mesophase structures are essentially nano-structured birefringent slabs.

The effect of the length of the spacer chain on the liquid-crystalline properties of the octamers of octasilsesquioxane, of general structure **38**, was

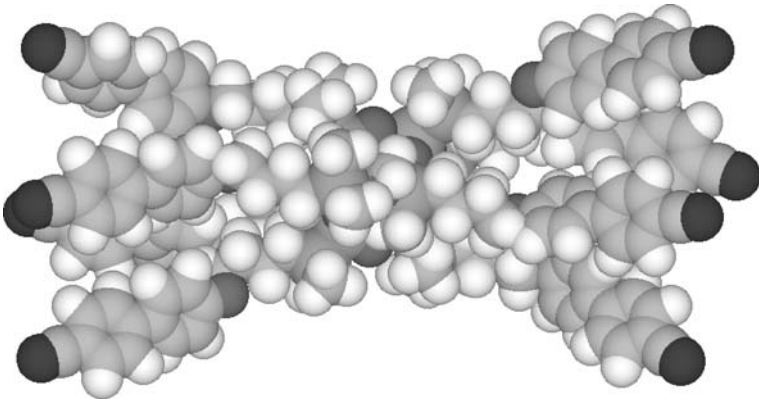

Fig. 36 Minimized structure of the octamer, **37**, showing that the dendrimer is cylindrical in shape

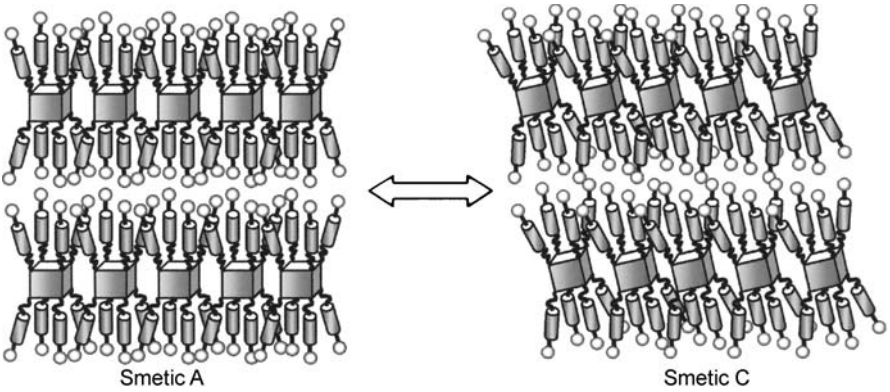

Fig. 37 The structures and phase transition for the smectic A and smectic C phases of multipede **37** where the spheres represent the terminal cyano moieties

investigated, see Fig. 38 and Table 1. This family of materials were found to exhibit only smectic A phases, however, as the aliphatic chain length of the spacer was increased, the mesophase stability increased. All of the family exhibited glassy phases on cooling the smectic A phase, interestingly the glass transition temperatures were below room temperature [84].

The number of mesogenic groups can be increased in the periphery by the hydrosilylation of the first-generation hexadecavinyl octasilsesquioxane dendrimer, see Fig. 39, with cyanobiphenyl mesogens containing terminal Si-H groups, thereby affording the liquid crystal multipede **39**, see Fig. 40, which contains 16 cyanobiphenyl groups attached to the dendritic core [86]. For this material, the ^{1}H NMR spectrum showed well-resolved resonances for all the protons of the cyanobiphenyl mesogenic groups, indicating complete conformational freedom of the mesogenic units in solution. Complementary ^{29}Si NMR spectroscopy shows that the reaction of the cyanobiphenyl mesogens with the vinyl units was incomplete, and although the distribution was much sharper than normally found for polymers, nevertheless, the material showed a degree of dispersity and is not a unique compound. The molecular weight of **39** was under-estimated by SEC, an effect frequently encountered in

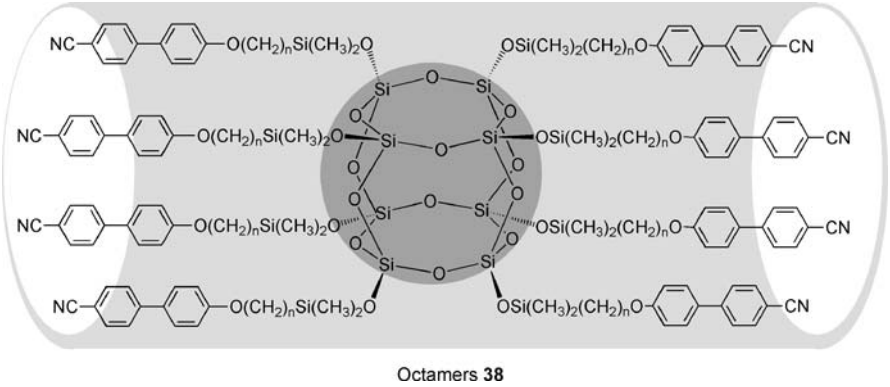

Fig. 38 Effect of spacer chain length on the liquid crystal properties of dendrimers of general structure **38**

Table 1 Transition temperatures (°C) as a function of methylene spacer length (*n*) for octamers **38**

Spacer chain length (*n*)	g to SmA	SmA to Iso Liq
4	11.0	93.9
6	0.3	116.5
11	–7.0	128.5

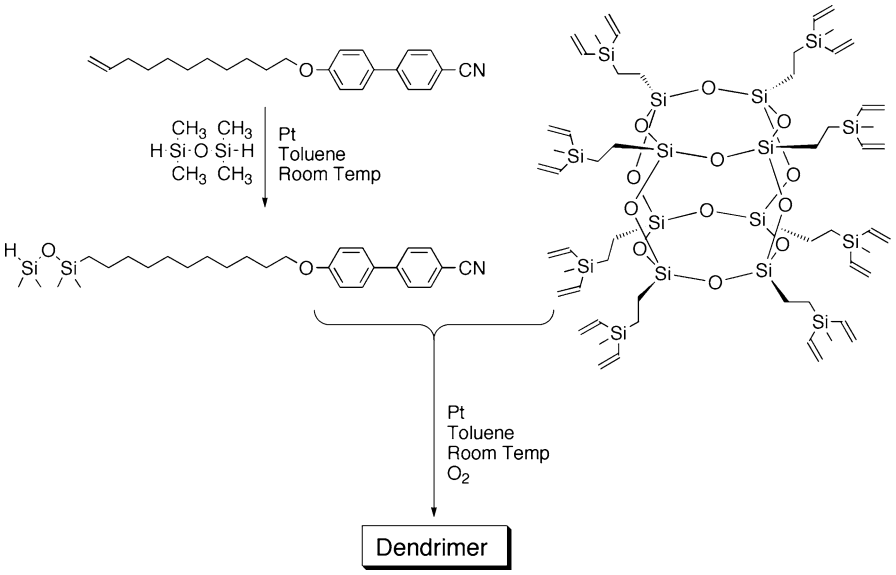

Fig. 39 Synthesis of supermolecule **39**

dendrimers, which has been interpreted as evidence of a globular conformation in solution.

Multipede **39** shows, see Fig. 40, a phase sequence of g –17.5 SmC 63.1 SmA_1 91.7 °C Iso Liq. Thus the effective doubling of the number of mesogenic units results in the lowering of the clearing point, the SmC to SmA transition and the glass transition relative to **37**. This thermal behavior is in contrast with that normally found for liquid crystal dendrimers based on flexible dendritic cores, where the clearing points increase and the glass transitions remain almost constant with generation number [87–91].

The mesophase behavior of **39** implies that the dendrimer must, like supermolecule **37**, also have a rod-like shape in order that it can pack in layers, where the molecules within the layers are disordered and the layer structure is diffuse, revealing that the mesogenic state deforms the globular environment of the dendrimer. This is remarkable given that the number of mesogenic units is doubled relative to the number of octasilsesquioxane scaffolds, see Fig. 41, and where as a consequence one would expect curvature in the packing of the mesogenic units to occur due to their bunching about the scaffolds. Again, unlike the parent mesogenic system, the smectic A phase of the dendrimer forms a monolayer smectic A phase (SmA_1). As with other dendrimers bearing terminal nitrile groups, a smectic C phase is also formed, which for the parent system is almost unheard of.

The point of bifurcation, so that 16 mesogenic units can be more easily located around the octasilsesquioxane core, can be achieved by moving the bifurcation point away from the central part of the scaffold as shown for

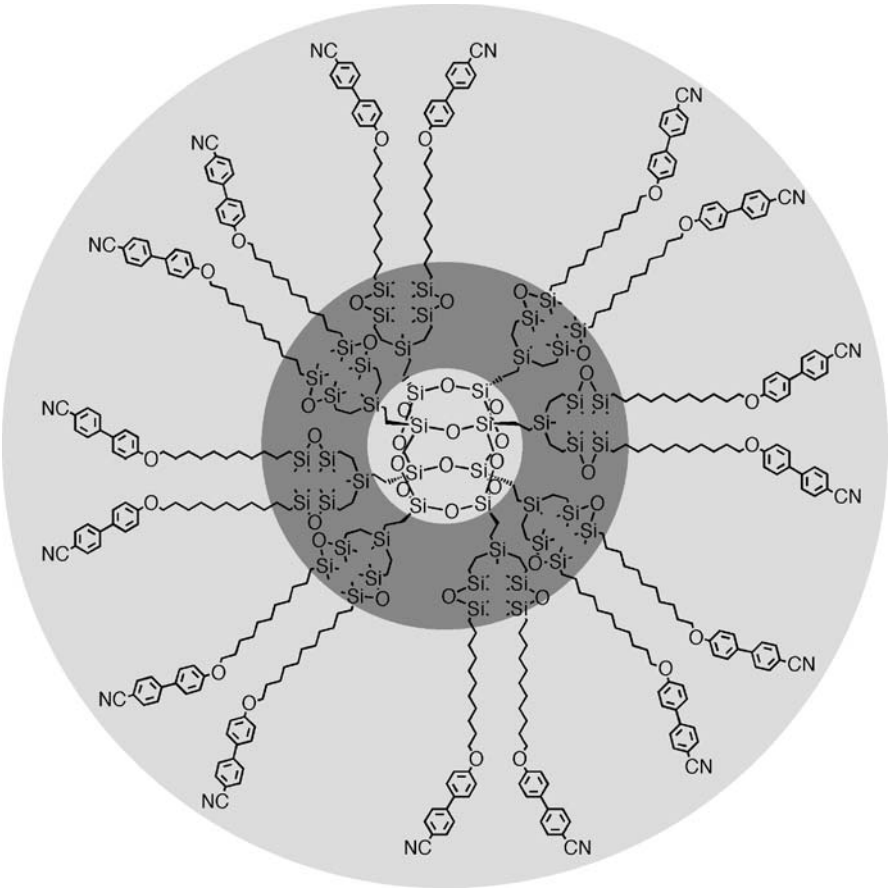

Fig. 40 Structure of dendromesogen **39**. The results below the structure show that it is not monodisperse

dendrimer **40**, see Fig. 42 [85]. In this case, however, the thermal stability of the smectic C phase is greatly reduced, whereas the stability of the smectic A phase is retained. However, because the mesogens are decoupled from the scaffold to a large degree, the material crystallized rather than formed a glassy phase.

As noted earlier, in general, as for traditional side-chain liquid crystal polymers, the end-on attachment of the mesogenic moieties affords smectic phases, whereas side-on mesogenic sub-units lead to nematic phases. By appending laterally attached chiral mesogenic units to the octasilsesquioxane scaffold the induction of the chiral nematic phase into this class of materials was targeted. Supermolecule **41**, see Fig. 43, the size of a small globular protein (i.e., $M_W = 6560$), was prepared as a single material with a dispersity of 1, and as predicted it exhibited a chiral nematic phase with a helical

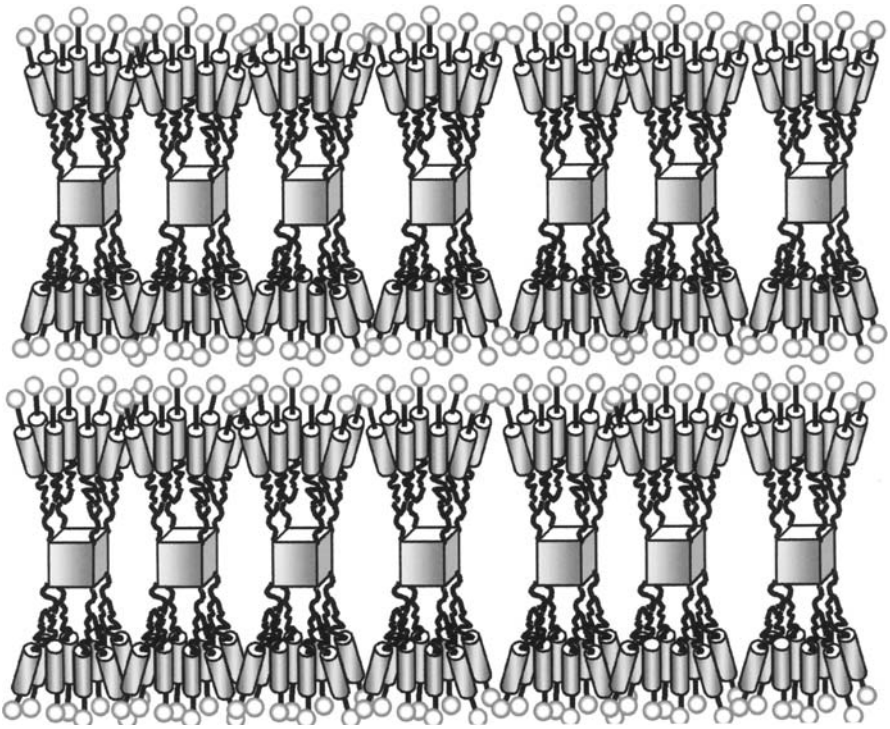

Fig. 41 Schematic drawing of the bilayer structure of the smectic A phase of multipede **39**. The 16 mesogenic units (cylinders and spheres which represent the cyano groups) per molecule are accommodated in the layers without the introduction of curvature in the packing of the mesogenic units together

macrostructure. Furthermore, the material exhibits an extraordinarily long temperature range for the chiral nematic phase. A transition from a glassy state to the chiral nematic phase occurs near to room temperature and then the phase extends over 90 degrees before transforming to the isotropic liquid at 116.9 °C [92].

The local structure of the chiral nematic phase is shown in Fig. 44 where the supermolecules are depicted as having rod-like/tubular structures where the mesogenic units are expected to intermingle between the supermolecules. The chiral nematic phase will have a helical macrostructure superimposed upon the local nematic ordering as shown in the figure. Remarkably, the material has a helical pitch of approximately 2 μm, which is a relatively short pitch considering the size of the polypede, and approximately the same as the pitch that would be produced by the individual mesogenic units without spacers being attached. However, unlike the situation for the mesogenic units, the pitch is relatively temperature insensitive. Thus the surface of the polypede acts as a molecular recognition surface, in a similar way to recognition sur-

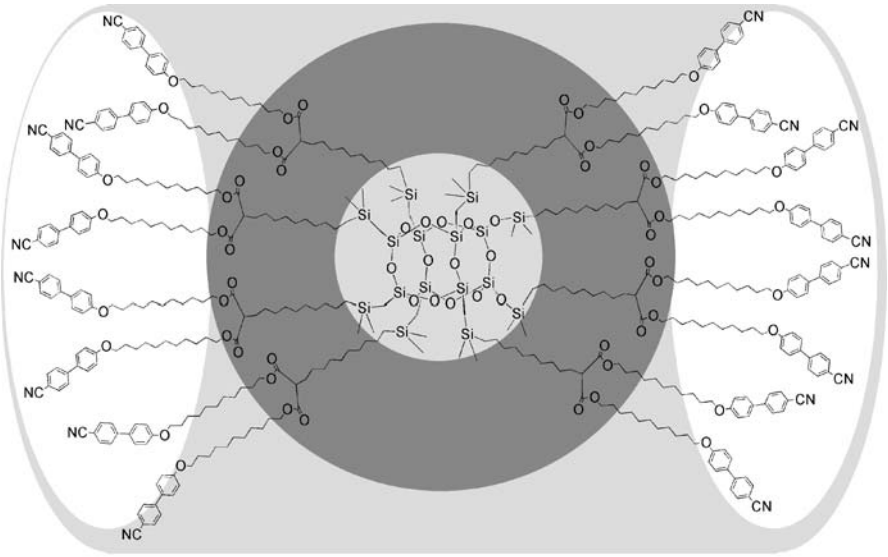

Cryst 35.1 (SmC 29.8) SmA 95.7 °C Iso Liq **40**

Fig. 42 Dendrimer **40** shows a bifurcation point that is removed from the central scaffold

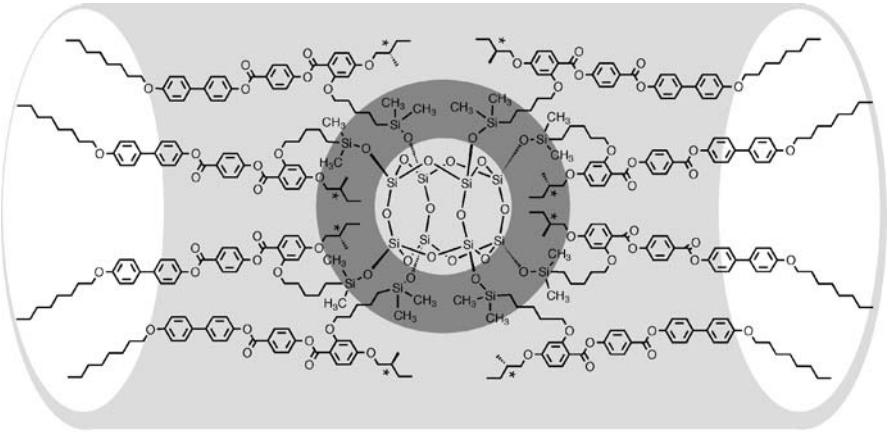

g 23.7 N* 116.9 °C Iso Liq **41**

Fig. 43 Laterally appended octamer of octasilsesquioxane, **41**, where the mesogens are chiral

faces are created in surfactant systems and Janus grains as described by de Gennes [93].

By changing the chiral moiety associated with the liquid crystal units, the physical properties of the supermolecular system can be changed and/or fine-tuned. For example, changing the chiral group from 2-methylbutyl to

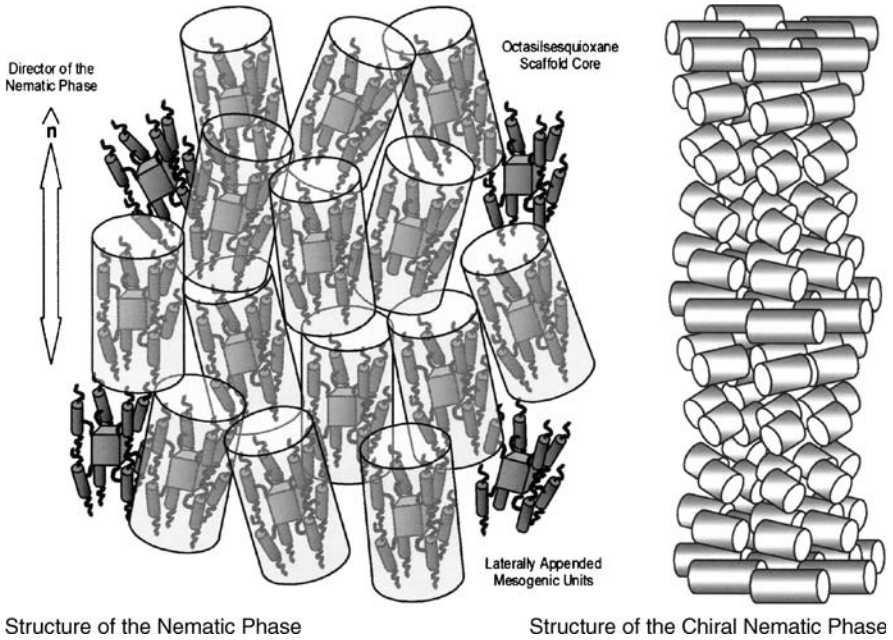

Fig. 44 Schematic representation of the local nematic structure and the helical structure of the chiral nematic phase of dendrimer **R**

2-octyl, as for polypede **42** (M_W = 6889) in comparison to **41**, the glass to chiral nematic phase transition is lowered to a value below room temperature, and similarly the clearing point is substantially reduced. However, the chiral nematic phase still exists over a temperature range of approximately 60 °C, which is quite remarkable considering that the low molar mass equivalents melt above 70 °C, thus supermolecular systems provide access to liquid crystal phases over much wider temperature ranges than the low-molar-mass equivalents [92].

The pitch of the helix for compound **42** was found to be approximately 0.2–0.3 μm, thus the material selectively reflects visible light over a wide temperature range. Moreover, the pitch is relatively temperature insensitive thus the material can be used in large area non-absorbing polarizers, or in optical notch filters or reflectors. In addition, in the glassy state the helical macrostructure of the chiral nematic phases is retained, thus similar applications are possible.

As with the terminally appended system **39**, dendritic growth of the octasilsesquioxane core allows twice the number of mesogenic units be bound to the central scaffold. Thus, the first generation octasilsesquioxane dendrimer **43**, see Fig. 46, which is the size of a small protein (M_W = 14653) possessing 16 side-on attached mesogenic units, was reported [94]. After purification of this material it was found to be monodisperse by Maldi-*tof*

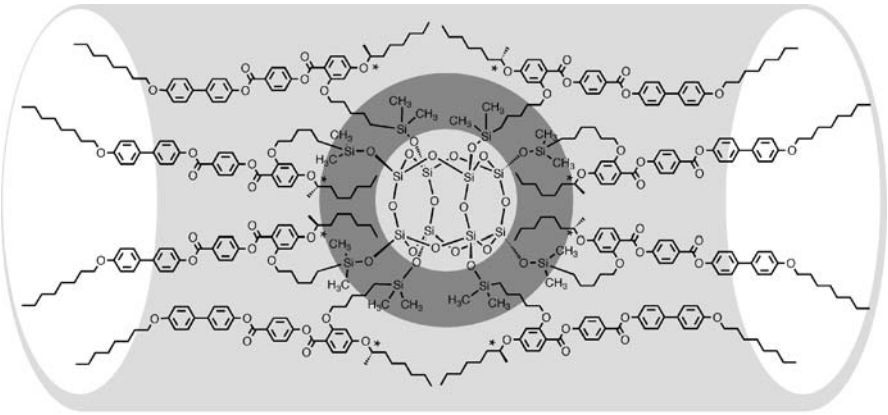

g 11.2 N* 72.0 °C Iso Liq **42**

Fig. 45 Supermolecular material **42** which has a relatively short pitch in the chiral nematic phase

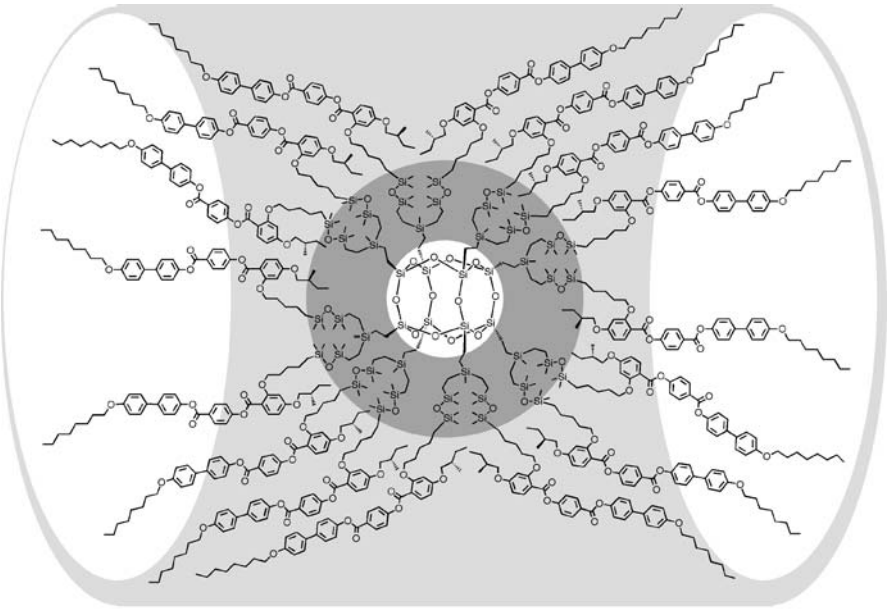

g 5.4 Col*$_{rd}$ 30 Col*$_{hd}$ 102.3 N* 107.7 °C Iso Liq **43**

Fig. 46 Supermolecular hexadecamer **43**, with 16 laterally appended mesogens

spectrometry, size exclusion chromatography and ^{29}Si NMR spectroscopy, see Fig. 47 for the NMR spectrum.

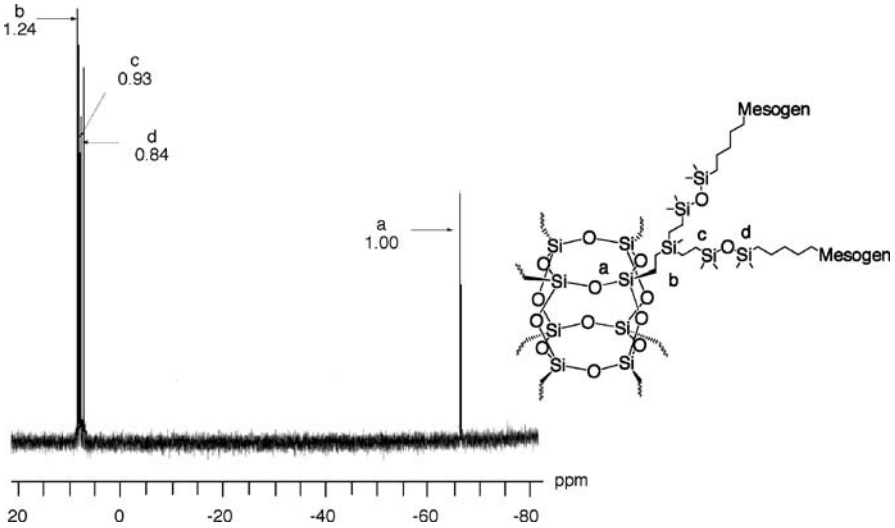

Fig. 47 The ^{29}Si NMR spectrum of supermolecule **43** showing the resonances for four identifiable silicon atoms

Compound **43** was found to exhibit a chiral nematic phase (see the texture in Fig. 48), hexagonal disordered columnar (see Fig. 49) and rectangular disordered columnar phases, in the sequence g 5.4 Col^*_{rd} 30 Col^*_{hd} 102.3 N* 107.7 °C Iso Liq [94]. Thus the increase in the number density of the mesogens bound to the central scaffold transforms the situation from the octamers **41** and **42**, which exhibit calamitic phases, to one where the hexadecamer **43** exhibits columnar phases. However, the formation of columnar phases when the dendrimer possesses rod-like mesogenic groups is not easy to vi-

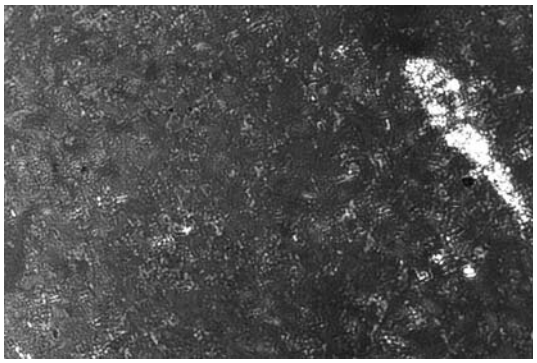

Fig. 48 The Grandjean plane texture of the chiral nematic phase of supermolecule **43**. There is a blue iridescent color which is due to the selective reflection of light from the helical macrostructure (×100)

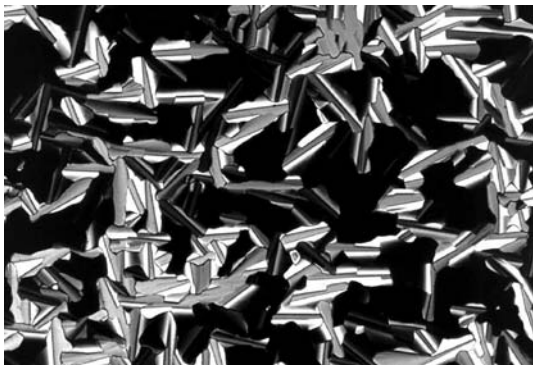

Fig. 49 The homeotropic and rectilinear defect textures of the hexagonal columnar phase of supermolecule **43** (×100)

sualize unless the mesogenic groups surround the octasilsesquioxane core to give a cotton-reel-like structure. From the point of view of the mesophase structure, the best fit to the X-ray data was obtained using such a "cotton-reel" model, see Fig. 50, which suggests that in the hexagonal columnar phase the dendrimer assumes a cylindrical shape that has approximately the same height as its diameter. The long axes of the mesogenic units are roughly par-

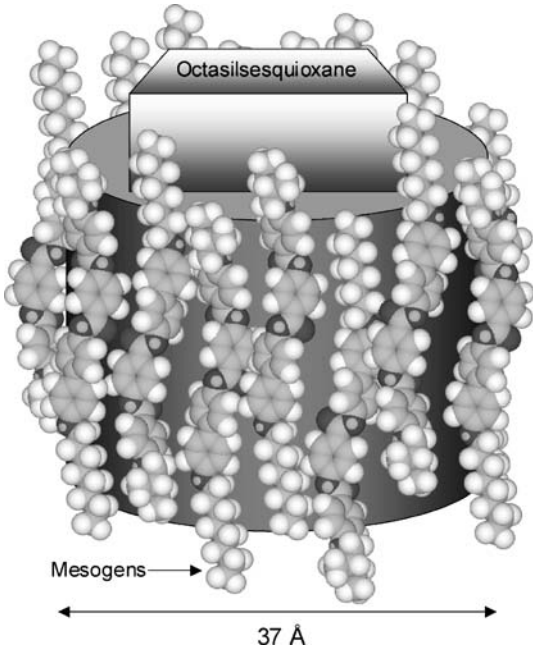

Fig. 50 Cotton-reel model of supermolecular material **43**

allel to or slightly tilted with respect to the rotational axis that is normal to the cylinder, i.e., they are nematic-like, and they are packed together side by side on the outer surface of the cylinder, in a disordered fashion, as shown in Fig. 51.

The mesogenic behavior of **43** emphasizes the role played by the octasilsesquioxane core when comparing with the related side-chain liquid-crystalline polysiloxanes [95, 96]. It is remarkable that the thermal stability of the chiral nematic phase is similar in both the polymer and the dendrimer, suggesting that the cubic core does not perturb significantly the associations between the mesogens necessary to support the chiral nematic phase.

Similarly, the formation of the columnar phases for dendrimer **43**, but not in the side-chain polysiloxanes, indicates that the silsesquioxane core assists in the interaction of neighboring units resulting in the formation of the hexagonal and rectangular columnar disordered structures, presumably through segregation of the siloxane cores from the mesogenic units in distinct columns. These remarkable new mesophase structures, which are essentially variations of "tubular nematic-columnar phases", are favored by the spacer length used to attach the mesogen to the dendrimer core, since it has been kept relatively short (five methylene units) in order to prevent full decoupling of the mesogenic motions from the silsesquioxane core and

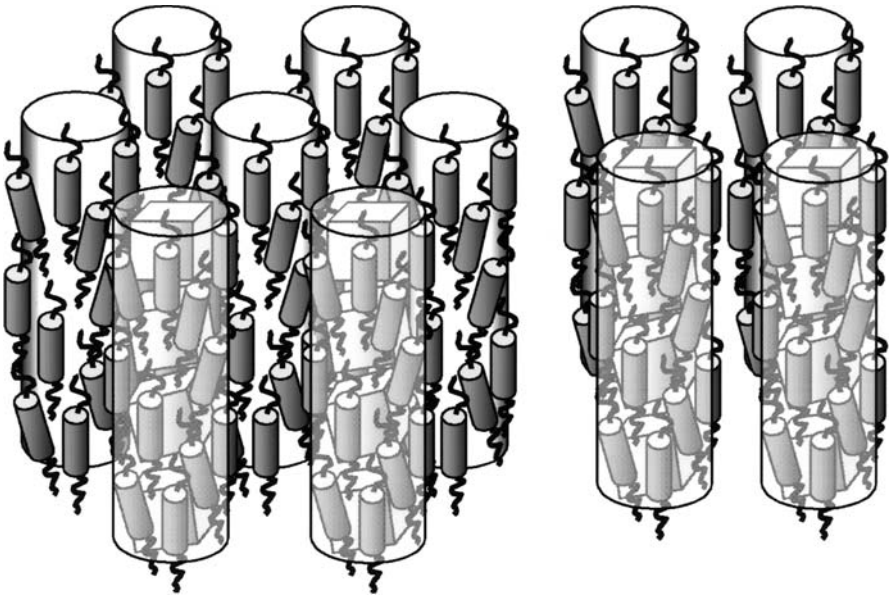

Fig. 51 Schematic structures of the hexagonal tubular nematic and rectangular tubular nematic phases. The mesogenic groups are roughly parallel to the columns but their positions are disordered. Thus the columns effectively act as the directors of the nematic phase

by forcing the mesogens to pack closely together around the dendritic core. The structures of the "hexagonal tubular nematic-columnar" and "rectangular tubular nematic-columnar" phases are shown schematically together in Fig. 51.

The hybrid structures of such "tubular nematic-columnar liquid crystal phases" lend themselves as potential model systems for the development of photonic band-gap materials, where large difference in refractive indices between the inorganic and organic sections can be engineered into the system through design and synthesis. In addition, the chiral nematic phase of the hexadecamer shows the selective reflection of blue light indicating that the pitch of the chiral nematic phase is sub-micron, approximately 0.2 to 0.3 μm.

By swapping the position of the chiral group of the mesogen with the linking group to the central scaffold, polypede **44**, see Fig. 52, is created where the mesogens are attached end-on. As predicted, the material does not exhibit columnar phases, but instead reverts to calamitic phases, with chiral nematic and chiral smectic C* phases being found. In terms of material properties, the nematic phase of the supermolecule possesses a helical macrostructure and therefore reflects light. The chiral smectic C* phase is ferroelectric as was shown by electrical field studies, however, the polarization was not determined because of the slowness of the response of the material.

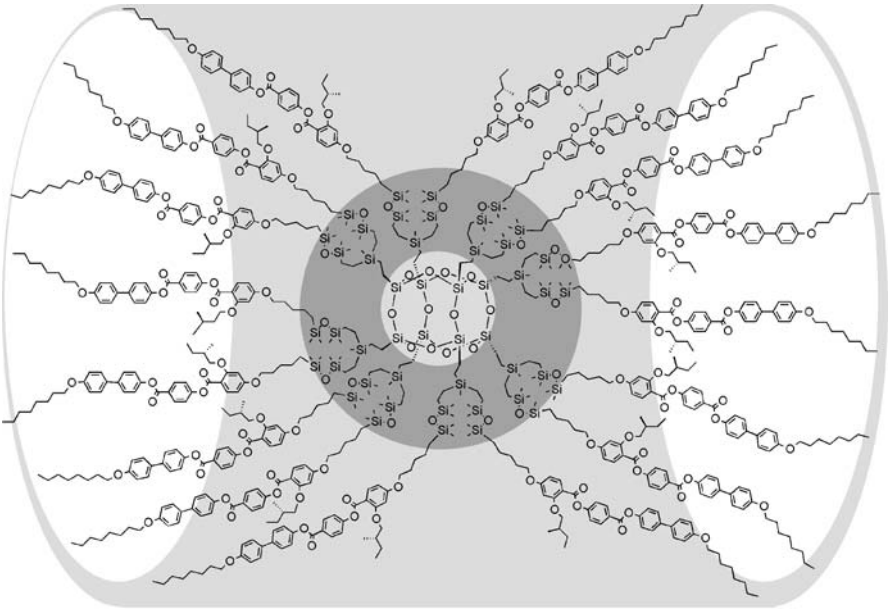

Cryst 133 SmC* 162.3 N* 165.3 °C Iso Liq **44**

Fig. 52 Hexadecamer supermolecule **44**

2.6
Effect of Hard Core Scaffolds – Fullerene

Apart from employing octasilsesquioxane as the central scaffold, other rigid cage structures can be used as the central building block, for example [60]fullerene. The hexa-adducts of [60]fullerene can give a spherical distribution of mesogenic substituents about the central scaffold, and thus these types of supermolecular material have similar topologies to those of the octa- and hexa-substituted silsesquioxane. Not surprisingly, therefore the fullero-dendrimers exhibit similar mesophase behavior to the silsesquioxane dendrimers. For example, compound **45**, shown in Fig. 53 [76] is similar in topology to supermolecule **43** shown in Fig. 40. Material **45** exhibits a relatively high glass-transition temperature, 80 °C, followed by a transition to a smectic A phase. No other liquid crystal phase is observed and the liquid crystal state collapses to the liquid at 133 °C. The octasilsesquioxane, **43**, exhibits the following phase sequence and transition temperatures; g –17.5 SmC 63.1 SmA_1 91.7 °C Iso Liq. Thus it can be seen that the lower glass transition reveals the presence of smectic polymorphism. Often because of higher glass transition temperatures or melting points, fullero-dendrimers with terminally appended mesogens tend not to exhibit smectic C phases.

Terminally appended chiral mesogens have also been investigated through the deployment of cholesteryl substituents [97]. For example, material **46** has been prepared and shown to exhibit a smectic A phase, thus it has properties

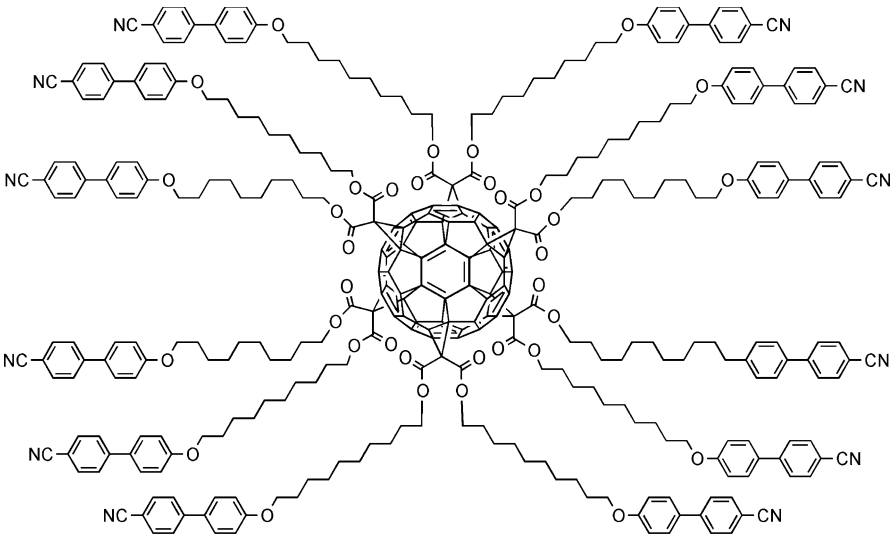

g 80 SmA 133 °C Iso Liq **45**

Fig. 53 Supermolecular fullero-dendrimer **45**

similar to that of material **45**. The clearing point is relatively high; however, due to the inclusion of chiral groups, the glass transition is low. The wider temperature range for liquid crystal properties to be observed, however, does not reveal any other phases than smectic A.

2.7 Effect of Hard Core Scaffolds – Molecular "Boojums"

The incorporation of lateral mesogenic substituents onto a [60]fullero-scaffold, particularly chiral mesogens, can lead to interesting structural behavior and properties. For example, supermolecular material **47**, shown in Fig. 55, has a structure that utilizes the same laterally appended mesogens as in material **43** shown in Fig. 46, but this time attached to a [60]fullerene (C_{60}) central core unit [98]. Through bifurcation, 12 mesogenic units were symmetrically positioned about the C_{60} core, thereby creating a spherical architecture. Again, because of the lateral attachment of the mesogenic units, a chiral nematic phase is exhibited by this material. The material forms a glass at 47 °C, and upon heating a chiral nematic phase is stable up to 103 °C. Unlike compound **43**, however, for **47** no columnar phases were observed, thereby strengthening the view that [60]fullerene suppresses mesophase polymorphism.

The mesophase defect textures exhibited by **47** were typical of those normally found for a chiral nematic phase, except they were only revealed upon annealing, which is probably a function of the viscosity of the material. Thus the sample was annealed just below the clearing point. After 24 h, large areas of the preparation evolved to show fingerprint defects and the Grandjean plane

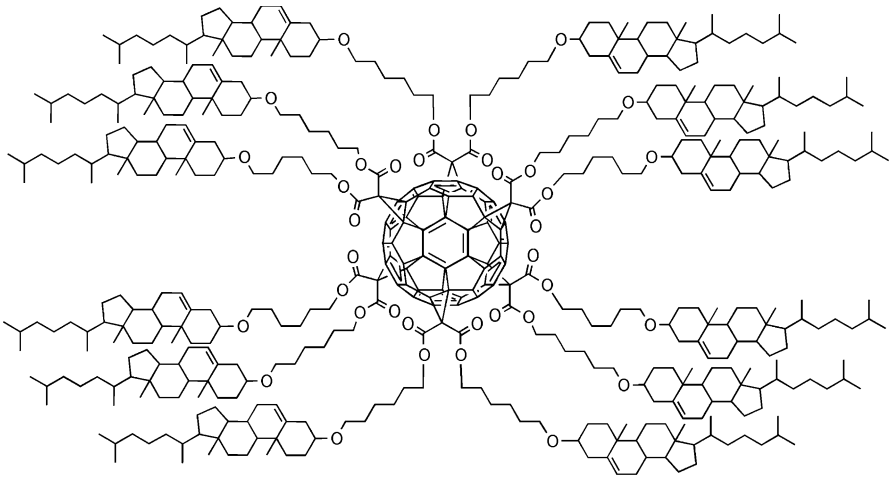

g Room Temperature SmA 165 °C Iso Liq **46**

Fig. 54 Chiral supermolecular fullero-dendrimer **46**

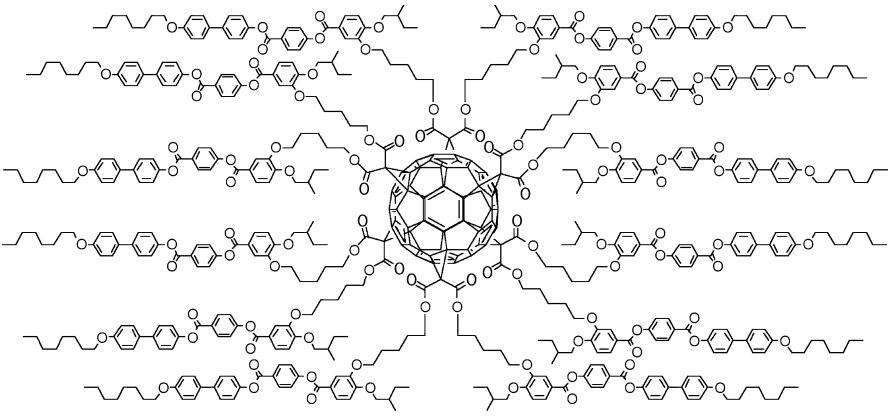

g 47 N* 103 °C Iso Liq **47**

Fig. 55 Supermolecular material **47** which possesses a "boojum-like" structure and exhibits a chiral nematic phase

texture (see Fig. 56). From the Grandjean plane texture, the twist sense of the helical structure was found to be left-handed. The pitch was determined by measuring the number of pitch bands per unit length from the fingerprint texture. A value of 2.0 μm for the pitch length was obtained at room temperature. The value was found to be similar to those of the chiral mesogen unit (1.7 μm) and the malonate precursor (1.9 μm). Thus the fullerene moiety is shielded very effectively among the laterally attached mesogens, without disturbing the helical supramolecular organization of the mesophase. Furthermore, as the mesogenic units are symmetrically distributed all over the fullerene sphere they effectively isolate it, thereby decreasing the possibility of aggregation of the C_{60} units, which is detrimental to mesophase formation.

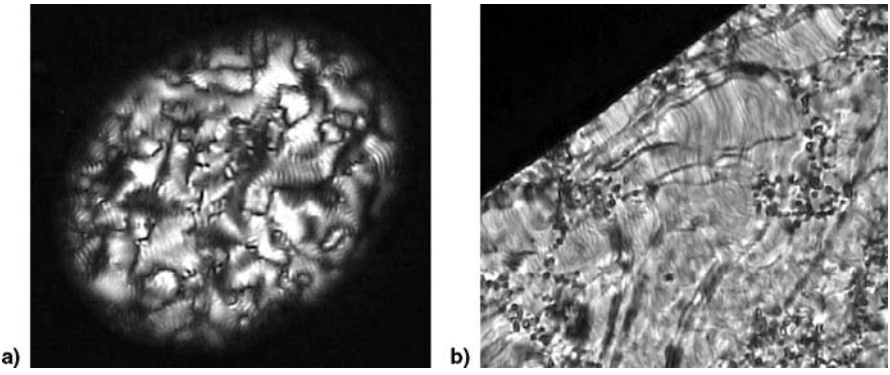

Fig. 56 **a** fingerprint texture for an uncovered droplet of compound **47**, and **b** the Grandjean texture of the chiral nematic phase

It is also interesting to consider how the selection process for the helical organization of material **47** is generated upon cooling from the isotropic liquid. As the C_{60} core of the material is spherical, and the mesogenic units are attached by relatively short methylene spacer units, it is not unreasonable to assume that, in the liquid phase, the mesogenic units are symmetrically disposed about the central core. Cooling into the chiral nematic phase, however, the helical organization was be expected to be a result of the organized packing of the dendritic supermolecules, i.e., they are considered to be no longer spherical in shape. However, it was found that when the diameter of the C_{60} core is compared to the length of the mesogenic units, it is clear that flexible, random packing of the mesogenic units about the core in the liquid crystal state was not possible, and that the mesogens are required to be organized in their packing arrangements relative to one another, both on the surface of the dendrimer and between individual dendrimer molecules. One possibility was postulated where the mesogenic units are oriented parallel to one another, thus when the material cools into the liquid-crystalline phase directional order of the mesogens is selected by the external environment, such as the surface. In doing so, this information is transmitted to the other mesogens associated with the spherical dendrimer and further to the neighboring dendritic supermolecular compounds. Alternatively, for an individual dendrimer it was proposed that the direction of the mesogens would spiral around the C_{60} core to give poles at the top and bottom of the structure, as shown in Fig. 57. Thus the spherical dendrimer was projected to have a well-defined chiral surface, thereby resulting in the creation of a chiral nanoparticle, i.e., a molecular "*Boojum*". When the chiral nanoparticles pack together they were expected to do so through chiral surface recognition processes, resulting in the formation of a helical supramolecular structure. Consequently, the chiral supermolecular nanoparticles transmit their local organization through

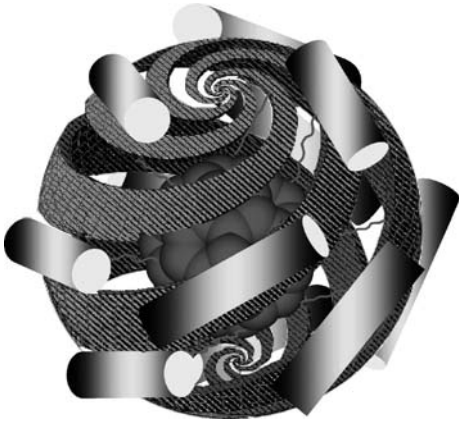

Fig. 57 Proposed helical structure of a molecular "Boojum"

amplification to adjacent molecules resulting in values of the helical twisting power that are higher and the pitch shorter than might be expected for such large molecular entities.

3 Multipedes

As noted in the introduction, multipedes are essentially a step away from polymer and dendritic systems towards the complex super- and supramolecular materials found in living organisms, where materials with selective functional properties are incorporated into self-assembling and/or self-organizing states of matter. If we consider firstly the two polypedes **48** and **49**, tetramer **48** has four laterally appended chiral mesogenic groups and therefore exhibits a chiral nematic phase as expected. Similarly, tetramer **49**, which has terminally appended cyanobiphenyl mesogenic groups, exhibits a smectic phase as expected, see Fig. 58.

Replacement of one of the mesogenic groups in either of the tetramers by a mesogenic group from the other tetramer results in two new supermolecules **50** and **51**, see Fig. 59 [99]. These materials are no longer tetramers, but are molecules in their own right with discrete structures. The introduc-

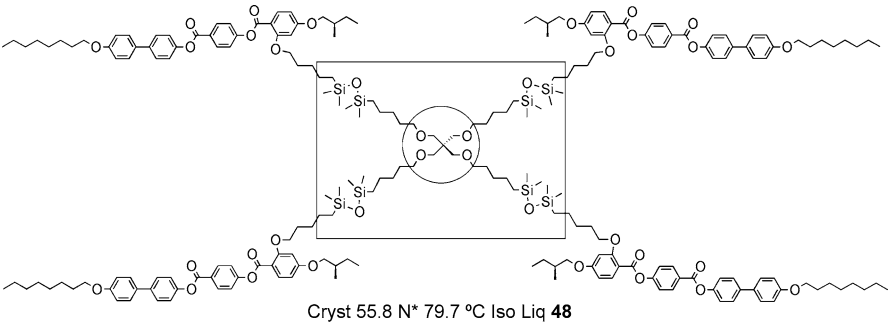

Fig. 58 Comparison of liquid-crystalline tetramers possessing laterally, **48**, and terminally appended, **49**, mesogens

tion of a terminally appended mesogen into a supermolecule which has predominantly laterally appended mesogens in the periphery, as for **50**, results in a lowering of the relative melting point, but the mesomorphic properties remain nematic, which is expected as the terminally appended mesogen serves to increase the disordering in the system.

However, when a laterally appended mesogen is introduced into a system where all of the other mesogens are terminally appended, as for **51**, the laterally appended mesogen acts as a disruptor to the orderly packing of the molecules together. This results in the suppression of the formation of smectic modifications and support for nematic phases. Thus compound **49**, which

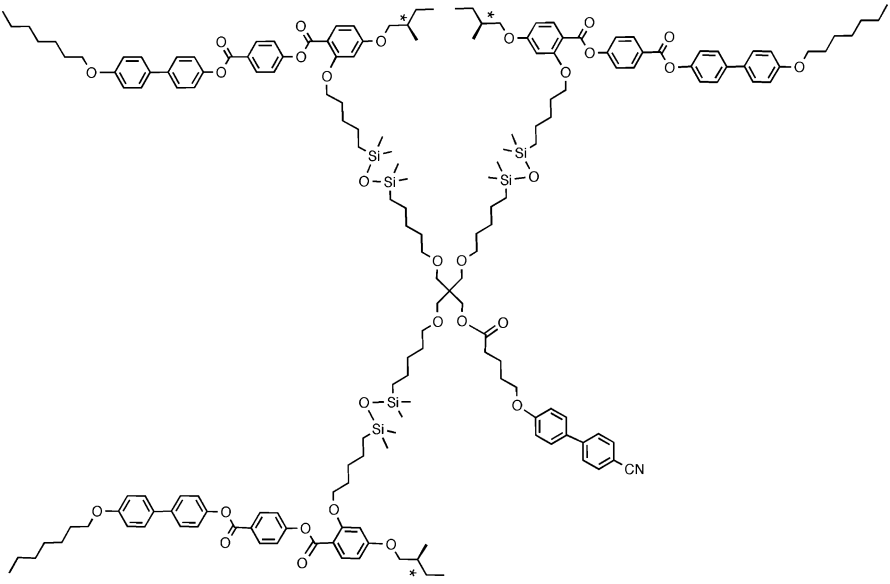

Cryst 36.2 N* 58.8 °C Iso Liq **50**

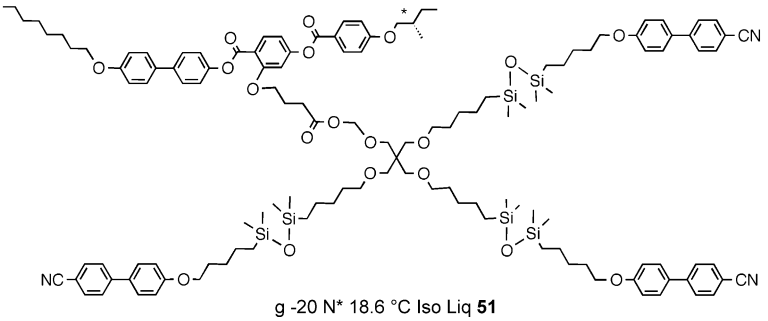

g -20 N* 18.6 °C Iso Liq **51**

Fig. 59 Comparison of liquid-crystalline multipedes possessing mixed laterally, **50**, and terminally appended, **51**, mesogens

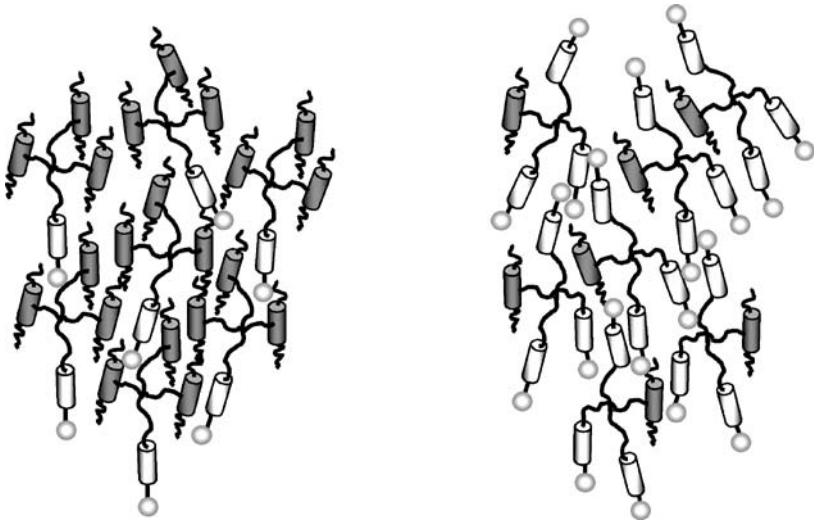

Fig. 60 Schematic representation of the nematic phases formed by multipedes **50** and **51** which have mixed lateral and terminal mesogenic groups

is smectic A, is converted into a chiral nematic phase, see **52**. A comparison of the nematic structures of **50** and **51** is shown in Fig. 60.

Interestingly, material **51** has a nematic phase at room temperature, with a glassification point at –20 °C. In comparison 4-pentyl-4′-cyanobiphenyl has a melting point of 24 °C and a clearing point of 34 °C. Furthermore, mechanical shearing of specimens of the nematogenic materials **50** and **51** show that the samples have low viscosity, indicating that the materials have rheological properties similar to those of low-molar-mass mesogens.

Fine tuning of material properties therefore can be achieved by using mixtures of mesogens attached to the periphery of the scaffold. In addition, the disordering induced can substantially lower melting points and widen temperature ranges of desirable liquid crystal phases. Furthermore, such materials are miscible with low-molar-mass materials, and can be used to modify their physical properties.

3.1
"Janus" Liquid-Crystalline Multipedes

One of the more intriguing and challenging aspects in materials science is understanding the molecular recognition and self-assembling processes in materials with diversely functionalized faces or sides, which can yield supramolecular objects that may recognize and select left from right, or top from bottom, as described by de Gennes [93]. For example, Janus grains [100], block co-polymers in the form of Janus micelles [101], segregated amphiphilic den-

drimers [102–105], shape-persistent macromolecules [106], and polar colloidal particles [107] are abiotic examples of such materials that self-organize, like proteins, in a pre-programmed fashion.

A recent molecular design, "Janus" liquid-crystalline molecular materials in the form of segmented structures that contain two different types of mesogenic units has recently been reported [108, 109]. Janus materials favor different types of mesophase structure, grafted onto the same scaffold, to create giant molecules that contain different hemispheres ("Janus" refers to materials with two faces, such as fluorocarbon/hydrocarbon or hydrophilic/hydrophobic, etc., for example Janus amphiphilic dendrimers have been reported [110–114]).

The complementary materials **52** and **53**, based on a central scaffold made up of pentaerythritol and tris(hydroxymethyl)aminomethane units linked together, where one unit carries three cyanobiphenyl (CB) (smectic preferring), see Fig. 61, and the other three chiral phenyl benzoate (PB) (chiral nematic preferring) mesogenic moieties, see Fig. 62, or *vice-versa* were investigated [115], see Fig. 63.

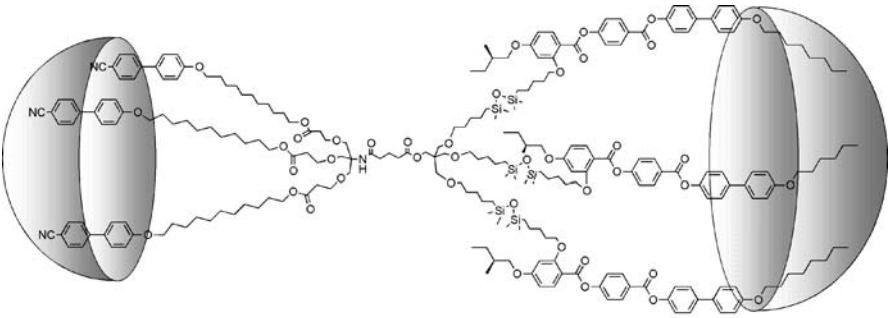

Fig. 61 Janus liquid crystal **52**

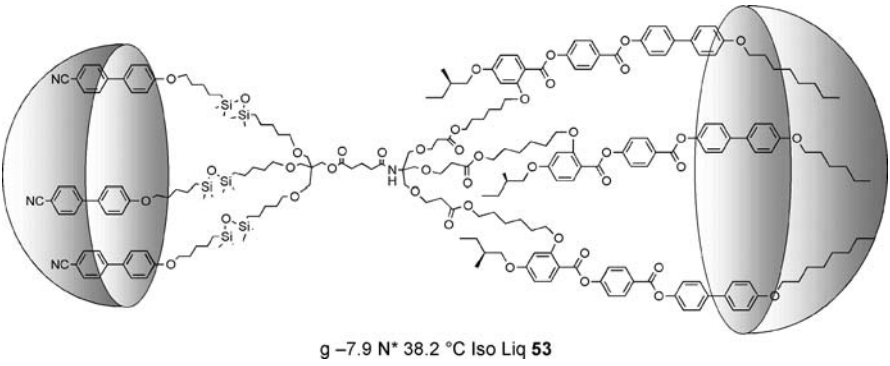

Fig. 62 Janus liquid crystal **53**

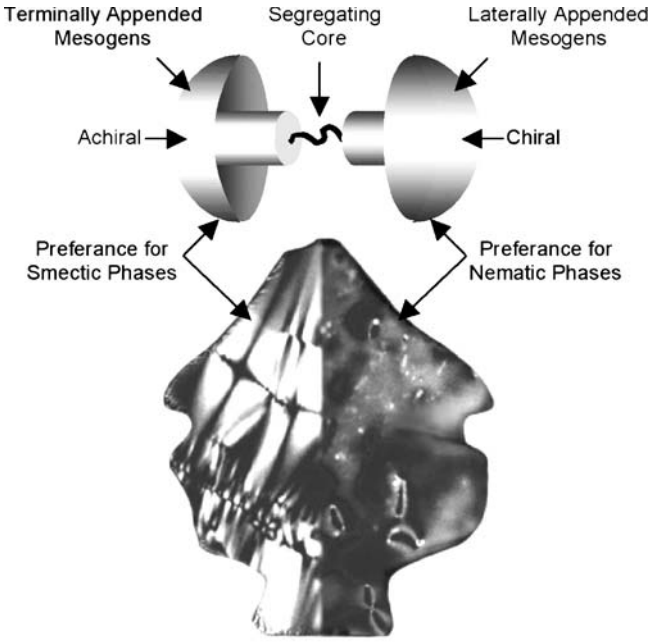

Fig. 63 Conceptual design of Janus liquid-crystalline supermolecular systems, where the Janus head is composed of a nematic liquid crystal (*right*) and a smectic liquid crystal *left*

Both Janus compounds, **52** and **53**, were isolated as single compounds in a glassy state at room temperature. The predicted and experimental isotopic distribution for the mass ion overlay each other identically confirming the purity of the material and demonstrating the utility of Maldi-*tof* in the determination of structure in supermolecular systems.

On heating **52**, a broad melting endotherm with onset at 33.8 °C (ΔH = 6.26 kJ mol^{-1}) was followed by a transition from the liquid crystal state to the liquid at 60.8 °C (ΔH = 2.73 kJ mol^{-1}). The cooling cycle from the isotropic liquid showed a broad, weak exotherm, onset at 60.3 °C, marking the transition to the chiral nematic phase. A second exotherm occurred on cooling, onset 36.1 °C, marking a second-order transition to a chiral smectic C* phase. Further cooling induced a glass transition at approximately –2.8 °C. This sequence of events was reproducible in subsequent heating and cooling cycles. It is noteworthy that the transitions have extremely low ΔH values, suggesting that the system is relatively disordered and highly flexible. In addition, it is important to note that the formation of chiral mesophases by compound **52** means that the nematic phase is thermochromic and the smectic C* phase is ferroelectric and pyroelectric and will exhibit electrostrictive properties.

In contrast, compound **53** exhibits only one enantiotropic transition by DSC, which occurs between a chiral nematic phase and the isotropic liquid, in

the form of a weak and broad peak at 38.2 °C (ΔH = 0.87 kJ mol^{-1}). The only other thermal event present was a glass transition below room temperature at –7.9 °C. Only when the sample was left standing at room temperature for 3 weeks did a broad, strong endotherm with onset at 31.6 °C with a shoulder at 42.6 °C occur. However, these thermal events were not present in successive heating and cooling cycles, suggesting that crystallization only occurs on standing after a long period of time.

Comparison of the phase behavior of compounds **52** and **53** shows clearly that the overall topology of the molecule in respect to the inner core (i.e., which hemisphere carries what mesogen) plays a significant role in determining the type of mesophase formed, since in both cases the number of mesogens of each type and the core are the same and simply by placing them in different hemispheres changes the mesophase exhibited.

The manipulation of the structural fragments (mesogenic units, central scaffold, and linking units) in the molecular design of such supermolecular systems potentially allows one to vary mesophase type and therefore the physical properties and potential applications of materials. Thus the molecular design of these systems is flexible and potentially capable of incorporating functional units, thereby allowing us to take some steps towards the molecular and functional complexity found in living systems.

3.2
Functional Liquid-Crystalline Supermolecules

The concept of creating functional materials by incorporating a certain functionality within a liquid-crystalline molecule, through covalent attachment, is a bottom-up approach to self-organizing functional materials. In the following examples, fullerene is incorporated as the functional unit into self-organizing supermolecular systems. Fullerene is of interest because of its unusual physical properties, and it is fascinating to see if such a large non-mesogenic unit affects mesomorphic behavior. Moreover, the synthesis of fullerene-containing liquid crystals is expected to open new avenues in the design of self-organized structures containing the fullerene unit [116–122]. This approach to self-organization appears to be particularly interesting for other functional groups which are not well adapted to being organized in nanoscale architectures.

The first set of examples described are those which examine the proportion of mesomorphic groups that are required in the structure of a supermolecule for it to be mesogenic, and secondly to investigate the incorporation of second functional group in the system which might contribute to the activity of the fullerene unit, see Fig. 64. The parent multipede **54** [123] exhibits a smectic A phase with a clearing point of 168 °C, the functional material **55** clears at 171 °C, and similarly functional multipede **56** clears at 169 °C [124]. All three materials also exhibit glassy states with transitions to the smectic A phase at

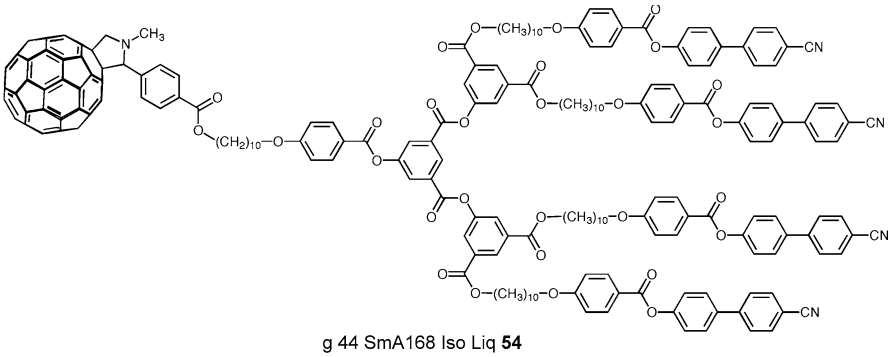

g 44 SmA168 Iso Liq **54**

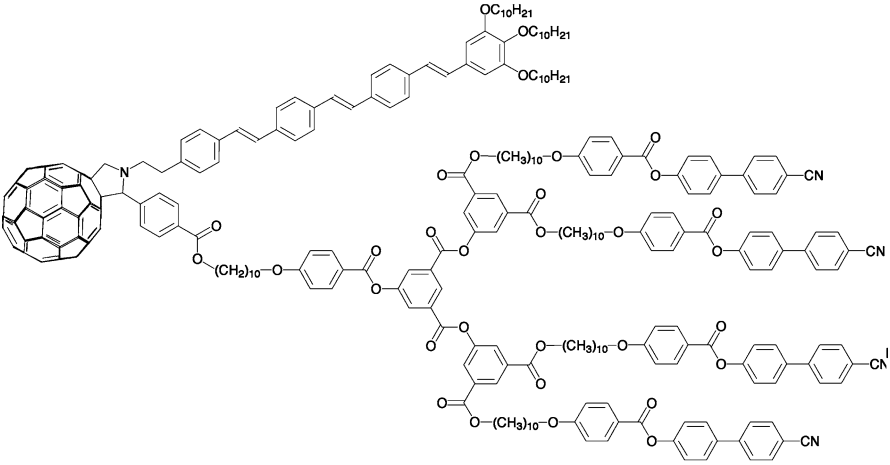

g 50 SmA171 Iso Liq **55**

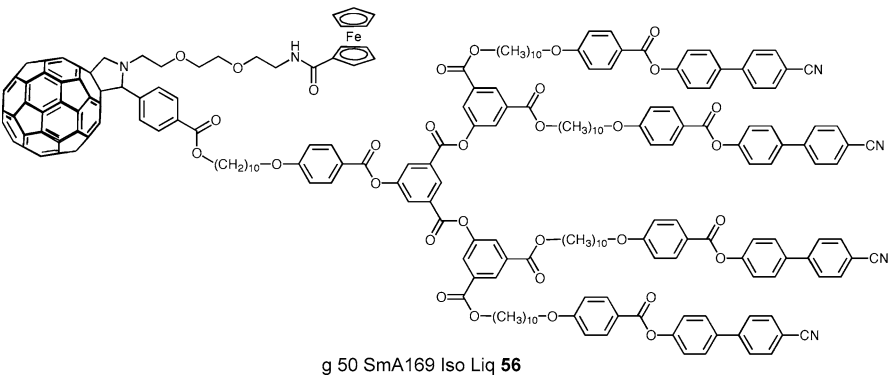

g 50 SmA169 Iso Liq **56**

Fig. 64 Comparison of the transition temperatures of functional supermolecular systems that demonstrate that mesogenic groups can be used to control their self-organization

very similar temperatures. The structural difference between the three arise from the incorporation of a π-conducting group (**55**), or a ferrocenyl group (**56**) attached to the C_{60} core unit. The three materials differ greatly in structure, however, the liquid crystal properties are almost invariant with structure. These results indicate that the self-organizing properties of the three materials are dominated by the mesogenic dendron which is attached to the C_{60} unit, and that the non-mesogenic parts of each material have little or no effect. These accumulative results demonstrate that the incorporation of mesogenic units into a supermolecular structure can be utilized in the self-organization and self-

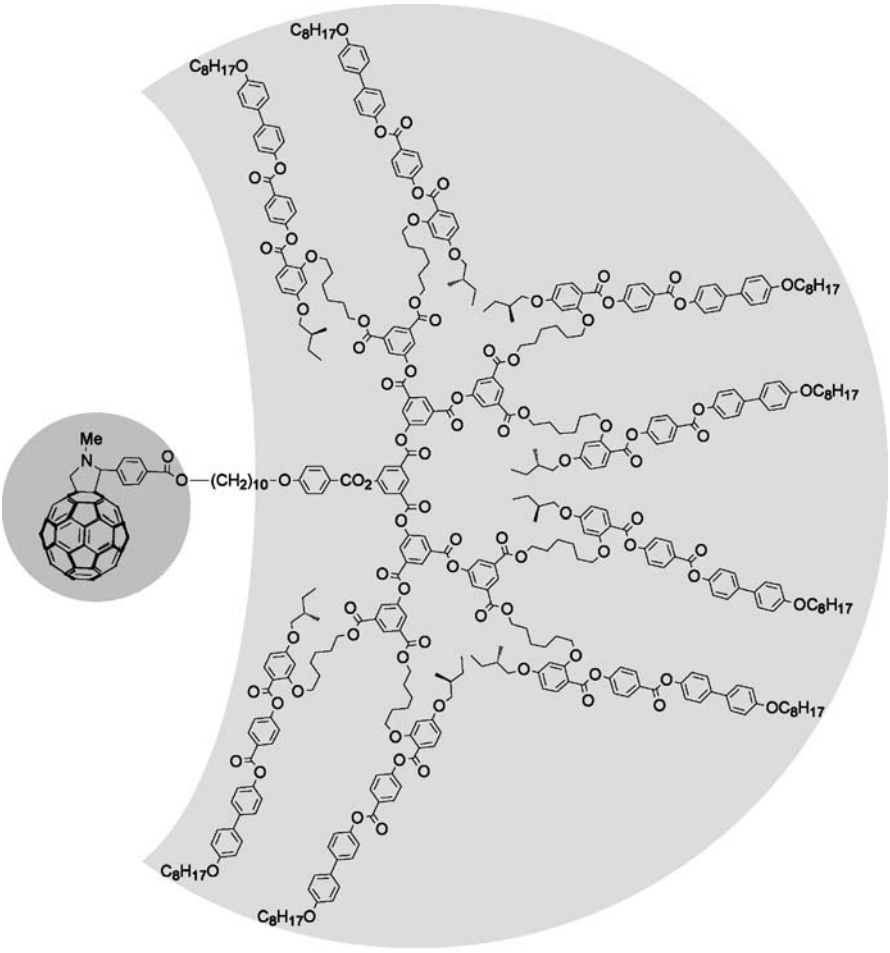

K 50.5 M 66.9 Iso °C (M = Unidentified mesophase) **57**

Fig. 65 Functional fullero-supermolecule **57**

assembly properties, while at the same time retaining the functionality of the supermolecule. These are properties not unlike those of a protein.

In the examples given in Fig. 64, the mesomorphic groups used for the self-organization process are cyanobiphenyls. As with many of the other examples used previously in this article, lateral substitution of the mesogens can be used to control the self-organization process to yield nematic phases. The fist example given is for supermolecular material **57**, as shown in Fig. 65. Although this material demonstrates that liquid crystal properties can be obtained when a dendron is attached to a fullerene unit which is exposed on one side of the resulting supermolecule, it nevertheless does not exhibit a nematic phase, but instead an hitherto unidentified more ordered phase.

The exposure of the fullerene unit is shown in Fig. 66. The mesogenic groups cluster together as they stabilize an ensemble that would support the formation of a liquid crystal phase. The exposed fullerene is then free to interact with other fullerenes, thereby potentially stabilizing the formation of a lamellar phase.

Nematic phases can be induced to form, however, by bifurcation at the surface of the fullerene unit and the incorporation of mesogens that are laterally attached. For example fullerene multipede **58**, see Fig. 67, shows an enantiotropic chiral nematic phase, with a phase sequence of g 26 N* 69 °C Iso Liq, which is useful for applications. The values of the pitch of the helix of the chiral nematic phase obtained indicate that C_{60} fits within the helical structure formed by the mesogens themselves without causing any significant perturbation of the pitch, see Fig. 68. This, in turn, implies that although the large C_{60} unit disturbs the mesogenic interactions, therefore lowering the clearing point, it can be effectively camouflaged within the self-organizing chiral ne-

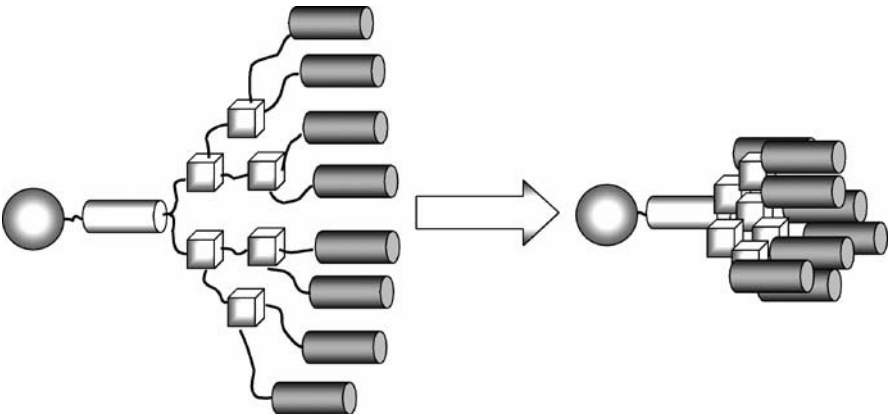

Fig. 66 Clustering of the mesogenic groups together in order to support the formation of a lamellar phase, thereby leaving the fullerene unit exposed and free to interact with other fullerene units

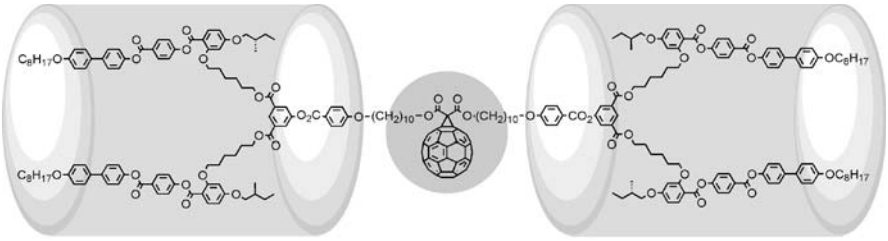

g 26 N* 69 °C Iso Liq **58**

Fig. 67 A chiral nematic fullero-multipede, **58**

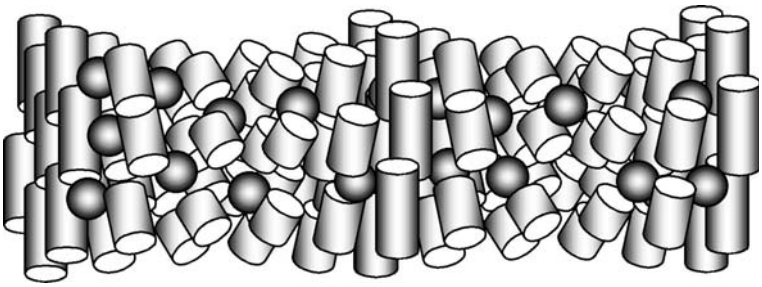

Fig. 68 The helical structure of the chiral nematic phase of a fullero-multipede. The C_{60} units are shown as spheres dispersed within the helical structure of the cylindrical array of mesogenic units

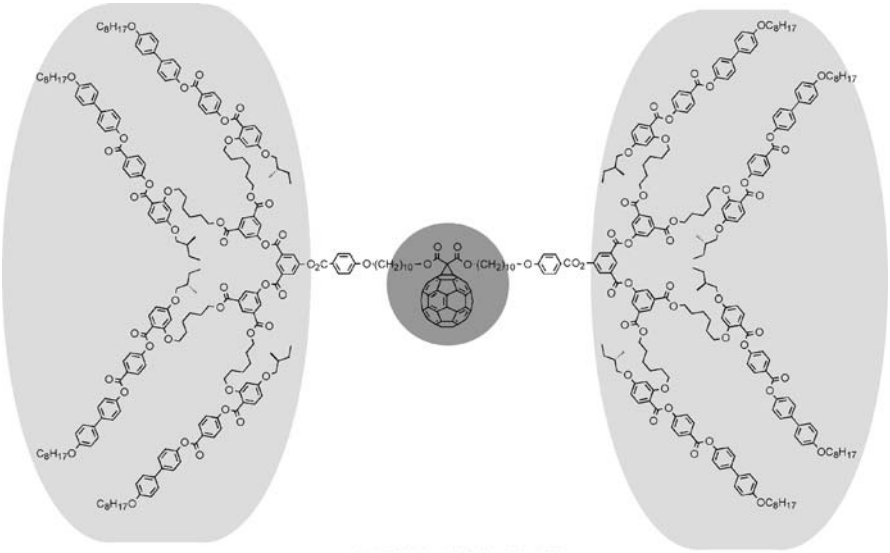

g 24.3 N* 80.6 °C Iso Liq **59**

Fig. 69 A chiral nematic fullero-multipede, **59**

matic medium, provided that enough mesogenic sub-units are available in the dendritic addend, without markedly suppressing the liquid-crystalline state.

When the number density of the mesogens is increased, thereby reducing the weight fraction of fullerene units in the supermolecular structure, see **59** in Fig. 69, the liquid crystal phases become increasingly more stable and the spherical fullerene unit becomes increasingly hidden within the liquid crystal matrix [125]. This result indicates that the liquid crystal units have the ability to incorporate and organize non-mesogenic functional units into the self-organizing state, without too much detriment to the liquid crystal itself.

Thus, we can apparently control the periodic ordering of non-mesogenic functional units through the process of self-organization. Similar approaches recently have been taken by Sakai and Matile [126] and Zhuravel et al. [127], but in both of these cases, amino acids were used to induce self-assembly, and ultimately self-organization.

3.3
Complex Functional Multipedes

Current research by Kato, Stoddart and Sauvage has demonstrated how the self-organization properties of liquid crystals can be used in the self-assembling of functional systems to give an oriented and organized bulk material [128, 129]. Figure 70 shows a novel system, **60**, where the properties of liquid crystals have been combined with that of rotaxanes to create a self-organizing molecular switch [128]. This material self-organizes to give a smectic A phase, which has a temperature range from 7 to 146 °C. Bistable switching was observed through examination of the electrochemical response which was characterized by cyclic voltammetry.

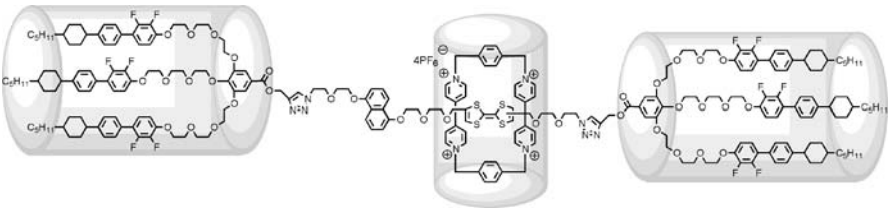

Fig. 70 A self-organizing rotaxane system, **60**, which forms a smectic A phase

4
Summary

In this brief review, we have demonstrated the potential for creating a wide variety of novel supermolecular materials with designer structural and functional properties. In our own development of new materials we have borne in

mind the philosophy and approach used by living systems in the creation of monodisperse and discrete supermolecular materials with specific functionality. In particular, the design features employed in the creation of proteins have been used in the creation of materials which do not bear any common atomistic relationship with proteins themselves. In this way, this new field lies open for the development of materials for which their design is only limited by human imagination.

Acknowledgements The authors are very grateful to The Leverhulme Trust, the European Science Foundation, ESF, and the Engineering and Physical Sciences Research Council, EPSRC, for financial support.

References

1. Lehn J-M (1995) Supramolecular Chemistry: Concepts and Perspectives. Wiley, Weinheim
2. Lehn J-M (2002) Science 295:2400
3. Whitesides GM, Grzybowski B (2002) Science 295:2418
4. Kato T (2002) Science 295:2414
5. Elemans JE, Rowan AE, Nolte RJM (2003) J Mater Chem 13:2661
6. Demus D, Goodby JW, Gray GW, Spiess H-W, Vill V (eds) (1998) Handbook of Liquid Crystals, vols 1–3. Wiley, Weinheim
7. Bunning TJ Kreuzer FH (1995) Trends Polym Sci 3:318
8. Goodby JW, Mehl GH, Saez IM, Tuffin RP, Mackenzie G, Auzely-Velty R, Benvegnu T, Plusquellec D (1998) Chem Commun, p 2057
9. Tschierske C (1998) J Mater Chem 8:1485
10. Goodby JW (1999) Curr Opin Solid State Mater Sci 4:361
11. Tschierske C (2002) Curr Opin Coll Interface Sci 7:69
12. Goodby JW (2002) Curr Opin Coll Interface Sci 7:326
13. Percec V, Bera TK, Glodde M, Fu Q, Balagurusamy VS, Heiney PA (2003) Chem Eur J 9:921
14. Ponomarenko SA, Boiko NI, Shibaev V (2001) Polym Sci Ser C 43:1
15. Percec V, Glodde M, Bera TK, Miura Y, Shiyanovskaya I, Singer KD, Balagurusamy VSK, Heiney PA, Schnell I, Rapp A, Spiess H-W, Hudson SD, Duank H (2002) Nature 419:384
16. Tomalia DA (2003) Nat Mater 2:711
17. Newkome GR, Moorefield CN, Vögtle F (2000) Dendrimers and Dendrons. Concepts, Syntheses, Applications. Wiley, Weinheim
18. Fréchet J-M (2003) J Polym Sci Part A: Polym Chem 41:3713
19. Grayson SM, Fréchet J-M (2001) Chem Rev 101:3819
20. Tully DC, Fréchet J-M (2001) Chem Commun, p 1229
21. Percec V, Holerca M (2000) Biomacromolecules 1:6
22. Syamakumari A, Schenning APHJ, Meijer EW (2002) Chem Eur J 8:3353
23. Precup-Blaga FS, Schenning APHJ, Meijer EW (2002) Macromolecules 36:565
24. Gehringer L, Guillon D, Donnio B (2003) Macromolecules 36:5593
25. Saez IM, Goodby JW (2005) J Mater Chem 15:26
26. Tschierske C (2001) J Mater Chem 11:2647
27. Kato T, Mizoshita N, Kishimoto K (2006) Angew Chem Int Ed 45:38

28. Emsley JW, Luckhurst GR, Shilstone GN, Sage I (1984) Mol Cryst Liq Cryst Lett 102:223
29. Imrie CT, Henderson PA (2007) Chem Soc Rev 36:2096
30. Praefcke K, Kohne B, Singer D, Demus D, Pelzl G, Diele S (1990) Liq Cryst 7:589
31. Hardouin F, Achard MF, Jin J-I, Shin J-W, Yun Y-K (1994) J Phys II (Paris) 4:627
32. Imrie CT, Luckhurst GR (1998) J Mater Chem 8:1339
33. Griffin AC, Sullivan SL, Hughes WE (1989) Liq Cryst 4:677
34. Nishiyama I, Yamamoto J, Goodby JW, Yokoyama H (2001) J Mater Chem 11:2690
35. Nishiyama I, Yamamoto J, Goodby JW, Yokoyama H (2002) J Mater Chem 12:1709
36. Nishiyama I, Yamamoto J, Goodby JW, Yokoyama H (2002) Liq Cryst 29:1409
37. Nishiyama I, Yamamoto J, Goodby JW, Yokoyama H (2002) Ferroelectrics 276:255
38. Nishiyama I, Yamamoto T, Yamamoto J, Goodby JW, Yokoyama H (2003) J Mater Chem 13:1868
39. Nishiyama I, Yamamoto J, Goodby JW, Yokoyama H (2003) J Mater Chem 13:2429
40. Nishiyama I, Yamamoto J, Yokoyama H, Goodby JW (2003) Mol Cryst Liq Cryst 400:21
41. Nishiyama I, Yamamoto J, Yokoyama H, Mery S, Guillon D, Goodby JW (2004) Trans Mats Res Soc Jpn 29:785
42. Nishiyama I, Yamamoto J, Goodby JW, Yokoyama H (2004) Chem Mater 16:3212
43. Nishiyama I, Yamamoto J, Goodby JW, Yokoyama H (2004) Liq Cryst 31:1495
44. Nishiyama I, Yamamoto J, Goodby JW, Yokoyama H (2004) Proc SPIE 5518:201
45. Nishiyama I, Yamamoto T, Yamamoto J, Yokoyama H, Goodby JW (2005) Mol Cryst Liq Cryst 439:1921
46. Goodby JW, Pindak R (1981) Mol Cryst Liq Cryst 75:233
47. Goodby JW (1981) Mol Cryst Liq Cryst Lett 72:95–99
48. Yelamaggad CV, Anitha Nagamani S, Hiremath US, Shankar Rao DS, Krishna Prasad S (2001) Liq Cryst 28:1581
49. Yelamaggad CV, Achalkumar AS, Rao DS, Prasad SK (2007) Org Lett 9:2641
50. Elsäßer R, Mehl GH, Goodby JW, Veith M (2001) Angew Chem Int Ed 40:2688
51. Elsäßer R, Mehl GH, Goodby JW, Veith M (2001) Phosphorus Sulfur Silicon Relat Elem 168:341
52. Elsäßer R, Mehl GH, Goodby JW, Rodriguez-Martin D, Richardson RM, Photinos DJ Veith M (2003) Mol Cryst Liq Cryst 402:237
53. Mehl GH, Elsäßer R, Goodby JW, Veith M (2001) Mol Cryst Liq Cryst 364:219
54. Newkome GR, Weiss CD, Moorfield CN, Weiss I (1997) Macromolecules 30:2300
55. Percec V, Cho WD, Ungar G, Yardley DJP (2001) J Am Chem Soc 123:1302
56. Zeng XB, Ungar G, Lin YS, Percec V, Dulcey SE, Hobbs JK (2004) Nature 428:157
57. Percec V, Mitchell CM, Cho WD, Uchida S, Glodde M, Ungar G, Zeng XB, Liu YS, Valagurusamy VSK, Heiney PA (2004) J Am Chem Soc 126:6078
58. Grimsdale AC, Müllen K (2005) Angew Chem Int Ed 44:5592
59. Clark CG, Wenzel RJ, Andreitchenko EV, Steffen W, Zenobi R, Müllen K (2007) J Am Chem Soc 129:3292
60. Hoeben FJM, Jonkheijm P, Meijer EW, Schenning PHJ (2005) Chem Rev 105:1491
61. Kato T (2002) Curr Opin Solid State Mater Sci 6:51
62. Donnio B, Buathong S, Bury I, Guillon D (2007) Chem Soc Rev 36:1495
63. Deschenaux R, Donnio B, Guillon D (2007) New J Chem 31:1064
64. Shibaev VP (2006) Liq Cryst 33:1497
65. Cammidge AN, King ASH (2006) Tetrahedron Lett 47:5569
66. Wilson MR (2005) Int Rev Phys Chem 24:421

67. Rueff JM, Barbera J, Marcos M, Omenat A, Martin-Rapun R, Donnio B, Guillon D, Serrano JL (2006) Chem Mater 18:249
68. Percec V, Holerca MN, Nummelin S, Morrison JL, Glodde M, Smidrkal J, Peterca M, Rosen BM, Uchida S, Balagurusamy VSK, Sienkowska MJ, Heiney PA (2006) Chem Eur J 12:6216
69. Percec V, Won BC, Peterca M, Heiney PA (2007) J Am Chem Soc 129:11265
70. Kaucher MS, Peterca M, Dulcey AE, Kim A, Vinogradov S, Hammer DA, Heiney PA, Percec V (2007) J Am Chem Soc 129:11698
71. Percec V, Kawasumi M (1992) Macromolecules 25:3843
72. Stebani U, Latterman G (1995) Adv Mater 7:578
73. Stebani U, Lattermann G, Wittenberg M, Wendorf J (1996) Angew Chem Int Ed 35:1858
74. Ponomarenko SA, Rebrov EA, Bobrovsky AY, Boiko NI, Muzafarov AM Shivaev VP (1996) Liq Cryst 21:1
75. Lorenz K, Hölter D, Stühn B, Mülhaupt R, Frey H (1996) Adv Mater 8:414
76. Donnio B, Guillon D (2006) Adv Polym Sci 201:45
77. Mehl GH, Goodby JW (1996) Chem Ber 129:521
78. Mehl GH, Goodby JW (1999) Chem Commun, p 13
79. Goodby JW (1998) In: Demus D, Goodby JW, Gray GW, Spiess H-W, Vill V (eds) Handbook of Liquid Crystals Vol 2A: Low Molecular Weight Liquid Crystals, Chap 1. Wiley, Weinheim, pp 3–21
80. Saez IM, Styring P (1996) Adv Mater 8:1001
81. Mehl GH, Saez IM (1999) Appl Organomet Chem 13:261
82. Busson P, Ihre H, Hult A (1998) J Am Chem Soc 120:9070
83. Elsaßer R, Mehl GH, Goodby JW, Photinos DJJ (2000) Chem Commun, p 851
84. Mehl GH, Goodby JW (1996) Angew Chem Int Ed Engl 35:2641
85. Mehl GH, Thornton AJ, Goodby JW (1999) Mol Cryst Liq Cryst 332:2965
86. Saez IM, Goodby JW (1999) Liq Cryst 26:1101
87. Baars MWPL, Söntjens S, Fischer HM, Peerlings HWI, Meijer EW (1998) Chem Eur J 4:2456
88. Ponomarenko SA, Boiko NI, Shibaev VP, Richardson RM, Whitehouse IJ, Rebrov EA, Muzafarov AM (2000) Macromolecules 33:5549
89. Donnio B, Barberá J, Jiménez R, Guillon D, Marcos M, Serrano JL (2002) Macromolecules 35:370
90. Rueff JM, Barberá J, Donnio B, Guillon D, Marcos M, Serrano JL (2003) Macromolecules 36:8368
91. Gedde UW, Hult A, Andersson G (2201) Macromolecules 34:1221
92. Saez IM, Goodby JW (2001) J Mater Chem 11:2845
93. de Gennes P-G (1992) Angew Chem Int Ed Engl, p 842
94. Saez IM, Goodby JW, Richardson RM (2001) Chem Eur J 7:2758
95. Lewthwaite RA, Gray GW, Toyne KJ (1992) J Mater Chem 2:119
96. Lewthwaite RA, Gray GW, Toyne KJ (1993) J Mater Chem 3:241
97. Felder-Flesch D, Rupnicki I, Bourgogne C, Donnio B, Guillon D (2006) J Mater Chem 16:304
98. Campidelli S, Brandmüller T, Hirsch A, Saez IM, Goodby JW, Deschenaux R (2006) Chem Commun, p 4282
99. Saez IM, Goodby JW (2003) J Mater Chem 13:2727
100. Cassagrande C, Veyssié M (1988) CR Acad Sci (Paris) II 306:1423
101. Erhardt R, Zhang M, Böker A, Zettl H, Abetz C, Frederik P, Krausch G, Abetz V, Müller AHE (2003) J Am Chem Soc 125:3260

102. Hawker CJ, Wooley KL, Fréchet J-M (1993) J Chem Soc Perkin Trans 1, p 1287
103. Grayson SM, Fréchet J-M (2000) J Am Chem Soc 122:10335
104. Pesak D, Moore JS (1997) Tetrahedron 53:15331
105. Gillies ER, Fréchet JM (2004) J Org Chem 69:46
106. Zhang W, Moore JS (2006) Angew Chem Int Ed 45:4416
107. Cayre O, Paunov VN, Velev OD (2003) J Mater Chem 13:2445
108. Saez IM, Goodby JW (2003) Chem Commun, p 1726
109. Schulz WG, Braddock M (eds) (2003) Chem Engin News 10:10
110. Bury I, Heinrich B, Bourgogne, Guillon D, Donnio B (2006) Chem Eur J 12:8386
111. Dirksen A, Meijer EW, Adriens W, Hackeng TM (2006) Chem Commun, p 1667
112. Yuan F, Wang W, Yang M, Zhang X, Li J, Li H, He B (2006) Macromolecules 39:3982
113. Apko C, Weber E, Reiche J (2006) New J Chem 30:1820
114. Ropponen J, Nummelin S, Rissanen K (2004) Org Lett 6:2495
115. Saez IM, Goodby JW (2003) Chem Eur J 9:4869
116. Lenoble J, Campidelli S, Maringa N, Donnio B, Guillon D, Yevlampieva N, Deschenaux R (2007) J Am Chem Soc 129:9941
117. Campidelli S, Deschenaux R, Swartz A, Aminur Rahman GC, Guldi, Milic, Vázquez, Prato M (2006) Photochem Photobiol Sci 5:1137
118. Lenoble J, Maringa N, Campidelli S, Donnio B, Guillon D, Deschenaux R (2006) Org Lett 8:1851
119. Even M, Heinrich B, Guillon D, Guldi DM, Prato M, Deschenaux R (2001) Chem Eur J 7:2595
120. Chuard T, Deschenaux R (2002) J Mater Chem 12:1944
121. Campidelli S, Deschenaux R, Eckert JF, Guillon D, Nierengarten J–F (2002) Chem Commun, p 656
122. Sawamura M, Kawai K, Matsuo Y, Kanie K, Kato T, Nakamura E (2002) Nature 419:702
123. Campidelli S, Lenoble J, Barberá J, Paolucci F, Marcaccio M, Paolucci D, Descechenaux R (2005) Macromolecules 38:7915
124. Campidelli S, Deschenaux R, Eckert JF, Guillon D, Nierengarten JF (2002) Chem Commun, p 656
125. Campidelli S, Eng C, Deschenaux R, Saez IM, Goodby JW (2002) Poster No 789, 19th International Liquid Crystal Conference, Edinburgh
126. Sakai N, Matile S (2003) Chem Commun, p 2514
127. Zhuravel MA, Davis NE, Nguyen ST, Koltover I (2004) J Am Chem Soc 126:9882
128. Aprahamian I, Yasuda T, Ikeda T, Saha S, Dichtel WR, Isoda K, Kato T, Stoddart FJ (2007) Angew Chem Int Ed 46:4675
129. Baranoff ED, Voignier J, Yasuda T, Heitz V, Sauvage JP, Kato T (2007) Angew Chem Int Ed 46:4680

Struct Bond (2008) 128: 63–98
DOI 10.1007/430_2007_061

Published online: 18 August 2007

Liquid Crystalline Assembly of Rod–Coil Molecules

Ja-Hyoung Ryu · Myongsoo Lee (✉)

Center for Supramolecular Nano-Assembly and Department of Chemistry, Yonsei University, 120-749 Seoul, Korea
mslee@yonsei.ac.kr

Abstract The development of novel supramolecular materials with nanometer-scale architectures and the effect of these architectures on the materials' properties are currently of great interest in molecular design. Liquid crystalline assemblies of rod-like mesogenic molecules containing flexible coils (rod–coil molecules) provide a facile entry into this area. Rod–coil molecules have been demonstrated to self-assemble into a rich variety of different liquid crystalline structures of nanoscale dimensions through the combination of shape complementarity and repulsive interaction of rigid and flexible parts as an organizing force. The mesophases include smectic, hexagonal or rectangular columnar, bicontinuous cubic, hexagonal channeled lamellar, barrel-like, honeycomb-like, and discrete micellar phases. The unconventional mesophases are induced by changing the rod-to-coil volume fraction, controlling the number of rod–coil repeating units, designing novel shapes of rod–coil molecules, and increasing the rod–coil molecular length.

Keywords Liquid crystal · Rod–coil · Self-assembly · Block copolymer · Microphase separation

1 Introduction

The development of new materials based on self-organizing systems has had a great deal of attention due to their potential in the construction of well-defined supramolecular nanostructures [1–6]. Self-assembling molecules, which include liquid-crystals [7–10], block copolymers [11–13], hydrogen bonded complexes [14, 15], and coordination polymers [16–18] are widely studied for their great potential as advanced functional materials. Especially, the construction of novel supramolecular architectures with well-defined shape and size by using rod building blocks is one of the most important subjects in organic materials chemistry because they can exhibit novel electronic and photonic properties as a result of both their discrete dimensions and three dimensional organization [19–22].

In contrast to organic molecules with low molecular weight, rod–coil systems consisting of rigid rod and flexible coil segments are excellent candidates for a large variety of ordered supramolecular structures covering several length-scales via a process of spontaneous organization [23, 24]. The rod–coil molecular architecture imparts microphase separation of the rod and coil blocks into ordered periodic structures in nanoscale dimensions due to the mutual repulsion of the dissimilar blocks and the packing constraints imposed by the connectivity of each block, while the anisometric molecular shape and stiff rod-like conformation of the rod segment imparts orientational organization. In order to balance these competing parameters, rod–coil molecules self-organize into a variety of supramolecular structures with domain sizes that general coil–coil copolymers could not show, and it can be controlled by variation of the rod-to-coil volume fraction [25–28]. Typical examples of the main types of rod–coil molecules forming supramolecular structures with mesophase are shown in Fig. 1. Basically, these rod–coil oligomers can be divided into two major classes: those containing monodisperse rod segments and those containing polydisperse rod parts.

In contrast to coil–coil block molecules, microphase separated structures in rod–coil block molecules can form, even though the molecular weight of each block is very small, due to large chemical differences between each block. The stiffness-asymmetry of rod–coil molecules that enhances the Flory–Huggins χ-parameter in comparison with coil–coil copolymers, results in well-ordered self-assembled structures of lower molecular weight. At the interface separation of the rod and coil domains, the relatively smaller area per junction favored by the rod block results in chain stretching of the coil block, which is energetically unfavorable. Considering the energetic penalties associated with chain stretching of the coil block and interfacial energy resulting from the interfaces separating the rod and coil domains, the theoretical works on rod–coil systems have predicted nematic–smectic A and smectic A–smectic C transitions in the melt [25, 26]. Other theoretical works

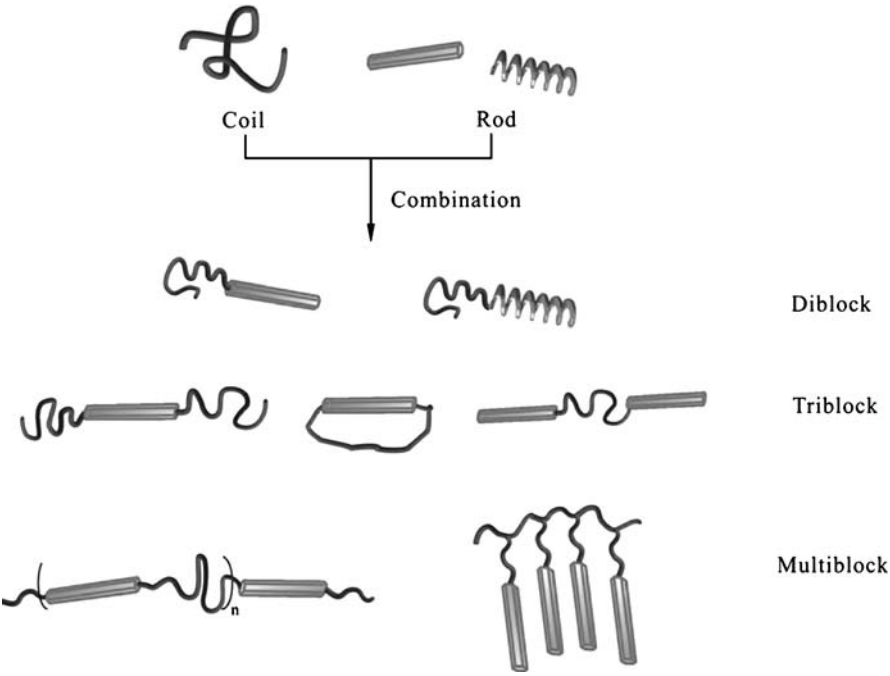

Fig. 1 Typical examples of rod–coil molecules

have dealt more with the phase behavior of rod–coil diblocks in a selective solvent for the coil segment [28]. These works have predicted various micellar structures for sufficiently large coil volume fractions, in addition to the familiar lamellar structures.

This chapter will present an overview of recent work in designing rod–coil systems, demonstrating their self-organization capability into a variety of liquid crystalline phases.

2
Diblock Rod–Coil Systems

2.1
Rod–Coil Diblock Copolymers Based on Perfectly Monodisperse Rods

It is well known that the connection of oligo(alkylene ether) chains into a calamitic rigid rod at the terminals destabilizes the thermotropic mesophases [8]. However, mesomorphic properties can be obtained by molecules with extended rigid rod segments as a result of the microphase segregation between the polar flexible oligo(alkylene oxide) ethers and rigid rod seg-

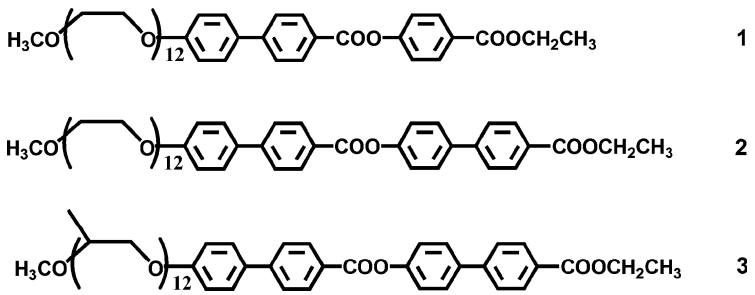

ments [2, 29]. The rod–coil molecules based on three phenyl units (**1**) as a rod segment, for example, exhibits only an isotropic phase after crystalline melting [30] while the molecule (**2**) based on four phenyl units as a rod segment shows a smectic A mesophase [29]. In the case of rod–coil molecule with short rod length, the coil segment may couple with the anisotropic rod owing to the relatively high miscibility between coil and rod segments, which can disturb the anisotropic aggregation of rod blocks. However, as the rod length increases, the immiscibility between chemically different flexible and rigid chains increases. This allows the increasing lateral intermolecular interactions of rigid segments. As a result, a layered smectic liquid crystalline phase can be induced, as exhibited by **2**. If the coil volume fraction increases, smectic ordering of rod segments becomes unstable due to a large space crowding; consequently, the lamellar structure will transform into cylindrical micelles, which allows more volume for coils to explore. In contrast to the molecule **2**, the molecule **3** based on a poly(propylene oxide) (PPO) coil shows a hexagonal columnar structure [31]. This large structural variation between the molecularly similar systems is probably caused by the larger spatial requirement of the bulkier PPO coil in comparison with the poly(ethylene oxide) (PEO).

In a systematic work on the influence of the coil length on phase behavior, rod–coil molecules (**4**) with PPO having different degrees of polymerization but the identical rod segment were prepared [32, 33]. A dramatic structural change in the mesophase of this rod–coil system was observed with variation in the coil length, as determined by a combination of techniques consisting of differential scanning calorimetry (DSC), optical polarized microscopy and X-ray scattering. Rod–coil molecules with seven propylene oxide (PO) repeating units exhibit a layered structure, while rod–coil molecules with 12 PO repeating units exhibit an optically isotropic cubic phase. This structure was identified by X-ray scattering methods to be a bicontinuous cubic (cub) structure with *Ia3d* symmetry. Further increasing the coil length induces a hexagonal columnar mesophase, as in the case of the molecule with 20 PO repeating units (Fig. 2). Organization of the rod–coil molecules into a cross sectional slice of a cylinder for cubic and columnar phases gives rise to an aromatic core with approximately square cross section. The sizes and

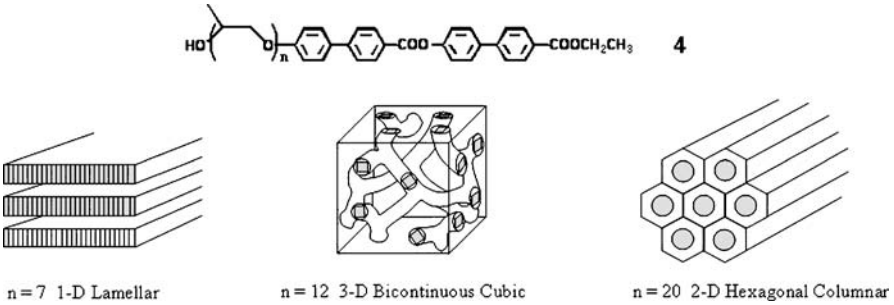

Fig. 2 Mesophases of the rod–coil diblock molecules by the increasing volume fraction of coil segments

periods of these supramolecular structures are typically in a range of less than 10 nm. This structural variation can be explained by considering the fact that increasing coil volume fraction leads to a structure with larger interfacial area, similar to the well-known conventional diblock copolymer phase behavior [13, 34, 35].

A strategy to manipulate supramolecular structures assembled from rod segments may be accessible by the alteration of the coil architecture (linear (**5**) versus branched (**6**)) in the rod–coil system [36]. On the basis of SAXS and TEM results, rod–coil molecules (**5**) with a linear PPO coil showed a honeycomb-like lamellar rod assembly with hexagonally arrayed PPO coil perforations, while the rod–coil molecules (**6**) with a dibranched PPO coil self-organized into rod-bundles with a body-centered tetragonal symmetry surrounded by a PPO coil matrix (Fig. 3). The notable feature is that a sim-

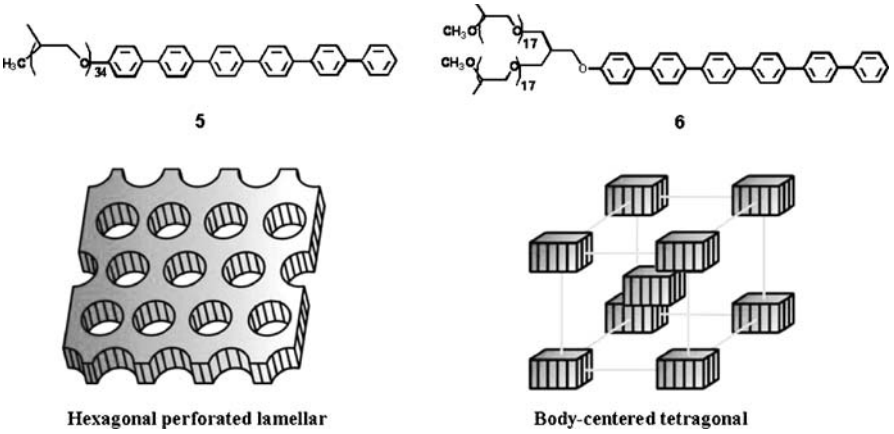

Fig. 3 3D supramolecular structural change from organized honeycombs (**5**) to organized bundles (**6**), dependent upon the coil architectural variation of the rod–coil molecule

ple structural variation from linear to dibranched chains generates a three-dimensional (3D) supramolecular structural inversion from organized coil perforations in rod layers to organized discrete rod bundles in a coil matrix. This implies that the steric hindrance at the rod/coil interface arising from branched coils plays a crucial role in the self-assembly of rod segments, as well as the conformational entropy associated with coil length.

Stupp et al. reported on rod–coil copolymers consisting of an elongated mesogenic rod and a monodisperse polyisoprene [37–39]. These rod–coil copolymers organize into ordered structures that differ in terms of varying rod volume fraction, as monitored by transmission electron microscopy and electron tomography. Depending on the rod volume fraction (f_{rod}), rod–coil oligomers either form strip-like morphologies or self-assemble into discrete aggregates that are organized in an hexagonal superlattice, with domain sizes typically between 5–10 nm. The authors also synthesized rod–coil copolymers containing oligostyrene-block-oligobutadiene as the coil block and rigid biphenyl units connected by ester linkages as the rod block [40–42]. Polarized optical microscopy showed that molecule **7** undergoes a phase transition from the smectic to the isotropic state. On the basis of TEM and X-ray data, it was suggested that the rod–coil molecules pack into the mushroom-shaped nanostructure with a height of 8 nm and a diameter of 2 nm. Each supramolecular nanostructure was estimated to contain approximately 23 molecules. Most importantly, this nanostructure was proposed to impart the spatial isolation of cross-linkable oligobutadiene blocks required to form a well-defined object. Therefore, polymerization might be confined to the volume of the supramolecular cluster. Thermal polymerization of rod–coil molecules in liquid crystalline state produced high molar-mass products with a very narrow polydispersity within a range of 1.15 to 1.25 and a molecular weight of approximately 70 000, as confirmed by GPC (Fig. 4). The macromolecular objects obtained reveal an anisotropic shape (2 by 8 nm) similar to that of supramolecular clusters, as determined by electron microscopy and small-angle X-ray scattering. Polarized optical microscopy showed that polymerization of the molecules into macromolecular objects results in a strong stabilization of the liquid crystalline phase that remains up to a chemical decomposition temperature of 430 °C. This result is interesting because the self-assembly process provides a direct pathway for preparation of well-defined molecular nanoobjects with distinct and permanent shapes through polymerization within supramolecular structures.

Yu et al. reported the synthesis of rod–coil block copolymers containing oligo(phenylene vinylene)s (OPV) coupled to either polyisoprene or poly(ethylene glycol) [43, 44]. These OPV showed a reversible thermotropic liquid–crystalline transition. The liquid–crystalline texture observed using a polarizing microscope shows a typical Schlieren pattern, which is evidence for the presence of nematic phases. TEM and small-angle X-ray scattering revealed alternating strips of rod-rich and coil-rich domains. The domain sizes

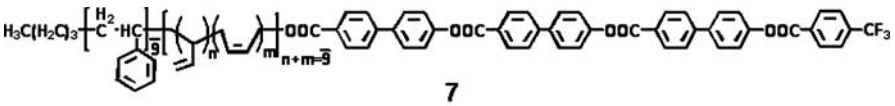

7

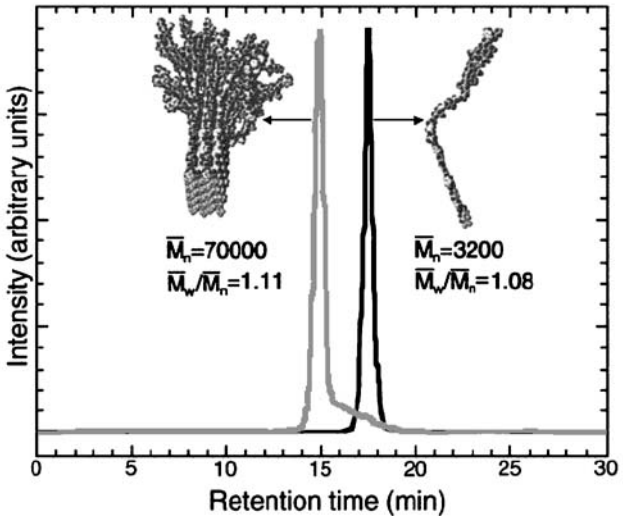

Fig. 4 GPC traces of rod–coil copolymer (7) and macromolecular object. Reprinted with permission from [40–42]. © 2001 American Association for the Advancement of Science

of the strips suggested that the supramolecular structures could be bilayer lamellar structures.

Incorporation of a rigid wedge-shaped building block into a diblock molecular architecture gives rise to a novel class of self-assembling systems consisting of a rigid wedge and a flexible coil because the molecule shares certain general characteristics of both dendrons and block copolymers. Lee et al. reported the self-assembling behavior of wedge–coil diblock molecules consisting of a rigid wedge and a flexible PEO coil in the melt state [45]. All of the molecules had a thermotropic liquid–crystalline structure after melting. The wide-angle X-ray diffraction patterns of all the molecules in the melt state are characterized by a diffuse scattering, which confirms their liquid–crystalline nature. However, a significant structural variation in the melt state was observed as the length of the PEO segment was varied, as evidenced by optical microscopic textures and small-angle X-ray diffraction patterns. The variation in the supramolecular structure can be rationalized by considering the microphase separation between the dissimilar parts of the molecule and the space-filling requirement of the flexible PEO chains (Fig. 5). The molecules based on a short PEO chain can be packed with a radial arrangement to fill the space efficiently, which results in a spherical supramolecular structure. Increasing the length of the PEO chain results in more space for

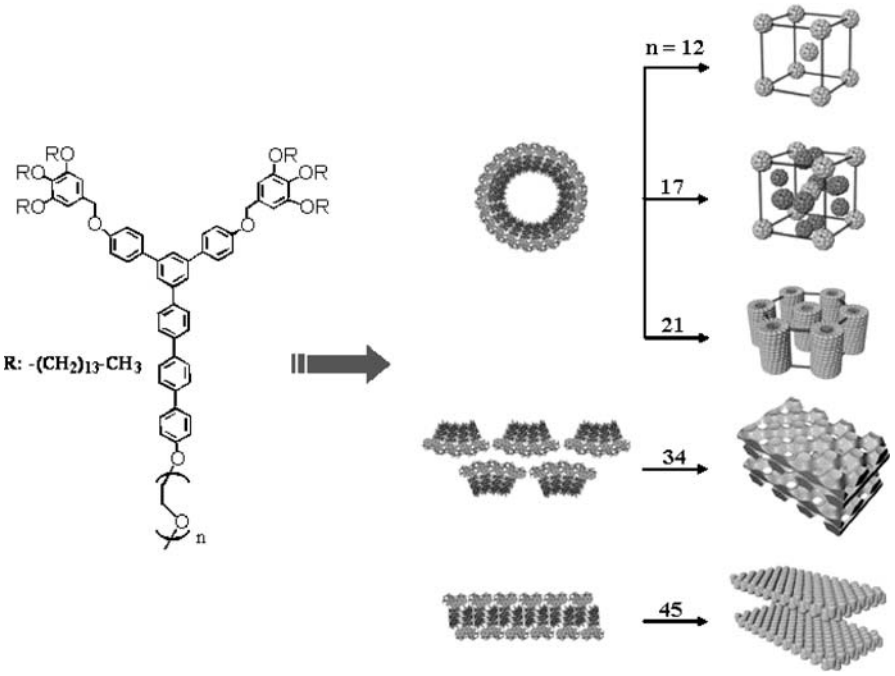

Fig. 5 Liquid crystalline structures formed by wedge-shaped molecules depend on the length of PEO

the chains being required while maintaining the radial arrangement of the rigid segments. Consequently, the discrete PEO domains will be extended to an infinitely long cylindrical domain in which the coils are less confined, which results in the formation of a 2D hexagonal columnar structure. Further increasing the length results in the rigid wedge-shaped segments assembling into a perforated lamellar structure with a radial arrangement of rigid segments, which allows a greater volume for the PEO chains to explore compared to that of the columnar structure. The radial arrangement of the wedge-shaped rigid segments eventually transforms into a parallel arrangement with interdigitation, to produce a flat interface while maintaining a constant density of the rigid hydrophobic domain. This transformation results in a monolayer lamellar structure as in the case of a molecule based on longest PEO chain.

Compared to other self-assembling systems based on dendritic molecules [46–48], the remarkable feature of the wedge-shaped building blocks investigated is their ability to self-assemble not only into spherical cubic and columnar structures, but also into an unusual bilayer lamellar structure with in-plane hexagonally ordered coil perforations. This approach of controlling supramolecular structures using wedge-shaped building blocks and only

a small variation in the length of grafted coils allows unexpectedly complex liquid crystalline structures to be produced.

2.2 Rod–Coil Diblock Copolymers Based on Polydisperse Rods

In contrast to the rod–coil diblock copolymer consisting of perfectly monodisperse rods, the liquid crystalline morphologies of rod–coil diblock copolymer containing polydisperse rods seem to be studied in less detail. In certain cases, the polydisperse nature of the rod-segments could hinder self-assembly into regularly ordered supramolecular structures. However, due to relatively simple synthetic procedures, liquid crystalline polymer can be of benefit for new materials with controlled internal dimensions ranging from the nanometer to macroscopic scale.

Poly(hexyl isocynate) is known to have a stiff rod-like conformation in the solid state and in a wide range of solvents, which is responsible for the formation of a nematic liquid crystalline phase [49, 50]. The inherent chain stiffness of this polymer is primarily determined by chemical structure rather than by intramolecular hydrogen bonding. This results in a greater stability in the stiff rod-like characteristics in solution. The lyotropic liquid crystalline behavior in a number of different solvents was extensively studied by Aharoni et al. [51–53]. In contrast to homopolymers, interesting new supramolecular structures can be expected if a flexible block is connected to the rigid polyisocyanate block (rod–coil copolymers) because the molecule imparts both microphase separation characteristics of the blocks and a tendency of rod segments to form anisotropic order.

Thomas and coworkers reported rod–coil diblock copolymers consisting of poly(hexyl isocyanate) as the rod block and polystyrene as the coil block [54, 55]. A block copolymer consisting of poly(hexyl isocynate) with DP of 900 and polystyrene with DP of 300 displays liquid crystalline behavior in concentrated solutions, suggestive of an anisotropic order of rod segments [54]. Transmission electron microscopy of bulk and thin film samples cast from toluene solutions showed the existence of a zigzag morphology with a high degree of smectic-like long range order. With additional research into the influence of the rod volume fraction on the phase behavior, the authors studied the rod–coil copolymers with varying compositions of rod blocks [55]. Transmission electron microscopy revealed phase-separated morphologies with rod-rich regions and coil-rich regions in which rod segments are organized into tilted layers analogous to those observed in smectic phases.

The authors also investigated the rod–coil block copolymer consisting of poly(3-(triethoxysilyl)propyl isocyanate) (23 kg/mol) (PIC) as a rigid rod and polystyrene (39 kg/mol) (PS) as a coil block [56]. Initial isotropic solutions of rod–coils undergo multiple ordering transitions until a final smectic microdomain structure develops in the dry state. The intermediate nematic

state is able to dynamically respond to external fields and form periodic defects. Depending on the evaporation of solvent, they showed that hierarchical morphology was induced in a rod–coil block copolymer film.

When the rod blocks contained reactive side groups with a composition having a large coil-to-rod volume ratio (PIC 23K, PS 200K), prism-like micelle nanoobjects could be synthesized via self-assembly of rod–coil diblock copolymers [57]. The PIC domain was cross-linked thermally via condensation of triethoxysilyl side groups and the rod directors remain parallel to each other due to the liquid crystalline order. Thermal cross-linking of the rod blocks only took place within each micellar nanodomain because the high molecular weight PS blocks could completely separate from each other. The TEM images indeed showed prism-like nanoobjects, which suggests a tilted bilayer structure consisting of 300 aggregates of the rod–coil block copolymer, as shown in Fig. 6. The result presents a novel method for forming anisotropic organic particles with potential multifacial surface characteristics.

De Boer et al. reported on the synthesis of a donor–acceptor, rod–coil diblock copolymer with the objective of enhancing the photovoltaic efficiency of the poly(phenylenevinylene)-C_{60} system by incorporation of both components in a rod–coil molecular architecture that self-assembled through microphase separation [58]. These rod–coil copolymers showed nematic liquid crystalline phase and exhibit thermotropic transition at two regions. The first transition is attributed to the melting of the side chains, and the second higher one is an isotropic transition. Consequently, the diblock copolymers possess complex and rich phase behavior due to the combination of a mesogenic rod-like block and the adjacent coil-like block. The morphology of the polymer in bulk can play an important role in determining the photovoltaic cells, which the combination of a poly(*p*-phenylenevinylene)-type polymer as the donor material and C_{60} as acceptor has effectively utilized.

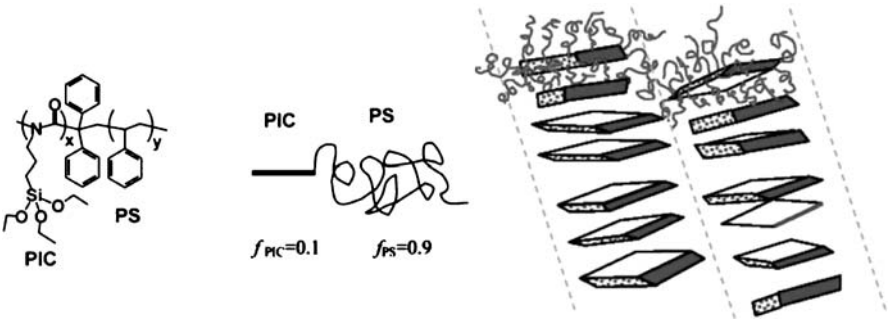

Fig. 6 Semectic ordering of the anisotropic nanoobjects formed from PIC(23K)/PS(200K). Reprinted with permission from [57]. © 2004 American Chemical Society

2.3 Rod–Coil Diblock Copolymers Based on Peptide Rods

Polymers with a stiff helical rod-like structure have many advantages over other synthetic polymers because they possess stable secondary structures due to cooperative intermolecular interactions. Examples of polymers with helical conformation are polypeptides in which the two major structures include α-helices and β-sheets. The α-helical secondary structure enforces a rod-like structure, in which the polypeptide main chain is coiled and forms the inner part of the rod [59]. This rod-like feature is responsible for the formation of the thermotropic and lyotropic liquid crystalline phases. Polypeptide molecules with α-helical conformation in solution are arranged with their long axes parallel to each other to give rise to a nematic liquid crystalline phase. However, even long chain polypeptides can exhibit a layered supramolecular structure when they have a well-defined chain length. For example, the monodisperse poly(α,L-glutamic acid) prepared by bacterial synthetic methods assembles into smectic ordering on length scales of tens of nanometers [60, 61].

Incorporation of an elongated coil-like block to this helical rod system in a single molecular architecture may be an attractive way of creating new supramolecular structures due to its ability to segregate incompatible segments of individual molecules. The resulting rod–coil copolymers based on a polypeptide segment may also serve as models providing insight into the ordering of complicated biological systems. Low molecular weight block copolymers consisting of poly(γ-benzyl-L-glutamate) with DP of 10 or 20 and polystyrene with DP of 10 were synthesized by Klok, Lecommandoux, and a coworker [62]. Both the rod–coil polymers were observed to exhibit thermotropic liquid–crystalline phases with assembled structures that differ from the lamellar structures. Incorporation of a polypeptide segment into a polystyrene segment was observed to induce a significant stabilization of the α-helical secondary structure, as confirmed by FT-IR spectra. However, small-angle X-ray diffraction patterns indicated that α-helical polypeptides do not seem to assemble into hexagonal packing for the rod–coil copolymer with ten γ-benzyl-L-glutamate repeating units. The amorphous character of the polystyrene coil is thought to frustrate a regular packing of the α-helical fraction of the short polypeptide segments. Increasing the length of the polypeptide segment to a DP of 20 gives rise to a strong increase in the fraction of diblock copolymers with α-helical polypeptide segment. By studying this block copolymer with small-angle X-ray analysis, a 2D hexagonal columnar supramolecular structure was observed with a hexagonal packing of the polypeptide segments adopting an 18/5 α-helical conformation with a lattice constant of 16 Å. The authors proposed a packing model for the formation of the double-hexagonal organization. In this model, the rod–coil copolymers are assembled in a hexagonal fashion into infinitely long

columns, with the polypeptide segments oriented perpendicularly to the director of the columns. The subsequent supramolecular columns are packed in a superlattice with hexagonal periodicity parallel to the α-helical polypeptide segments, with a lattice constant of 43 Å.

In addition, the authors reported that two series of peptide rod–coil block copolymers based on γ-benzyl-L-glutamate or ε-benzyloxycarbonyl-L-lysine as a rod building block and a short oligo(styrene) (DP = 10) coil self-assembled into well-ordered structures, and that the conformation of the α-helical peptide rod is sensitive to temperature [63]. Under ambient conditions, the peptide segments of the diblock oligomers largely possess an α-helical secondary structure, indicating the rod–coil architecture of the molecules as confirmed by FT-IR spectra. For all molecules, increasing the length of the peptide segment results in a stabilization of the α-helical secondary structure and ultimately allows a regular organization of the rod-like peptide blocks. The small-angle X-ray diffraction pattern of peptide block copolymers based on short γ-benzyl-L-glutamate also indicates a columnar hexagonal arrangement, except for one composed of the shortest peptide segments ($n = 10$). However, in case of the long γ-benzyl-L-glutamate peptide segments ($n = 20, 40$), increasing temperature transforms the organized structure from hexagonal columnar into lamellar structure due to the change of the peptide conformation from

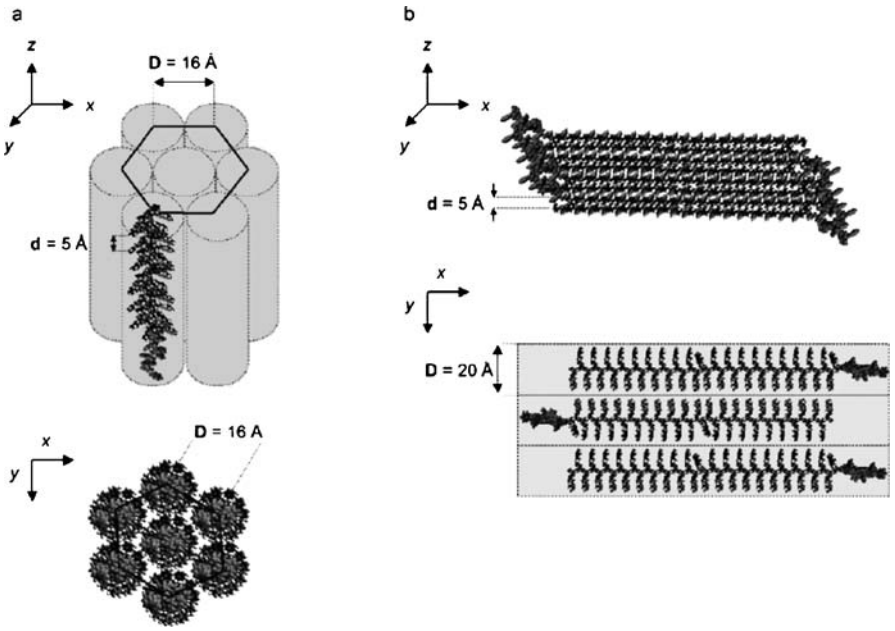

Fig. 7 **a** Columnar hexagonal and **b** lamellar β-sheet organization of the (styrene)$_{10}$-*b*-(γ-benzyl-L-glutamate)$_n$ diblock oligomers (PS$_{10}$-*b*-PBLG$_n$). Reprinted with permission from [63]. © 2001 American Chemical Society

α-helix to β-sheet (Fig. 7). The block length required to allow such a transition varies from ~40 repeat units for the PS_{10}-*b*-$PBLG_n$ diblock oligomers to ~80 α-amino acids for the PS_{10}-*b*-$PZLys_n$ series, reflecting the lower α-helix-forming propensity of Z-Lys in comparison with Bn-Glu.

In contrast to peptide diblock copolymers based on general polymers, Deming and Pochan et al. reported on unique copolymers that are completely peptidic [64]. Leucine (L), racemic copolymers of L- and D-leucine (racL), or a random copolymer of L and valine (V) blocks with the inherent secondary structures of random coil (racL or LV) or rigid rod (L), were attached to PBLG molecules. In PBLG diblock copolymers with relatively small additional blocks, cholesteric liquid crystalline ordering was observed in bulk films. However, depending on the kinetics of film formation and the amount of non-PBLG block, the nanostructure or microstructure were able to be controlled. These purely peptidic block molecules can provide the opportunity to pattern materials with peptidic functionalities by taking advantage of block copolymer phase behavior and liquid crystal ordering.

Very recently, the self-assembly of poly(γ-benzyl-L-glutamate)-*b*-poly(L-lysine) rod–coil copolypeptide via ionic complexation was reported by Ikkala, Hadjichristidis and coworkers [65]. Complexation between the anionic surfactants dodecyl benzenesulfonic acid and the cationic poly(L-lysine) chains occurs via proton transfer from the acid group to the base, resulting in electrostatically bonded comb-like structures, and fluid-like liquid crystalline structures at room temperature due to efficient plasticization of dodecyl benzenesulfonic acid.

3
Triblock Rod–Coil System

3.1
ABC Coil–Rod–Coil Triblock Copolymers

If a chemically distinct hydrophobic chain is attached to the opposite ends of rod segment, segregation of incompatible chain ends takes place and leads to an ordered phase composed of three distinct sub-layers [66]. Coil–rod–coil ABC triblock molecules give rise to the formation of self-assembled structures with higher interfacial areas in comparison with AB diblock molecules. In contrast to that of diblock molecules based on a PEO coil, which show isotropic or smectic phase depending on the coil length, the ABC triblock molecule exhibits a hexagonal columnar mesophase [67]. Molecule (**9**) with 22 ethylene oxide (EO) repeating units, for example, exhibits hexagonal columnar mesophase which, in turn, undergoes transformation into a discrete spherical micellar structure in which rod segments are packed into a discrete bilayer lamellar structure that is encapsulated with PEO coils

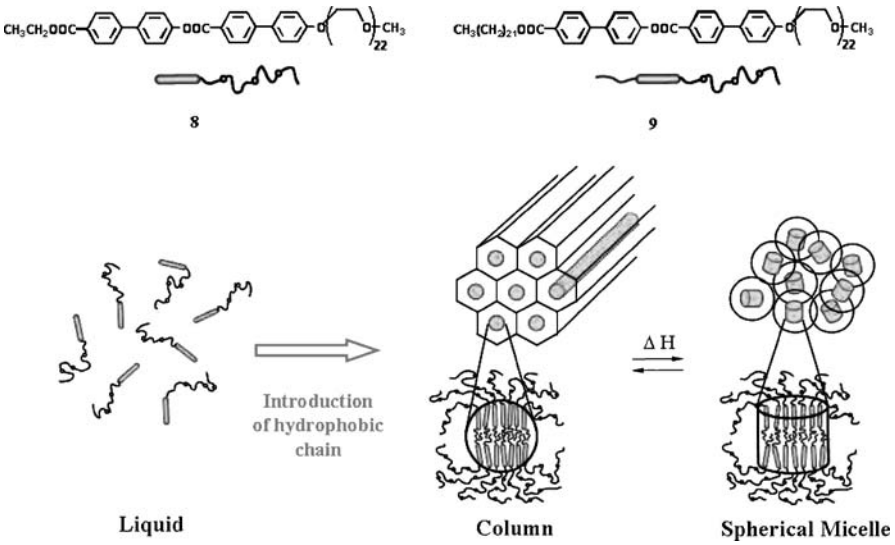

Fig. 8 Induction of the mesophase in rod–coil molecules via hydrophobic forces

(Fig. 8). Small-angle X-ray diffraction in the optically isotropic state revealed a strong primary peak together with a broad peak of weak intensity at about 1.8 relative to the primary peak position, indicating that the spatial distribution of centers of the spherical micelles has only liquid-like short range order, most probably due to random thermal motion of spherical micelles [68, 69]. From the observed primary peak of X-ray diffraction, the diameter of spheres was estimated to be approximately 12 nm. Considering that diblock rod–coil molecule (**8**) with 22 EO repeating units shows only an isotropic phase after crystalline melting, it is likely that hydrophobic forces play an important role in the self-assembly of the molecules into discrete nanostructures.

A novel strategy for manipulating the supramolecular nanostructure may be accessed by binding the C coil block of a coil–rod–coil ABC triblock molecule (**9**) into a tetrabranched triblock molecule (**10**) at a specific coil volume fraction [70]. This binding may slightly modify the entropic contribution of the coil C part in the coil–rod–coil ABC system. In comparison with the monomer, the tetramer has restricted chain end mobility through covalent linkage. Consequently, this effect may bring about the formation of a novel supramolecular nanostructure. Tetramerization of the molecule **9** provides an unusual example of the formation of a 3D tetragonally perforated lamellar liquid crystalline phase as an intermediate phase between conventional lamellar and columnar structures (Fig. 9). The supramolecular structure consists of liquid crystalline rod layers with in-plane tetragonally ordered coil perforations stacked in an AB–BA sequence. The perforations are likely to be filled by docosyl chains, most probably due to the large chemical difference

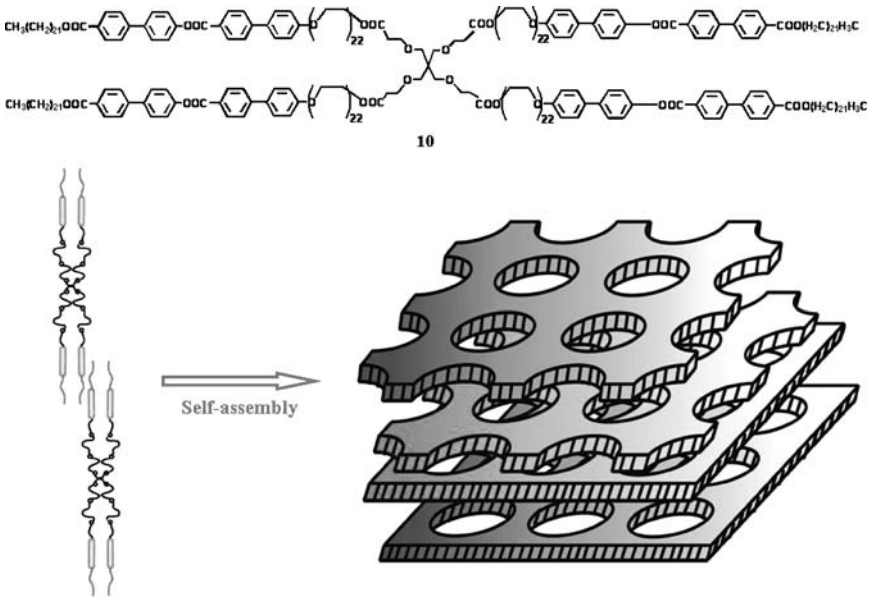

Fig. 9 Tetragonal perforated lamellar structure in an AB–BA sequence formed by tetra-branched triblock molecule

between the rod and PEO coil segments. The 3D lattice is built up of two interpenetrating centered 3D lattices. In comparison with the phase behavior of **9**, the remarkable feature of **10** is that attachment of coil–rod–coil molecules into a central point induces a perforated lamellar liquid crystalline phase with a 3D tetragonal symmetry that is thermodynamically stable. Upon melting of rod segments in **9**, there is adequate free volume for PEO to form a 2D hexagonal columnar mesophase. Attachment of four PEO chains to a central point, however, has the effect of reducing the freedom of movement for the flexible chains, which in turn suppresses the ability of the rod segments to form a columnar mesophase with a larger interfacial area. Consequently, certain supramolecular structures with reduced interfacial area, such as a perforated lamellar structures, are preferred over the columnar phase exhibited by the monomer.

Incorporation of a dendritic building block into the end of an incompatible linear chain gives rise to novel self-assembling systems because the molecule shares certain general characteristics of both block copolymers and small amphiphiles. Amphiphilic dendrimers containing an extended rigid rod block represent another class of self-assembling systems that are increasingly used for the construction of supramolecular architectures with well-defined shape. The introduction of a hydrophobic docosyl chain and hydrophilic dendrimer into each end of an extended rigid segment would give rise to a unique amphiphilic ABC triblock system consisting of a hydrophilic dendritic block,

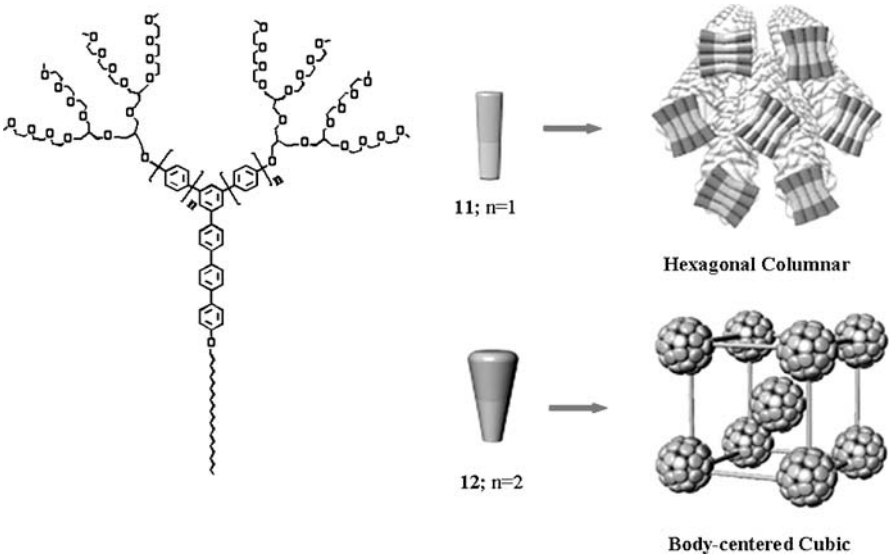

Fig. 10 Rod shape-dependent supramolecular structures

rigid aromatic, and hydrophobic docosyl chain [71]. The small-angle X-ray diffraction pattern of **11** displays sharp reflections that correspond to a 2D hexagonal columnar structure with a lattice constant of 8.1 nm. This dimension implies that the rod-like rigid segments arrange axially with their preferred direction within a cross-sectional slice of the column, in which docosyl chains pack in an interdigitated fashion and distort conformationally (Fig. 10). In contrast, the small-angle X-ray diffraction patterns of **12** show a strong reflection together with a number of low intensity reflections at higher angles, indexed as a 3D body-centered cubic phase with a lattice parameter of 11.6 nm [72, 73]. Considering the space-filling requirement and cone-shaped building block, the radial arrangement of the rigid segments is expected to be the best way to close-pack the hydrophobic core, leading to a discrete nanostructure. Accordingly, **12** based on a more wedge-like aromatic segment can be described to self-organize into an optically isotropic cubic phase consisting of a 3D body-centered arrangement of discrete aggregates, as shown in Fig. 10.

Amphiphilic molecules consisting of oligo(phenylene vinylene) (OPV) asymmetrically end-substituted with a hydrophilic PEO segment and a hydrophobic alkyl chain induce self-assembly into both thermotropic and lyotropic lamellar liquid crystalline phases [74]. Depending on the length of PEO block, the mesostructures were controlled. When PEO chains are short, the amphiphilic molecule showed a mosaic birefringence texture from polarized optical microscopy, which is defined smectic B (S_B) mesophase. Increasing the length of PEO chain frustrates ordering of OPV aggregation and results

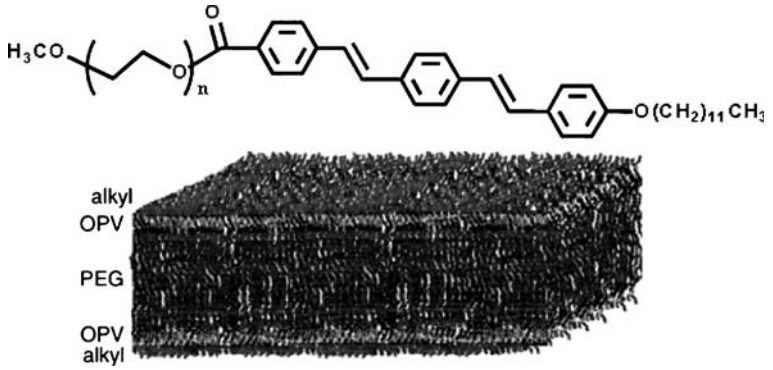

Fig. 11 Bilayer packing of amphiphilic OPV molecules. Reprinted with permission from [74]. © 2005 American Chemical Society

in smectic C (S_C) and smectic A (S_A) phases. The interlayer spacing is approximately equal to the fully extended lengths of the molecules, indicating significant interdigitation and/or tilt within a bilayer smectic structure. The X-ray data confirmed that OPV amphiphiles form an interdigitated bilayer smectic phase as shown in Fig. 11. Liquid crystallinity will be used to control OPV aggregation, influencing exciton mobility, fluorescence, and potentially leading to improved charge carrier mobility in heterojunction solar cells or enabling more efficient, polarized emission from organic light-emitting diodes.

Very recently, Lin et al. synthesized asymmetrical molecules consisting of a novel conjugated aromatic core containing fluorene, thiophene, and biphenyl groups and two kinds of PEO chains ($DP = 17$ and 44) on one side and alkoxy groups with different lengths ($-OC_8H_{17}$ and $-OC_{16}H_{33}$) on another side of the rigid core and their mesophases characterized [75]. Asymmetrical amphiphilic molecules based on short PEO chain ($DP = 17$) display the smectic phases. However, amphiphilic molecules based on longer PEO chain ($DP = 44$) show two kinds of columnar phases, hexagonal columnar and rectangular columnar. The immiscibility between the hydrophilic flexible chains and the hydrophobic rods leads to stronger lateral interaction of rigid rods and induces the smectic phases. By increasing the hydrophilic ethylene oxide units, the immiscibility increases and microphase separation is enhanced to form more order columnar phases.

3.2
ABA Coil–Rod–Coil Triblock Copolymers

In the case of symmetric coil–rod–coil molecule, the rod segment is connected with coil segments at both ends. This gives rise to the formation of the liquid crystalline structure with higher interfacial area in comparison with rod–coil diblock systems at similar coil volume fraction. For example, the

triblock molecule (**13**) with coil volume fraction, $f_{coil} = 0.47$ exhibits a bicontinuous cubic phase instead of smectic phase [76, 77]. Similarly to diblock rod–coil systems, increasing the volume fraction induces a hexagonal columnar mesophase as in the case of **14**.

Remarkably, molecules with a longer length of coil (**15**) assemble into discrete supramolecular aggregates that spontaneously organize into a 3D tetragonal phase with a body-centered symmetry in the solid state and mesophase as determined by small-angle X-ray scattering. Based on X-ray data and density measurements, the inner core of the supramolecular aggregate is composed of the discrete rod bundle with a cylindrical shape of 5 nm in diameter and 3 nm in length. It is encapsulated with phase-separated PPO coils, which gives rise to the formation of non-spherical oblate aggregate (Fig. 12). The supramolecular rod bundles subsequently organize into a 3D body-centered tetragonal symmetry. The oblate shape of supramolecular aggregates is believed to be responsible for the formation of the unusual 3D tetragonal phase (M_{tet}). This unique phase behavior mostly originates from the anisotropic aggregation of rod segments with their long axes within microphase-separated aromatic domains. Consequently, rod bundles with puck-like cylindrical shape would give rise to oblate micelles, which can pack more densely into an optically anisotropic 3D tetragonal lattice, rather than an optically isotropic cubic lattice. These results demonstrate that the linear combination of flexible coils in both terminals of rod segment leads to discrete micellar aggregates that organize into a body-centered tetragonal liquid crystalline phase above a certain coil volume fraction.

Another possible way to manipulate the liquid crystalline structure could be provided by systematic variation of the rod length at constant rod-to-coil

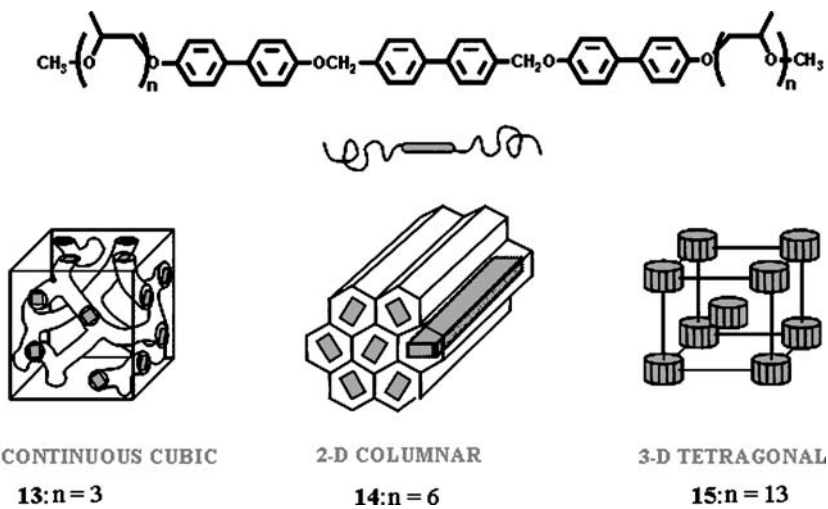

Fig. 12 Mesophase structures of the ABA coil–rod–coil triblock molecules

volume ratio. In particular, increasing the length of the rod segment should disturb the assembly of the rigid rod segments into discrete bundles due to larger rod-to-rod interactions. Rod–coil molecules **15**, **16**, and **17** have an identical rod-to-coil volume fraction ($f_{rod} = 0.22$). As mentioned above, the triblock molecule **15** based on three biphenyl units exhibits a tetragonal micellar liquid crystalline phase. In great contrast, the rod segment of **16** based on longer chain length self-assembles into a honeycomb-like layered liquid crystalline phase (HC) as a lower temperature mesophase in which hexagonally ordered perforations within a layer are filled by coil segments [78]. These layers, in turn, are stacked spontaneously in an ABAB fashion to generate a 3D hexagonal order. A DSC heating trace of **16** shows a crystalline melting transition at 136 °C, followed by a birefringent liquid crystalline phase that undergoes transformation into another liquid crystalline phase at 157 °C. On heating to 157 °C, the honeycomb-like mesophase transforms into a 3D tetragonal micellar liquid crystalline phase. On slow cooling from the isotropic liquid, the formation of fern-like domains growing in four directions with an angle of approximately 90°, which coalesce into a mosaic texture, could be easily observed using polarized optical microscopy, indicating the presence of a 3D tetragonal mesophase.

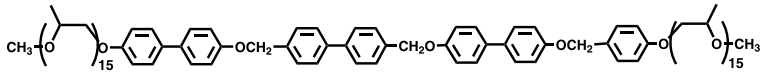

16

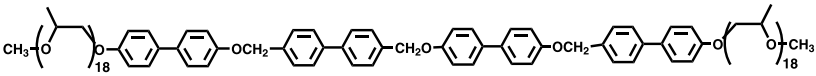

17

Further increasing the length of rod segment suppresses the formation of a 3D tetragonal mesophase, while inducing only a honeycomb-like liquid crystalline phase as in the case of the molecule **17**. These results indicate that the self-assembled 3D liquid crystalline phase changes significantly from organized rod bundles in a coil matrix (tetragonal structure) to organized coil perforations in rod layers (honeycomb structure) on increasing the rod length. This direct structural inversion is also accompanied by changing temperature. Therefore, changing temperature produces an effect similar to varying the molecular length. This example proves that the molecular length in rod–coil systems also has a large impact on the organized structure formed by self-assembly of rod–coil molecules.

The opposite way to modulate the supramolecular structure can be provided by variation in the coil structure while maintaining the rod segment constant. The influence of cross-sectional area of coil segment upon the self-assembly behavior were explored by ABA type coil–rod–coil molecules **15** and **18** that have identical coil volume fraction ($f_{coil} = 0.78$) relative to mesogenic rod segment, but different coil segments, i.e., PPO and PEO, re-

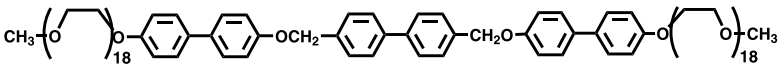

18

spectively [77]. As mentioned, **15** containing the PPO coils self-organizes into a 3D body-centered tetragonal lattice. In contrast, **18** shows significantly distinct self-assembly behavior. The optical microscopic observation of an arced pseudo-focal conic texture and the small-angle X-ray diffraction measurement both indicate that the supramolecular structures in mesophases are honeycomb-like lamellar structures where hexagonally perforated layers ($P6_3/mmc$ symmetry) are stacked in ABAB order.

The different self-assembly behavior of **15** and **18** with identical coil volume fraction points out the significance of coil cross-sectional area for the packing of rod segments. It can be rationalized by the consideration of coil density at the rod/coil interface as dependent upon coil cross-section. For a given space at the rod/coil junction, the coils with larger cross-sectional area cause more space crowding. The steric repulsion resulting from the space crowding leads to the stretched conformation of coils, leading to the coil stretching penalty [9c]. The morphological transition from continuous (the honeycomb-like lamellar structure of **18**) into discrete rod packing structures (the tetragonal structure of **15**) allows coils enough room to lower the coil conformational energy. Finally, self-assembly of rods can be fine-tuned in 3D nanospace since, in addition to coil volume fraction, coil cross-section is an independent parameter in building a variety of supramolecular structures.

A method for manipulating the size of the discrete nanostructures assembled from conjugated rod building blocks may be accessible by attaching chemically dissimilar, flexible dendritic wedges to their ends. Dumbbell-shaped molecules consisting of three biphenyls connected through vinyl linkages as a conjugated rod segment and aliphatic polyether dendritic wedges with different cross-sections (i.e., dibranch (**19**), tetrabranch (**20**) and hexabranch (**21**)) self-assemble into discrete bundles that organize into 3D superlattices [79]. Molecule **19**, based on a dibranched dendritic wedge, organizes into primitive monoclinic-crystalline and body-centered, tetragonal liquid crystalline structures, while molecules **20** and **21**, based on tetra- and hexabranched dendritic wedges, respectively, form only body-centered, tetragonal liquid crystalline structures (Fig. 13). X-ray diffraction experiments and density measurements showed that the rod-bundle cross-sectional area decreases with increasing cross-section of the dendritic wedges. The number of molecules per bundle decreases systematically with increasing cross-section of the dendritic wedge. Consequently, the size of the rod-bundle in cross-sectional area decreases in nanoscale dimension from 17.0 to 11.5 to 9.6 nm^2 for **19**, **20**, and **21**, respectively. The variation of rod bundle size in cross-section can be rationalized by considering both the steric repulsion between the bulky dendritic wedges and the nanophase separation between

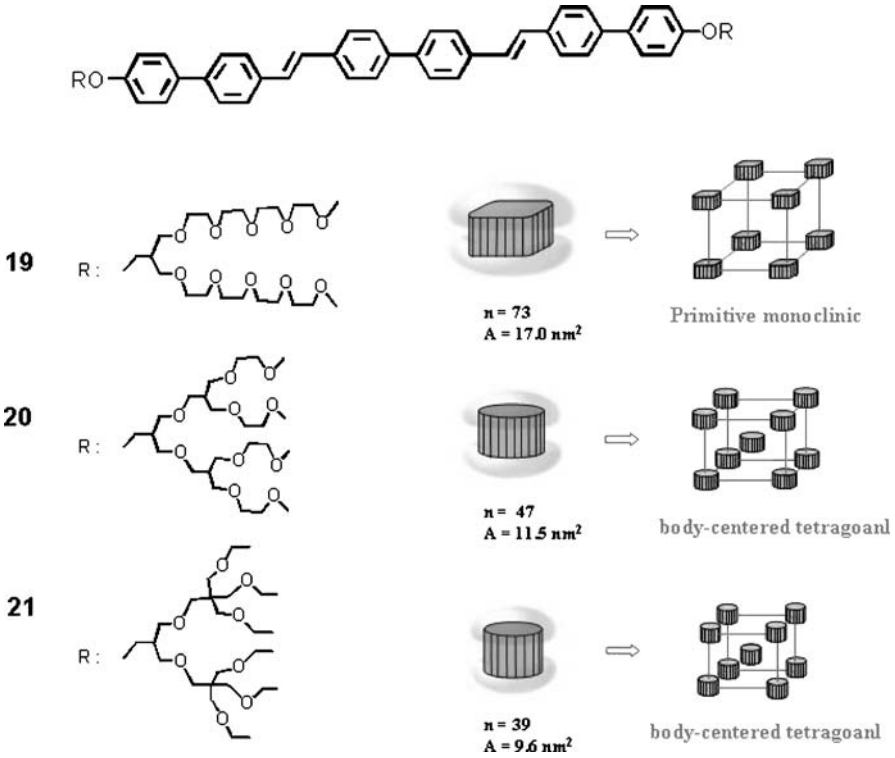

Fig. 13 Structural analysis of the supramolecular bundles assembled from molecular dumbbells **19–21**

the dissimilar parts of the molecule [32, 33, 80, 81]. Anisotropic ordering of the rod building blocks in the molecule should exclude chemically dissimilar dendritic segments. Because dendritic wedges have a large cross-section, they will encounter strong repulsive forces when trying to accommodate the density of the ordered rod building blocks. These repulsive forces could balance the favorable aggregation of rod building blocks and generate the finite aggregation of dumbbell-shaped molecules. As the cross-sectional area of the dendritic wedges increases, so do the repulsive forces between them. Consequently, this increase in steric repulsion could give rise to smaller aggregates that allow more space for the dendritic building blocks to adopt a less strained conformation.

If supramolecular bundles are formed spontaneously in bulk films, by inclusion of appropriate reactive groups it should be possible to convert these into molecular objects by cross-linking, while maintaining the precise size and shape of the rod bundles. A coil–rod–coil triblock molecule **22** based on linear PPO ($f_{coil} = 0.73$) with a reactive rod block self-assembles into discrete rod bundles that are encapsulated by PPO coils and subsequently organize

into a 3D hexagonal close-packed structure ($P6_3/mmc$ space group symmetry) in the melt state, confirmed by optical polarized microscopy and X-ray diffraction measurements [82]. Cross-linking of **22** under UV irradiation of 254 nm in a liquid crystalline phase under nitrogen atmosphere for several hours resulted in the formation of a completely soluble macromolecule. GPC traces showed that the molecular weight appeared to be 270 kDa, with a narrow molecular weight distribution after polymerization. Small-angle X-ray scattering revealed several reflections corresponding to a 3D hexagonal lattice with essentially the same lattice constants as those of the coil–rod–coil molecule, indicative of the preservation of the ordered symmetry and the dimensions of the discrete objects after polymerization. On the basis of these lattice constants and measured density, the number of constituent units in each object was estimated to be approximately 112. The 3D hexagonal close-packed structure was observed to recover after isolation from the solutions and transform into an isotropic liquid in the bulk state in a reversible way, suggesting that the macromolecular objects are shape-persistent in solution as well as being an isotropic liquid phase of the bulk (Fig. 14).

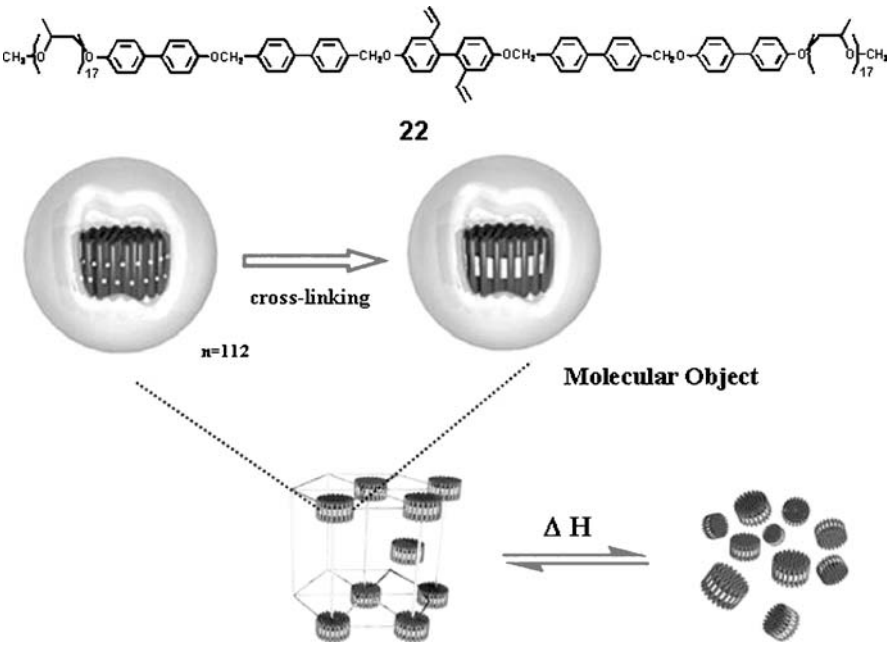

Fig. 14 Hexagonal close-packed liquid crystalline structure of the object and its transformation in to an isotropic liquid state

In contrast to linear coil, the triblock molecule **23**, consisting of bis(pentaethylene glycol) dendrons as coil segments at both ends of the rod with same rod building block, self-organizes into 2D columnar and 3D bicon-

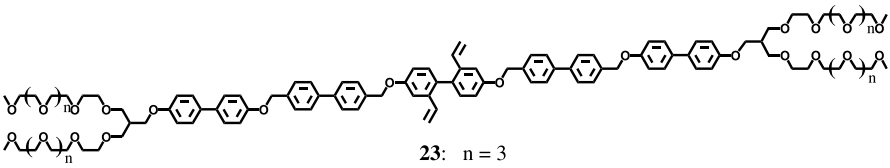

23: n = 3

tinuous cubic structures at the liquid crystalline state [83]. Photopolymerizations of **23** in liquid crystalline state proceed with preservation of the ordered supramolecular architectures and maintenance of the lattice dimensions. Photopolymerization of **23** in the bicontinuous cubic liquid crystalline state gives rise to a 3D ordered nanostructure, while in the hexagonal columnar liquid crystalline state it produces a 2D ordered nanostructure that in aqueous solution can be dispersed into individual nanofibers with a uniform diameter. The covalent stitching of reactive rod segments within the ordered state by photopolymerization offers a strategy to construct shape-persistent organic nanomaterials with well-defined size and shape, which potentially have applications in macromolecular electronics, nanoreactors, and hybrid nanomaterials.

A strategy to control the aggregation structure assembled from a rod building block may be accessible by incorporation of side groups into a rod block [84]. The side groups could lead to loose packing of the extended rod segments, which may modify the resulting supramolecular structure. A coil–rod–coil molecule (**24**) consisting of five biphenyl units connected through ether linkages as a rod block and PPO coils with the number of repeating units of 17, self-assembles into hexagonal perforated layers stacked in ABAB order in the melt. In contrast, a coil–rod–coil molecule (**25**) containing methyl

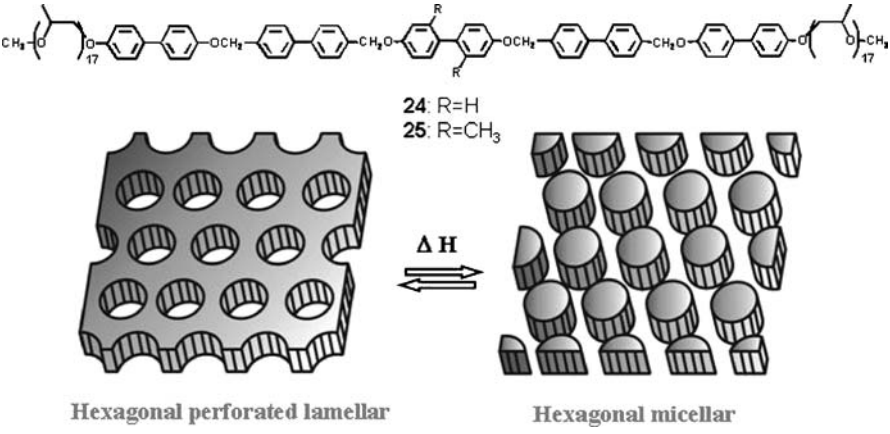

Fig. 15 Self-assembly of coil–rod–coil molecule **25** into the hexagonal perforated lamellar structure and subsequent conversion to hexagonal closed-packed bundles

side groups in its center shows an unusual supramolecular structural inversion, from perforated layers to discrete bundles, while maintaining a 3D hexagonal superlattice (Fig. 15). This phase transition on heating is most probably due to larger entropic contribution to the free energy associated with coil stretching [27, 85]. This indicates that the introduction of methyl side groups into a rod segment leads to the transformation of a 3D hexagonal perforated lamellar structure into a 3D hexagonally organized discrete bundles. This notable feature is that the incorporation of alkyl side groups into the center of a rod segment generates the structural inversion from organized coil perforations in rod layers to organized discrete rod-bundles in a coil matrix, while maintaining a 3D hexagonal superlattice. It is also remarkable that this structural inversion, retaining a 3D hexagonal superlattice, occurs directly without passing through any intermediate structures in a reversible way by changing the temperature. This abrupt structural change in rod-assembly may offer an attractive potential for use in supramolecular switch and thermal sensor.

3.3
BAB Rod–Coil–Rod Triblock Copolymers

Kato et al. reported on rod–coil–rod molecules consisting of rigid mesogenic cores and flexible PEO coils [86]. The small triblock molecule (**26**) was observed to exhibit smectic A liquid crystalline phase as determined by a combination of optical polarized microscopy and differential scanning calorimetry. The incorporation of $LiCF_3SO_3$ into the rod–coil–rod molecules shows significant mesophase stabilization. X-ray diffraction patterns revealed that complexation of **26** ($[Li^+]/[EO] = 0.05$) drastically reduces the layer spacing from 44 to 23 Å. This decrease is thought to be due to the interaction of the lithium salt with the ether oxygen, which results in a more coiled conformation of the PEO coil. Ion conductivities were also measured for complexes forming homeotropically aligned molecular orientation of the smectic phase. Interestingly, the highest conductivity was observed for the direction parallel to the layer (Fig. 16). However, the conductivities decrease in the polydomain sample, which disturbs the arrangement of ion paths. These results suggest that the self-organized rod–coil salt complexes can provide access to a novel strategy to construct ordered nanocomposite materials exhibiting low dimensional ionic conductivity.

Recently, rod–coil–rod triblock copolymers based on polydimethylsiloxane and polypeptide were reported by Rodriguez-Hernadez and coworkers [87]. In similar to rod–coil diblock copolymer with poly [poly(γ-benzyl-L-glutamate)], this triblock copolymer shows double hexagonal structure. The hexagonal array formed by α-helices remains stable at high temperatures. However, at a higher organization level the second hexagonal structure is lost at temperatures exceeding 160 °C. Moreover, this higher-level hexagonal

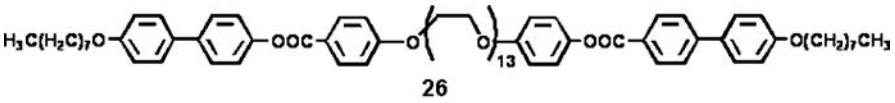

26

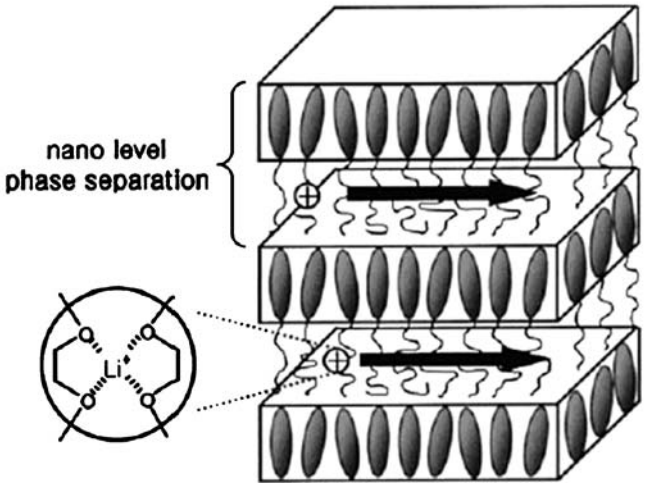

Fig. 16 Li^+ ion conduction for the complex of **26** in smectic A phase. Reprinted with permission from [86]. © 2000 American Chemical Society

structure can be reorganized on cooling indicating that this transition is reversible.

3.4 Novel Rod–Coil Triblock Copolymers

Precise control of supramolecular objects requires the rational design of molecular components, because the information determining their specific assembly should be encoded in their molecular architecture. Lee and coworkers reported on novel rod–coil molecules based on a hexa-*p*-phenylene rod and PEO chains that are fused together into a macrocyclic ring [88, 89]. The rod–coil macrocycle was observed to undergo double phase transitions in the crystalline state and to form ordered mesophases at higher temperature, as confirmed by differential scanning calorimetry. In the first crystalline state, **27** self-assembles into infinitely long ribbon-like 1D aggregates with uniform width and thickness. The cyclic geometry of the coil attached to one side of the rod would prohibit the 2D growth of a self-assembled structure. Instead, the aromatic rod segments should be strongly driven to aggregate in one dimension to produce a laterally stacked bilayer through microphase separation between the rod and coil segments, and π–π interactions. In the second crystalline state, the rod segments of **27** self-assemble into discrete ribbon-like

aggregates with a laterally stacked bilayer encapsulated by cyclic aliphatic chains in which the rod building blocks are arranged with their long axes parallel to each other. Subsequently, the ribbon nanostructures self-organize into a 3D body-centered orthorhombic superlattice (Fig. 17a). Both steric forces and crystallization of the rod segments are believed to play an important part in the formation of discrete ribbons [27]. The tendency of the rod building blocks to pack into a parallel arrangement accompanies a strong coil deformation on heating. To reduce the energetic penalty associated with coil deformation, while maintaining crystalline order of the rod segments, infinitely long ribbons would break up into discrete ribbons that allow coils to splay at the periphery of the supramolecular unit. In the birefringent mesophase of **27**, small-angle X-ray scattering showed several reflections, corresponding to a 3D body-centered tetragonal superlattice with lattice parameters of 6.1 and 5.9 nm Wide-angle scattering showed only a broad halo, indicative of liquid crystalline order of the rod segments within domains. On cooling from the optically isotropic mesophase, straight lines growing in four directions with an angle of 90° could be observed in the polarized optical microscope with a final development of mosaic texture, indicative of the presence of a 3D noncubic lattice [76]. On further heating to the optically isotropic mesophase, the small-angle X-ray scattering pattern showed three sharp peaks that could be indexed as a 3D body-centered cubic phase with a lattice parameter of 5.7 nm. According to the number of molecules per aggregate, by using the lattice constants and densities, aggregates of **27** were estimated to contain about 40 molecules each. Considering microphase separation between the rod and coil segments, the aggregation of 40 rod–coil macrocyclic molecules in an ag-

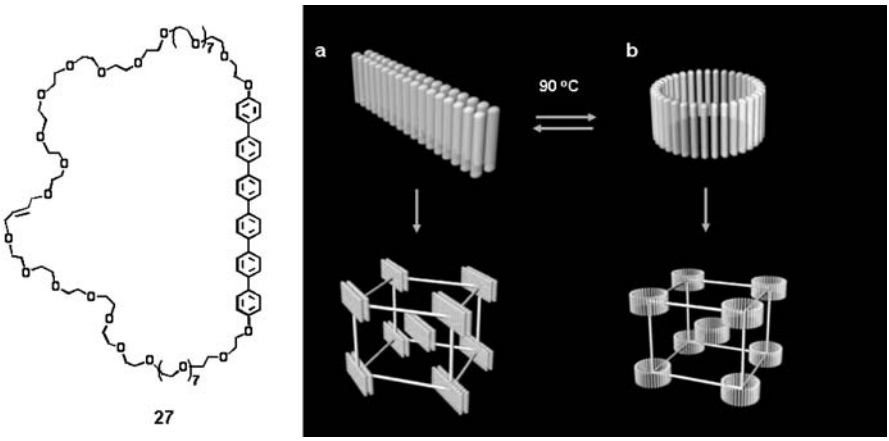

Fig. 17 Supramolecular architectures from self-assembly of rod–coil macrocycles. **a** Body-centered orthorhombic structures from ribbon-like aggregates; **b** body-centered tetragonal structures from barrel-like aggregates

gregate can be viewed as generating a barrel-like supramolecular structure in which the rods are aligned axially with their preferred direction, and both the interior and exterior of the barrel are filled by the coil segments (Fig. 17b). These results indicate that a flat discrete ribbon-like aggregate transforms into a curved barrel-like structure on crystal melting of the rod segments. This transformation may be rationalized by considering end-to-end connection by rolling of the discrete ribbon [90]. With increasing temperature, space crowding of coil segments would be larger because of greater thermal motion of the flexible chains. A ribbon-like ordering of the rod segments would confine flexible coil segments to a flat interface, forcing a strong deformation of the flexible coils and making the system energetically unfavorable. To release this deformation without sacrificing anisotropic order of the rod segments, the flat ribbons would roll to form curved barrels.

Tschierske and coworkers reported on new complex liquid crystalline phases of polyphilic block molecules or their metal complex [91–93]. These triblock rod–coil molecules consist of a rod-like *p*-terphenylene unit, and two hydrophobic alkyl chains at both ends of the rod, and oligo(ethylene glycol) with a terminal carbohydrate unit at a lateral position of the rod [94]. Depending on the size of the hydrophilic and hydrophobic segments, a series of unusual liquid crystalline phases were detected (Fig. 18). When the carbohydrate unit is directly conjugated to the rod building block, a simple smectic (S_A) phase was observed. In this liquid crystalline phase, the molecules are

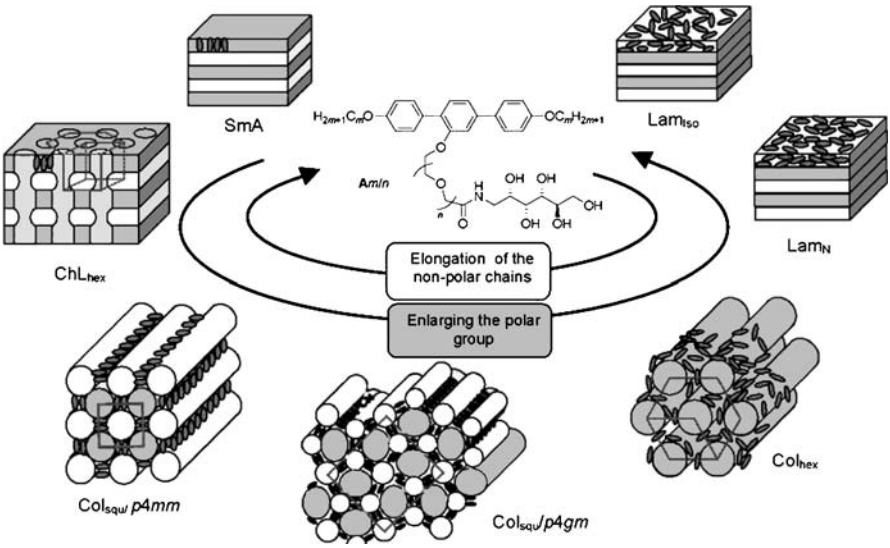

Fig. 18 Supramolecular architectures from self-assembly of facial rod–coil molecules with lateral hydrophilic groups as a function of the size of polar lateral and hydrophobic terminal groups. Reprinted with permission from [94]. © 2005 American Chemical Society

organized in layers, where the terphenyl units and the lateral carbohydrate units are incorporated in the layer and these sublayers are separated by layers of alkyl chains. Increasing the space unit (oligo(ethylene glycol)) transformed smectic mesophase into a hexagonal channeled layer phase (ChL_{hex}). This mesophase appears almost completely black between crossed polarizers and shows a very high viscosity, indicating an optically uniaxial mesophase with a 3D lattice. Small-angle X-ray diffraction pattern shows five spots that could be indexed as a 3D hexagonal lattice (*P*6/*mmm*). This mesophase consists of alternating layers of aromatic units and aliphatic chains, penetrated at right angles by columns with undulating profiles containing the polar lateral groups. Accordingly, the structure consists of layers perforated by an array of polar channels, which are arranged on a 2D hexagonal lattice.

When the space units were increased further, rod–coil molecules form square columnar mesophases confirmed by optical polarized microscopy and X-ray diffraction pattern. The polar column is located inside the square, providing strong attractive intermolecular interactions via hydrogen bonding and the hydrophobic columns containing alkyl chains are at the corners interconnecting the aromatic rods end-to-end. For the columnar mesophases, the rigid-rod segments tend to restrict the side length of the polygons within relatively narrow limits, giving rise to columns with a well-defined polygonal shape. The lateral chains fill the interior of the polygons; the terminal chains form the corners of these polygons and connect the rigid rods. Thus, the number of sides of the polygons critically depends on the volume of the lateral chain and the length of the molecule. Extending the hydrophilic chain, raising the temperature, or reducing the alkyl chain length leads to a transition from square to hexagonal columnar phases. Due to amphotropic characteristics of rod–coil molecules, new types of laminated mesophases also were induced by solvent (Fig. 18).

4
Multiblock Rod–Coil System

4.1
Main-Chain Rod–Coil Copolymers

The rod–coil approach as a means to manipulate supramolecular structure as a function of rod volume fraction was reported to be extended to main chain multiblock copolymer systems, which generate bicontinuous cubic and hexagonal columnar mesophases depending on the rod-to-coil volume fraction [95, 96]. For example, rod–coil multiblock copolymer (**28**) based on short length of coil (rod volume fraction, $f_{rod} = 0.38$) exhibits a bicontinuous cubic mesophase, while copolymer (**29**) based on higher coil volume fraction ($f_{rod} = 0.29$) shows a hexagonal columnar mesophase. A notable feature

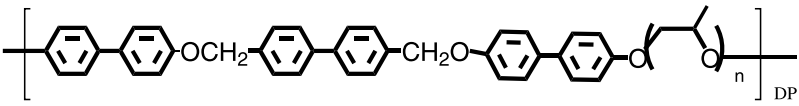

28 n = 12
29 n = 18

of this system is the ability of the main-chain liquid crystalline polymers based on a rod building block to self-assemble into ordered structures with curved interfaces. Formation of supramolecular columnar and bicontinuous cubic assemblies in the rod–coil copolymers is in marked contrast to the general behavior of conventional liquid crystalline polymers based on rod-like mesogens and segmented copolymers based on alternating rigid and flexible segments [97, 98]. Formation of the ordered structures with interfacial curvature from the main-chain rod–coil copolymers can be rationalized by considering entropic penalties associated with coil stretching and anisotropic arrangement of rod segments. Bulky PPO coils induce curvature at the rod/coil interface (arising from the connectivity of the rod and coils), constraint of constant density, and minimization of coil stretching. At the interface separating the rod and coil domains in the layered smectic structure, the relatively smaller area per junction favored by rod block results in chain stretching of the coil block, which is energetically unfavorable. Therefore, the rod–coil copolymers self-assemble into bicontinuous cubic or hexagonal columnar structures with larger interfacial area, instead of a layered smectic structure.

In contrast to this, another strategy for manipulating the supramolecular structure at constant rod-to-coil volume ratio can also be accessible by varying the number of grafting sites per rod, which might be closely related to the grafting density at the interface separating rod and coil segments. For this reason, **30**, **31** and **32**, with rod–coil repeating units consisting of three biphenyl units connected by methylene ether linkages as the rod block and PPO with 13 PO repeating units as the coil block, were prepared [99]. All of the oligomers are self-organized into ordered supramolecular structures that differ significantly on variation of the number of repeating units, as confirmed by X-ray scattering. The molecule **30** shows a bicontinuous cubic liquid crystalline structure. In contrast, the molecule **31** shows a 2D rectangular crystalline and a tetragonal columnar (col_t) liquid crystalline structures, while the molecule **32** displays a hexagonal columnar structure in both their solid state and mesophase (Fig. 19). These results show that self-assembled liquid crystalline structures, from 3D bicontinuous cubic, 2D tetragonal, to 2D hexagonal lattices are formed by rod–coil structures that differ only in the number of repeating units.

This interesting variation of self-assembled structures, at an identical rod-to-coil volume ratio, can be explained by considering the density of grafting sites at the interface separated by rod and coil. On increasing the number

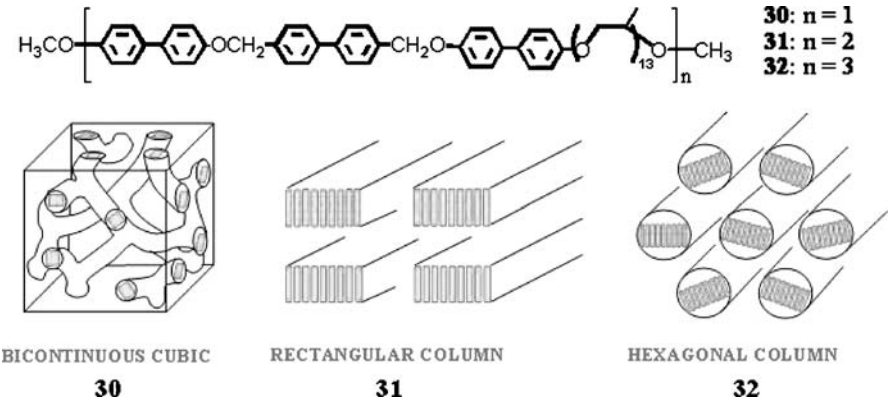

Fig. 19 Mesophase of the rod–coil multiblock molecules depending on rod–coil repeating units

of rod–coil repeating units, the density of grafting sites at the interface will be increased due to an increase in the average number of coils grafted to a rod, which results in strong entropic penalty associated with coil stretching at the rod–coil interface. To reduce this coil stretching, a bicontinuous cubic structure of the monomer would break up into 2D cylindrical domains in which less confinement and deformation of coil segments occur. These results demonstrate that systematic variation of the number of repeating units in the rod–coil multiblock oligomers can provide a strategy to regulate the liquid crystalline phase, from bicontinuous cubic, 2D tetragonal columnar, to 2D hexagonal columnar structures.

Picken et al. recently reported on the phase behavior of a series of rod–coil multiblock copolymers comprised of alternating poly(*p*-phenylene terephthalamide) as a rod building block and polyamide blocks as a coil part [100]. When the mole fraction of rod parts exceeds 0.5 these polymers show lyotropic liquid crystalline structure in concentrated sulfuric acid solution. The critical concentration for the formation of a nematic phase increases with increasing fraction of the flexible fragments in the block copolymer, and coupling of flexible chains to rod-like oligomers increases the stability of the liquid crystalline phase. This means that the liquid crystallinity involves induced orientation of the flexible polyamide coils. The incorporation of aramid blocks in the copolymer induces stretching of the flexible coils, and this stretching will make the copolymer stiffer.

4.2
Side-Chain Rod–Coil Copolymers

A novel strategy for manipulating the supramolecular structure can also be accessed by converting the rod–coil monomer into a side chain polymer. Lee

et al. reported on the supramolecular behavior of the liquid crystalline state of rod–coil monomers and their corresponding polymer, consisting of a rigid rod made up of two biphenyls connected through ester linkages and flexible PPO coils (Fig. 20) [101]. Polymerization of the rod–coil monomer into a side chain polymer gives rise to a large structural transformation from 2D hexagonal to 3D cubic structures. Polymerization of the acryl group stitches coil segments into a polymer backbone and produces selective shrinkage of coil domains in the microphase-separated supramolecular structure. This is responsible for the transformation of the hexagonal columnar structure exhibited by the monomer into a bicontinuous cubic structure that allows less volume for the coil upon polymerization.

Incorporation of aromatic rigid-rod segments in the side chain of block copolymer can play a role in forming well-ordered nanostructures. Finkelmann et al. reported that block copolymer consisting of poly(hexyl methacrylate) as a coil and an azobenzene moiety as a rod showed liquid crystalline mesophases including smectic A and bicontinuous cubic phase [102]. Based on TEM experiments, the smectic layers of rod units are oriented either parallel or perpendicular to the lamellar morphology. The deformation of the anisotropic phase structure leads to the formation of a gyroid morphology. Hayakawa et al. also reported on side-chain rod–coil block copolymer composed of a poly(styrene-*b*-substituted isoprene) with an oligothiophene derivatives [103]. DSC and X-ray data showed characteristics of a liquid–crystalline smectic mesophase of the π-stacked oligothiophene blocks. TEM images indicated that the phase-separated polystyrene and polyisoprene with oligothiophene-modified side chain were aligned layer by layer due to the self-assembly characteristic of the diblock copolymer. The combination of a liquid-crystal phase and phase-separated nanodomain structures formed extremely regular hierarchical structures.

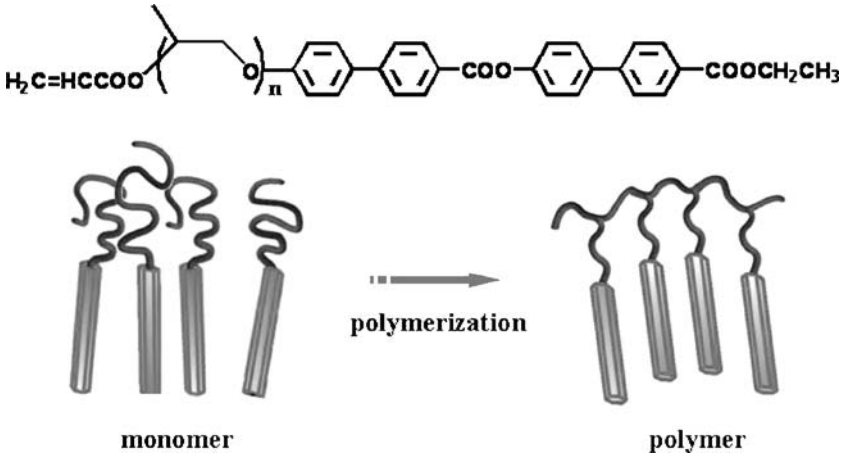

Fig. 20 Side-chain rod–coil polymer from polymerization

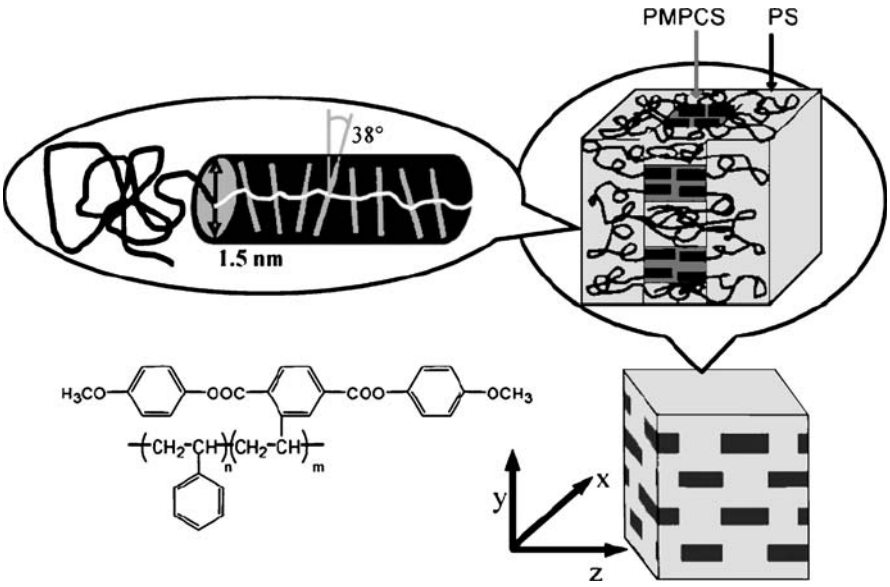

Fig. 21 Perforated lamellar structure hierarchically formed by poly(styrene-*b*-(2,5-bis[4-methoxyphenyl] oxycarbonyl)styrene) structure. Reprinted with permission from [107]. © 2005 American Chemical Society

By laterally linking aromatic mesogens directly to polymer backbones, mesogen-jacketed liquid crystalline polymers as a rod–coil copolymer can be achieved [104–106]. Zhou and coworkers reported on the supramolecular structures of these type of rod–coil copolymers composed of poly(styrene-*b*-(2,5-bis[4-methoxyphenyl] oxycarbonyl)styrene) [107]. The strong interaction between the side-chain mesogens and polymer backbone induces formation of rigid columns of mesogens. The macromolecular columns possess orientational order and then these rigid columns self-assemble into a columnar nematic of hexagonal mesophase. On increasing the volume fraction of polystyrene blocks, the mesophases change from lamellar to perforated lamellar structures, where the polystyrene perforates the macromolecular rigid column layer of poly(2,5-bis[4-methoxyphenyl]oxycarbonyl)styrene (Fig. 21).

5 Conclusions

A variety of different supramolecular structures can be formed by self-assembly of mesogenic rod building blocks with terminally attached polyether coils. This unique phase behavior seems to originate from a combination of organizing forces. These include the mutual repulsion of the dissimilar blocks and packing constraints imposed by the connecting of each block, and the

tendency of the rod block to form orientational order. The incorporation of different rod-like segments such as helical rods, low molar mass mesogenic rods, and conjugated rods as a part of the main chain in rod–coil molecular architecture has already proven to be an effective way to manipulate supramolecular structures in nanoscale dimensions. Depending on the relative volume fraction of rigid and flexible segments, and the chemical structure of these segments, rod–coil copolymers and their low molar mass homologs self-assemble into a variety of supramolecular structures through the combination of shape complimentarity and microphase separation of rod and coil segments as an organizing force. The supramolecular structures assembled by rod segments in rod–coil systems include sheets, cylinders, finite nanostructures, and even perforated sheets that organize into 1D, 2D, and 3D superlattices, respectively. It should be noted that self-assembly can be used to prepare well-defined macromolecular nanoobjects that are not possible to prepare by conventional synthetic methodologies, when the rod–coil copolymers self-assemble into discrete supramolecular structures. In this respect, many synthetic strategies have been developed that allow the incorporation of functional rod segments into well-defined rod–coil architectures for specific properties. Electron transfer, second harmonic generation, and piezoelectricity have been reported for supramolecular structures of rod–coil copolymers containing conjugated rods or highly polar end groups [108–110]. Many more rod–coil systems are expected to be developed soon for possible applications as diverse as molecular materials for nanotechnology, supramolecular reactors, periodic porous materials, transport membranes, and biomimic materials.

References

1. Lehn JM (1995) Supramolecular chemistry, concepts and perspective. VCH, Weinheim
2. Lee M, Cho BK, Zin WC (2001) Chem Rev 101:3869
3. Klok HA, Lecommandoux S (2001) Adv Mater 13:1217
4. Stupp SI, Pralle MU, Tew GN, Li L, Sayar M, Zubarev ER (2000) MRS Bull 42
5. Loos K, Munoz-Guerra S (2000) Microstructure and crystallization of rigid-coil comblike polymers and block copolymers. In: Ciferri A (ed) Supramolecular polymers, Chap 7. Dekker, New York
6. Ryu JH, Cho BK, Lee M (2006) Bull Korean Chem Soc 27:1270
7. Collings PJ, Hird M (1997) Introduction to liquid crystals: chemistry and physics. Taylor and Francis, London
8. Tschierske C (2001) J Mater Chem 11:2647
9. Kato T, Mizoshita N, Kishimoto K (2006) Angew Chem Int Ed 45:38
10. Mingos DMP (1999) Liquid crystal II. Springer, Berlin Heidelberg New York
11. Föster S, Plantenberg T (2002) Angew Chem Int Ed 41:688
12. Föster S, Antonietti M (1998) Adv Mater 10:195
13. Khandpur AK, Föster S, Bates FS, Hamley IW, Ryan AJ, Bras W, Almdal K, Mortensen K (1995) Macromolecules 28:8796

14. Zeng F, Zimmerman SC (1997) Chem Rev 97:1681
15. Brunsveld L, Folmer BJB, Meijer EW, Sijbesma RP (2001) Chem Rev 101:4071
16. Hennigar TL, MacQuarrie DC, Losier P, Rogers RD, Zaworotko MJ (1997) Angew Chem Int Ed 36:972
17. Kaes C, Hosseini MW, Rickard CEF, Skelton BW, White AH (1998) Angew Chem Int Ed 37:920
18. Cui Y, Lee SJ, Lin W (2003) J Am Chem Soc 125:6014
19. Tschierske C (1998) J Mater Chem 8:1485
20. Berresheim AJ, Müller B, Müllen K (1999) Chem Rev 99:1747
21. Steffen W, Köhler B, Altmann M, Scherf U, Stitzer K, Loye HC, Bunz UHF (2001) Chem Eur J 7:117
22. Jeneckhe SA, Chen XL (1999) Science 283:372
23. Lee M, Yoo YS (2002) J Mater Chem 12:2161
24. Stupp SI (1998) Curr Opin Colloid Interface Sci 3:20
25. Semenov AN, Vasilenko SV (1986) Sov Phys JETP 63:70
26. Semenov AN (1991) Mol Cryst Liq Cryst 209:191
27. Williams DRM, Fredrickson GH (1992) Macromolecules 25:3561
28. Halperin A (1990) Macromolecules 23:2724
29. Lee M, Oh NK (1996) J Mater Chem 6:1079
30. Lee M, Oh NK, Choi MG (1996) Polym Bull 37:511
31. Lee M, Oh NK, Zin WC (1996) Chem Commun, p 1787
32. Lee M, Cho BK, Kim H, Zin WC (1998) Angew Chem Int Ed 37:638
33. Lee M, Cho BK, Kim H, Yoon JY, Zin WC (1998) J Am Chem Soc 120:9168
34. Hamley IW, Ropp KA, Rosedale JH, Bates FS, Almdal K, Mortensen K (1993) Macromolecules 26:5959
35. Bates FS, Schulz MF, Khandpur AK, Foster S, Rosedale JH, Almdal K, Mortensen K (1994) Faraday Discuss Chem Soc 98:7
36. Park MH, Ryu JH, Lee E, Han KH, Chung YW, Cho BK, Lee M (2006) Macromol Rapid Commun 27:1684
37. Radzilowsk JL, Wu JL, Stupp SI (1993) Macromolecules 26:879
38. Radzilowsk JL, Stupp SI (1994) Macromolecules 27:7747
39. Radzilowsk JL, Carragher BO, Stupp SI (1997) Macromolecules 30:2110
40. Stupp SI, Lebonheur V, Walker K, Li LS, Huggins KE, Keser M, Amstutz A (1997) Science 276:384
41. Zubarev ER, Pralle MU, Li L, Stupp SI (1999) Science 283:523
42. Zubarev ER, Pralle MU, Sone ED, Stupp SI (2001) J Am Chem Soc 123:4105
43. Li W, Wang H, Yu L, Morkved TL, Jaeger HM (1999) Macromolecules 32:3034
44. Wang H, Wang HH, Urban VS, Littrell KC, Thiyagarajan P, Yu L (2000) J Am Chem Soc 122:6855
45. Kim JK, Hong MK, Ahn JH, Lee M (2005) Angew Chem Int Ed 44:328
46. Ungar G, Liu Y, Zeng X, Percec V, Cho WD (2003) Science 299:1208
47. Kato T, Matsuoka T, Nishii M, Kamikawa Y, Kanie K, Nishimura T, Yashima E, Ujiie S (2004) Angew Chem Int Ed 43:1969
48. Fréchet JMJ (2002) Proc Natl Acad Sci USA 99:4782
49. Bur AJ, Fetters LJ (1976) Chem Rev 76:727
50. Fetters LJ, Yu H (1971) Macromolecules 4:385
51. Aharoni SM (1979) Macromolecules 12:94
52. Aharoni SM, Walsh EK (1979) Macromolecules 12:271
53. Aharoni SM (1980) J Polym Sci Polym Phys Ed 18:1439
54. Chen JT, Thomas EL, Ober CK, Hwang SS (1995) Macromolecules 28:1688

55. Chen JT, Thomas EL, Ober CK, Mao G (1996) Science 273:343
56. Park JW, Thomas EL (2003) Adv Mater 15:585
57. Park JW, Thomas EL (2004) Macromolecules 37:3532
58. van der Veen MH, de Boer B, Stalmach U, van de Wetering KI, Hadziioannou G (2004) Macromolecules 37:3673
59. Gallot B (1996) Prog Polym Sci 21:1035
60. Zhang G, Fournier MJ, Mason TL, Tirrell DA (1992) Macromolecules 25:3601
61. Yu SM, Conticello VP, Zhang G, Kayser C, Fournier MJ, Mason TL, Tirrell DA (1997) Nature 389:167
62. Klok HA, Langenwalter JF, Lecommandoux S (2000) Macromolecules 33:7819
63. Lecommandoux S, Achard MF, Langenwalter JF, Klok HA (2001) Macromolecules 34:9100
64. Minich EA, Nowak AP, Deming TJ, Pochan DJ (2004) Polymer 45:1951
65. Hanski S, Houbenov N, Ruokolainen J, Chondronicola D, Iatrou H, Hadjichristidis N, Ikkala O (2006) Biomacromolecules 7:3379
66. Stadler R, Auschra C, Beckmann J, Krappe U, Voigt-Martin I, Leibler L (1995) Macromolecules 28:3080
67. Lee M, Lee DW, Cho BK, Yoon JY, Zin WC (1998) J Am Chem Soc 120:13258
68. Schwab M, Stuehn B (1996) Phys Rev Lett 76:924
69. Sakamota N, Hashimoto T, Han CD, Vaidya N (1997) Macromolecules 30:1621
70. Oh NK, Zin WC, Im JH, Ryu JH, Lee M (2004) Chem Commun, p 1092
71. Jang CJ, Ryu JH, Lee JD, Sohn D, Lee M (2004) Chem Mater 16:4226
72. Percec V, Cho WD, Ungar G, Yeardley DJP (2001) J Am Chem Soc 123:1302
73. Yeardley DJP, Ungar G, Percec V, Holerca MN, Johansson G (2000) J Am Chem Soc 122:1684
74. Hulvat JF, Sofos M, Tajima K, Stupp SI (2005) J Am Chem Soc 127:366
75. Lin HC, Lee KW, Tsai CM, Wei KH (2006) Macromolecules 39:3808
76. Lee M, Cho BK, Jang YG, Zin WC (2000) J Am Chem Soc 122:7449
77. Cho BK, Chung YW, Lee M (2005) Macromolecules 38:10261
78. Cho BK, Lee M, Oh NK, Zin WC (2001) J Am Chem Soc 123:9677
79. Lee M, Jeong YS, Cho BK, Oh NK, Zin WC (2002) Chem Eur J 8:876
80. Henglein A (1989) Chem Rev 89:1861
81. Murray BC, Norris DJ, Bawendi MG (1993) J Am Chem Soc 115:8706
82. Jin LY, Ahn JH, Lee M (2004) J Am Chem Soc 126:12208
83. Jin LY, Bae J, Ryu JH, Lee M (2006) Angew Chem Int Ed 45:650
84. Jin LY, Bae J, Ahn JH, Lee M (2005) Chem Commun, p 1197
85. Müller M, Schich M (1996) Macromolecules 29:8900
86. Ohtake T, Ogasawara M, Ito-Akita K, Nishina N, Ujie S, Ohno H, Kato T (2000) Chem Mater 12:782
87. Ibarboure E, Rodríguez-hernández J, Papon E (2006) J Polym Sci Part A Polym Chem 44:4668
88. Yang WY, Ahn JH, Yoo YS, Oh NK, Lee M (2005) Nat Mater 4:399
89. Yang WY, Lee E, Lee M (2006) J Am Chem Soc 128:3484
90. In M, Aguerre-Chariol O, Zana R (1999) J Phys Chem B 103:7747
91. Chen B, Baumeister U, Diele S, Das MK, Zeng XB, Ungar G, Tschierske C (2004) J Am Chem Soc 126:8608
92. Chen B, Zeng XB, Baumeister U, Diele S, Ungar G, Tschierske C (2004) Angew Chem Int Ed 43:4621
93. Chen B, Zeng XB, Baumeister U, Ungar G, Tschierske C (2005) Science 307:96

94. Chen B, Baumeister U, Pelzl G, Das MK, Zeng XB, Ungar G, Tschierske C (2005) J Am Chem Soc 127:16578
95. Lee M, Cho BK, Kang YS, Zin WC (1999) Macromolecules 32:7688
96. Lee M, Cho BK, Kang YS, Zin WC (1999) Macromolecules 32:8531
97. Eisenbach CD, Heinemann T, Ribbe A, Stadler E (1994) Macromol Symp 77:125
98. Osaheni JA, Jenekhe SA (1995) J Am Chem Soc 117:7389
99. Lee M, Cho BK, Oh NK, Zin WC (2001) Macromolecules 34:1987
100. de Ruijter C, Jager WF, Li L, Picken SJ (2006) Macromolecules 39:4411
101. Cho BK, Choi MG, Zin WC, Lee M (2002) Macromolecules 35:4845
102. Schneider A, Zanna JJ, Yamada M, Finkelmann H, Thomann R (2000) Macromolecules 33:649
103. Hayakawa T, Horiuchi S (2003) Angew Chem Int Ed 42:2285
104. Zhou QF, Zhu XL, Wen ZQ (1989) Macromolecules 22:491
105. Zhang D, Liu YX, Wan XH, Zhou QF (1999) Macromolecules 32:5183
106. Gopalan P, Ober CK (2001) Macromolecules 34:5120
107. Tenneti KK, Chen X, Li CY, Tu Y, Wan X, Zhou QF, Sics I, Hsiao BS (2005) J Am Chem Soc 127:15481
108. Pralle MU, Whitaker CM, Braun PV, Stupp SI (2000) Macromolecules 33:3550
109. Tew GN, Pralle MU, Stupp SI (2000) Angew Chem Int Ed 39:517
110. Stalmach U, de Boer B, Videlot C, van Hutten PF, Hadziioannou G (2000) J Am Chem Soc 122:5464

Struct Bond (2008) 128: 99–117
DOI 10.1007/430_2007_075

Published online: 12 December 2007

Liquid Crystalline Blue Phases

Hirotsugu Kikuchi

Institute for Materials Chemistry and Engineering, Kyushu University,
6-1 Kasuga-Koen, 816-8580 Kasuga, Fukuoka, Japan
kikuchi@cm.kyushu-u.ac.jp

Abstract Blue phases are known to appear in chiral liquid crystals in a small temperature range between the chiral nematic phase and the isotropic one. They are optically active, non-birefringent, and they show Bragg diffraction of light in the visible wavelength, measuring several hundred nanometers. Their exotic structures and properties result from the competition between chiral forces and packing topology. Recently, the blue phases have attracted the attention in the field of optoelectronics and photonics. The following article summarizes the basic properties, especially the frustration in the double twist molecular alignment which is the origin of stabilization of the blue phase, and history of the blue phase studies, and describes significant advances that have been recently reported.

Keywords Blue phase · Frustration · Double twist · Electrooptic effect · Photonic crystal

1 Introduction

"So, are they called 'blue phases' because they are blue?" This is a question often asked by many. It is true that the naming might have originated from

the color, however, the color alone does not reveal the true nature of such phases. So mysterious are blue phases, in fact, that scholars had no other basis on which to name them but to refer to their color. This overly simple name seems to reveal all the more how confused the researchers involved in the first understanding of these phases must have been.

Early studies on blue phase were assuredly marked by one astonishing discovery after another, such as the narrow stable temperature range, optical isotropy, three-dimensional order, and frustration. These unique characteristics, not observed in any other liquid crystal phases, have enthralled these pioneering researchers, as is obvious from their writings.

Blue phases, once a subject of academic and basic studies only, are now attracting the attention of researchers in a range of application-based fields. These phases, once a headache for many scientists, are in no way easy to understand, even for the leading engineers of today. This chapter aims to present, as plainly as possible, the history of study on blue phases, some of their essential nature, and the recent progress made in the field.

2
What are Blue Phases?

Blue phases are liquid crystal phases that appear between chiral nematic phases with relatively short helical pitches and isotropic phases. Generally, blue phases have the following characteristics:

1. Narrow temperature range (typically ca. 1 K);
2. Optical isotropy;
3. Optical activity;
4. There are three kinds of phases, blue phase I (BP I), blue phase II (BP II), and blue phase III (BP III), in order of increasing temperature.
5. BP I has body-centered cubic symmetry, BP II has simple cubic symmetry, and BP III has isotropic symmetry.
6. The unit lattices of BPs I and II have a lattice parameter of approximately 200 to 300 nm, with Bragg diffraction in the ultraviolet and visible region. Understanding of the basic nature of blue phases up to the 1990s was summarized in many distinguished articles [1–6].

3
Discovery of Blue Phases

As is well known, Reinitzer and Lehmann discovered liquid crystals some 120 years ago, in 1888. A letter exchanged between these two pioneering researches contained descriptions suggestive of blue phases even at that time.

As a cholesteric compound slowly cools from the isotropic phase, blue scattering can be seen momentarily immediately prior to the phase transition to the chiral nematic (cholesteric) phase. One of the discoverers of liquid crystals, Reinitzer, did not miss this extremely subtle phenomenon [7]. However, it took another 80 years before blue phases were recognized by the academic world as specific liquid crystal phases. Although this long delay may have arisen because the initial discovery was ahead of its time, the lag also reveals how these phases were ignored for many years. Not even a single paper on blue phases can be found for the 34 years from 1922 to 1956. Two major reasons for why these phases failed to catch the attention of researchers is that the phases did not exhibit birefringence, a most typical characteristic of liquid crystals, and that the stable temperature range was extremely narrow (typically ca. 1 K). For over 80 years, and even though the unusual phenomenon of blue phases was occasionally encountered by researchers, the observation was ascribed to a metastable state of the chiral nematic phase, and further investigation of the phase's true nature was never pursued.

Then, between 1970 and 1990, this misunderstanding was resolved, and the study of blue phases abruptly became popular, particularly in the field of physics, leading to the discovery of frustrated phases, one of the most remarkable events in the entire history of materials science. Now, it must not be forgotten that one factor leading to this great discovery was the development of liquid crystal chemistry in the 1950s. While industrial applications of liquid crystals were not predicted back then, the foundations of the synthetic chemistry of liquid crystals had been laid. George William Gray, a British chemist, was one of the builders of this foundation. He conducted systematic studies of the phase transition of cholesteric compounds and discovered that the strange phenomenon of the blue phase, as witnessed by Reinitzer, commonly takes place in many of the cholesteric compounds [8]. Then, in 1969, Saupe made the most foresighted proposal in the history of blue phase studies [9]. He focused on the empirically discovered fact that the state of this phenomenon is optically isotropic while having unusually strong optical activity, and thus proposed an innovative model of a huge cubic crystal formed by the three-dimensional expansion of a twisted structure of chiral molecules. This model, although ultimately found erroneous in certain details, provided a largely accurate description of the true nature of blue phases. The model suggested a state in which three-dimensional order exists between a chiral nematic phase with one-dimensional order and a disordered isotropic phase. It can be easily imagined that such a hypothesis was very bold in Saupe's time. It is thus admirable that Saupe had this profound insight in the days when blue phases were still in the dark and the very name, "blue phases", was non-existent.

In 1973, Coates and Gray came up with the name, "blue phases", to indicate this unusual state, and began to treat the phase as one of the liquid crystal phases [10]. At last, the era of widespread study of blue phases had arrived.

A search of the Web of Science using “blue phase” or “blue phases” as a keyword reveals a rapid expansion in the number of studies since then, from only seven in the 1970s to 174 in the 1980s and 232 in the 1990s.

4 Simple and Double Twists

The results of experiments examining light diffraction proved that blue phases form huge cubic crystals with a lattice parameter approximately equivalent to the wavelengths of light (around a few hundred nanometers). This means that a single unit lattice contains as many as 10^7 molecules. The toughest challenge the researchers of blue phases faced was identifying the structural arrangement of this many molecules within such a lattice. The basic form of this arrangement is a “twist”.

Let us consider molecular arrangements based on the twist. As shown in Fig. 1, a chiral nematic phase consists of a helical structure of molecular arrangements. Such a structure is commonly found in nature and is one of the typical self-assembled molecular arrangements. Generally, a liquid crystal phase with a helical structure either consists of or contains chiral molecules. Due to the intermolecular interaction among the chiral molecules, the rod-shaped liquid crystal molecules become more stable when their long axes are slightly twisted together, rather than aligned in parallel. It is understood that the liquid crystal molecules form a helix, since the sense of the twist is the same for all molecules. In this case, the twisted molecular structure is formed along a single axis in the lateral molecular direction (perpendicular to the long axis), and is known as a “simple twist”. Each molecule rotates rapidly

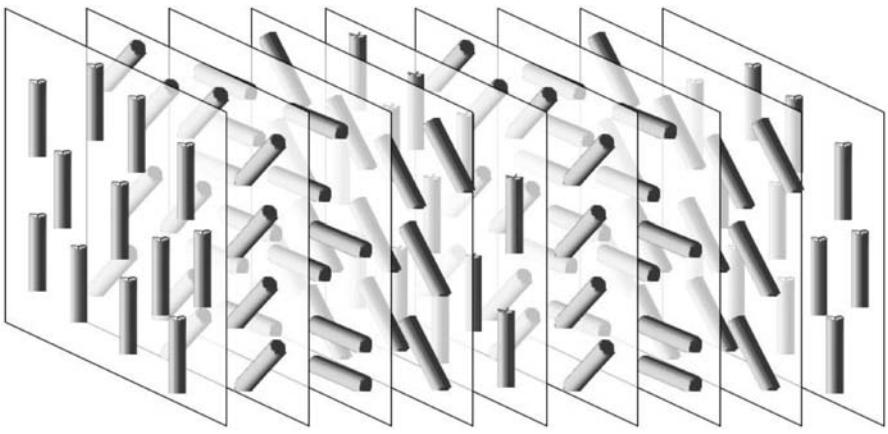

Fig. 1 Helical arrangements of molecules in a chiral nematic phase

around its long axis, and the intermolecular interaction should therefore work isotropically in all of the lateral directions. For this reason, the interaction is expected to induce twist arrangements for all the neighboring molecules in the lateral directions. It should be noted, however, that a simple twist results in directions, perpendicular to the helical axis, in which no twisting is induced. That is to say, the molecular interaction to be twisted isotropically in all of the lateral directions is not satisfied in the simple twist. Why does the chiral nematic phase form a simple twist despite of the unsatisfactory arrangement? Now let us consider the geometrical continuity of twisting arrangements. As shown in Fig. 2, the rod-shaped molecules are arranged so that their long axes are parallel to the x-axis, with no twisting along the long axis of molecules. Then, beginning at Point A on the x-axis, the molecules are arranged in a twist along the y-axis. Similarly, the twisting arrangement along the y-axis begins with Point B on the x-axis, separated from Point A. When the angle of twisting reaches 90°, the molecules are arranged along the x-axis so that they meet each other from either direction. In the case of a simple twist along the x-axis, the molecules are not twisted along the y-axis. Thus, the angles of the molecules from Points A and B match, as shown in Fig. 2a in the meeting point. This holds true even if the molecule twisting angle is other than 90° at the points where the angle changes. If, however, the molecules are twisted along both the y- and x-axes (double twist), the angles of molecules from both points are mismatched (Fig. 2b) in the meeting point, except the distance between Points A and B coincidentally corresponds to half the helical pitch. Next, let us expand such twisting arrangements globally to the entire space. In the case of the simple twist, when the angle of one molecule is determined at one point, the angle of a molecule at any given position can be determined regardless of

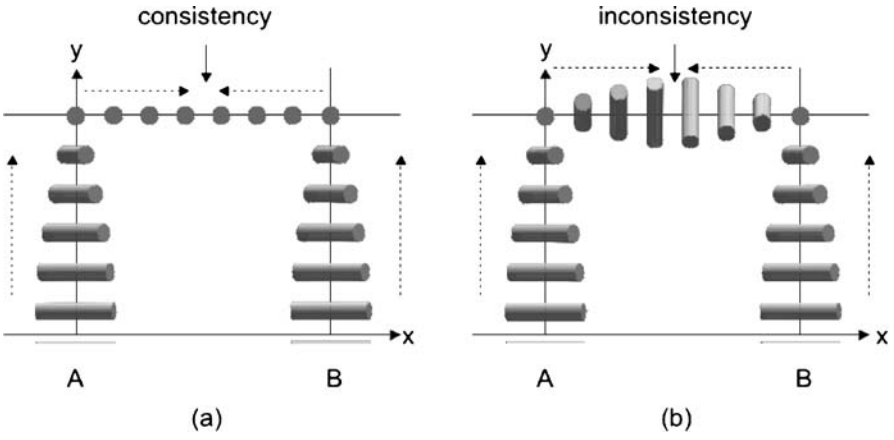

Fig. 2 Frustration in twisted arrangements. **a** In the case of simple twists, arrangements from Points A and B, which are separated, do not result in inconsistency. **b** Double twists result in inconsistency

the route of molecule arrangement. In this way, all the angles of molecules can be regulated. In other words, all molecules in the simple twist can be arranged continuously in three-dimensional space. On the other hand, if the molecules are twisted along two axes even when the angle of a molecule is determined at one point, its angle at another location differs depending on the route of arrangement, as shown in Fig. 2b [11]. In short, the double twist within the entire space inevitably results in a defect of discontinuous arrangements of the molecular angles. The topological effect forcing the chiral liquid crystal to become continuous by preventing this defect effectively and autonomously restricts the twisting arrangement to a single axis alone in a chiral nematic

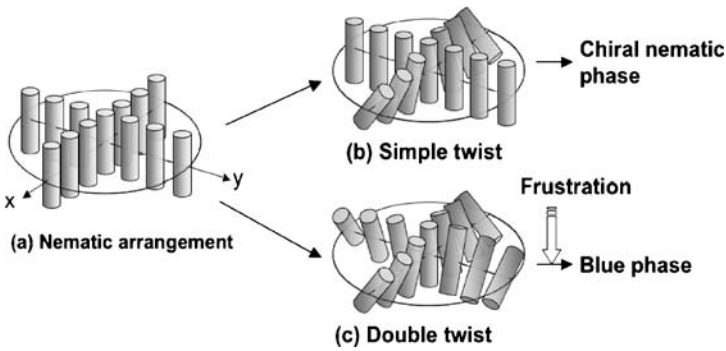

Fig. 3 Comparison of simple-twist and double-twist arrangements

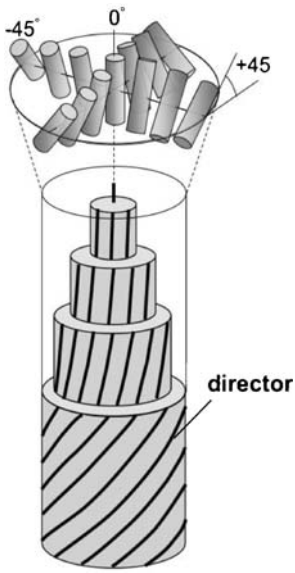

Fig. 4 Model of molecule arrangements within a double-twisted cylinder

phase. This is the reason why the simple twist is common structure in nature rather than the double twist.

In the simple twist, the twisting forces in a direction other than the twisted axis are suppressed as mentioned above. What happens if these forces become large? Twisting in all lateral directions of molecules results in a structure like that shown in Fig. 3c. Such an arrangement is called a double twist. Complete double twisting exists only at the central molecule and its surrounds, that is, the double twist becomes weaker as it spreads radially. The molecules at and around the center are more stable than in the case of a simple twist, since twisting in all lateral directions is allowed. The organized structure formed within such a stable area is the double-twisted cylinder shown in Fig. 4. Double twisting, if expanded to a broader area, results in a defect. For this reason, as pointed out earlier, a double-twisted cylinder structure can not be a basic structure that occupies a space continuously. Blue phases, however, are built upon such a double-twisted cylinder structure that maintains this inconsistency, as described in the next section.

5
Structure of Blue Phases

A double-twisted structure is unable to continuously occupy a three-dimensional space. Thus, if such a structure is expanded to a three-dimensional space, a defect inevitably occurs. Since the generation of such a defect involves some energy, the entire system becomes unstable. Unless there is some gain that exceeds such a loss in stability, a phase containing a double twist cannot become stable. In the case of blue phases, the gain is a strong twisting force. The stronger the twisting force, the more stable the double-twisted structure becomes. As the system reaches the temperature of a disorderly isotropic phase, the loss caused by the defect is relatively alleviated and a double-twisted structure is more likely to form. In the event that such a gain from a double-twisted structure exceeds the loss caused by defects, blue phases appear. For this reason, blue phases appear in the temperature range close to that of an isotropic phase, in a chiral nematic phase, which is shorter-pitched, that is, which contains larger twisting forces. Blue phases are exceptional in that they must coexist with defects. In short, the local tendency for stability towards a double twist and the global tendency for stability towards the defect-free space counteract each other. If the former tendency exceeds the latter, blue phases appear. If the latter prevails, the result is a chiral nematic phase. A system in which the locally stable structures create such competitive interaction, where the global ground state does not settle down to a single state, is called a frustration system. A blue phase is precisely such a system. Among all the phases of liquid crystals, blue phases were the first to be treated as frustrated phases. Other frustration systems include spin glasses of magnetic alloys, Frank-Kasper phases of transi-

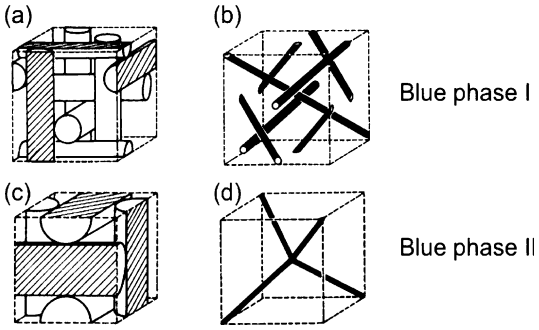

Fig. 5 Structures of Blue Phases I and II. The *rods* in (**a**) and (**c**) represent double-twist cylinder. The *black lines* in (**b**) and (**d**) represent disclination lines

tion metal alloys, and vortex lattices of superfluids and superconductors. Such frustration systems are known for their peculiar characteristics.

Figure 5 shows the structures of BP I (Fig. 5a,b) and BP II (Fig. 5c,d), identified through many different experiments and theoretical calculations [4, 5, 12]. BPs I and II have body-centered cubic symmetry and simple cubic symmetry, respectively. The cylinders in Fig. 5a and c indicate double-twisted cylinders, and the black lines in Fig. 5b and d indicate the disclination, defect lines. These are unusual structures of lattices, and appear as logs stacked up at right angles. Within each of the double-twisted cylinders, each molecule is twisted by 90° along its radius. On the outermost circumference of a cylinder, the molecules are twisted by 45° with respect to the cylinder axis, from – 45° at one end to + 45° at the other. This is equivalent to a quarter pitch, where a single pitch corresponds to a twist of 360°. The diameter of a single double-twisted cylinder is typically 100 nm or so. Thus, assuming that the molecular diameter is 0.5 nm, approximately 200 molecules are gradually twisted. The lattice parameter for BP I corresponds to 1 pitch of twisting, while that in BP II corresponds to 0.5 pitches. These pitch lengths usually differ slightly from those of a chiral nematic phase, which is a lower-temperature phase. It is amazing that such a complex, hierarchical structure forms in a sort of self-organized way as a result of repetitions of the twisted arrangement of molecules. Diffraction peaks appear at (110), (200), and (211), etc., in BP I, and (100) and (110), etc., in BP II as a result of the long wavelength. These diffractions satisfy the equation:

$$\lambda = \frac{2na}{\sqrt{h^2 + k^2 + l^2}}, \tag{1}$$

where λ, n, and a denote the wavelength of incidence, refractive index, and lattice constant, and h, k, and l are the Miller indices. In BP I, $h + k + l$ is an even number. Figure 6 shows an example of the reflectance spectrum of BP I. Unlike a chiral nematic phase, multiple reflection peaks are present in

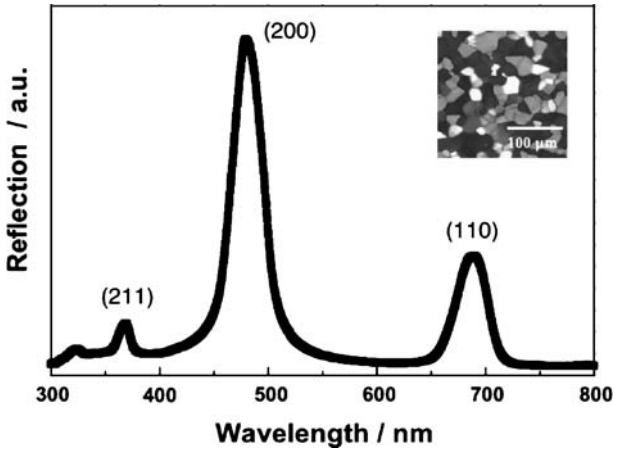

Fig. 6 Reflectance spectrum of Blue Phase I and polarizing optical micrograph of typical platelet texture

the spectrum. With typical blue phases, the blue range is formed by light diffracted from the (110) and (200) directions of BP I and the (100) direction of BP II. This range appears blue to the naked eye, giving rise to the name "blue phase." The disclination caused by frustration in the molecular arrangement passes through a corner at which three double-twisted cylin-

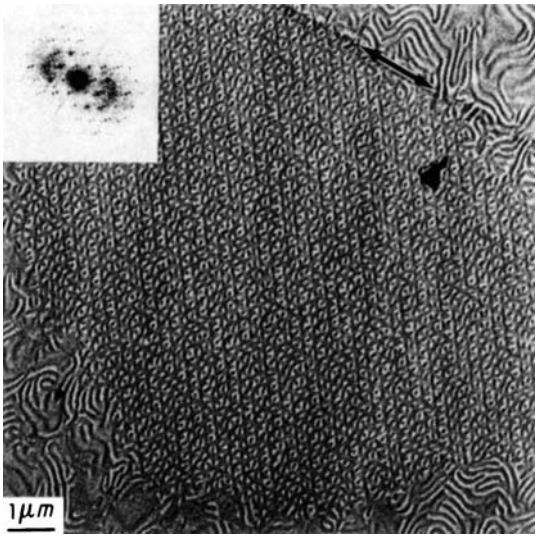

Fig. 7 Example of a transmission electron microscopy image of a section of a quenched blue phase [14]

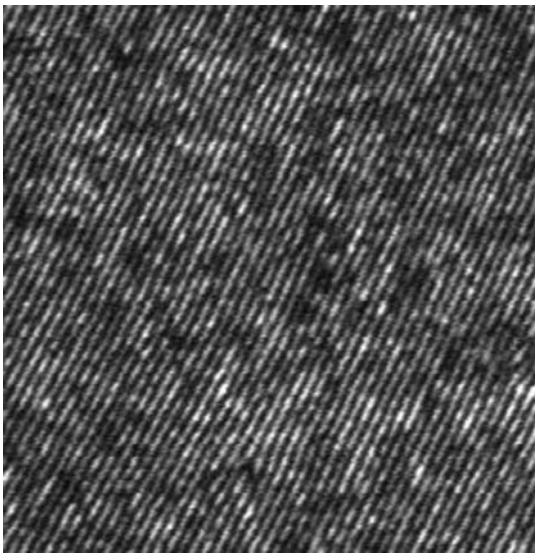

Fig. 8 Confocal laser scanning micrograph of polymer-stabilized blue phase I [16]

ders exist at right angles to each other. The symmetry of the disclination alignments is body-centered cubic in BP I and simple cubic in BP II. The disclination core is estimated to have a diameter of about 10 nm. Inside such a core, it is hypothesized that there is a disordered arrangement of molecules, as in an isotropic phase.

Recently, direct observations of the blue phase lattice structure have been attempted by freeze-fracture electron microscopy [13, 14] (Fig. 7), atomic force microscopy for quenched blue phases [15], and confocal laser scanning microscopy [16] (Fig. 8).

Researchers have confirmed the existence of BP III, the structure of which is predicted to be more amorphous with the short-distance order of double twist alone. However, further details of this phase have yet to be cleared.

6
New Materials Exhibiting Blue Phases

Recent progress in material science, notably with the development of new materials exhibiting blue phases, has generated a renewed interest in the incorporation of the functional properties with the unique structure of frustrated phases. Synthesis of a monosubstituted ferrocene-based chiral Schiff's base derivative which exhibits TGBA and blue phases has been reported [17] (Fig. 9). Other metallomesogens leading to blue phases have been found for palladium complexes [18] (Fig. 10). Optically active materials incorporating

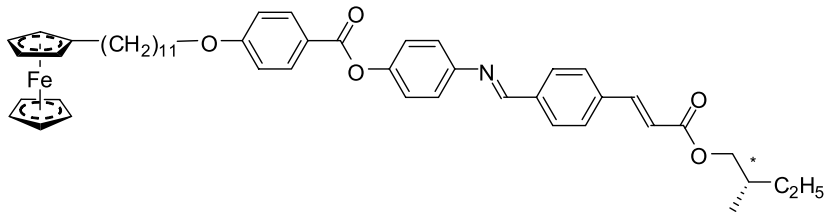

Fig. 9 Chemical structure of the ferrocene-based chiral Schiff's base derivative [17]

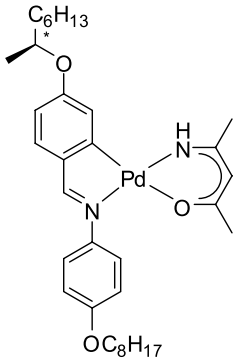

Fig. 10 Chemical structure of the chiral palladium complex [18]

a 2,4-disubstituted oxazoline ring have been shown to induce blue phases when they are added to the host mixture at low concentrations [19]. New chiral discotic triphenylene derivatives exhibit a blue phase and a ferroelectrically switchable columnar mesophase [20]. Many interactions are involved in the doping effect of chiral dopants to host liquid crystals to induce blue phases [21].

7
Expanding the Stable Temperature Range of Blue Phases

Frank, who is famous for his theory of liquid crystal elasticity, once said of blue phases, "They are totally useless, –", indicating that while academically interesting, no practical applications can be expected of such phases. Standing in the way of any practical application of blue phases is, obviously, the narrow temperature range at which they appear. Although the unique characteristics of blue phases are very attractive, the temperature range at which they are available is only on the order of 1 K, which prohibits consideration with regard to potential applications. Recently, however, there have been some attempts to expand this temperature range.

Kitzerow et al. in 1993 formed blue phases of polymeric liquid crystal monomers and polymerized these monomers while maintaining the blue-phase structure, leading to a solid resin of fixed blue-phase structure [22]. Such a substance, although maintaining the blue-phase structure, provided none of the dynamics of liquid crystal, since all the constituent molecules were polymerized.

In 2002, Kikuchi et al. reported that the temperature range of the blue phase can be expanded by several tens of degrees Celsius by forming a small quantity of polymers at a ratio of 7–8 wt % within the blue phase. In this system, referred to as "polymer-stabilized blue phases" (Fig. 11) [23], the molecules retain their dynamics and exhibit rapid electro-optical responses to an applied electric field. It is considered that the blue phase is stabilized when the polymers formed within the blue phase are condensed into disclinations, and the disclinations are then thermally stabilized. In 2005, Yoshizawa, et al. synthesized T-shaped and dimeric liquid crystal molecules, which broadened the temperature range of blue phases to 13 K [24] (Fig. 12). It was suggested that this expanded temperature range is ascribable to the biaxiality of the T-shaped liquid crystal molecules. Also in 2005, Coles et al. reported that in dimer liquid crystals with large flexoelectricity, the temperature range of the blue phase was larger than 44 K [25] (Fig. 13). Flexoelectric-

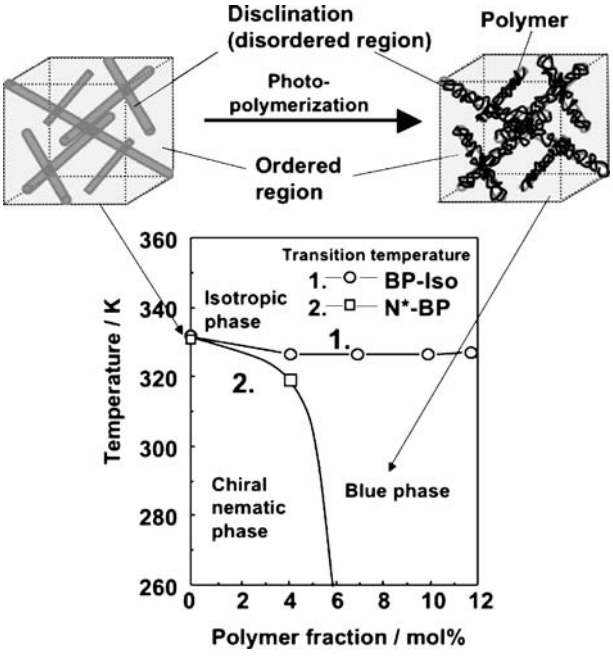

Fig. 11 Phase diagram of polymer-stabilized blue phases and schematic illustration of aggregation state of polymers [23]

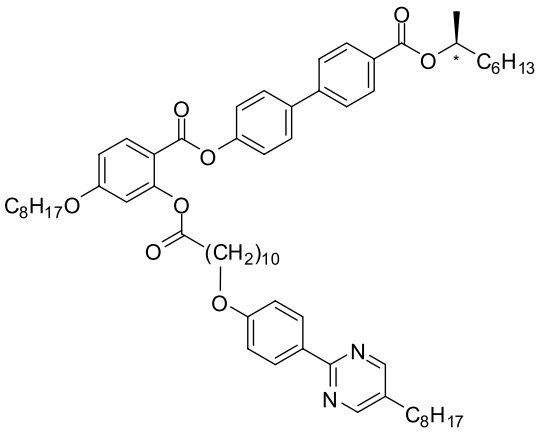

Fig. 12 Chemical structure of T-shaped dimeric liquid crystal molecules that broadened the temperature range of blue phases to 13 K [24]

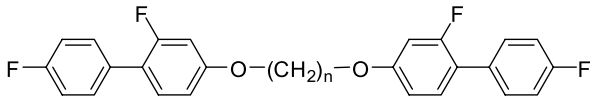

Fig. 13 Chemical structure of materials exhibiting a blue phase with a wide temperature range [25]

ity was suggested to stabilize the disclination. This system is very interesting with respect to potential application, since the diffraction wavelengths of the blue-phase lattice can be changed reversibly by applying an electric field. A theoretical approach for stabilizing the blue phases has been investigated within the framework of Landau–de Gennes theory [26].

Technologies to expand the narrow temperature range of blue phases have thus been in rapid development in recent years. At last, it seems that we have arrived at the dawn of an era in which real progress will be made towards realizing practical applications of blue phases.

8
Smectic Blue Phase

New chiral phases, called smectic blue phases (BPSm), have been discovered in a small temperature range with the following phase sequence: TGB-$BP_{Sm}1$-$BP_{Sm}2$-$BP_{Sm}3$-Iso, without any intermediate chiral nematic phase between the BPSm and TGB phases [27, 28]. X-ray scattering studies showed that unlike the traditional blue phases, the smectic blue phases possess the quasi-long-range smectic order in addition to three-dimensional orienta-

tional order [29, 30]. Although a blue phase with smectic ordering was reported before the observation of the smectic blue phases, it was a supercooled state [31, 32]. On the other hand, the smectic blue phases are thermally equilibrium phases. The lattice parameter of the smectic blue phases is in the ultraviolet range, preventing any optical scattering of visible light (Kossel diagram), which is commonly used to study the symmetry of cholesteric blue phases. Therefore the structure of the smectic blue phases has been investigated by X-ray scattering and crystal faceting. The X-ray scattering patterns of the monodomains have provided the symmetries of the smectic blue phases: the $BP_{Sm}2$ appears hexagonal [33] whereas the $BP_{Sm}1$ has a structure that depends on the phase sequence. The $BP_{Sm}1$ exhibits a cubic symmetry in the case of a TGB_A-$BP_{Sm}1$ transition [34] and is labelled $BP_{SmA}1$; but the symmetry of the $BP_{Sm}1$ is hexagonal for TGBC-$BP_{Sm}1$ phase sequence [35], called $BP_{SmC}1$. The $BP_{Sm}3$ has an amorphous structure of the same macroscopic symmetry as that of the isotropic phase. However, the results obtained by the X-ray scattering indicate the directions where the smectic order is enhanced, providing indirect information of the symmetry of the orientational unit cell. The observations of faceted monocrystals, which provide direct information of the symmetry of the orientational unit cell, reveal that the symmetry of the $BP_{Sm}2$ is orthorhombic [36]. Kamien proposed a model of smectic double-twist cylinders linking smectic A order and twist not only in one di-

Fig. 14 Image of smectic blue phase based on uniform layer spacing of the Schwartz P surface [38]

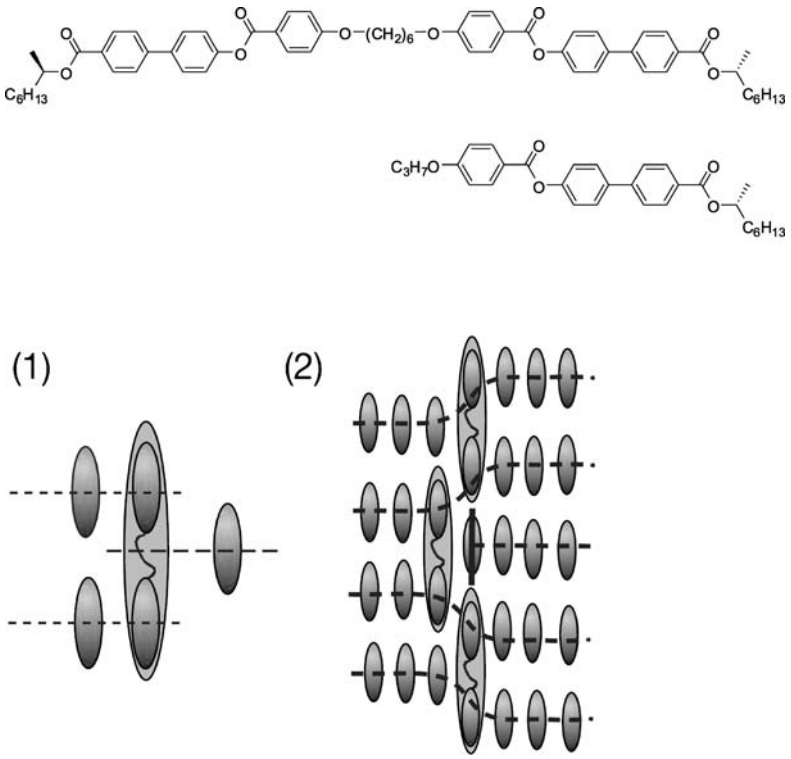

Fig. 15 Chemical structures of the monomer and twin dimer, and schematic representation of molecular arrangement in the mixture of the monomer and twin dimer in the novel smectic blue phase, SmBPiso [39]

rection as in TGB phases but also in two spatial directions [37]. Recently another geometrical model based on minimal surfaces has also been proposed [38] (Fig. 14). A novel smectic blue phase with spherical symmetry has been found in a two-component mixture containing a chiral monomer and its twin containing two repeat units of the first molecule connected by a linear hydrocarbon spacer. The anomalous softening of elasticity due to a strong reduction in entropy caused by mixing the monomer and the twin permits the seamless coexistence of these two competing liquid crystal orders. The new phase spontaneously exhibits an optically isotropic but uniformly iridescent color and automatically acquires spherical symmetry, so that the associated photonic band gap maintains the same symmetry despite the local liquid crystalline order [39] (Fig. 15).

9
Photonics of Blue Phases

It can be expected that blue phases consisting of three-dimensional periodic structures on scales equivalent to the wavelength of visible light can be applied in photonics [40–42]. Recently, researchers have paid attention to artificial crystals with periodic optical structures on the order of visible wavelengths, known as photonic crystals. Much effort has been made toward the study and development of technologies to manufacture such crystals. Blue phases have an edge over the top-down method of micro fabrication, since these phases form three-dimensional photonic lattices in a self-organizing manner. Cao et al. dispersed some fluorescent dye in BP II and activated them with a pulsed light source and the result was lasing in three spatial directions, proving that blue phases exhibit three-dimensional photonic characteristics [43]. Yokoyama et al. used polymer-stabilized blue phases to show that lasing from the lattice structures of blue phases takes place over a broad temperature range of 35 K, and found that the lasing threshold and line width are smaller than for lasing arising from a chiral nematic phase [44](Fig. 16). Studies on the application of blue phases to photonics have in this way seen rapid progress recently.

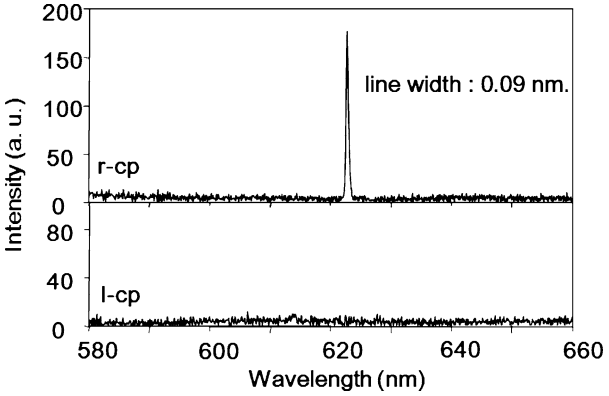

Fig. 16 Laser emission spectra from the polymer-stabilized blue phase of the (110) crystal [44]

10
Electro-optics of Blue Phases

Kikuchi and coworkers found the rapid electro-optical effect in polymer-stabilized blue phases and presented the major potential of such phases in application to display devices and optical modulation devices [45, 46]. Tra-

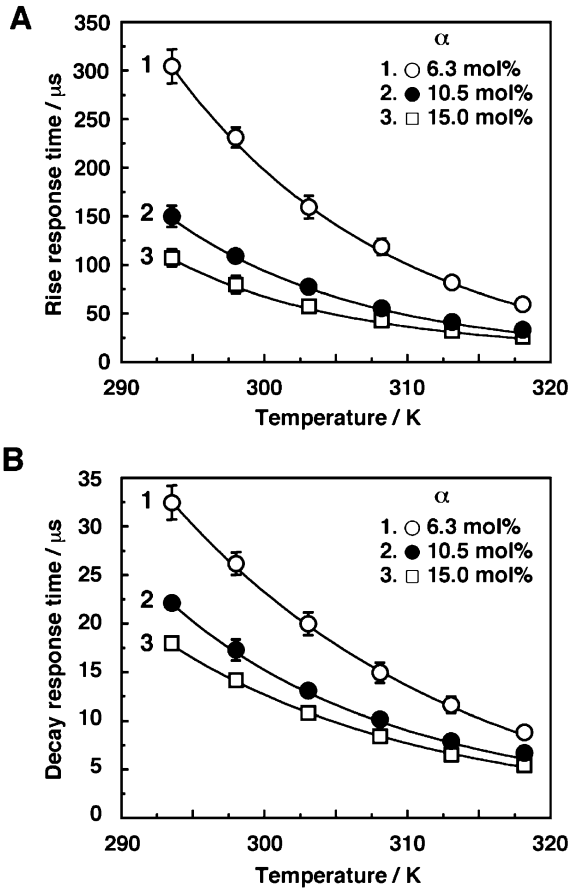

Fig. 17 Temperature dependence of electro-optical response time for the polymer-stabilized blue phases (polymer fraction: $\alpha = 6.3$, 10.5, 15.0 mol %) in the rise process (**A**) and decay process (**B**) [46]

ditional liquid crystal display devices have several problems, such as slow response (millisecond order), the need for initial orientation by surface treatments, and viewing-angle dependence. In contrast, polymer-stabilized blue phases provide faster response (10 to 100 μs), and are optically isotropic and therefore require no treatment for initial orientation and have small viewing-angle dependence (Fig. 17). If the remaining problems of high driving voltage can be resolved, then we will be much closer to seeing real applications of blue phases.

11 Conclusions

The blue phase models shown in Fig. 5 appear in textbooks on liquid crystals. Yet how many people can capture a complete image of the structures immediately? How can such complex structures form by themselves? Do people truly understand what blue phases really are? This structural mystery remains, even for those with a good understanding of these phases. The researchers who identified these structures must have been amazed at their findings, which were well beyond their own expectations. At the same time, it is very interesting that some incredible structures exist in biologic materials and living organisms. Collagen is made of huge molecules that form triple helices, and in its aggregates, a blue-phase structure exists [47]. Some also say that rats' teeth have a structure similar to those of blue phases [48]. Why have some living organisms chosen such structures? Future findings on these issues will undoubtedly be of keen interest.

It is considered that liquid crystals that are soft and have long-distance order may form certain complex hierarchical structures other than blue phases. In fact, recent discoveries of new liquid crystal phases have arisen one after another. While many think of liquid crystals as display materials with the range of applications seemingly exhausted, it is more likely that applications other than displays are only beginning to appear.

References

1. Crooker PP (1983) Mol Cryst Liq Cryst 98:31
2. Stegemeyer H, Blumel T, Hiltrop K, Onusseit H, Porsch F (1986) Liq Cryst 1:1
3. Cladis PE (1987) Theory and Applications of Liquid Crystals. Springer, Berlin Heidelberg New York
4. Wright DC, Mermin ND (1989) Rev Mod Phys 61:385
5. Crooker PP (2001) Chirality in Liquid Crystals. Springer, Berlin Heidelberg New York
6. Oswald P, Pieranski P (2005) Nematic and Cholesteric Liquid Crystals. Taylor & Francis, Boca Raton, London, New York, Singapore
7. Reinitzer F (1888) Montash Chem 9:421
8. Gray GW (1956) J Chem Soc 3733
9. Saupe A (1969) Mol Cryst Liq Cryst 7:59
10. Coate D, Gray GW (1973) Phys Lett 45A:115
11. Sethna JP (1985) Phys Rev B 31:6278
12. Meiboom S, Sethna JP, Anderson PW, Brinkman WF (1981) Phys Rev Lett 46:1216
13. Costello MJ, Meiboom S, Sammon M (1984) Phys Rev A 29:2957
14. Delacroix H, Gilli JM, Erk I, Mariani P (1992) Phys Rev Lett 69:2935
15. Hauser A, Thieme M, Saupe A, Heppke G, Kruerke D (1997) J Mater Chem 7:2223
16. Kikuchi H, Hirata S, Uchida K (2007) Mol Cryst Liq Cryst 465:283
17. Seshadri T, Haupt HJ (1998) Chem Commun (7):735
18. Buey J, Espinet P, Kitzerow HS, Strauss J (1999) Chem Commun (5):441
19. Lamb AGM, Eastwood AJ, Kelly SM, Goodby JW (1998) Ferroelectrics 212:317

20. Heppke G, Kruerke D, Lohning C, Lotzsch D, Moro D, Muller M, Sawade H (2000) J Mater Chem 10:2657
21. Nakata M, Takanishi Y, Watanabe J, Takezoe H (2003) Phys Rev E 68:041710
22. Kitzerow HS, Schmid H, Ranft A, Heppke G, Hikmet RAM, Lub J (1993) Liq Cryst 14:911
23. Kikuchi H, Yokota M, Hisakado Y, Yang H, Kajiyama T (2002) Nat Mater 1:64
24. Yoshizawa A, Sato M, Rokunohe J (2005) J Mater Chem 15:3285
25. Coles HJ, Pivnenko MN (2005) Nature 436:997
26. Alexander GP, Yeomans JM (2006) Phys Rev E 74:061706
27. Li MH, Nguyen HT, Sigaud G (1996) Liq Cryst 20:361
28. Li MH, Laux V, Nguyen HT, Sigaud G, Barois P, Isaert N (1997) Liq Cryst 23:389
29. Pansu B, Li MH, Nguyen HT (1997) J Phys II France 7:751
30. Pansu B, Li MH, Nguyen HT (1998) Eur Phys J B 2:143
31. Onusseit O, Stegemeyer H (1991) Liq Cryst 10:869
32. Demikhov E, Stegemeyer H, Tsukruk V (1992) Phys Rev A 46:4879
33. Pansu B, Grelet E, Li MH, Nguyen HT (2000) Phys Rev E 62:658
34. Grelet E, Pansu B, Li MH, Nguyen HT (2001) Phys Rev Lett 86:3791
35. Grelet E, Pansu B, Nguyen HT (2001) Phys Rev E 64:010703
36. Grelet E, Pansu B, Li MH, Nguyen HT (2002) Phys Rev E 65:050701
37. Kamien RD (1997) J Phys II France 7:743
38. DiDonna BA, Kamien RD (2003) Phys Rev E 68:041703
39. Yamamoto J, Nishiyama I, Inoue M, Yokoyama H (2005) Nature 437:525
40. Hornreich RM, Shtrikman S, Sommers C (1993) Phys Rev E 47:2067
41. Huang CY, Scott JJ, Petschek G (1998) Phys Rev Lett 80:5603
42. Etchegoin P (2000) Phys Rev E 62:1435
43. Cao W, Munoz A, Palffy-Muhoray P, Taheri B (2002) Nat Mater 1:111
44. Yokoyama S, Mashiko S, Kikuchi H, Uchida K, Nagamura T (2006) Adv Mater 18:48
45. Kikuchi H, Hisakado Y, Uchida K, Nagamura T, Kajiyama T (2004) Proc SPIE Liquid Cryst VIII 5518:182
46. Hisakado Y, Kikuchi H, Nagamura T (2005) Adv Mater 17:96
47. Lepescheux L (1988) Biol Cell 62:17
48. Calvert P (1995) Biomimetics. AIP Press, New York

Struct Bond (2008) 128: 119–149
DOI 10.1007/430_2007_066

Published online: 23 October 2007

Supramolecular Interactions in the Formation of Thermotropic Liquid Crystalline Polymers

Stuart J. Rowan (✉) · Patrick T. Mather (✉)

Department of Macromolecular Science and Engineering,
Case Western Reserve University,
2100 Adelbert Road, Cleveland, OH 44106-7202, USA
stuart.rowan@case.edu, ptmather@syr.edu

Abstract This review will focus on recent developments that have occurred since 2000 on the utilization of specific supramolecular interactions to form polymeric aggregates which exhibit thermotropic liquid crystalline (LC) properties.

Keywords Liquid Crystals · Polymers · Self Assembly · Supramolecular Chemistry · Thermotropic

1 Introduction

Liquid crystalline polymers (LCPs) are those macromolecular systems that adopt varying levels of orientational and spatial order upon increasing the concentration of a solution (lyotropic) or decreasing the temperature (thermotropic). Incorporating geometrically anisotropic moieties within a polymer architecture can drive the formation of liquid crystalline (LC) phases from strictly steric repulsion considerations [1–3], principally in the form of slender rods (calamitic) or flat disks (discotic). The calamitic LCPs have been the most commonly studied and have been the subject of several outstanding reviews, including wholly aromatic [4], rigid-flexible segmented [5], and side-chain [6] architectures. As shown in Fig. 1, calamitic LCPs incorporate mesogens (rigid rod-like molecules) either as a main component of their

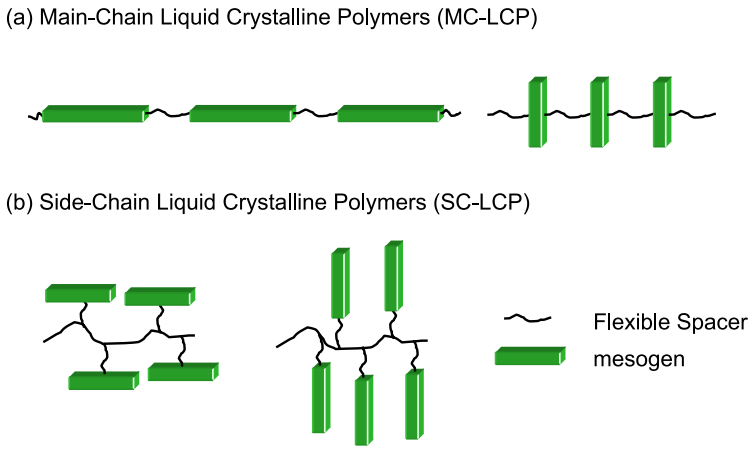

Fig. 1 Common architectures for thermotropic liquid crystalline polymers

backbone or as a pendant group. The former are referred to as *main-chain* LC polymers (MC-LCPs), while the latter are termed *side-chain* LC polymers (SC-LCPs). In both cases, mesogens are linked either to each other or with the polymer backbone through a more flexible chain, often an alkyl chain, termed the *flexible spacer*. In SC-LCPs, the mesogens are attached to the polymer backbone by one end (side-chain LCP) or laterally (side-on LCP). Similarly, MC-LCPs can be formed by two possible arrangements of the flexible spacers and mesogens: the mesogens can be linked to the flexible spacer by either their ends, or laterally. Interestingly, Griffin has used some of the latter as an approach to design synthetic auxetic materials (i.e., materials that expand perpendicularly to the direction of the stress applied, negative Poisson ratio) [7].

In the area of main-chain LCPs, several approaches toward spacer incorporation have been adopted, including copolymerization of semiflexible polyethylene terephthalate (PET) with rod-like poly(4-hydroxy benzoic acid) [8], polycondensation of aliphatic dicarboxylic acids with mesogenic bisphenols [9], and especially polycondensation of hydroquinones (substituted or not) with α,ω-bis benzoic acids (such as 4,4′-dicarboxy-α,ω-diphenoxyhexane) bearing the spacer molecule [10, 11]. Additionally, semiflexible polyethers with comparatively lower transition temperatures have been prepared from dibromoalkanes and mesogenic diols using a phase transfer catalyst approach [12]. Numerous studies of the phase behavior and physical properties of segmented LCPs has revealed a critical role of the spacer length, along with any mesogen pendent group, in determining the crystallinity, the LC phases observed, and the phase transition temperatures. Perhaps the most intriguing aspect of these studies, reviewed by Sirigu, [5] is the remarkable “odd-even” alternation in phase transition temperature(s)

with increasing spacer length, indicating substantial conformational differences between segmented LCPs with an odd number of methylene spacer units (lower transition temperatures) and their even-numbered counterparts. Recently, we have introduced the use of acyclic diene metathesis (ADMET) polymerization as an approach to the preparation of main-chain LCPs [13]. The preparation of side-chain LCPs is comparatively simpler [6] and involves chain-growth polymerization of vinyl- or vinylidene-functionalized mesogens. Alternatively, mesogens may be post-polymerization grafted (the so-called polymer analogous synthesis) to polymers which contain appropriate functional groups on the backbone [14, 15].

Recently, the use of specific non-covalent interactions has lead to the development of a wide range of supramolecular polymers [16–19]. In this class of interesting polymers small molecule and/or polymeric units are designed to contain supramolecular motifs in order to self-assemble a desired polymeric aggregate. One major advantage of such a self-assembly process is the ability to control the resulting supramolecular architecture of the polymer aggregates by simply tailoring the structure of the starting units. Another aspect that differentiates supramolecular polymers from more conventional covalent bonded structures is their dynamic nature, which has potentially significant consequences for the thermomechanical properties of such systems [20]. The properties of such non-covalently bound aggregates have a strong dependence not only on their core components but also on the nature (stability and dynamics [21]) of the supramolecular interactions that control the self-assembly process. The degree of the interaction between the starting units depends, to a large extent, on the strength of the supramolecular interaction, and the unit concentration, as well as a range of environmental conditions (such as temperature, pH, solvent, etc).

The ability to combine supramolecular chemistry with liquid crystallinity is very attractive for several reasons. It has been well known for a long time in the liquid crystal community that non-covalent interactions have a great effect on a material's liquid crystallinity. Therefore, it is expected that designing specific non-covalent interactions into monomer units can result in a number of effects, including inducing liquid crystallinity upon non-mesogenic starting materials, changing the nature of the LC phase and/or changing the stability of the LC phase. Furthermore, the combination of the dynamic behavior of the supramolecular polymer along with the temperature sensitivity of the LC phase offers exciting opportunities for (multi-step) stimuli-responsive materials. From the point of view of supramolecular materials it has been proposed that the order imposed by liquid crystallinity can been utilized to enhance the interaction between constituent molecules, thus allowing access to SLCPs with relatively weak hydrogen bonding interactions between monomers [22–38].

Over the years there have been a number of excellent papers [39–41] that cover different aspects of this burgeoning field. The field of supramolecular materials and LCPs is a large one and includes the supramolecular ordering of

mesogen-containing polymers as well as supramolecular systems which organize in solution (lyotropic) and/or in the melt (thermotropic). The purpose of this paper is to focus on recent developments, which have occurred since the turn of the century, on the utilization of specific supramolecular interactions to form polymeric aggregates which exhibit thermotropic LC properties.

1.1 Background on Combining Supramolecular Chemistry and Liquid Crystallinity

The design of polymeric molecules which combine tailored supramolecular interactions with liquid crystallinity has been around since the late 1980s and early 1990s. Pioneering work by Fréchet, Kato [42–45], Lehn [46–50] and Griffin [51–54], and others during this period demonstrated that specific supramolecular interactions, in the form of hydrogen bonding, can be used to access supramolecular LCPs (SLCPs). Figure 2 shows a selection of the early SLCPs, designed by these groups, in which hydrogen bonding plays an import role in forming the structure.

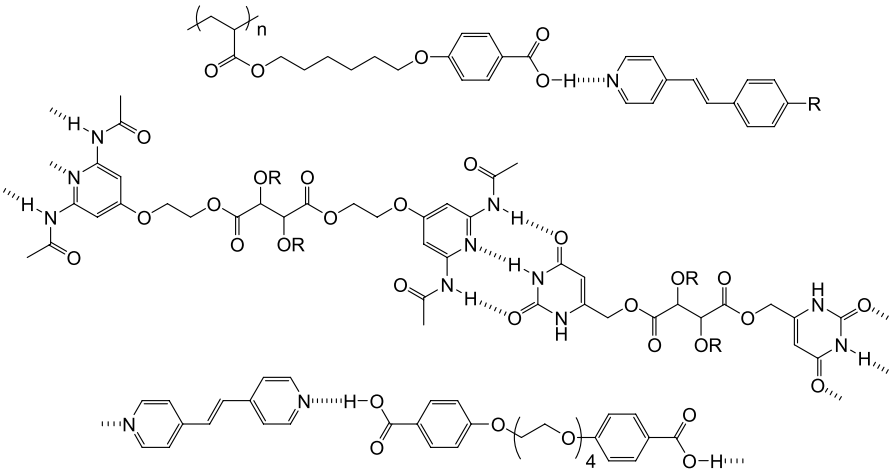

Fig. 2 A selection of early examples of supramolecular liquid crystalline polymers designed by Fréchet and Kato [42–45], Lehn [46–50] and Griffin [51–54]

In principle, there are a number of ways that supramolecular chemistry can be utilized to influence/access LC polymeric systems. One way is to access different polymeric architectures, such as main-chain, side-chain, or network structures (Fig. 3). For example, main-chain SLCPs can be formed through the aggregation of low(er) molecular weight ditopic compounds whose chain ends interact with each other through specific non-covalent interactions. Conceptually, this can occur in a number of different ways. The simplest conceptual

class of a main chain SLCP is one that has self-complementary units attached to either end of a mesogenic core and thus results in a self-assembling $(A)_n$ polymer (Fig. 3a). If the supramolecular motif used in the assembly of the polymer is asymmetric (i.e., consists of two different complementary units) then the supramolecular polymer will only be formed when both of these complementary units are present and in equal proportions. A heteroditopic monomer, in which both complementary units are placed on the same molecule, results in

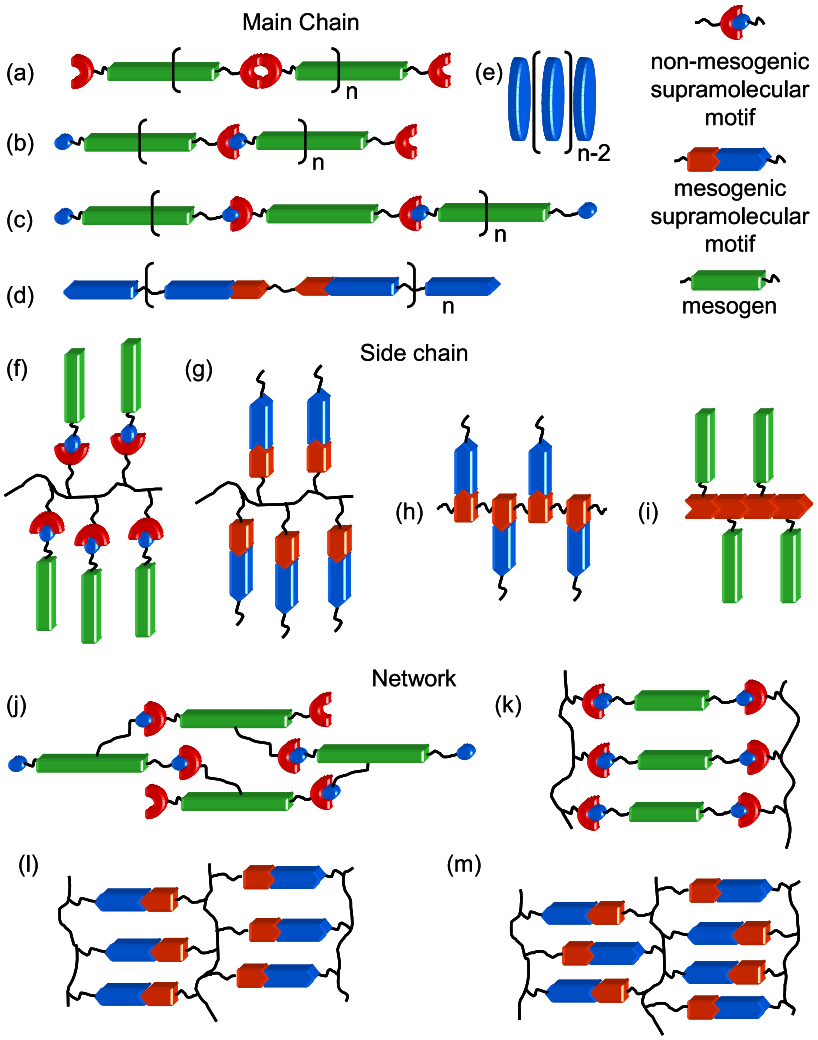

Fig. 3 Schematic representations of some possible supramolecular liquid crystalline polymer architectures. **a–e** Different classes of main-chain structures. **f–i** Different side chain polymers. **j–m** Different types of networks

a self-assembling $(A\text{-}B)_n$ polymer (Fig. 3b). However, homoditopic monomers, which have one of the complementary units placed on both ends of the core (e.g. A-A or B-B), will only exhibit polymer-like properties upon mixing the two complementary monomers (e.g., Fig. 3c). In all the above examples the core is mesogenic; however, this does not necessarily have to be the case. An additional subset of main-chain SLCPs involves aggregates in which the mesogenic component is the supramolecular motif itself. Such supramolecular mesogens can, of course, be formed through either self-complementary units or with (as is shown in Fig. 3d) a hetero-supramolecular motif. An alternative approach is to use ditopic molecules that interact through two faces of a rigid, usually disk-like component (Fig. 3e), rather than through the ends of a chain. This leads to 1-dimensional polymeric structures which tend to form columnar LC phases.

Pre-made polymer backbones with supramolecular binding sites can be used to access side-chain SLCPs with a monotopic small mesogenic molecule (Fig. 3f). Similar architectures are accessed if the supramolecular motif itself is mesogenic (Fig. 3g). If the supramolecular motif is mesogenic and one of its components is part of the polymer backbone, then the addition of its complement will yield side-chain SLCPs whose mesogen consists of part of the main-chain as well as the side chain (Fig. 3h). Alternatively, a small mesogen-containing molecule can access side chain SLCPs if the supramolecular motif can form polymeric tape-like structures (Fig. 3i). The use of oligotopics that are either small molecules (Fig. 3j) or polymers (Fig. 3k) rather than ditopic monomers can access LC branched or network structures. Of course, in the

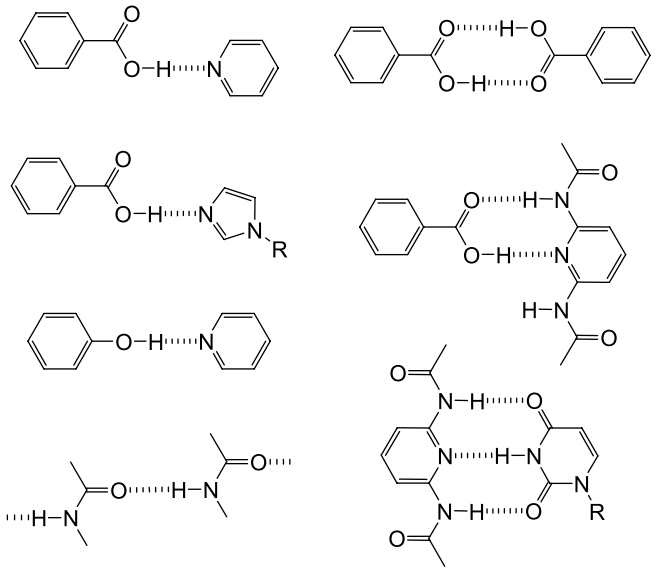

Fig. 4 A selection of some supromolecular motifs used to access supramolecular liquid crystals

last two classes, while the figures show the use of two different complementary units to form these structures, derivatives in which the supramolecular units are either self-complementary and/or form the mesogenic unit are also possible. In this last case, there are two additional types of networks that can be formed, namely blends of two polymers containing complementary units, (Fig. 3l) or a copolymer in which the two complementary units are in the same backbone (Fig. 3m).

There are potentially a large number of supramolecular motifs that can be designed into a molecule or polymer to allow access to supramolecular liquid crystals. Figure 4 shows just a selection of some hydrogen bond motifs that have been utilized in the early development of supramolecular liquid crystals. As we shall see, some of these motifs, particularly the benzoic acid/pyridine and amide motifs, have continued to be popular choices in the design of new SLCPs.

2
Recent Developments (2000–)

2.1
Main-Chain SLCPs

Over the last decade the area of supramolecular polymerization, i.e., the self-assembly of small monomeric units into polymer-like materials through the use of non-covalent interactions, has received a growing amount of attention. Conceptually, a simple way to achieve such supramolecular polymers is by the attachment of appropriate supramolecular motifs onto the ends of a core unit (Fig. 2a–e). The backbones of the resulting self-assembled polymeric systems will therefore contain non-covalent bonds, in addition to covalent bonds, which collectively impart upon the system reversibility (i.e., a dynamic degree of polymerization) and temperature sensitivity. This behavior, in turn, offers the potential to develop polymeric materials where the melt viscosity at elevated temperatures is more akin to a monomeric-like state, and thus allows for the utilization of mild (low pressure and stress) processing conditions. One interesting opportunity offered by such systems is the ability to self-assemble functional units into processable polymeric materials, which, for example, exhibit attractive electronic and/or optical properties [55–62]. The properties of such non-covalently bound aggregates have a strong dependence not only on their functional core components but also on the nature (stability and dynamics) of the supramolecular motifs which control the self-assembly process. In addition, if the supramolecular motif used in the assembly of the polymer is asymmetric (i.e., consists of two different complementary units) then the supramolecular polymer, along with any potential functionality that results, will only be formed when both of these complementary units are present.

An example of such a supramolecular-aided function is the growing area of supramolecular LC materials. In such systems, molecular shape anisotropy is important for the formation of an LC phase. For example, rigid and semi-rigid molecules which have a high aspect ratio often exhibit LC behavior. Therefore, the self-assembly of small (semi)rigid units into a larger linear array, with a high axial ratio, can result in the appearance of an LC phase. The induction of a LC phase in such a case is a macroscopic expression of the molecular recognition designed into the molecules. Furthermore, the formation of such an LC phase, with its long range order, can also aid the formation of higher molecular weight aggregates.

Rowan, Mather et al. [63–65] have examined the use of complementary nucleobase interactions to allow the formation of supramolecular LC materials of the main type shown in Fig. 3a and b. In these cases, a rod-like mesogen–bis(phenylethynyl)benzene–was functionalized symmetrically (homoditopically) with thymine (**T**) or N^6-anisoyl protected adenine ($\mathbf{A}^{An}$) using alkoxy spacers of varying length to yield molecules of the type: $\mathbf{B}^{P}$-**1**-$\mathbf{B}^{P}$, where $\mathbf{B}^{P}$ depicts the variable nucleobase moiety, $\mathbf{A}^{An}$ or **T** (Fig. 5).

It was found that the single-component systems featured quite high crystal melting transitions, presumably owing to the high symmetry of the bis(phenylethynyl)benzene mesogen combined with minimal supramolecular polymerization. These high-melting transitions had the effect of narrowing the range of liquid crystallinity to ca. 10 °C. Interestingly, however, it was observed [63, 64] that when homoditopic molecules featuring complementary nucleobase pairs were mixed in 1 : 1 stoichiometry (**T**-**1**-**T** + $\mathbf{A}^{An}$-**1**-$\mathbf{A}^{An}$) a significant broadening of temperature range for liquid crystallinity was witnessed. The broadening of liquid crystallinity was attributed to the formation of large, linear supramolecular aggregates only possible when complementary nucleobase pairs are mixed. This conclusion was further substantiated by the report of fiber-forming capacity from the LC phase of the same mixtures. Using X-ray diffraction, it was found that the LC phase formed was generally smectic-C, with layer spacings of 40–50 Å (depending on spacer length) and

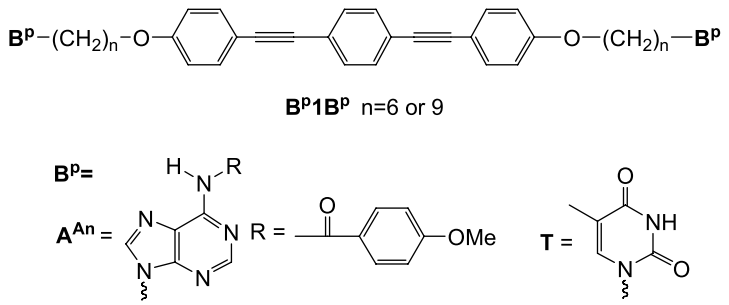

Fig. 5 Structures of the homoditopic (A–A, B–B) nucleobase terminated bis(phenylethynyl)benzene monomers ($\mathbf{B}^{P}$**1**$\mathbf{B}^{P}$) investigated by Rowan, Mather et al. [63–65]

apparent mesogen tilting within the layers from 27° to 30°. Further work by the same group investigated the influences of complementary mixture stoichiometry and thermal history on LC phase behavior [65]. There it was found that departure from 1 : 1 stoichiometry hampered liquid crystallinity. Further, the precise thermal history of such a 1 : 1 blend had a large impact on phase behavior, a finding attributed by a propensity for the high-melting N^6-anisoyl-adenine functionalized mesogen to phase separate from the mixture under certain conditions.

A commonly studied motif for the main-chain SLCPs involves chains of hydrogen bonding between dicarboxylic acids and bipyridyls, building on some early work by Griffin et al. in this area [66]. Such SLCPs tend to be of the mesogenic supramolecular type shown in Fig. 3d, where the non-covalent interaction is part of the mesogen. More recently, Griffin et al. [67] found that a stoichiometric mixture of tetraethyleneglycoxy-bis(2,6-dimethyl-4-benzoic acid) (**2**) and 4,4′-(*p*-phenylenedi-1,2-ethenediyl)bipyridyl (**3**) (Fig. 6) led to a nematic LC material with polymer-like fiber-forming capacity. In particular, the stoichiometric mixture featured an enantiotropic nematic phase sequence of (K 150 N 175 I) on heating and (I 175 N 88 K) on cooling. In contrast, the two starting compounds (bisbenzoic acid and bipyridyl compounds) underwent direct melting from the crystalline to isotropic phases. For this system it was argued that the liquid crystallinity is afforded by enhancement in the mesogen length/diameter (L/D) ratio from 3.3 (15.5 Å/5 Å) for the bipyridine derivative to 6 (31 Å/5 Å) for the hydrogen-bonded mesogenic unit.

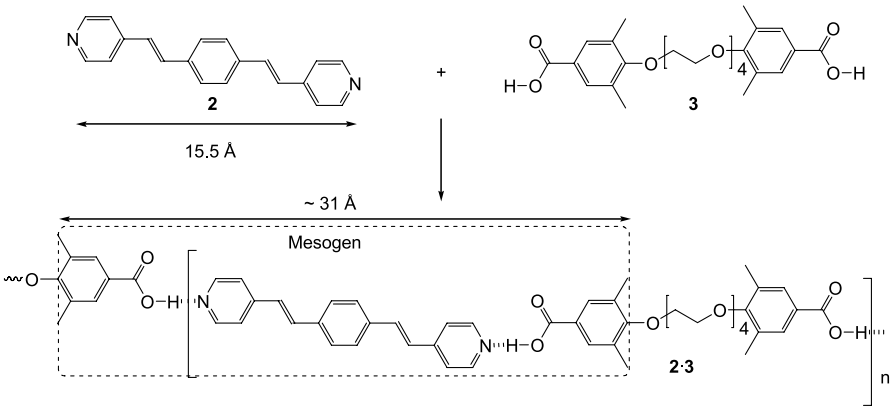

Fig. 6 Structures of the non-mesogenic bis-pyridyl (**2**) and bis-benzoic acid (**3**) monomers studied by Griffin et al. [67] and the proposed structure of the main chain liquid crystalline supramolecular polymer (**2**·**3**) highlighting the length of supramolecular mesogen

He et al. [68] examined the effect of adding flexibility to the hydrogen bond acceptor bis-pyridyl units. They attached stilbazole derivatives to either end of differently sized oligo(ethylene oxide) spacers (**4**) (Fig. 7). Mixing

these difunctional proton acceptors with bis-benzoic acids, which also bear oligo(ethylene oxide) spacers, allowed the investigation of how flexibility influences the LC properties of such supramolecular polymers. As is seen in covalently bonded segmented LC polymers, a decrease in the isotropic-nematic transition temperature (upon cooling) was observed for stoichiometric mixtures. Both nematic and smectic-A phases were observed for many compositions, with isotropization temperatures in the range 170 °C < T_{NI} < 190 °C.

In a similar vein, Weigel et al. [69] have also studied main-chain SLCPs exploiting the carboxylic acid/pyridine hydrogen-bonding motif, in their case examining oligo(ethylene glyol)s symmetrically endcapped with 6-hydroxy-2-naphthoic acid as the hydrogen bond donor. For the hydrogen bond acceptors, a variety of pyridine-terminated molecules were studied, including 4,4′-azopyridine, and 4,4′-(*p*-phenylenedi-1,2-ethylenediyl)bispyridyl, among others. The researchers observed, using DSC and POM, that over narrow temperature ranges a liquid crystal phase appeared and that, like the work of He, increasing the spacer lengths afforded lower isotropization temperatures. Further work by the same group [70] demonstrated how the nature of the mesogenic supramolecular motif affects the LC properties. By combining different aromatic bisacids (**5**, **6**, **7**) with a series of bisazopyridine phenol derivatives (**8**, **9**) (Fig. 7) they showed that LC transition temperatures are raised with increasing mesogen rigidity and aspect ratio. For example, as in the case of covalently bonded LCPs, it was found that the 6-hydroxy-2-naphthoic acid unit (**6**)–in this case serving as the hydrogen bond donor–offers a clearing transition (e.g., **6**·**8b**: I 142.7 N 40.4 K) higher than that of the benzoic acid version (e.g., **5**·**8b**: I 131.5 N 60.2 K), but lower than the high transition temperatures witnessed for the biphenyl benzoic acid (e.g., **7**·**8b**: I 209.0 N 127.0 K) derivatives.

Liquid crystallinity has also been observed from supramolecular polymerization of bipyridyl mesogens without a need for an aromatic mesogenic component of the hydrogen donor. Bhowmik et al. [71] investigated the self-assembly of 4,4′-bipyridyl (**BP**) with two aliphatic dicarboxylic acids: adipic acid (**AA**; HOOC-$(CH_2)_4$-COOH) and sebacic acid (**SA**; HOOC-$(CH_2)_8$-COOH). Despite the simplicity of using only commercially available building blocks (monomers), rich LC behavior was observed. In particular, DSC and POM studies revealed that the supramolecular homopolymers **BP** : **SA** and **BP** : **AA** exhibited smectic phases with phase sequences on heating of (K 127 Sm 172 I) and (K 143 Sm1 177 Sm2 181 I), respectively. Copolymerization, namely mixing in different ratios of SA and AA while keeping the acid/pyridine ratio at 1 : 1, was observed to broaden the temperature range for liquid crystallinity quite substantially through melting point reduction (both T_m and heat of fusion). For example, the 50 : 50 copolymer (K 120 Sm 165 I), though the melting transition was barely detectable by DSC.

An interesting example of how non-mesogenic rigid supramolecular main-chain polymers can affect LC environments has recently been shown [72]

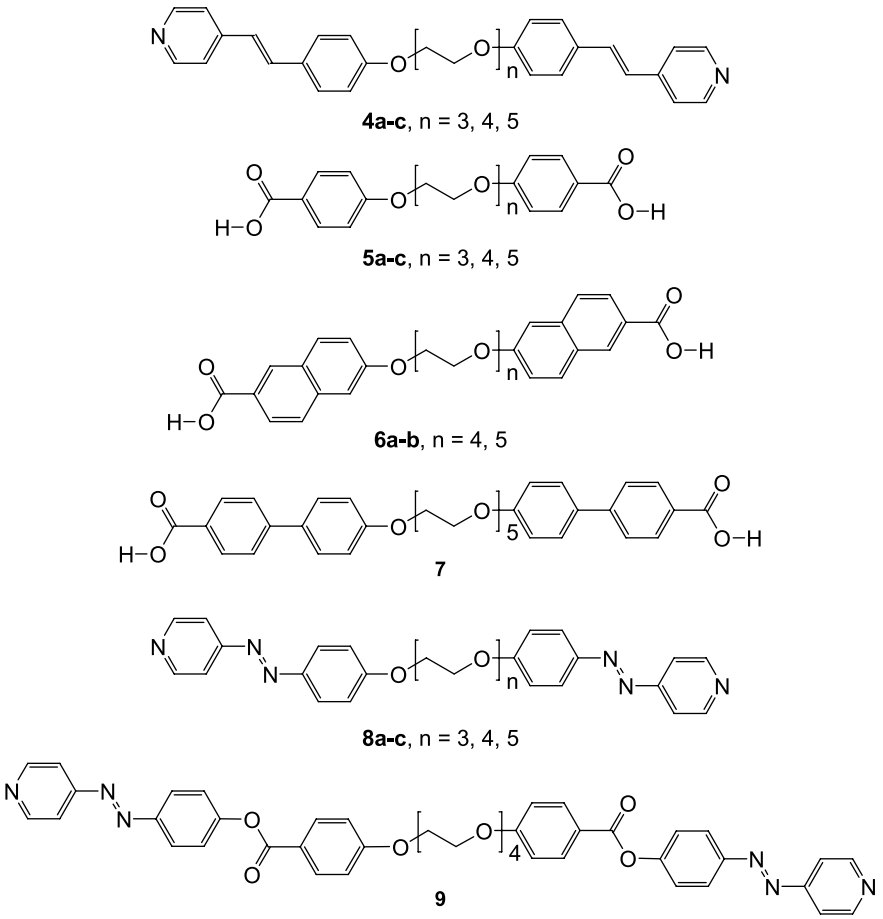

Fig. 7 A selection of bis benzoic acids and bis pyridine derivatives which have been used to access main-chain liquid crystalline polymers

by Hoogboom and Swager. Poly(phenylene ethynylene) derivatives (Fig. 8) that were endcapped with the four-fold hydrogen-bonding ureidopyrimidinone (Upy) motif and containing pendent iptycene groups on every second backbone aromatic ring were synthesized. The iptycene moieties had previously been shown by the same group to create a strong coupling between a rigid polymer and the molecular director of nematic liquid crystals. When such compounds were dissolved in the nematic solvent, 5CB, a strong enhancement of the dichrotic ratio as well as the apparent polymer conjugation length were witnessed for the case of Upy-capped PPE when compared to non-functionalized counterparts. Moreover, it was proven that the length of the main chain supramolecular polymer has an effect on the dichroic ratio. The addition of chain terminating mono-Upy compounds which result in the

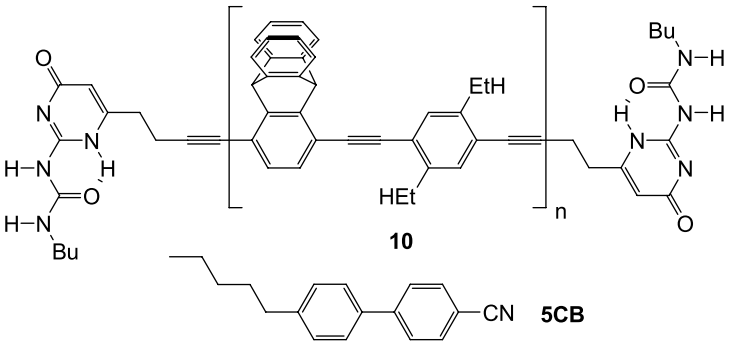

Fig. 8 The structure of the ureidopyrimidinone (Upy) end-capped, pendant iptecene poly(*p*-phenylene ethylene) derivative (**10**) prepared by Hoogboom and Swager [72] to investigate alignment in the liquid crystal 4-*n*-pentyl-4′-cyanobiphenyl (**5CB**)

depolymerization of the supramolecular polymer also results in a drop of the dichroic ratio.

Hydrogen-bonding is not the only supramolecular interaction that can be used to access main-chain SLCPs. Recently, halogen-bonding [73], namely the non-covalent interaction D···X-Y between an electronegative atom D (such as O, N) and a halogen atom X, has been used as another approach to the formation of main-chain supramolecular polymers [74]. In an analogous study to the benzoic acid/pyridine mediated main-chain SLCPs systems discussed previously, Xu and He prepared a series of 1,*n*-bis(4-iodo-2,3,5,6-tetrafluorophenoxy)-alkane compounds (**11a–d**, *n* = 6, 8, 10, 12) and studied its complexes with a series of bispyridine derivatives (e.g., **4a–c**) (Fig. 9). Thus, in this case, the iodotetrafluorophenoxy moieties replaced the benzoic acid binding units used in the previous studies. It should be noted that the presence of the fluorines is important here as their electron withdrawing

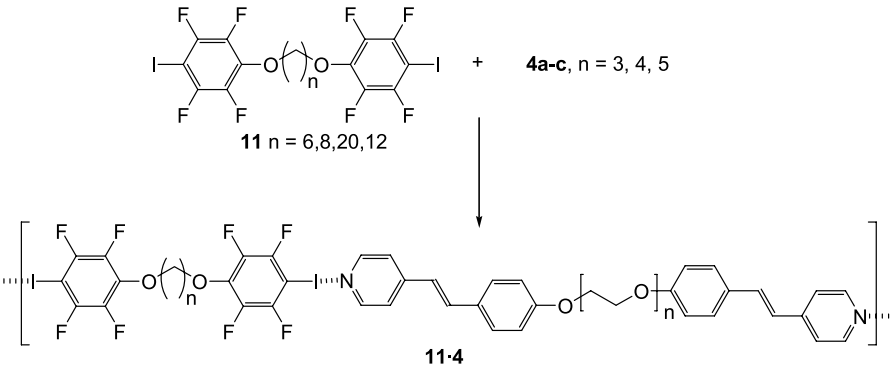

Fig. 9 A halogen-bond mediated main-chain supramolecular liquid crystalline polymer **11·4**

ability reduces the electron density on the iodine atom promoting the N–I halogen bond. Interestingly, the flexibility in **4** appears important for forming LC material with **11**, as complexes of **11** with rigid bispyridine derivatives (e.g., 4,4′-bipyridine) formed only crystalline compounds that melted to an isotropic liquid. However, when both the halogen "donor" compound and bispyridyl compound included flexible spacers, **4·11**, monotropic (unstable to crystallization) nematic phases were observed upon cooling. It should be noted that while these supramolecular materials did form liquid crystal phases, they were generally not as stable as those materials formed from the benzoic acid/pyridine supramolecular motif.

2.2 Supramolecular Columnar Structures

There has been a great amount of work in recent years focused on the formation of 1-dimensional polymers aggregates (Fig. 3e) that form columnar liquid crystal phases. Most of these aggregates utilize π-π-stacking to aid their assembly. For the purpose of this paper we will focus in this section only on systems which utilize specific, tailored supramolecular interactions that have been designed into the monomer to aid the formation of the desired columnar aggregates. A key example of such a system which has attracted some attention is the benzene-1,3,5-tricarboxamide moiety (Fig. 10a). Early work by Matsunaga et al. demonstrated that simple alkyl group derivatives (**12**) of these compounds do form mesophases (e.g., for $n = 12$, K 88 M 212 I) [75]. In order for such molecules to form hydrogen bonded columnar aggregates, the three amide moieties have to distort out of conjugation with the aromatic core (Fig. 10b). Nuckolls et al. showed that long chain alkoxy- [76, 77] or alkyne-substituents [78] on the 2,4 and 6 positions of the benzene-1,3,5-tricarboxamide unit (**13** and **14**, respectively) resulted in the formation of hydrogen-bonded polymeric aggregates that form more stable columnar LC phases (K 98 M 294 I) than the phases observed with the materials without the 2,4,6-substitution (K 88 M 212 I) [75]. The benzene-1,3,5-tricarboxamide core appears to be a flexible platform allowing access to a wide range of LC materials [79, 80]. From the examples reported it appears that while increasing the bulk on the amide positions (as in **15**, Fig. 10c) yields wider LC temperature ranges, primarily as a consequence of reducing the compounds melting point, the clearing temperature is reduced (K – 4 M 178 I). This would be consistent with bulkier groups reducing packing efficiency and destabilizing molecular aggregation. The same benzene-1,3,5-tricarboxamide core has also been used by Meijer et al. to access much larger discotic materials, such as **16** (Fig. 10c), in which the amides are involved in intramolecular hydrogen bonding, rigidifying and preorganizing the mesogenic disc [79, 81].

A number of supramolecular discotic systems have been investigated in which hydrogen bonding has been used to form or stabilize the disc rather

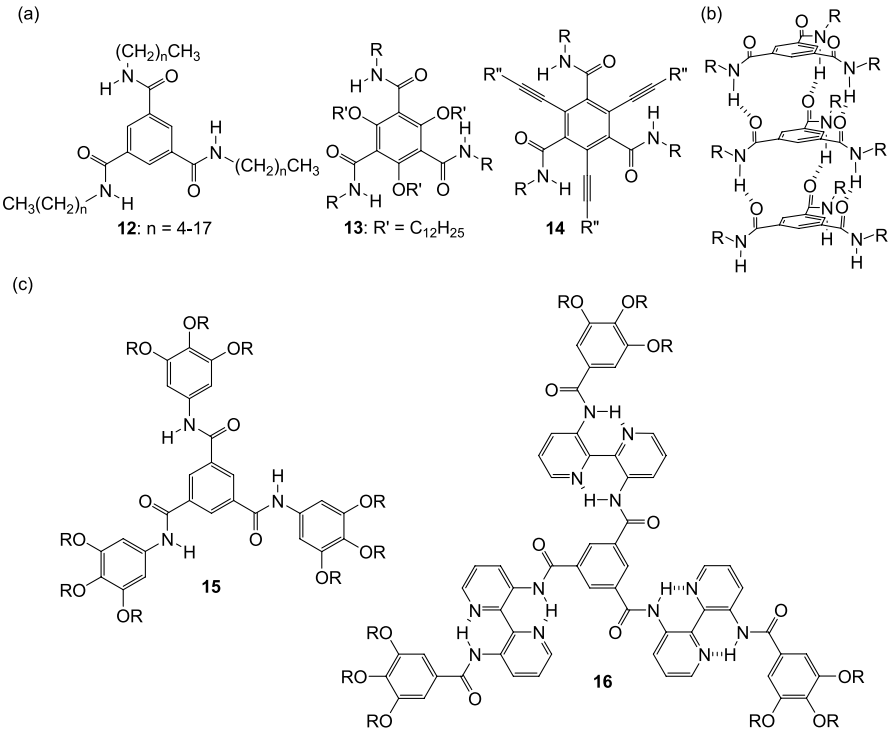

Fig. 10 **a** Chemical structures of benzene-1,3,5-tricarboxamide derivatives (**12**–**14**) which form columnar phases through the assembly of **b** hydrogen-bonded stacks and **c** examples of larger benzene-1,3,5-tricarboxamide derivatives, a bulky derivative (**15**) and a large intra-hydrogen-bond stabilized disc **16**, both of which are known form stable columnar phases

than simply being used to hold pre-made discs together as is discussed above. For example, Meijer et al. have reported the self-assembly of disc-like structures driven by self-complementary four hydrogen bonded array motifs. Figure 11a shows examples of two four hydrogen-bond motifs, ureidiotriazene (**17**) and ureidopyrimidinone (**18**) derivatives [82] which upon dimerization form columnar mesophases (K 25 M 131 I and 25 M 180 I, respectively for R = $C_{12}H_{25}$; M is an undefined mesophase). The same group has also shown that tethering two of these supramolecular motifs with an appropriate spacer results in ditopic materials (**19** and **20**) that also yield stable columnar mesophases (Fig. 11b) [83]. These systems are akin to the main-chain polymers discussed in the previous section but on account of a combination of the nature of the spacer, π-π stacking and phase segregation, they form polymeric stacks that organize into columnar mesophases. In the case of the ureidopyrimidinone derivatives (**19**) the nature of the alkyl length, which was varied from 5 to 8, resulted in dramatic changes in the stability of the mesophase. For example, for

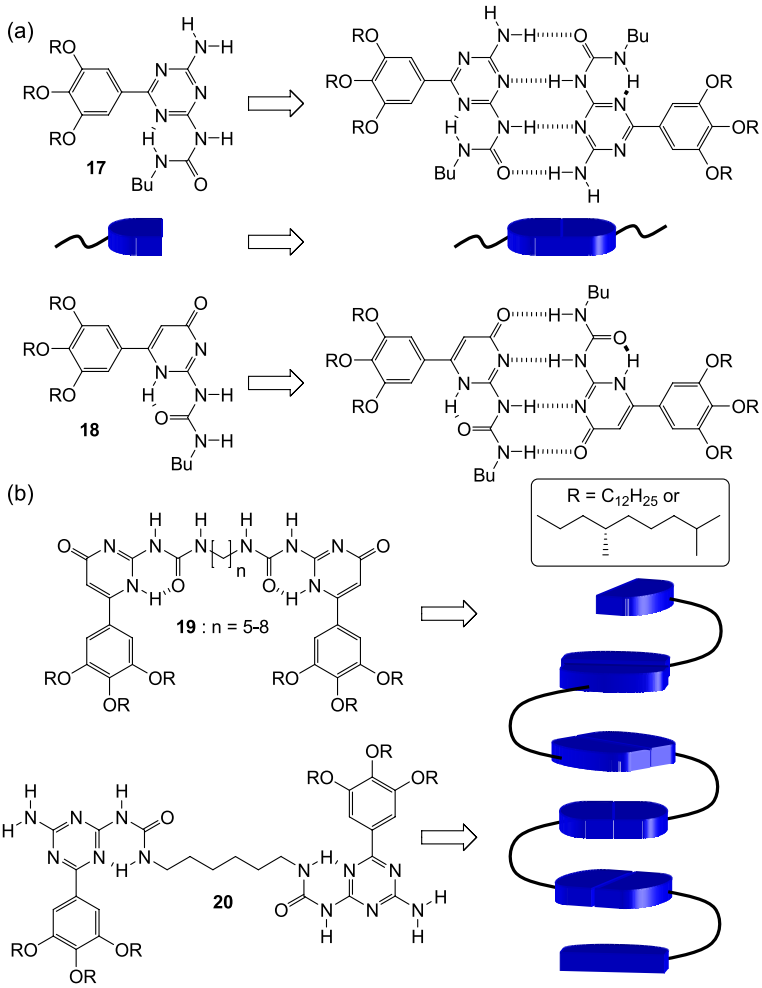

Fig. 11 **a** Chemical structures of mono functional ureidotriazene **17** and ureidopyrimidinone **18** derivatives and their mode of association into mesogenic dimers. **b** Bifunctional derivatives **19** and **20** and a schematic representation of their proposed self-assembly into main-chain supramolecular polymeric columns

the chiral mono-derivative T_{M-I} is 98 °C while T_{M-I} for $n = 7$ is 147 °C and is 207 °C for $n = 8$.

Other more complex supramolecular assemblies of disc-like architectures have also been reported. For example, self-assembly around a trifunctional core can yield columnar mesophases. This can be achieved by addition of appropriately long chain substituted benzoic acid derivatives (**21**) to a tris(imidazole) base (**22**) leading to the formation of a four component supramolecular disc (**21**$_3$·**22**) (Fig. 12a) which exhibits columnar mesophases.

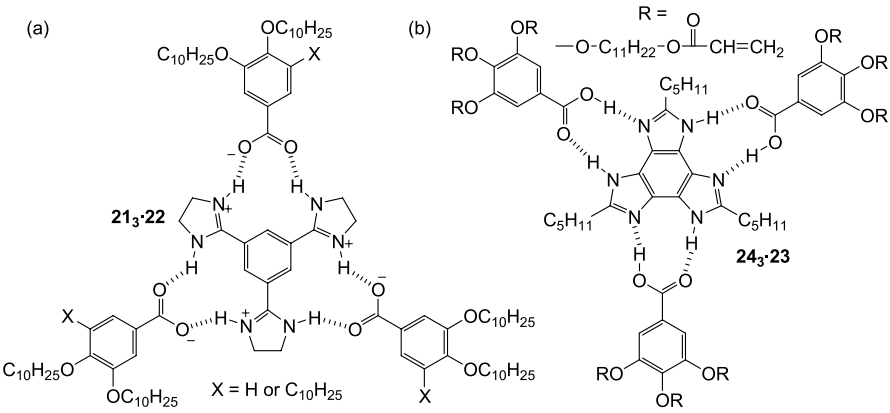

Fig. 12 Chemical structures of mesogenic 3 : 1 discotic complexes based on complexes of benzoic acid derivatives (**21** or **24**) with **a** a *tris*(imidazoline) **22** or **b** a benzotri(imidazole) **23** core

Interestingly, the 3 : 1 complex with the less symmetrical 3,4-substituted benzoic acid shows a more stable mesophase (K 79 M 244 I) than the derivative formed from the 3,4,5 substituted benzoic acid (K 63 M 214 I). A related system has also been reported which uses a benzotri(imidazole) (**23**) as the trifunctional core unit (Fig. 12b) along with benzoic acid derivatives (**24**). This 1 : 3 complex exhibits a hexagonal columnar mesophase between 23 °C and 75 °C. The acrylate moieties on the alkoxyl chains could be photopolymerized to covalently "fix" the LC phase. Removal of the supramolecularly bound benzotri(imidazole) core yields a nanoporous polymer film containing hexagonally-ordered channels–opening the door to the potential application of these materials in such areas as separation, nano-composites, and catalysis.

Interactions other than hydrogen bonding have been utilized in the construction of columnar structures. The aromatic nature of most of the compounds used in discotic systems enables the tailoring of the π-π interactions in order to aid the formation and stability of the desired polymeric stacks. It has been known for a number of years that "doping" electron-rich discotics with electron-poor aromatics leads to mesophases with enhanced stability. For example, the electron rich 2,3,6,7,10,11-hexakis(pentyloxy)triphenylene (**25**, $n = 4$) exhibits a Col_h phase (hexatic columnar) between 69–122 °C, while its 1 : 1 mixture with 2,4,7-trinitrofluoren-9-one (**26**) has a mesophase between 49–232 °C. The complementary interaction between the two aromatic components results in the formation of alternating AB stacks. Park and Hamilton introduced the use of the C_3-symmetric mellitic triimide (**27**) as the electron-deficient component which also forms columnar phases when mixed with derivatives of **25** [84, 85]. It is interesting to note that the stacking of aromatic units often yields offset stacks, in agreement with the Sanders–Hunter model of π-π stacking, which is of course not ideal for the formation

of columnar mesophases. The addition of alkyl chains encourages more overlap of the aromatic cores on account of alkyl-alkyl interactions and phase segregation. Electron-rich/electron-poor aromatic pairs structurally achieve a similar result by maximizing π-system overlap.

Bushby et al. were able to access similar AB stacks with derivatives of **25** using aromatic units, which are not electron-poor [86–88]. They showed that hexakis(4-nonylphenyl)triphenylene (**28**, $n = 8$) forms alternating stacks with **25** (Fig. 13). Unlike the electron-deficient derivatives mentioned previously, which exhibit single liquid crystal phases over a wide composition range of the two components, phase separation between the **25**:**28** and the **25** or **28** mesogenic phases occurs [89]. The driving force for the AB stack formation is a combination of a number of different non-covalent interactions which the authors termed "complimentary polytopic interactions" (CPIs).

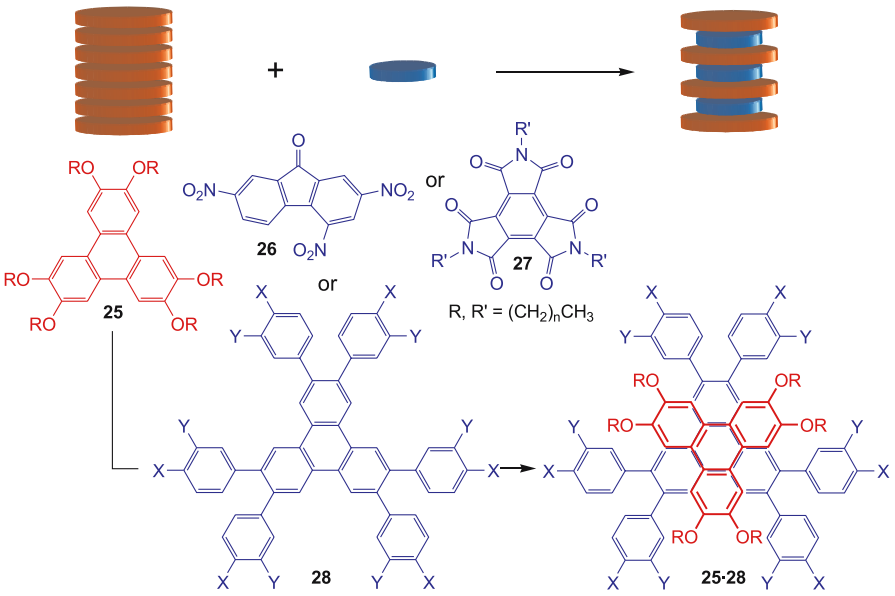

Fig. 13 Self-assembly of alternating stacks can be achieved with an electron-rich **25** and electron-poor **26** or mellitic triimde **27**. Alternatively, complimentary polytopic interactions (CPI) can be used to organize **25** and **28** as shown, yielding the desired assemblies

Electron donor–acceptor (EDA) stacks have been accessed by Percec et al. [90] using partially fluorinated dendrons (Fig. 14) to form LC columnar phases. The self-assembly of the dendrons is primarily driven by phase segregation of the fluorinated chains and the aromatic units. Functionalization of the dendrons at their apex with either an aromatic electroactive donor (**29a**) or an acceptor (**29b**) group yields LC columnar structures, further aided by the additional interaction between the aromatic units, which have optoelec-

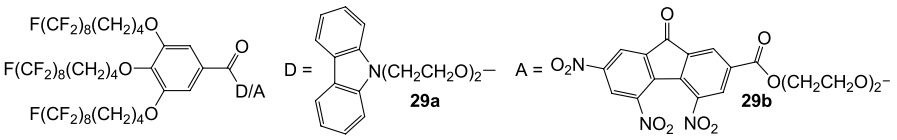

Fig. 14 Examples of dendrons **29a** and **29b** studied by Percec et al. [90] which self-assemble into columnar structures with electroactive aromatic groups at the core

tronic elements present in their cores. The charge carrier mobilities in these LC stacks were two to five orders of magnitude greater than those found in similar amorphous materials. EDA stacks at the center of the columnar liquid crystals can be accessed by mixing a donor and an acceptor containing dendrons or by even mixing amorphous donor (acceptor)-containing linear polymers with an acceptor (donor) dendron.

2.3 Side-Chain and Network SLCPs

Figure 3f–m shows the variety of ways that can be used to access side-chain and network SLCPs. For example, one route involves the binding of monotopic small mesogenic molecules to sites along a polymer backbone to yield "grafted" structures (Fig. 3f). Prior to 2000, a number of such polymers had been reported, for example, using poly(vinyl pyridine) with carboxylic acid end-functionalized mesogens [42–45, 91–95] or poly(acrylic acid) with imidazole end-functionalized mesogens [96]. Using the latter system as the basis for their mesogenic polymers, Ober, Thomas et al. developed temperature-dependent photonic bandgap materials [97]. They used a block copolymer of poly(styrene) (PS, 500 kg/mol) and poly(methacrylic acid) (PMAA, 96 kg/mol) (**30**) which phase segregates into hexagonally packed cylinders of PMAA embedded within a PS matrix. The addition of the imidazole end-functionalized mesogen **31** (0.6 molar ratio mesogen to acrylic acid repeat units) to the block copolymer yields a SLCP on account of the hydrogen bonding of the mesogenic molecule to the PMAA block (Fig. 15a). This, along with the increased volume fraction of the PMAA-LC block, results in films of this material that form lamellar structures consisting of alternating PS and PMMA-LC domains, with a periodicity ca. 170 nm, that are orientated parallel to the surface. The liquid crystal domains show smectic ordering and a broad smectic-to-isotropic transition from 65–85 °C. Without any heat treatment these films are green in color; however, upon heating into the isotropic regime (80 °C) the films turn red-orange. This irreversible change in color is a consequence of the change in the peak reflectance of about 40 nm which is assigned to the randomized orientation of the mesogens in the isotropic state changing the refractive index contrast of the layers. Using similar materials, the same group demonstrated that SLCPs could undergo orientational switching

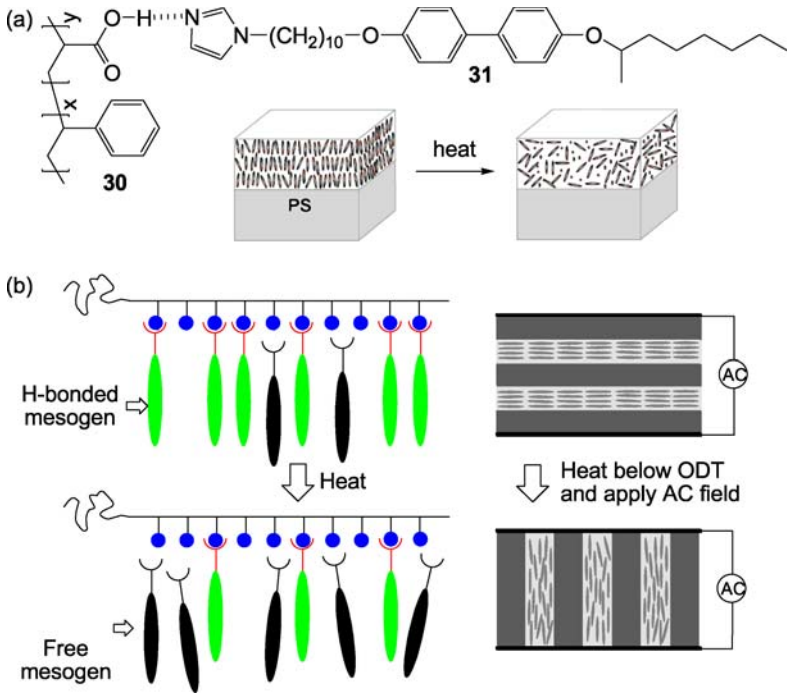

Fig. 15 **a** The structure of the side chain SLC block copolymer **30·31** used by Ober and Thomas to access temperature-dependant photonic band gap materials **b** A Schematic of the proposed model for "free" mesogen formation believed to be important for the re-orientation of blends heated below ODT in an applied AC field

of both the mesogens and microdomains with AC fields [98]. In this case, a lower molecular weight polystyrene-*block*-acrylic acid (25 and 5.3 kg/mol), to enhance the mobility of the system, was used as the block copolymer. The addition of the mesogen (0.8 molar ratio mesogen to acrylic acid repeat units) to this system resulted in films which again formed lamellar morphologies (6 nm thickness) in which one of the domains exhibits a smectic phase. SAXS data indicated that the smectic phase destabilizes at 110 °C and that the material shows an order–disorder transition (ODT) occurring at ca. 170 °C. It should be noted that, from POM observations, the films do not go isotropic until 135 °C, suggesting the presence of an additional LC phase. The lamellar morphologies formed run parallel to the (electrode) surface on account of a shear-induced alignment that occurred during sample preparation. Simple heating of the film above the ODT resulted in complete loss of orientation upon cooling. However, if the film is heated above the ODT and cooled under an AC field ($1 \sim 2\ V\mu m^{-1}$ with a frequency of 10 Hz) alignment of the lamellar structure occurs normal to the electrode (perpendicular orientation). More interestingly, the parallel orientation can be directly converted into the per-

pendicular orientation by heating the sample above the T_g of both blocks but below the ODT under the AC field. Control experiments showed that such alignment switching does not occur with the block copolymer by itself or with a side chain polymeric aggregates in which the side chains are non-mesogenic side chains, demonstrating the importance of liquid crystallinity to the orientational switching. Furthermore, structurally similar covalent side-chain LCPs and a SLCP with a lower fraction (0.5 molar ratio) of the mesogen also showed no orientational switching. The proposed mechanism for this process involved the presence of some "free" mesogen, which from FT-IR is present in the SLCP with a 0.8 molar ratio of the mesogen that helps to plasticize both blocks, resulting in "higher mobility" of the material and thus allowing the electric field induced orientational switching below the ODT (Fig. 15b).

Other non-covalent interactions, for example, ionic interactions, can be used to bind a mesogen to a polymer backbone. Thünemann et al. showed that poly(ethylene oxide)-block-poly(L-lysine) (**32**), in which the lysine units are positively charged, can form side-chain SLCPs with negatively charged mesogenic units, such as the discotic-columnar phase forming hexabenzocoronene (**33**) [99]. This side-chain SLCP forms two thermotropic liquid crystal columnar phases, exhibiting an order-order transition at 54 °C on heating. The proposed structure involves poly(L-lysine), which forms a α-helical structure surrounded symmetrically by six columns of hexabenzocoronene cores (Fig. 16).

Most of the work to date has focused on side-chain SLCPs in which the polymeric component is linear. However, there have been a few reports recently in

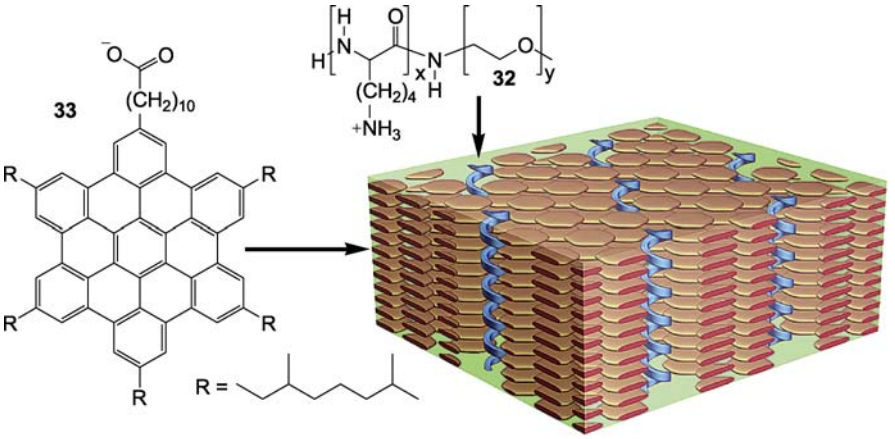

Fig. 16 The molecular structure of two components, poly(ethylene oxide)-*block*-poly(L-lysine) (**32**) and hexa-peri-hexabenzocoronene (**33**), used to form an ionic complex SLCP and a model of its α-helical-*within*-discotic columnar structure. Each α-helical poly(L-lysine) chain is surrounded symmetrically by six columns of **33** (disks) [99]

which mesogenic groups are bound to dendritic or hyperbranched polymers. Tsiourvas, Paleos et al. have reported a couple of systems for which they have studied the properties of complexes of the cholesterol carboxylic acid derivative **34** and pyridine end-capped dendrimers [100] or hyperbranched polymers [101]. Amine-terminated diaminobutane poly(propyleneimine) dendrimers functionalized with 3-pyridyl isothiocyanate (**35**, generation 2–5) formed smectic-A LC phases upon the addition of an equimolar quantity (relative to the number of pyridyl moieties) of **34** (Fig. 17a). All the systems formed glassy birefringent materials at room temperature, which became birefringent fluids above T_g (ca. 55 °C). No other transitions were observed. The smectic periodicities only slightly increased with generation ranging from 5.4 nm in generation 2 to 5.6 nm in generation 5, suggesting that the flexible dendrimer forms a "flattened" conformation between the orthogonally oriented hydrogen bonded pyridyl-cholesteryl moieties. Similar types of structures have been proposed for structurally similar covalent derivatives [102]. The same group went on to study hyperbranched polymers using the same supramolecular motif and mesogen (Fig. 17b). This time, the polymer was a pyridine end-capped hyperbranched polyether polyol **36**. As in the case of the dendritic SLCPs discussed

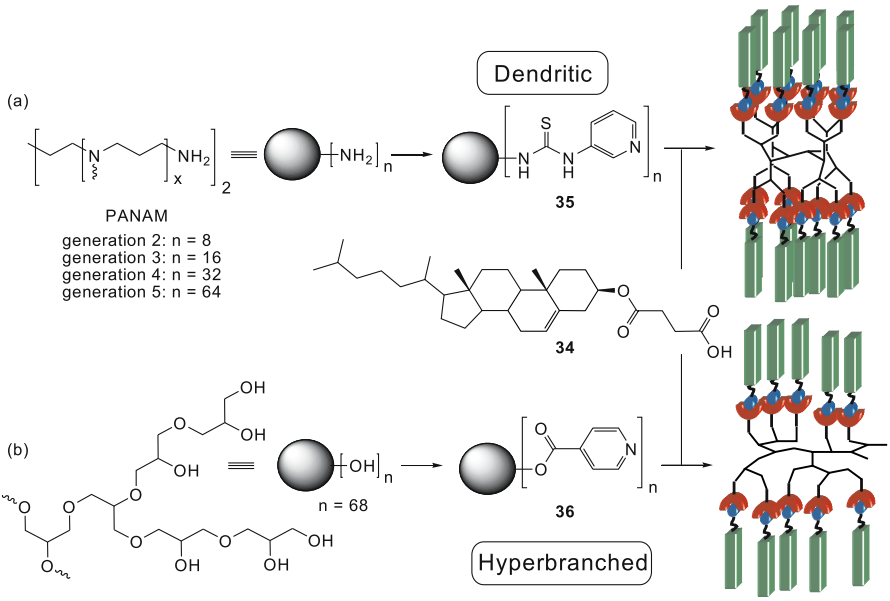

Fig. 17 **a** The chemical structure of the pyridyl-functionalized PANAM **35** and the schematic of the smectic phase which is formed upon complexation with 3-cholesteryloxycarbonylpropanoic acid **34** **b** The chemical structure of the pyridyl-functionalized hyperbranched polyol **36** and schematic of the smectic phase which is formed upon complexation with **34**

above, the complexes of these materials form smectic-A phases and the smectic distances suggest that the hyperbranched polymer forms a flattened structure.

Dendritic SLCPs, which use ionic interactions to bind the mesogen and dendrimer, have also been reported by Tsiourvas et al. [103]. In a study similar to those mentioned above, amine-terminated diaminobutane poly(propyleneimine) dendrimers were directly complexed with the cholesterol carboxylic acid derivative. From a supramolecular point of view this system is more complicated than the studies with the pyridyl end-functionalized dendrimers in that there are potentially two different binding motifs that can occur: namely, the carboxylic acid can either bind to a primary or a tertiary amine. The studies show that in the 1 : 1 (mesogen to primary amine) complexes about 70% of the primary amines are protonated for generations 1 and 2 while only 50% are protonated in generations 4 and 5, suggesting that the mesogens are interacting with both sites. All of the generations form smectic glass phases at room temperature which become smectic C* phases above T_g (ca. 38 °C). At higher temperatures ca. 105 °C for generations 1 and 2 and ca. 90 °C for generations 4 and 5, the smectic layer thickness increases which is assigned as an order-order transition from smectic C* to smectic A. It is interesting to note that no smectic C phase is observed for the previously discussed structurally-similar covalent or hydrogen bonded derivatives. It is argued that the presence of additional "internal" tertiary amine binding sites is a possible cause of this.

Some of the earliest examples [42–45] of SLCPs belonged to the class of side-chain materials in which the supramolecular motif itself is the mesogen (Fig. 3g). In those materials pyridine/benzoic acid was used as the binding motif. Since 2000 there have been a number of publications which have utilized this motif to access side-chain SLCPs. For example, supramolecular LC polyurethanes can by accessed by adding 4-dodecyloxybenzoic acid to a polyurethane which has pyridyl units incorporated into its backbone [104]. Both side-chain and side-chain network SLCPs which are formed through the pyridine/benzoic acid association have been recently reported by Lin et al. [105]. They investigated the LC behavior of a series of benzoic acid and stilbazole-containing monomers and polymers (Fig. 18). Formation of the side-chain SLCPs generally results in an increase in the smectic temperature range over the control monomeric complexes, presumably as a result of the reduced crystallinity of the polymer components. In fact, the side chain SLCPs formed from the stilbazole polymer **37** and monomeric benzoic acid derivative **38** do not crystallize at all, forming glassy smectic phases (G 78 S_A 127 I). Interestingly, however, side chain SLCPs with the binding motif reversed (i.e. formed from the benzoic acid polymer **39** and monomeric stilbazole derivative **40**) form crystalline materials at lower temperature (< 111 °C) and do exhibit higher clearing temperatures (S_A 150 I). The difference observed here is assigned primarily to the reduced packing efficiency (relative to the benzoic acid polymers) of the stilbazole poly-

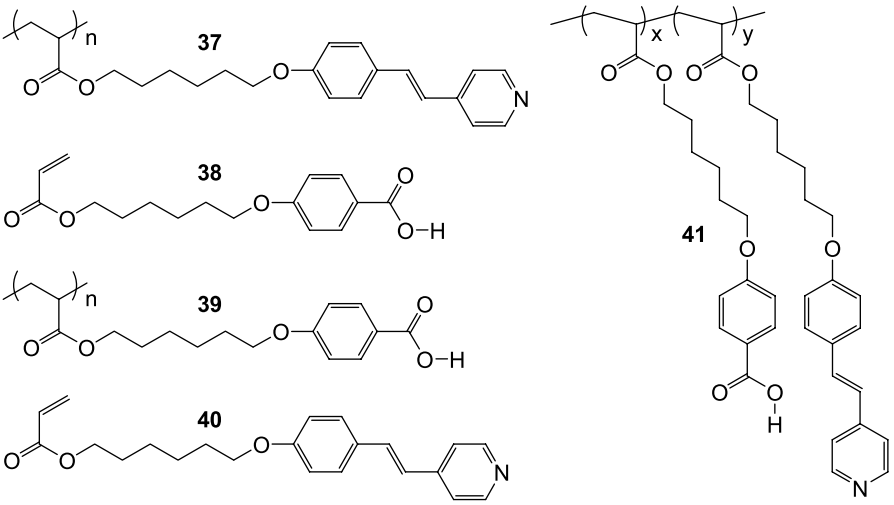

Fig. 18 Chemical structures of monomers and polymers used by Lin et al. to access side chain and network SLCPs

mers leading to reduced stability (a lower clearing temperature) of the LC phase and formation of LC phases at lower temperatures. This nicely demonstrates the importance of carefully designing the nature of the supramolecular motif in such side chain SLCPs. SLCP networks formed using these same materials were also investigated. A series of supramolecular polymers (**41**) with different mole fractions of benzoic acid units were used to compare the blend of the two complementary polymers (**37** and **39**) with a copolymer which contains both binding motifs. It was found that the copolymer **41** forms LC materials with a much wider mole fraction of benzoic acid derivatives than the blends of **37** and **39** (0.42–0.89 vs 0.4–0.55), which is consistent with the formation of more homogenous structures in the copolymers. In general, for both systems the higher the crosslinked density (i.e., the closer to a 1 : 1 molar ratio of benzoic acid:stilbazole) the more stable the LC phase is, although it should be noted that higher isotropization temperatures are observed with an increase in the ratio of benzoic acid moieties. This is presumably a consequence of the ability of the benzoic acid units to form hydrogen bonding homo-complexes via carboxylic acid dimers. The same groups went on to investigate related SLCP networks in which the benzoic acid containing polymer was "crosslinked" with a bis(pyridyl) small molecule, demonstrating that these complexes also formed smectic phases [106].

An example of side-chain SLCPs whose mesogen consists of part of the main-chain as well as the side chain (Fig. 3h) has been reported by Kato et al. [107]. In this case the hydrogen bond mesogenic motif utilized was a benzoic acid (as part of the small molecule side chain **42**) with a 2,6-diamino-

pyridine (as part of the polyamide **43** backbone) moiety. It was demonstrated in these systems that stable (up to ca. 200 °C) mesophases could be formed if there is a substitutent meta to the benzoic acid. If no meta substitutent is present, then no mesophase was formed. It was hypothesized that the substitution helps to fill in extra space in the supramolecular aggregate (Fig. 19) thus helping to stabilize the orientations in the mesogenic complexes.

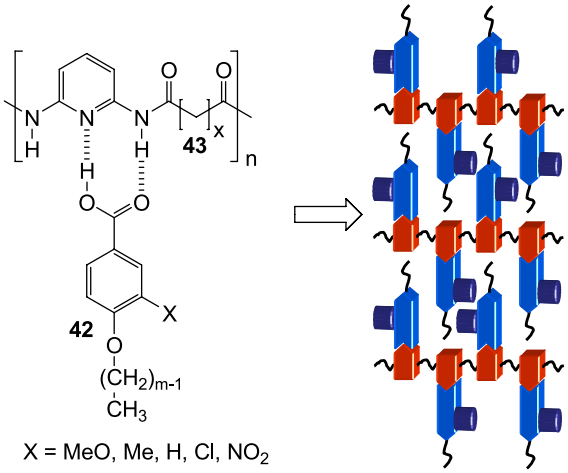

Fig. 19 The structure of the polymeric complex of benzoic acid derivatives **42** with the 2,6-diaminopyridyl-containing polyamides **43** and a schematic of the proposed molecular arrangement of its LC phase

All of the supramolecular motifs discussed so far are closed systems, i.e., only two components interact. However, there are a number of supramolecular motifs that self-assemble into open linear aggregates. Here, attaching appropriate side-chains to such motifs offers an alternative way to access side-chain SLCPs (Fig. 3i) in which the polymeric backbone consists of both covalent and non-covalent bonds. Kato et al. have reported a series of studies with folic acid derivatives **44** to access thermotropic LC materials (Fig. 20). It was found that the nature of the side chains plays an import role in the mesomorphic behavior of these systems. Molecules with small alkyl chains ($n = 6, 11$) attached to the glutamic acid residue in the folic acid form smectic phases with periodic distances consistent with the hydrogen-bonded tape side-chain SLCPs. Increasing the size of the alkyl chains ($n = 14, 16$) changes the nature of the hydrogen-bonding assembly from linear tapes to macrocyclic quartets, which in turn yields a discotic mesogenic unit and results in columnar phases. For the $n = 11$ compound, the smectic phase can be converted into the columnar phase by the simple addition of alkali metal ions, which are known to template the formation of cyclic quartets [108, 109]. Further increase in

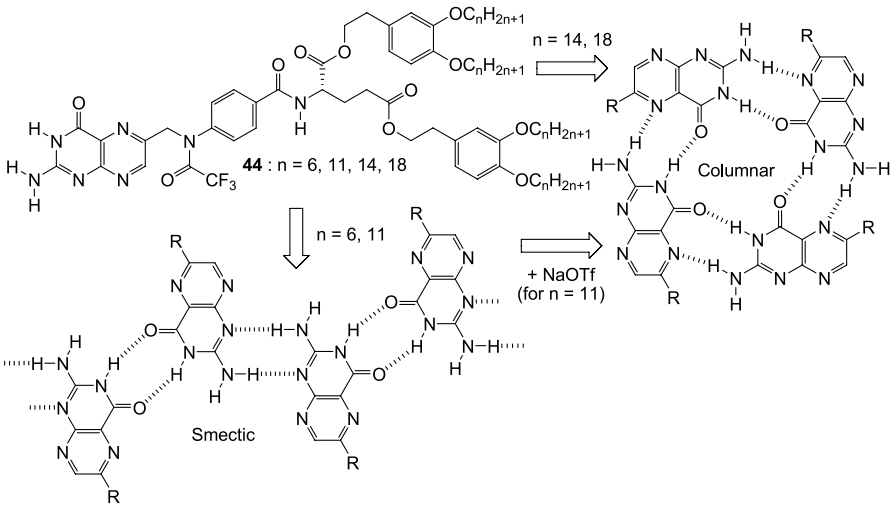

Fig. 20 The chemical structure of a thermotropic folic acid derivative **44** and its proposed self-assembly into smectic or columnar phases

the size of the side chains through attachment of dendritic oligo(glutamic acid) derivatives to the folic acid result in the formation of cubic as well as columnar phases [110, 111]. A number of other related supramolecular tape side-chain LCPs has also been reported and include binding motifs such as aromatic amides [112, 113] and barbituric acid dye-melamine [114] tapes, both of which form columnar phases.

Rather than having the hydrogen bonding group at the end of the molecule, the placement of a hydrogen-bonding motif in the middle of the mesogen can have a profound affect on the nature and stability of the mesophase. For example, there have been a number of reports through the years of using lateral hydrogen bonding to help to stabilize smectic phases (Fig. 21a). In a recent example, Snieckus and Lemieux compared a series of fluorenone derivatives (**45a**), with no lateral hydrogen bond donors, with fluorenol derivatives (**45b**), which contain a hydrogen bonding group in a lateral position (Fig. 21b) [115]. They found that the fluorenones formed both smectic and nematic phases (K 74 SmC* 77 N 87 I for $n = 8$), while the fluorenols only formed smectic phases which were also much more stable (K 70 SmC* 116 I for $n = 8$). Kishikawa et al. showed [116] with a series of aromatic ester mesogens that replacing one ester with an amide not only increases the stability of the material but changes the type of the mesogenic phase formed (Fig. 21c). In the case of the ester derivative **46a** both smectic A and nematic phases (K 124 SmA 237 N 250 decomp) are formed while the amide-containing compound **46b** exhibits two smectic C phases and smectic A phase which is stable at much higher temperatures (K 202 SmC_x 206 SmC_y 280 SmA 237 decomp). FT-IR data suggest that in the SmC_x phase there are

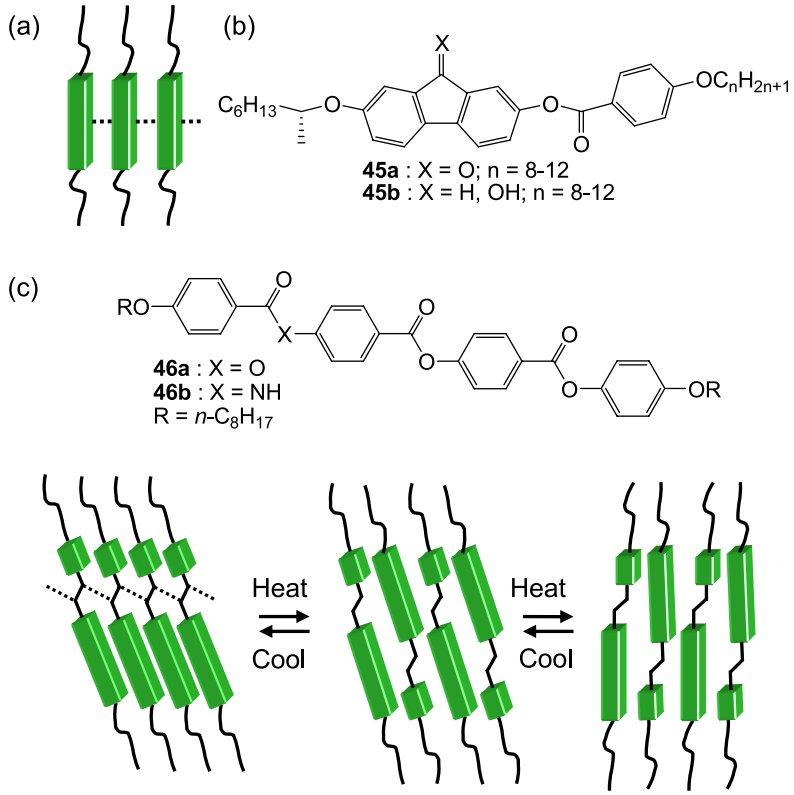

Fig. 21 **a** The schematic of lateral hydrogen bonding in a mesogenic phase. **b** The chemical structure of the fluorenone **54a** and fluorenol **54b** derivatives studied by Sniekus and Lemieux **c** Aromatic esters/amides **46a** and **46b** studied by Kishikawa and their proposed smectic phase assemblies

strong hydrogen bonding interactions present, leading the proposition of a syn-parallel (tape-like) arrangement for this phase. At higher temperatures a decrease in hydrogen bonding is observed as the phase transitions into a SmC_y and then a SmA phase. It is proposed than in these two phases the molecules are arranged in an anti-parallel manner to cancel out their large dipoles.

3 Perspectives and Outlook

It is clear that in recent times the toolbox of interactions and building blocks for SLCPs is at hand and that structure-property relationships have been established. A vast array of architectures and LC assemblies has been demon-

strated, but largely in a mode of structure-property relationship assessment within a homologous series of samples. What is now needed is research that examines the exploitation of the labile nature of supramolecular interactions within SLCP constituent chains. For example, main-chain SLCPs possess an ability to undergo dramatic molecular weight reduction through the reduction of the inter monomer supramolecular interactions, which in turn can directly impact liquid crystallinity. As such, the temperature-dependence of LC order and associated optical and mechanical characteristics deserves close attention and technological exploitation. Additives may reversibly impact hydrogen-bonding; for example, salts may alter the local dielectric environment, and thereby disfavor supramolecular assembly cascading to optical, and mechanical macroscopic properties may open the door to chemo-mechanical or chemo-optical transduction.

Supramolecular polymers, and SLCPs in particular, offer the intrinsic capacity to "self-heal" through the reversible nature of the non-covalent bonding between constituent monomers. However, this avenue of applied research has not been adequately studied and deserves attention. In particular, we envision studies that discern the separate roles of LC phase behavior and the supramolecular motif in dictating the material's ability to repair damage, whether autonomously or with limited intervention. Uniquely, SLCPs may offer the additional advantage of the optical evaluation of damage and its repair through the highly sensitive and space-amplifying nature of birefringence [117]. Thus, we anticipate multifunctional self-healing materials for SLCPS that combines re-bonding with facile healing assessment.

Significant advances have been witnessed in the separate areas of metal-based supramolecular polymers [118] and metallo-mesogenic liquid crystals [119], yet the two fields have not combined to yield any examples of metal-based SLCPs. Clearly, an opportunity exists in such an area. For example, polymers consisting of mesogenic ligands as repeating units may bind metal atoms (or cations) and such a binding may alter the LC phase behavior and optical characteristics. As another example, conventional LC polymers could be terminated with metal-binding ligands to yield telechelics LCPs that crosslink with metal incorporation. Certainly, many other examples can be conceived, and we anticipate significant activity in the near future.

Finally, the use of SLCPs as "reworkable" adhesives and coatings is an area for applied research in the field deserving attention. Here, the term "reworkable" refers to a capacity to repeatedly re-bond with the same adhesive material, as warranted by the application. For adhesives (which we will focus on here) it is necessary for the material to feature a very low viscosity during application–allowing a dimensionally thin bond to form–yet the low viscosity must convert to a high shear-strength solid to allow stress transfer from one part to the other, bonded part. Ordinarily, this conversion from liquid to solid is achieved though the covalent polymerization of multifunctional monomers, whether initiated by heat, light, or redox reactions. With such an

approach, the bond can only be broken by irreversible cohesive or adhesive failure, thus limiting the functionality of such materials. As an alternative, "hot melt adhesives" are thermoplastics that are intrinsically reworkable, yet suffer from a high viscosity that is too high for use in thin-dimension applications. Supramolecular polymers, and SLCPs in particular, may bridge the two approaches to adhesion by allowing melting to a monomer-like low viscosity (particularly low for the SLCP case) and strength growth during cooling and supramolecular polymerization. Because liquid crystallinity, itself, may enhance the degree of supramolecular polymerization (vide supra), the adhesive strength possible may well be higher for SLCPs as compared to their isotropic counterparts. Of course, if debonding is required in the future, supramolecular depolymerization can be triggered by heating and the adhesive reapplied as necessary.

We contend that the future is bright for the field of SLCPs and it is fully anticipated that the field will continue to grow. Sustained investigations into the chemistry and physics of SLCPs will position researchers for discovery of unanticipated compositions and properties, while application development building upon existing findings will make use of this exciting class of materials.

References

1. Flory PJ, Abe A (1978) Macromolecules 11:1119–1124
2. Warner M, Flory PJ (1980) J Chem Phys 73:6327–6332
3. Abe A, Ballauf M (1991) In: Cifferi A (ed) Liquid Crystallinity in Polymers: Principles and Fundamental Properties, Chap 4. John Wiley & Sons, Inc., New York USA
4. Han H, Bhowmik PK (1997) Prog Polym Sci 22:1431–1502
5. Sirigu A (1991) In: Cifferi A (ed) Liquid Crystallinity in Polymers. Principles and Fundamental Properties. VCH Publishers, Inc., New York
6. Dubois JC, Le Barny P, Noel C (1997) Acta Polym 48:47–87
7. Kang D, Mahajan MP, Petschek RG, Rosenblatt C, He C, Liu P, Griffin AC (1998) Phys Rev E 58:2041–2046
8. Jackson WJ Jr, Kuhfuss HF (1976) J Polym Sci Polym Chem Ed 14:2043–2058
9. Roviello A, Sirigu A (1975) J Polym Sci Polym Lett Ed 13:455–463
10. Griffin AC, Havens SJ (1981) J Polym Sci Polym Phys Ed 19:951–961
11. Mather P, Grizzuti N, Heffner G, Ricker M, Rochefort WE, Seitz M, Schmidt H-W, Pearson DS (1994) Liq Cryst 17:811–826
12. Percec V, Yourd R (1989) Macromolecules 22:524–537
13. Qin H, Chakulski BJ, Rousseau IA, Chen J, Xie X-Q, Mather PT, Constable GS, Coughlin EB (2004) Macromolecules 37:5239–5249
14. Kempe MD, Kornfield JA, Ober CK, Smith SD (2004) Macromolecules 37:3569–3575
15. Zhao Y, Dong S, Jamieson AM, Hu X, Lal J, Nazarenko S, Rowan SJ (2005) Macromolecules 38:5205–5213
16. Brunsveld L, Folmer BJB, Meijer EW, Sijbesma RP (2001) Chem Rev 101:4071–4097
17. Ciferri A (2002) Macromol Rapid Comm 23:511–529

18. Ciferri A (ed) (2005) Supramolecular Polymers, Second Edition. CRC Press, Taylor and Francis, Boca Raton, FL, USA
19. Lehn J-M (1990) Angew Chem Int Ed Engl 29:1304–1319
20. Sivakova S, Bohnsack DA, Suwanmala P, Mackay ME, Rowan SJ (2005) J Am Chem Soc 127:18202–18211
21. Yount WC, Loveless DM, Craig SL (2005) Angew Chem Int Ed 44:2746–2748
22. Kato T, Fréchet JMJ (1995) Macromol Symp 98:311–326
23. Kato T (1996) Supramolec Sci 3:53–59
24. Lee CM, Griffin AC (1997) Macromol Symp 117:281–290
25. Kamikawa Y, Nishii M, Kato T (2004) Chem Eur J 10:5942–5951
26. Cher Ling Toh CL, Xu J, Lu X, He C (2005) J Polym Sci Part A Polym Chem 43:4731–4743
27. Lehn J-M (1993) Makromol Chem Macromol Symp 69:1–17
28. Paleos CM, Tsiourvas D (1995) Angew Chem Int Ed 34:1696–1711
29. Muthukumar M, Ober CK, Thomas EL (1997) Science 277:1225–1232
30. Treybig A, Dorscheid C, Weissflog W, Kresse H (1995) Mol Cryst Liq Cryst 260:369–376
31. Torgova SI, Strigazzi A (1999) Mol Cryst Liq Cryst 336:229–245
32. Percec V, Heck J, Johansson G, Tomazos D, Kawasumi M, Chu P, Ungar G (1994) Mol Cryst Liq Cryst Sci Technol Sect A 419:384–387
33. Percec V (1997) Macro Symp 117:267–273
34. Spada GP, Gottarelli G (2004) Synlett 4:596–602
35. Lehn J-M (2002) Poly Int 51:825–839
36. Kato T, Mizoshita N, Kanie K (2001) Macromol Rapid Comm 22:797–814
37. Paleos CM, Tsiourvas D (2001) Liq Cryst 28:1127–1161
38. Ciferri A (1999) Liq Cryst 26:489–494
39. Kato T (1998) In: Demus D, Goodby JW, Gray GW, Spiess H-W, Vill V (eds) Handbook of Liquid Crystals, Vol 2B. Wiley-VCH, Weinheim, Germany, pp 969–979
40. Kato T (2000) Struct Bond 96:95–146
41. Kato T, Mizoshita D, Kishimoto K (2006) Angew Chem Int Ed 45:38–68
42. Kato T, Fréchet JMJ (1989) J Am Chem Soc 111:8533–8534
43. Kihara H, Kato T, Uryu T, Fréchet JMJ (1996) Chem Mater 8:961–968
44. Kato T, Hirota N, Fujishima A, Fréchet JMJ (1996) J Polym Sci Part A Polym Chem 34:57–62
45. Kato T, Fréchet JMJ (1995) Macromol Symp 98:311–326
46. Brienne MJ, Gabard J, Lehn J-M, Stibor I (1989) J Chem Soc Chem Comm 1868–1870
47. Lehn JM, Mascal M, DeCian A, Fischer J (1990) J Chem Soc Chem Comm 479–481
48. Gulik-Krzywicki T, Fouquey C, Lehn J-M (1993) Proc Natl Acad Sci USA 90:163–167
49. Kotera M, Lehn J-M, Vigneron J-P (1994) J Chem Soc Chem Comm 2:197–199
50. Kotera M, Lehn J-M, Vigneron JP (1995) Tetrahedron 51:1953–1972
51. Bladon P, Griffin AC (1993) Macromolecules 26:6604–6610
52. St Pourcain C, Griffin AC (1995) Macromolecules 28:4116–4121
53. Lee CM, Griffin AC (1997) Macromol Symp 117:281–290
54. He C, Donald AM, Griffin AC, Waigh T, Windle AH (1998) J Polym Sci Part B Poly Phys 36:1617–1624
55. Liang Z, Cabarcos OM, Allara DL, Wang Q (2004) Adv Mater 16:823–827
56. Kosonen H, Ruokolainen J, Knaapila M, Torkkeli M, Jokela K, Serimaa R, ten Brinke G, Bras W, Monkman AP, Ikkala O (2000) Macromolecules 33:8671–8675
57. Calzolari A, Di Felice R, Molinari E, Garbesi A (2002) Physica E 13:1236–1239
58. Tew GN, Pralle MU, Stupp SI (2000) Angew Chem Int Ed 39:517–521

59. Chen XL, Jenekhe SA (2000) Macromolecules 33:4610–4612
60. Weng W, Beck JB, Jamieson AM, Rowan SJ (2006) J Am Chem Soc 128:11663–11672
61. Knapton D, Weder C, Rowan SJ (2006) Macromolecules 39:651–657
62. Iyer P, Beck JB, Rowan SJ, Weder C (2005) Chem Comm 319–321
63. Sivakova S, Rowan SJ (2003) Chem Comm 19:2428–2429
64. Sivakova S, Wu J, Campo CJ, Mather PT, Rowan SJ (2006) Chem Eur J 12:446–456
65. Burke KA, Sivakova S, McKenzie BM, Mather PT, Rowan SJ (2006) J Polym Sci A Polym Chem 44:5049–5059
66. Alexander C, Jariwala CP, Lee CM, Griffin AC (1994) Macromol Symp 77:283–294
67. Lu XH, He CB, Terrell CD, Griffin AC (2002) Macromol Chem Phys 203:85–88
68. Toh CL, Xu JW, Lu XH, He CJ (2005) Polym Sci A Polym Chem 43:4731–4743
69. Riedel PJ, Kumpfer JR, Rogness DC, Wiegel KN (2006) J Appl Polym Sci 102:5890–5894
70. Rogness DC, Riedek PJ, Sommer JR, Reed DF, Wiegel KN (2006) Liquid Cryst 33:567–572
71. Bhowmik PK, Wang XB, Han HS (2003) J Polym Sci A Polym Chem 41:1282–1295
72. Hoogboom J, Swager TM (2006) J Am Chem Soc 128:15058–15059
73. Metrangolo P, Resnati G, Pilati T, Liantonio R, Meyer F (2007) J Polym Sci Part A Polym Chem 45:1–15
74. Xu JW, Liu XM, Lin TT, Huang J, He C (2005) Macromolecules 38:3554–3557
75. Matsunaga Y, Miyajima N, Nakayasu Y, Sakai S, Yonenaga M (1988) Bull Chem Soc Jpn 61:207–210
76. Bushey ML, Hwang A, Stephens PW, Nuckolls C (2001) J Am Chem Soc 123:8157–8158
77. Bushey ML, Hwang A, Stephens PW, Nuckolls C (2002) Angew Chem Int Ed 41:2828–2831
78. Bushey ML, Nguyen T-Q, Nuckolls C (2003) J Am Chem Soc 125:8264–8269
79. van Grop JJ, Vekemans JAJM, Meijer EW (2002) J Am Chem Soc 124:14759–14769
80. Hwang IH, Lee SJ, Chang JY (2003) J Polym Sci Part A Polym Chem 41:1881–1891
81. Palmans ARA, Vekemans JAJM, Fischer H, Hikmet RA, Meijer EW (1997) Chem Eur J 3:300–307
82. Hirschberg JHKK, Brunsfeld L, Ramzi A, Vekemans JAJM, Sijbesma RP, Meijer EW (2000) Nature 407:167–170
83. Hirschberg JHKK, Koevoets RA, Sijbesma RP, Meijer EW (2003) Chem Eur J 9:4222–4231
84. McMenimen KA, Hamilton DG (2001) J Am Chem Soc 123:6453–6454
85. Park LY, Hamilton DG, McGehee EA, McMenimen KA (2003) J Am Chem Soc 125:10586–10590
86. Arikainen EO, Boden N, Bushby RJ, Lozman OR, Vinter JG, Wood A (2000) Angew Chem Int Ed 39:2333–2336
87. Boden N, Bushby RJ, Liu Q, Lozman OR (2001) J Mater Chem 11:1612–1617
88. Boden N, Bushby RJ, Cooke G, Lozman OR, Lu Z (2001) J Am Chem Soc 123:7915–7916
89. Boden N, Bushby RJ, Lozman OR (2004) Mol Cryst Liq Cryst 411:345–354
90. Percec V, Glodde M, Bera TK, Miura Y, Shiyanovskaya I, Singer KD, Balagurusamy VSK, Helney PA, Schnell I, Rapp A, Spiess H-W, Hudson SD, Duan H (2002) Nature 419:384–387
91. Kato T, Fréchet JMJ (1989) Macromolecules 22:3818
92. Kato T, Wilson PG, Fujishima A, Fréchet JMJ (1992) Macromolecules 25:6836
93. Kato T, Kihara H, Ujiie S, Uryu T, Fréchet JMJ (1996) Macromolecules 29:8734

94. Kumar U, Kato T, Fréchet JMJ (1992) J Am Chem Soc 114:6630
95. Araki K, Fréchet JMJ, Kato T, Ujiie S, Iimura K (1992) Angew Chem Int Ed Engl 31:1531
96. Kawakami T, Kato T (1998) Macromolecules 31:4475
97. Osuji C, Chao C-Y, Bita I, Ober CK, Thomas EL (2002) Adv Funct Mater 12:753–758
98. Chao C-Y, Li X, Ober CK, Osuji C, Thomas EL (2004) Adv Funct Mater 12:364–370
99. Thünemann AF, Kubowicz S, Burger C, Watson MD, Tchebotareva N, Müllen K (2002) J Am Chem Soc 125:352–356
100. Felekis T, Tsiourvas D, Tziveleka L, Paleos CM (2005) Liq Cryst 32:39–43
101. Felekis T, Tziveleka L, Tsiourvas D, Paleos CM (2005) Macromolecules 38:1705–1710
102. Tsiourvas D, Felekis T, Sideratou Z, Paleos CM (2002) Macromolecules 35:6466–6469
103. Tsiourvas D, Felekis T, Sideratou Z, Paleos CM (2004) Liq Cryst 31:739–744
104. Ambrožič G, Žigon M (2000) Macromol Rapid Comm 21:53–56
105. Lin H-C, Hendrianto J (2005) Polymer 46:12146–12157
106. Lin H-C, Tsai C-M, Huang G-H, Tao Y-T (2006) Macromolecules 39:557–568
107. Ihata O, Yokota H, Kanie K, Ujiie S, Kato T (2000) Liq Cryst 27:69–74
108. Kanie K, Yasuda T, Ujiie S, Kato T (2000) Chem Comm 1899–1900
109. Kanie K, Nishii M, Yasuda T, Taki T, Ujiie S, Kato T (2001) J Mater Chem 11:2875–2886
110. Kato T, Matuoka T, Nishii M, Kamikawa Y, Kanie K, Nishimura T, Yashima E, Ujiie S (2004) Angew Chem Int Ed 43:1969–1972
111. Kamikawa Y, Nishii M, Kato T (2004) Chem Eur J 10:5942–5951
112. Pickaert G, Douce L, Ziessel R, Guillon D (2002) Chem Comm 1584–1585
113. Camerel F, Donnio B, Bourgogne C, Schmutz M, Guillon D, Davidson P, Ziessel R (2006) Chem Eur J 12:4261–4274
114. Würthner F, Yao S, Heise B, Tschierske C (2001) Chem Comm 2260–2261
115. McCubbin JA, Tong X, Wang R, Zhao Y, Snieckus V, Lemieux RP (2004) J Am Chem Soc 126:1161–1164
116. Kajitani T, Kohmoto S, Yamamoto M, Kishikawa K (2004) J Mater Chem 14:3449–3456
117. Shah RR, Abbott NL (2003) Langmuir 19:275–284
118. Burnworth M, Knapton D, Rowan SJ, Weder C (2007) J Inorg Organometal Polym Mater 17:91–103
119. Binnemans K, Gorller-Walrand C (2002) Chem Rev 102:2303–2345

Struct Bond (2008) 128: 151–179
DOI 10.1007/430_2007_071

Published online: 10 November 2007

Functional Liquid-Crystalline Polymers for Ionic and Electronic Conduction

Masahiro Funahashi · Harutoki Shimura · Masafumi Yoshio · Takashi Kato (✉)

Department of Chemistry and Biotechnology, School of Engineering, The University of Tokyo, 7-3-1 Hongo, Bunkyo-ku, 113-8656 Tokyo, Japan
kato@chiral.t.u-tokyo.ac.jp

Abstract Liquid-crystalline (LC) polymers that exhibit ionic or electronic conduction are described. Anisotropic and efficient transportation of electrons and ions is expected for these materials. The ordered LC nanostructures of LC polymers having ion- or electron-active moieties are important for efficient anisotropic transport. For electron-conductive materials, we focus on side-chain LC polymers.

Keywords Liquid crystal · Liquid-crystalline polymer · Side-chain polymer · Ion-conductor · Semiconductor

1 Introduction

For organic materials, electronic and ionic conduction are important topics [1]. Liquid-crystalline (LC) polymers are good candidates for materials that transport ions and electrons because their ordered nanostructures are expected to induce anisotropic and efficient conduction [2–10]. However, limited numbers of examples have been reported for electron- and ion-active LC polymers, compared to crystalline and amorphous polymers [3–10].

Ion transport plays an important role in electric energy generation systems such as batteries. Fast ionic transport between cathode and anode is indispensable for high power efficiency in electric cells. Ion-conductive polymers with high conductivity, flexibility, and self-standing shape are necessary for industrial applications [11, 12]. On the other hand, organic semiconductors with high electronic carrier mobility and mechanical flexibility are very important components in plastic electronics [13]. Polymeric semiconductors are promising candidates for opt-electronics materials applied to electronic papers [14] and chemical sensors [15].

Ionic conduction and electronic conduction are quite different physical phenomena; however, we can propose a common principle for material design of ion and electron conductive polymers with high carrier mobility as well as mechanical flexibility. In order to increase ionic and electronic carrier mobility, construction of nanostructures for one- or two-dimensional carrier transport is effective. In ionic conduction, ions are transported through the one-dimensional (1D) or two-dimensional (2D) paths with thermal segmental motions. Such a situation can be realized in LC phases that form 1D columnar or 2D smectic phases rather than amorphous phases [3–10]. Electronic carriers move between molecules via intermolecular π-orbital overlaps, influenced by structural and energetic disorders [16]. In columnar or smectic phases, 1D columnar stacking or 2D layer structures, with large intermolecular π-orbital overlaps and small disorders, are favorable for fast electronic carrier transport. In addition, large homogeneous domains formed in LC phases can suppress the formation of domain boundaries that inhibit smooth ionic and electronic carrier transport, unlike crystalline states. This behavior is favorable not only for electronic and ionic carrier transport but also for optical applications such as polarized light-emitting devices. Conjugated polymers have been studied intensively as organic semiconductors with good electrical properties and processability [17]; however, it is very difficult to produce macroscopically aligned thin films. From the viewpoint of industrial applications, LC polymers are therefore more promising materials because they have flexibility and a self-standing shape.

In addition, a new generation of LC materials such as polymers and oligomers [5, 9], supramolecular polymers [18–23], dendrimers [24, 25], and block copolymers [26, 27] have recently been developed as new functional materials. Supramolecular assemblies including π-conjugated systems with opt-electronic functionalities have also been investigated [28, 29]. The use of non-covalent interactions (such as hydrogen bonding) and ionic interactions has lead to the dynamic formation of supramolecular LC structures [18–22, 28]. The LC dendrimers and block polymers and oligomers exhibit a variety of nano-segregated liquid-crystalline structures (Fig. 1), such as micellar cubic (0D), columnar (1D), lameller or smectic (2D), and bicontinuous cubic phases (3D), leading to the introduction of anisotropic electric functions [4, 5, 30].

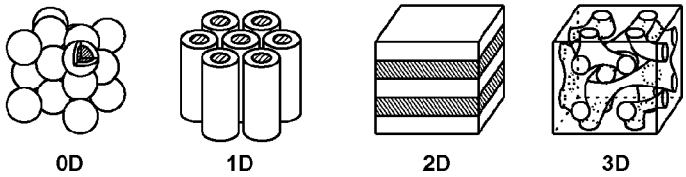

Fig. 1 Nano-segregated structures formed by self-assembly of LC molecules: *OD* 0-dimensional micellar cubic, 1*D* hexagonal columnar, 2*D* lamellar or smectic, and 3*D* bicontinuous cubic

In this review, we will focus on ion- and electron-conductive thermotropic LC polymers and oligomers. A variety of mesomorphic structures has been constructed utilizing non-covalent interactions, which influences ionic and electronic carrier transport processes.

2
Ion-Conductive Liquid-Crystalline Polymers

2.1
Organic Ion-Conductive Polymers

The development of high performance electrolytes is an important task in the production of devices for electric energy storage and delivery such as lithium ion batteries, capacitors, and electrochromic devices. Carbonate-based materials are one of the liquid electrolytes. Carbonate-based liquid electrolytes are now commonly used for the economical lithium ion batteries [31]. The solution of carbonate and lithium salts exhibits high ionic conductivity, on the order of 10^{-3} S cm^{-1} at ambient temperature.

The recent development of electrolytes is directed to the replacement of liquid electrolytes with solvent-free polymer electrolytes [32–36]. Polymer electrolytes have advantages as electrolytes because of their flexibility, lightness, easy processability, and safety. The complexes of poly(ethylene oxide)s (PEOs) with lithium salts have been intensively studied as solid polymer electrolytes since 1975 when Wright found that PEOs can be used as ion-conductive materials in such systems [37]. These polymers can operate both as separators that keep the distance between electrodes, and as electrolytes that lead to the production of batteries having overall polymer structures. Lithium cation dissolved in PEOs is stabilized by the ion–dipole interactions between lithium cations and the lone pairs of oxygen atoms in the PEO chains. The ions are conducted by the segmental motions of the ethylene oxide chains. A variety of PEO-based polymers, such as comb-shaped polymers containing highly mobile oligo(ethylene oxide) side chains [38], were prepared for the development of higher ion-conductive materials. However,

PEO-based amorphous polymers have apparently reached a limit in their conductivities on the order of 10^{-5}–10^{-4} S cm^{-1} at room temperature and approximately 10^{-3} S cm^{-1} at 100 °C.

Ionic liquids that are molten salts at ambient temperature [39–41] have attracted a great deal of attention as a new type of electrolyte [41]. They are composed of imidazolium and pyridinium cations, and perfluorinated anions such as BF_4^-, PF_6^-, and $(CF_3SO_2)_2N^-$. They exhibit high ionic conductivity in the range of 10^{-4}–10^{-1} S cm^{-1} at room temperature. Inorganic salts such as lithium salts can be dissolved in ionic liquids. A number of polymerizable ionic liquids have been developed and the effects of the species of cations and anions on ionic conductivities have been examined systematically [42, 43]. The ionic conductivities of polymerized ionic liquids were in the range of 10^{-6}–10^{-4} S cm^{-1} at room temperature. The conductivities of the polymers were several hundred times lower than those of the corresponding ionic liquid monomers. However, the ionic conductivities of such materials could be improved by changing the combination of cations and anions.

2.2 Low Molecular Weight Nanostructured Liquid-Crystalline Compounds

A new concept for enhancing the conductivities for materials based on PEOs and ionic liquids was the introduction of ordered LC nanostructures [4, 5, 44–56]. In PEO materials, lithium cations are tightly coordinated with the PEO chains. The ions are conducted in isotropic matrices by 3D migration processes. Also, ionic liquids themselves, and the ions dissolved in ionic liquids, move randomly in the isotropic liquid media. If the polyether and ionic moieties that function as ion-conductive parts are organized into LC nanostructures, efficient ion transportation and anisotropic ion conduction are expected by the formation of low-dimensional ion-conductive paths.

Although columnar LC materials such as azacrowns having peripheral long alkyl chains and crown ether-attached phthalocyanine were prepared as ion channels [57, 58], no ionic conductivities were reported. Percec, Ungar, and coworkers described ion conduction in a low molecular weight columnar liquid crystal [59]. Self-assembly of a fan-shaped molecule having a crown ether moiety **1** (Fig. 2) and sodium triflate formed hexagonal columnar LC phases forming ion channels. Low conductivities in the range of 10^{-10}–10^{-8} S cm^{-1} were observed for a non-aligned sample exhibiting the columnar phase by a direct current method. Also, the ionic conductivities of the non-aligned columnar LC complexes of a trimesic amide derivative with peripheral oligo(ethylene oxide) side chains and lithium perchlorate were measured by an alternating current impedance method [60]. The relatively high value of 10^{-6} S cm^{-1} in the hexagonal columnar phase at room temperature was recorded, although no 1D ion conduction along the direction

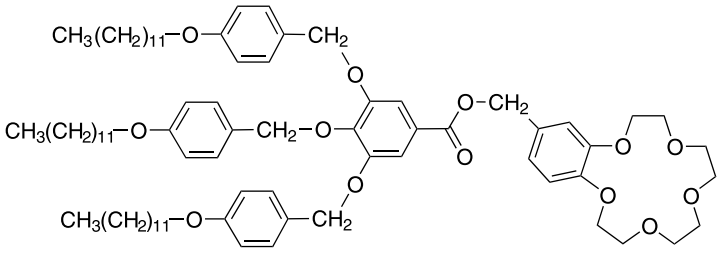

1

Fig. 2 Molecular structure of a columnar liquid crystal having a crown ether moiety

parallel to the column axis was expected because oligo(ethylene oxide) chains themselves do not form a columnar structure.

The self-assembly of LC block molecules composed of two or more covalently bonded immiscible molecular parts including an ion-conductive moiety leads to the formation of well-defined nano-segregated structures such as layer and columnar structures [4, 5, 26, 27, 30]. These anisotropic structures formed for LC block molecules having PEO and ionic liquid moieties would be useful for the anisotropic transportation of ions. Moreover, we considered that the macroscopic orientation of the nano-segregated LC structures plays a key role in the enhancement of the conductivities because the boundary in randomly oriented polydomains disturbs the anisotropic transportation of ions.

A rod–coil–rod type of twin mesogenic molecule having oligo(ethylene oxide) chains **2** (Fig. 3) was designed as a 2D ion conductor [44–47]. The lithium salt complexes of these molecules showed smectic LC phases. The lithium salts were incorporated into the oligo(ethylene oxide) layers of phase-segregated layered structures. Ionic conductivities of the aligned LC materials were measured by the alternating current impedance method. Highly anisotropic ion conduction along the layer structures was observed for complexes exhibiting LC smectic A and B phases aligned vertically on a glass substrate. The ionic conductivities parallel to the smectic layer were 1.9×10^{-4} S cm^{-1} in the smectic B phase at 79 °C and 5.5×10^{-4} S cm^{-1} in the smectic A phase at 152 °C. Then, perfluoroalkyl moieties were incorporated into twin mesogenic moieties containing PEO chains in order to stabilize the nano-segregated LC layered structures and to enhance the anisotropy of ion conduction [47]. The triply layered structures of perfluorocarbon, aromatic mesogen, and oligo(ethylene oxide) moieties led to the thermal stabilization of mesophases and a slight increase in anisotropy of ionic conductivities. A rod–coil molecule containing a tetra(ethylene oxide) chain was also prepared for the design of a 2D ion conductor exhibiting a smectic A phase at room-temperature [48]. The lithium triflate complex showed a smectic A phase over a wide temperature range, including room temperature. Uniaxially parallel alignment of the LC smectic A samples on rubbed polyimide

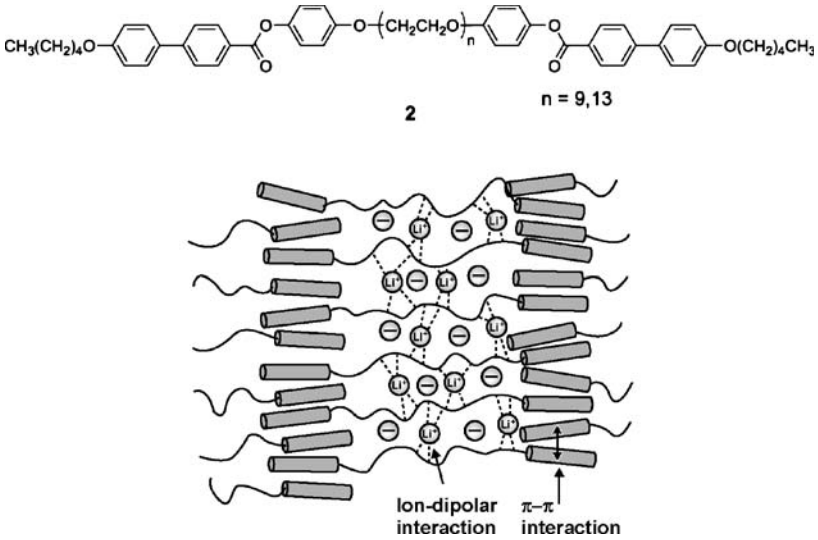

Fig. 3 Molecular structure of a rod–coil–rod twin mesogenic molecule containing an oligo(ethylene oxide) moiety, and its self-organized structure

surfaces was achieved. In the aligned LC smectic A phase, the ratio of ionic conductivities parallel and perpendicular to the smectic layer was 1.3×10^4.

Two-dimensional ion conduction was also achieved for the smectic liquid crystals consisting of the mixture of ionic liquids and hydroxyl-functionalized rod molecules [49–51] and smectic LC imidazolium salts having a long alkyl chain [52–55]. One-dimensional ion conduction was performed for aligned columnar LC phases forming ion-channels of fan-shaped imidazolium salts having a tris(alkoxy)phenyl moiety [56].

2.3 Nanostructured Liquid-Crystalline Polymers

Side-chain LC poly(siloxane)s **3** were prepared by Hsiue et al. (Fig. 4) [61]. The mesogenic side chains are linked to the siloxane backbone through oligo(ethylene oxide) moieties. These complexes with several alkali metal salts show relatively high ionic conduction in the order of 10^{-6} S cm^{-1} at ambient temperature. Percec prepared LC poly(siloxane)s **4** for potential use as 1D ion conductors [62]. Although no ionic conductivities were reported for these LC polymers, a possibility of an ion channel formed by poly(siloxane)s, which hold nematogenic side chains as shown in Fig. 5, was suggested. In this case, the mesogen is connected to the polymer main chain at the lateral position via an oligo(ethylene oxide) chain, and therefore the flexible poly(siloxane) is surrounded by the oligo(ethylene oxide) moieties and mesogenic groups, inducing a 1D structure.

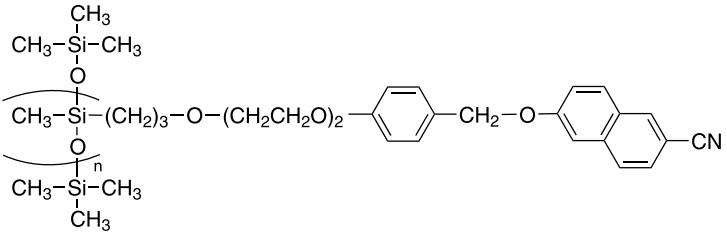

3

Fig. 4 Molecular structure of side chain type LC poly(siloxane) with PEO moiety

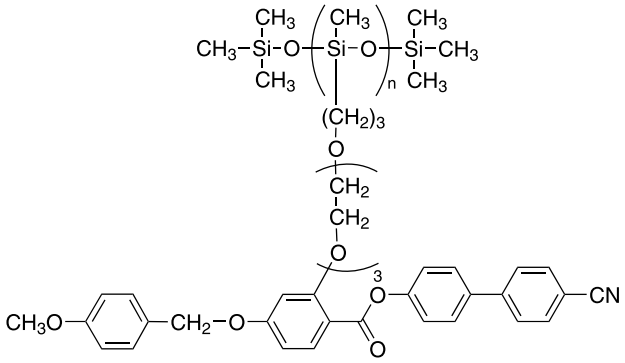

4

Fig. 5 Cylindrical structure formed by poly(siloxane)s having laterally substituted nematogenic groups

A rigid backbone was used by Wegner to build ion-conductive PEO-based polymers [63]. Oligo(ethylene oxide) chains were grafted from poly(*p*-phenylene) as shown in Fig. 6. The mixtures of polymers **5** and lithium salts show conductivities in the order of 10^{-6} S cm^{-1} at ambient temperature. The ionic conductivities can be improved to the order of 10^{-5} S cm^{-1} by plasticization of the materials with oligo(ethyleneglycol)-dimethylether.

Wright prepared PEO-based LC polymers having alkyl side chains **6** [64–66] as shown in Fig. 7. The alkyl side chains with linear conformation and coiled PEO chains induce a layered nanostructure, and the complexes of these polymers with lithium salts show conductivities in the order of 10^{-7} S cm^{-1} at ambient temperature.

The introduction of macroscopically oriented nanostructures is an essential approach for low-dimensional ion conduction, because the boundaries between the domains oriented randomly disturbs anisotropic ion conduction. However, as mentioned above, it was difficult to produce macroscopically aligned thin films with a low density of defects and domain boundaries, and therefore anisotropy in ionic conductivity has not been observed clearly.

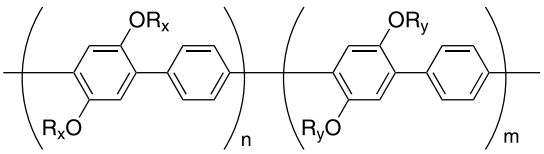

$R_x = (CH_2CH_2O)_xCH_3$

$R_y = (CH_2CH_2O)_yCH_3$

5

Fig. 6 Molecular structure of poly(*p*-phenylene) derivatives with a PEO group in their side chains

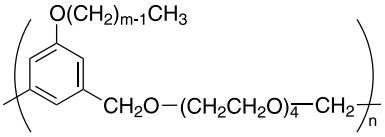

Fig. 7 Complexation of PEO-based LC polymers with lithium salts, and their nanostructure

Kato, Ohno and coworkers have used an in-situ photopolymerization technique to overcome the problem of the alignment of LC polymers [67–69]. Two-dimensionally ion-conductive polymer films (**7**) were obtained by photopolymerization of aligned monomer complexes. The monomer self-assembles into layered nanostructures, in which PEO moieties form nanosegregated ion transporting channels. The complex of the LC monomer with $LiOSO_2CF_3$ exhibits a smectic A phase. UV irradiation of the homeotropically aligned complex results in the formation of a free-standing film, as shown in Fig. 8 [67]. The film shows ionic conductivities in the order of 10^{-6} S cm^{-1} in the direction parallel to the layers, which is approximately 5000-times higher than that perpendicular to the layers. The value of the conductivity is not so high because the segmental motion of the PEO moiety is restricted between the polymer backbone and the mesogenic parts. The conductivity can be enhanced to the order of 10^{-3} S cm^{-1} by introducing a PEO moiety at the terminal of the side chain (**8**, Fig. 9) [68]. The corresponding acrylate monomer complex with $LiOSO_2CF_3$ (0.05 mol % to the oxyethylene) was polymerized in the smectic A phase at 60 °C by UV irradiation. Polymer **8** complexed with $LiOSO_2CF_3$ exhibits the glass transition at –45 °C and the solid–smectic A transition at 161 °C. The isotropization temperature is observed at 202 °C. At room temperature, conductivity in the range of 10^{-3} S cm^{-1} to the direction parallel to the layer is observed, even though the complex forms a solid state. These high ionic conductivities of the complex of **8** can be ascribed to the liquid-like layers in the solid oriented film.

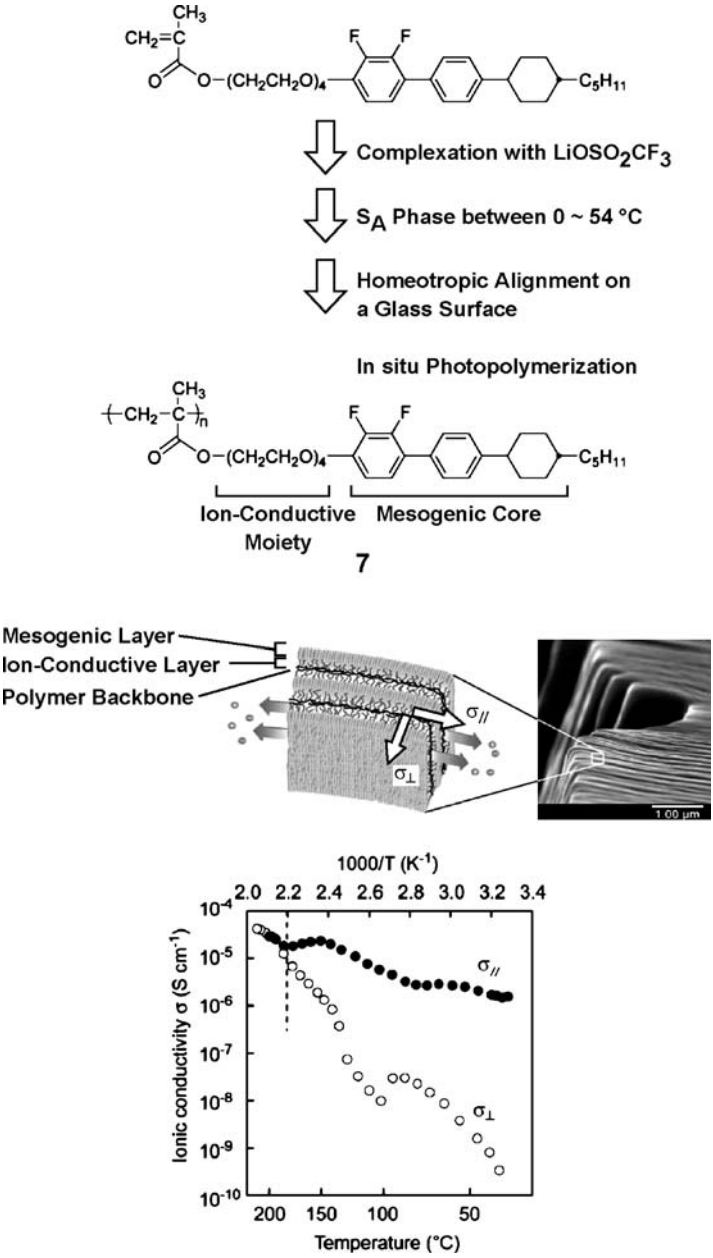

Fig. 8 Self-standing thin film of LC polymers with PEO moieties in their side chains

Anisotropically ion-conductive films have also been developed using liquid crystal nanostructures incorporating an imidazolium salt moiety at the end of the side chains. Two-dimensional ion conduction has been achieved using a li-

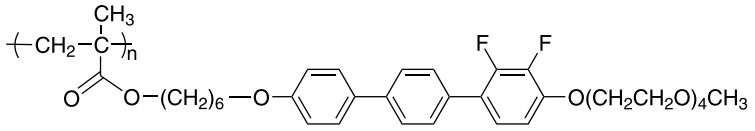

8

Fig. 9 Molecular structure of an LC polymer having a PEO moiety at the terminal of the side chain

quid crystal polymethacrylate with a rod-shaped mesogen **9** (Fig. 10) [69]. The corresponding monomers formed a homeotropic smectic A monodomain on glass substrate, and nanostructured films were obtained by in situ photopolymerization of them. One-dimensional ion-conductive films were also prepared

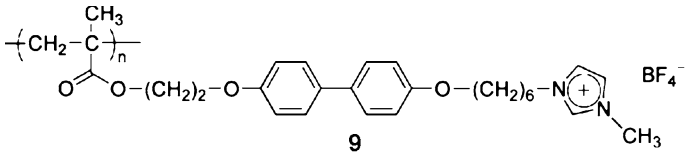

9

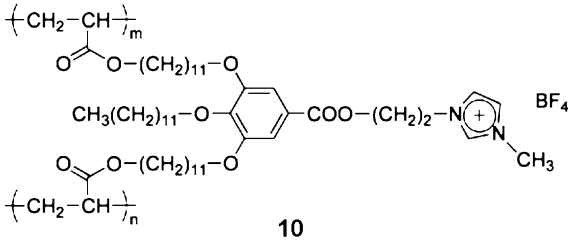

10

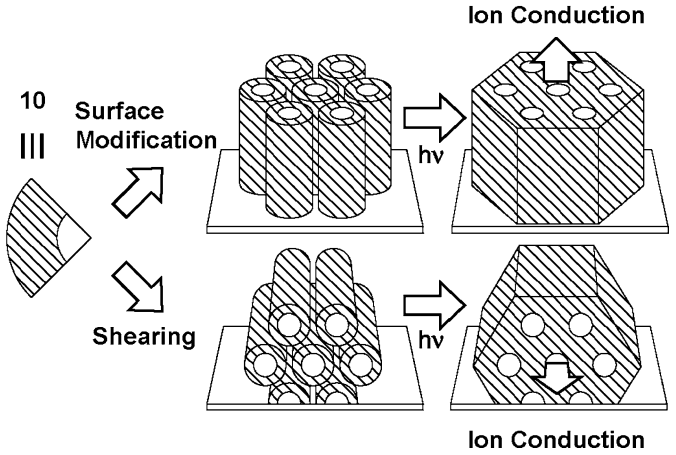

Fig. 10 2D and 1D ion-conductive LC polymers with imidazolium ionic moieties

from a columnar liquid crystal having two acrylate groups at the periphery (**10** in Fig. 10) [70]. Monomer **10** exhibits a columnar liquid crystal phase between 30 and 50 °C. The columns were oriented macroscopically in two directions by different methods: orientation perpendicular to the modified surfaces of glass

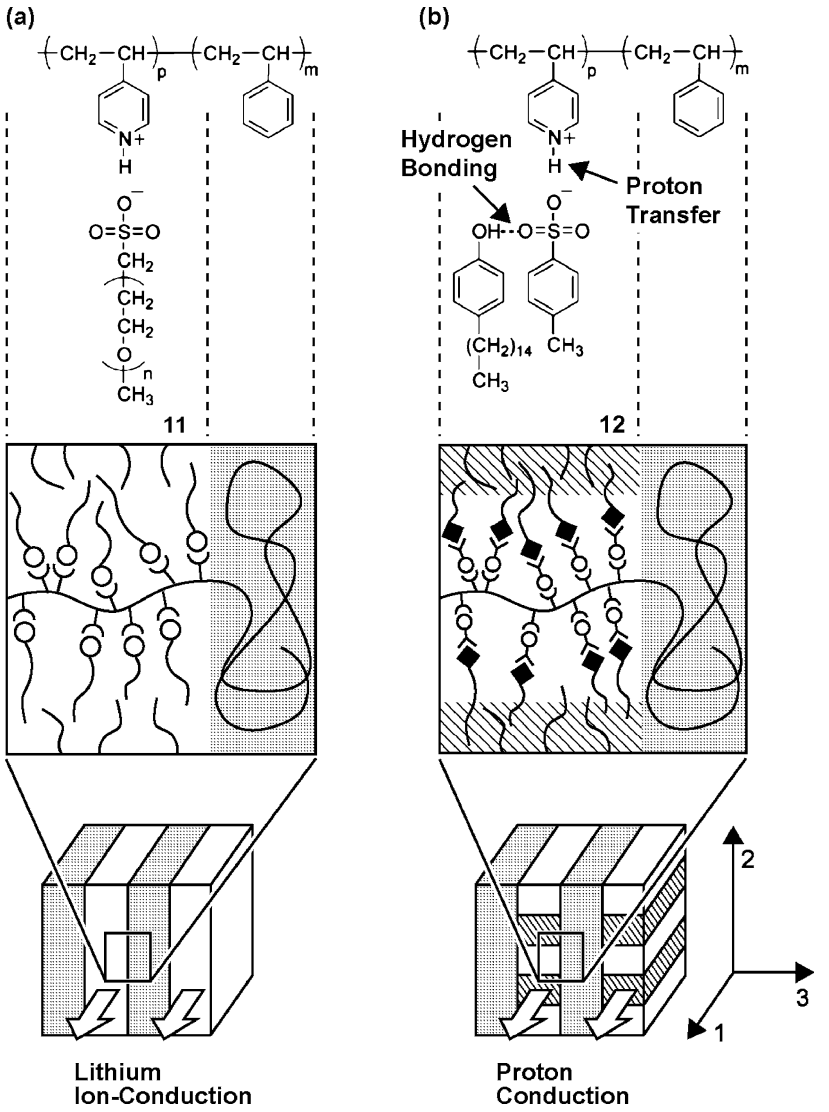

Fig. 11 **a** Polymer composites consisting of polystyrene-*block*-poly(4-vinylpyridine) (PS-*b*-PVP) and oligo(ethylene oxide)sulfonic acid. These composites can complex with $LiClO_4$, exhibiting high lithium ion conductivity. **b** PS-*b*-PVP polymers mixed with alkylphenol and toluenesulfonic acid, instead of oligo(ethylene oxide)sulfonic acid, exhibit proton conductivity

and indium tin oxide with 3-(aminopropyl)triethoxysilane, and orientation parallel to a glass surface by mechanical shearing. The polymerized film in the solid state shows ionic conductivities in the order of 10^{-6} S cm^{-1} in the direction parallel to the columnar axis at around 50 °C. The value is approximately 300-times higher than those perpendicular to the axis.

Supramolecular approaches [5, 7, 20–22] are also effective for ion conduction in polymers. Ikkala and ten Brinke prepared the complex of polystyrene-*block*-poly(4-vinylpyridine) (PS-*b*-PVP) and oligo(ethylene oxide)sulfonic acid **11** [71, 72]. The polymer self-assembles into lamellar nanostructures consisting of glassy hydrophobic polystyrene and hydrophilic PEO layers, as shown in Fig. 11. When $LiClO_4$ is dissolved in the polymer composites, lithium ions are complexed and transported in the hydrophilic PEO layers, resulting in high ionic conductivities on the order of 10^{-6} S cm^{-1} at ambient temperature.

It is interesting that proton conduction is also available in the polymer composites consisting of a similar polymer, toluenesulfonic acid, and 3-pentadecylphenol (**12**) as shown in Fig. 11 [73]. They form hierarchical lamellar nanostructures. The PS and PVP blocks are segregated at a larger scale. In the PVP blocks, additional lamellar substructures are formed through the nano-segregation of the alkyl chains and the PVP main chains. Monodomain orientation on the larger scale is achieved by applying shear force, resulting in anisotropic proton conduction [74].

Wiesner reported a new class of LC ion-conductors capable of switching ionic conduction, as shown in Fig. 12 [75–77]. The molecules with PEO block and dendritic block **13** show several low dimensional nanostructures.

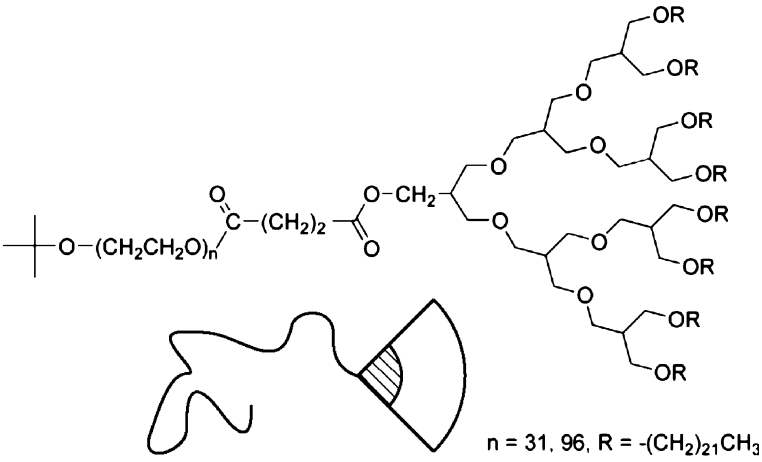

13

Fig. 12 Fan-shaped LC molecules consisting of dendritic alkyl chains and a PEO moiety at the focal point

Micellar cubic (0D), hexagonal columnar (1D), lamellar (2D), and bicontinuous cubic (3D) nanostructures are formed by self-assembly of **13**. For the complexes with $LiClO_4$, the ionic conductivities show discontinuous changes following the phase transitions with change of temperature or molecular structure of the dendritic moiety. For example, the conductivity of the complex of **13** with $LiClO_4$ drops from 4.6×10^{-6} to 1.2×10^{-9} S cm^{-1}, along the phase transition from crystalline lamellar to micellar cubic phases.

3
Electron-Conductive Side-Chain Liquid-Crystalline Polymers

3.1
Side-Chain Polymers and Low Molecular Weight Liquid Crystals

Not only conjugated polymers but also side chain type polymers, such as polyvinylcarbazole, have been applied to electronics devices. In particular, this kind of polymer has played an important role in xerographic photoreceptors utilizing their photoconductivity [78]. In this type of polymer, the dominant process of carrier transport is charge carrier hopping between chromophores containing π-conjugated aromatic system connected to the side chains. In this mechanism, charge carriers are localized on the chromophores and transferred between them via π-molecular orbital overlaps assisted by thermal activation and the electric field. Conventional side chain type photoconductive polymers are amorphous and, therefore, the positions of the chromophores as well as their HOMO and LUMO levels are disordered as shown in Fig. 13. These disorders and small intermolecular orbital overlaps cause low carrier mobility and strong dependence on temperature and electric field, compared to molecular crystals. This behavior is well described by the Gaussian disorder model proposed by Bässler [16].

Based on this model, we can expect that reduction of the energetic and positional disorders should increase carrier mobility and decrease dependence on temperature and electric field. One of the methods to reduce the disorders is introduction of mesogenic groups into the side chains of this kind of semiconductive polymer. The introduced mesogenic groups induce liquid crystal molecular order in which chromophores are aligned, reducing energetic and positional disorders as shown in Fig. 13b.

In general, for side chain liquid-crystalline polymers, macroscopic molecular alignment is not easy and therefore clear evidence of electronic charge carrier transport was confirmed first in liquid crystals with low molecular weight. In the 1990s, fast electronic conduction was verified in discotic columnar phases of triphenylene derivatives [79, 80] and hexabenzocoronene derivatives [81, 82] as well as smectic phases of 2-phenylbenzothiazole [83, 84] and 2-phenylnaphthalene derivatives [85], as shown in Fig. 14. Carrier

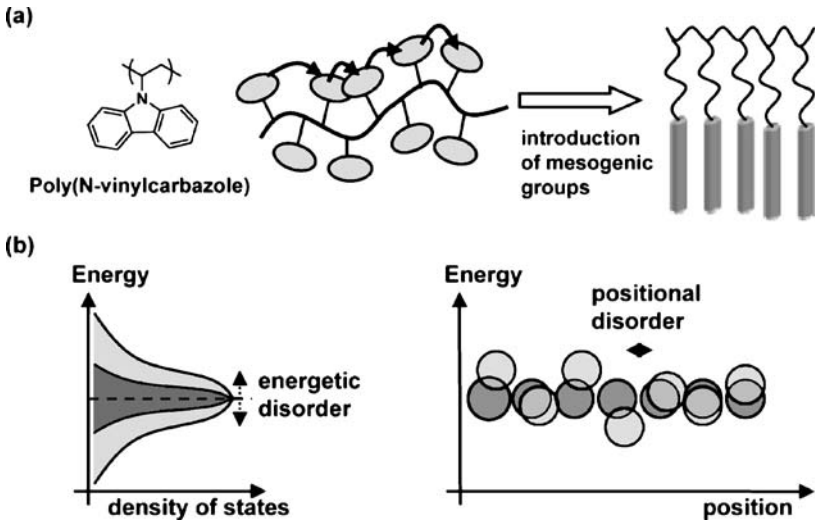

Fig. 13 **a** Charge carrier hopping between chromophores connected to the side chain, and the effect on molecular alignment of the introduction of mesogenic groups. **b** Resulting energy level distribution of the chromophores. Molecular alignment should result in narrower distribution of molecular orbital energy levels

mobilities in these columnar and smectic phases are on the order of 10^{-4} to 10^{-1} $cm^2\ V^{-1}\ s^{-1}$, which are several magnitudes larger than those of an electronic carrier in amorphous polymer semiconductors and of ions in isotropic liquids of organic compounds with low molecular weight (typically on the order of 10^{-7} to 10^{-5} $cm^2\ V^{-1}\ s^{-1}$). It should be noted that layer or columnar structures in which molecules align and stack are indispensable for fast electronic carrier transport, in contrast to the nematic phase which exhibits ionic conduction [86, 87] or relatively slow electronic charge carrier transport [88–90]. In fact, carrier mobility has clear relationships with molecular order within smectic layers or columns as shown in Fig. 15. Carrier mobility was on the order of 10^{-4} $cm^2\ V^{-1}\ s^{-1}$ in the smectic A or C phases of 2-phenylnaphthalene and dialkylterthiophene derivatives where no long range order existed within the smectic layer. However, it was on the order of 10^{-3} $cm^2\ V^{-1}\ s^{-1}$ in the smectic B or F phases, which had a hexagonal bond order within the smectic layers- It increased to around 10^{-2} $cm^2\ V^{-1}\ s^{-1}$ in the smectic E or G phases, where there was long range order in the molecular position within the layers [91]. The same tendency was also observed in the various columnar phases of the triphenylene derivatives [92].

A remarkable characteristic of carrier transport property in columnar and smectic phases is that carrier mobility is independent of temperature and electric field above room temperature [80, 83, 85]. A clear reason for this has not yet been confirmed although some models based on small polaron theory have been proposed [93].

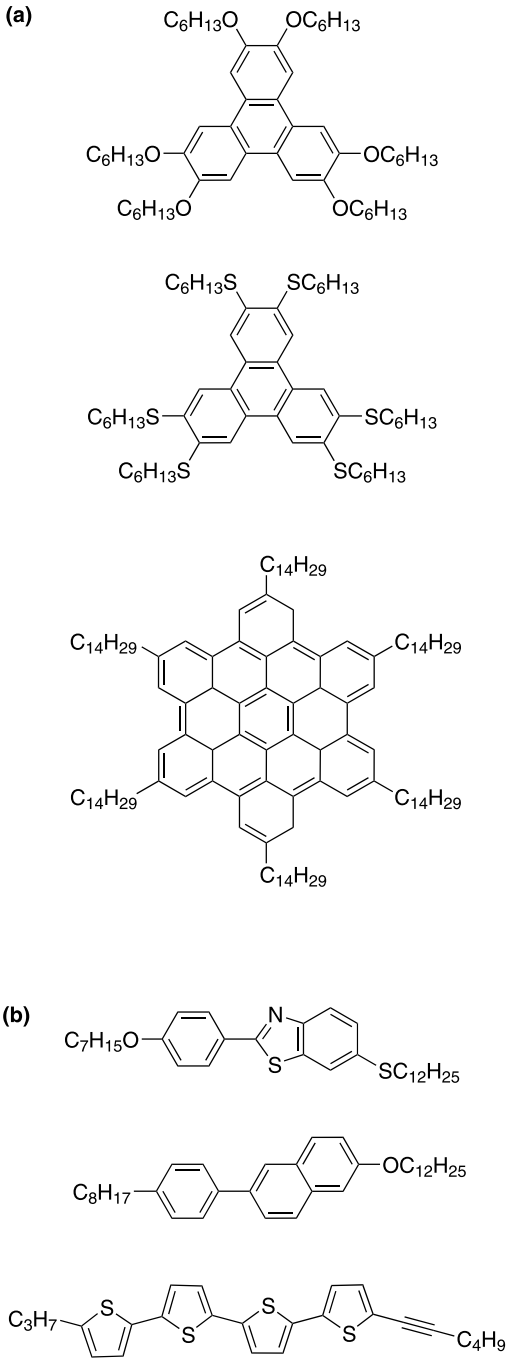

Fig. 14 Typical examples of liquid-crystalline semiconductors with low molecular weight exhibiting **a** columnar phases and **b** smectic phases

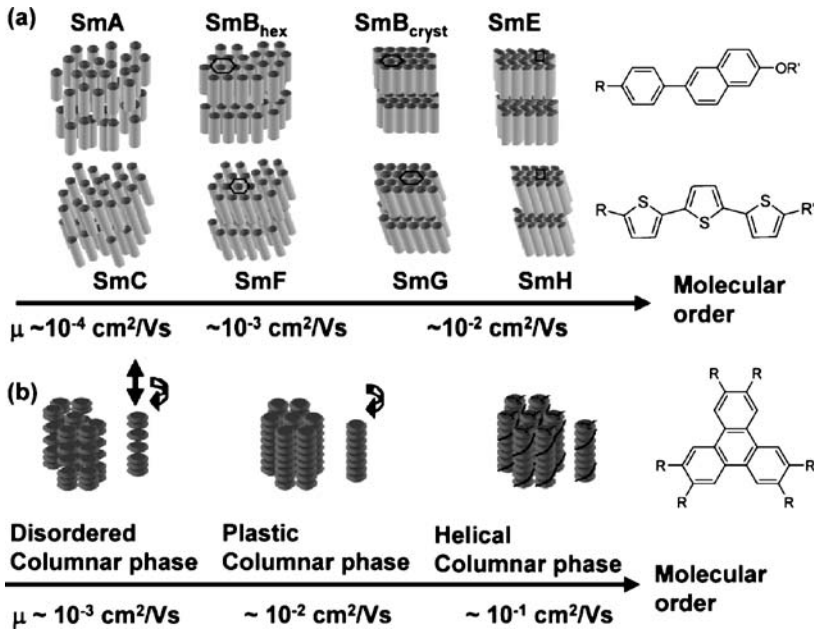

Fig. 15 Relationship between carrier mobility and molecular order in **a** smectic and **b** columnar liquid crystal phases

Thermally and mechanically stable thin film formation is indispensable for fabrication of practical electronic devices such as organic light-emitting diodes, field-effect transistors, and particularly for flexible electronic papers. There are two approaches for formation of thermally and mechanically stable thin films. One is formation of glassy semiconductors retaining ordered structures by cooling from liquid-crystalline states [94]. The other approach is polymerization of liquid-crystalline semiconductors with a reactive moiety.

3.2 Pioneering Works for Liquid-Crystalline Polymers

It is difficult to polymerize liquid-crystalline monomers retaining the highly ordered structure of the liquid crystal phases, which is requisite for fast carrier transport. Fabrication of macroscopically aligned thin films of side chain type liquid-crystalline polymers is generally difficult. In particular, it is very difficult to grow a large domain in the smectic phases of this type of liquid-crystalline polymer due to restriction of movement and the configuration of mesogenic groups. In contrast, photopolymerization of reactive mesogens is a relatively better method. Here, reactive mesogenic monomers aligned in their liquid crystal phases are polymerized by UV light, although optimization of polymerization conditions and selection of the reactive moiety is necessary.

It should be noted that initiators and impurities derived from them sometimes form carrier-trapping centers degrading carrier transport even in photopolymerized thin films.

As mentioned in Sect. 1, low carrier mobility and specific dependence on temperature and electric field have been recognized as phenomena caused by the large disorder of the semiconductive polymers, so some investigations to reduce disorder have been attempted. Ikeda et al. looked at the introduction of mesogenic groups into side chain type photoconductive polymers [95, 96]. As shown in Fig. 16, they synthesized random copolymers **14, 15** containing cyanobiphenyl or phenyl benzoate moieties, which are typical mesogens, as well as carbazole dimer units with radical polymerization. The synthesized polymers exhibited a nematic phase in a wide temperature range including room temperature. Thin films were fabricated by the solution cast method on substrates.

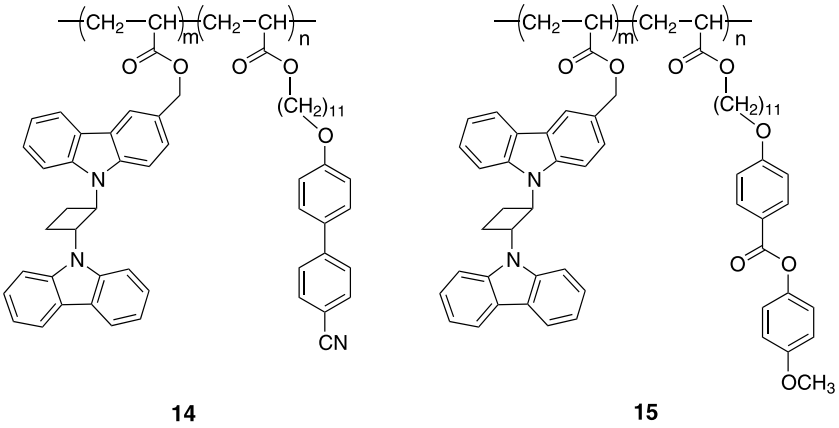

14 **15**

Fig. 16 Molecular structure of liquid-crystalline copolymers

Carrier transport characteristics were studied by the time-of-flight technique. Only hole transport was observed and its mobility was on the order of 10^{-7} cm^2 V^{-1} s^{-1} at room temperature, which was comparable to that of conventional non-mesogenic polyvinylcarbazole derivatives. It strongly depended upon electric field and temperature, which is similar to conventional amorphous semiconductive polymers. In this study, introduced mesogenic groups induced a nematic phase. However, the concentration of carbazole chromophores that were associated with carrier transport was reduced by the introduction of mesogenic groups, and the disorders were not greatly reduced because of low molecular ordering in the nematic phase.

In 1993, a research group at the University of Bayreuth confirmed fast electronic transport in the discotic columnar phase of hexaalkoxytriphenylene using the time-of-flight method [80], which made a strong impact on liquid

crystal research. As a next step, they attempted extension of the mesomorphic temperature range and stable thin film formation.

The group prepared discotic twin dimers **16** and **17** (shown in Fig. 17) and examined carrier transport in the columnar phase using the time-of-flight technique. These compounds exhibited a hexagonal columnar phase in a wide temperature range, including room temperature. A glassy phase retaining the columnar structure formed below room temperature because crystallization was inhibited due to restriction of molecular configuration. High carrier mobility exceeding 10^{-3} cm^2 V^{-1} s^{-1} was retained around room temperature [97]. In particular, compound **17** exhibited a highly ordered columnar phase in a wide temperature range, in which hole mobility determined by the time-of-flight technique reached 0.01 cm^2 V^{-1} s^{-1} around room temperature [98]. Around room temperature, the hole mobility was independent of temperature and electric field, which is characteristic for electronic carrier transport in columnar and smectic phases. Below its glass transition temperature (–20 °C), the hole mobility depended upon temperature and electric field, and the characteristics were similar to those of conventional amorphous organic semiconductors. They explained the carrier transport characteristics in the low temperature region using a 1D disorder model [98].

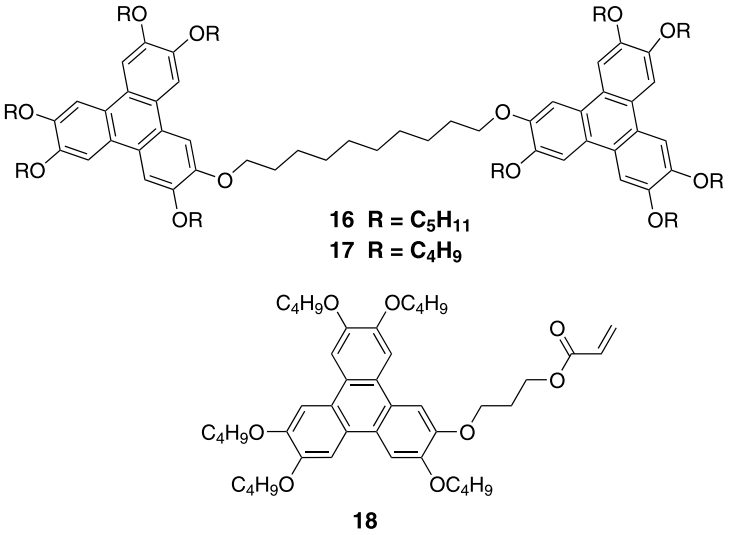

Fig. 17 Molecular structure of the triphenylene derivatives

Polymerization of mesogenic monomers is very effective for obtaining more stable ordered thin films. Triphenylene monomer containing acrylate moiety **18** was photopolymerized by UV light irradiation (Fig. 17). UV light was shone onto the mixture of the triphenylene derivative and a photoinitiator under inert atmosphere. Carrier transport characteristics of the ob-

tained films were studied by the time-of-flight technique. The tripheneylene monomer exhibited a hole mobility of 6×10^{-4} cm^2 V^{-1} s^{-1} in the columnar phase, and the hole mobility was retained at 5×10^{-4} cm^2 V^{-1} s^{-1} when the materials was mixed with the photo-initiator. The hole mobility decreased to 1×10^{-4} cm^2 V^{-1} s^{-1} at 80 °C after photopolymerization. Unlike monomeric triphenylene derivatives, the hole mobility was temperature-dependent, being 1×10^{-5} cm^2 V^{-1} s^{-1} at room temperature [99].

Application of triphenylene-based polymers as a hole transport layer in electroluminescence devices was also studied. The triphenylene polyacrylate was spun on ITO substrate, on which Alq_3 and Al cathode were vacuum-deposited; a brightness of 1390 cd m^{-2} was obtained at 4.5 V [100].

Because of the conformation change and defect formation during the photopolymerization process, long coherence length of the columns in the columnar phase was difficult to maintain. Therefore, the excellent carrier transport characteristics in the columnar phases of monomeric triphenylene derivatives could not be retained in the polymerized films.

3.3
Semiconductive Polymers with Nematic Phases

Various organic semiconductors have been used for electroluminescence devices [101]. Electroluminescence devices are suitable for flat panel displays and therefore they can be applied as backlights for liquid crystal displays, in which images are displayed by combining linearly polarized light, an optically anisotropic liquid crystal layer, and a polarizer. In order to generate linearly polarized light, another polarizer is essential, and therefore 50% of light absorbed by the polarizer is lost as heat [102]. Conventional organic semiconductors are amorphous and thus light emitted from devices based on amorphous organic semiconductors is not polarized. Polarized light-emitting devices, without using a polarizer, can contribute to an increase in energy performance. The films of liquid-crystalline semiconductors that have a uniaxial molecular alignment are promising candidates for such polarized light-emitting devices because their transition dipoles are uniaxially aligned in the films (as shown in Fig. 18). In addition, polarized light-emitting displays have a potential for 3D display [103].

It is easier to realize macroscopic uniaxial molecular alignment in a nematic phase than in 1D columnar and 2D smectic systems. In the application to electroluminescence devices emitting linearly polarized light, uniaxial molecular alignment is more important than good carrier transport properties. Kelly, O'Neill and coworkers synthesized liquid crystals containing fluorene moieties in central cores with a polymerizable group, the 1,4-pentadien-3-yloxy moiety [104–106]. These liquid crystals have extended π-conjugated systems that contribute to fast intermolecular charge transfer. A monomeric liquid-crystalline semiconductor that has the same aromatic core structure

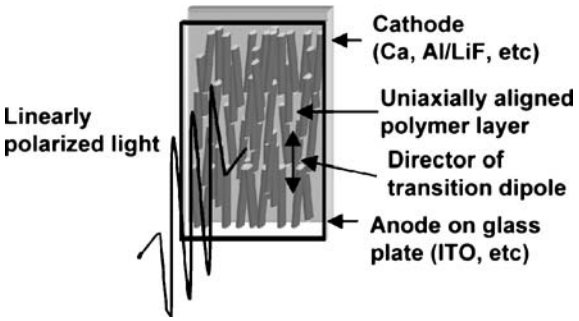

Fig. 18 Electroluminescence device based on a uniaxially aligned liquid-crystalline semiconductor layer emitting linearly polarized light

and branched alkyl chains exhibits a higher hole mobility (on the order of 10^{-4} cm^2 V^{-1} s^{-1}) in the glassy nematic than does an amorphous organic semiconductor [104]. Although the 1,4-pentadien-3-yloxy moiety was photopolymerizable and the polymerization rate was slower than those of acrylates and methacrylates, the photopolymerization reaction was controllable, resulting in suppression of formation of defects and disorder.

In 2000, the group reported the fabrication of electroluminescence devices that emitted green polarized light with a dichroic ratio of ten based on compound **19**. In general, uniaxial molecular alignment can be easily realized using rubbed polyimide films in a nematic phase. However, the rubbing process usually degrades the surface morphology of the alignment layers and generates dust, which is not suitable for thin film devices. In the photo-alignment layer, structural anisotropy induced by photochemical reaction is utilized and therefore the process is dustless, exhibiting good surface morphology. One problem is that conventional photo-alignment polymers are insulators, which inhibits carrier injection from an electrode to a semiconductor layer. In the devices, a photo-alignment layer was used that consisted of polyacrylate polymer with a photoreactive coumarine moiety and a triphenylamine derivative, which promoted hole injection. At high concentrations of the triphenylamine derivative, hole injection was surely promoted but molecular alignment severely degraded [105].

In 2005, Kelly and coworkers achieved full color polarized light-emitting displays. They synthesized three kinds of liquid crystals containing a bithienylfluorene moiety in their central core and photopolymerizable 1,4-pentadien-3-yloxy moieties in alkyl side chains (**20**, **21**, and **22**) as shown in Fig. 19. These three compounds emitted red, green, and blue fluorescence, respectively, and exhibited a nematic glass state around room temperature [103]. As a photo-alignment layer, they synthesized polyacrylate copolymer containing a liquid-crystalline semiconductor moiety with a bithienylfluorene as well as a photoreactive coumarine moiety in the side chains (**23**) as shown in Fig. 20.

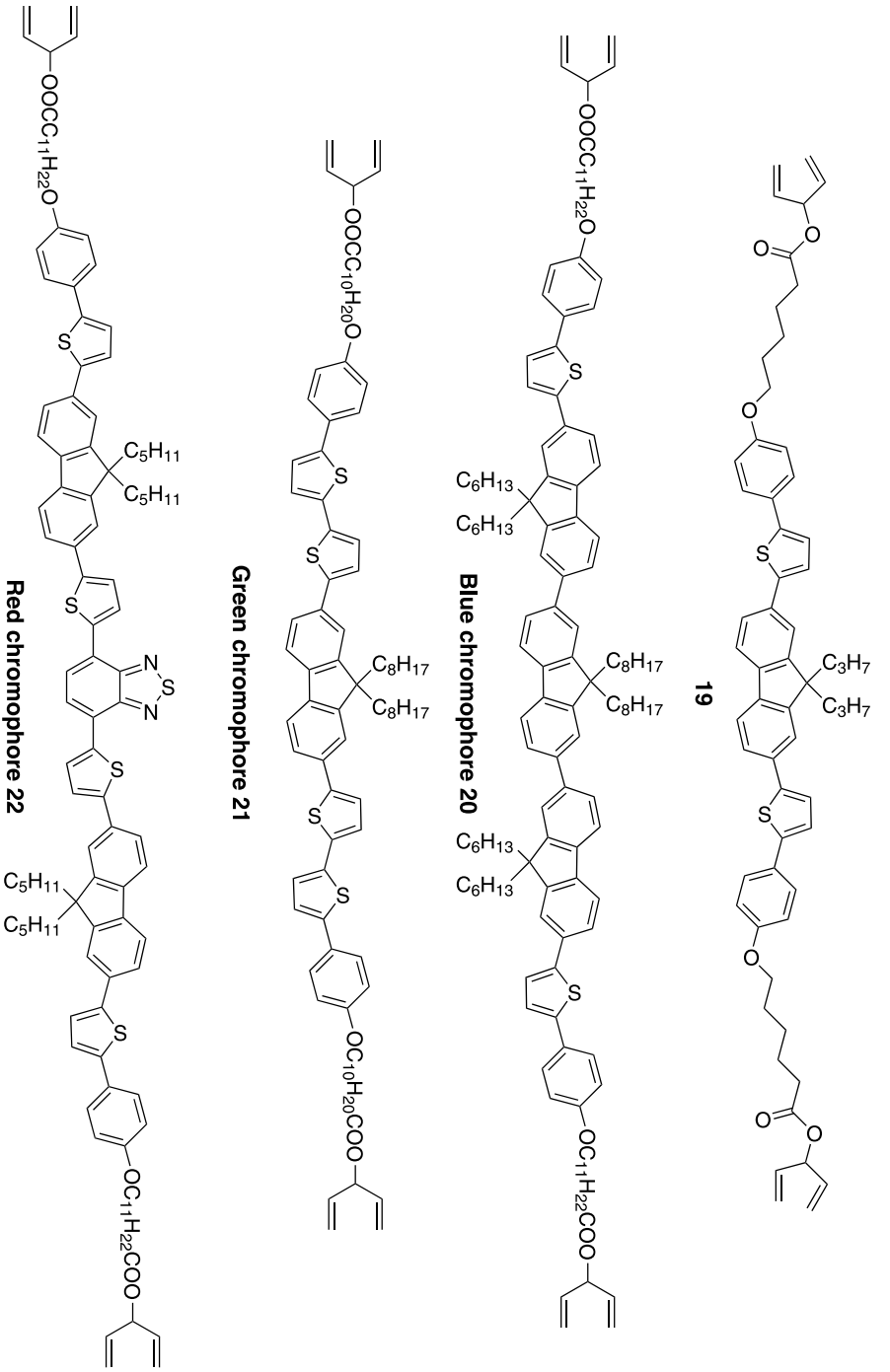

Fig. 19 Photopolymerizable LC semiconductors that exhibit nematic phase

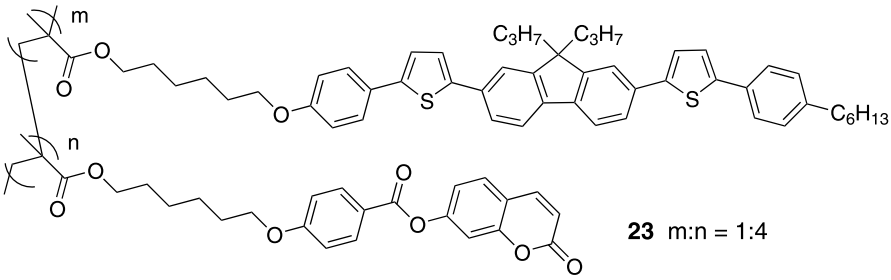

Fig. 20 Photo-alignment polymer consisting of photoreactive and semiconductive moieties

This polymer layer functioned not only as a hole injection layer but also as a molecular alignment layer. A high dichroic ratio exceeding 20 was observed in three color pixels [106].

Unlike thin film transistors, electroluminescence devices operate in a high electric field, and therefore homogeneity and low defect density of the thin films are more important than the carrier transport characteristics. In this sense, the approach to the use of nematic semiconductors by Kelly and O'Neill should be reasonable.

3.4 Photopolymerization in Smectic Phases

For application to thin film transistors (TFTs), which can operate electronic papers, high carrier mobility exceeding 0.01 $cm^2\ V^{-1}\ s^{-1}$ is necessary. For this purpose, nematic semiconductors with low molecular order, resulting in relatively low carrier mobility, are not suitable. For application of thin films of semiconductors to TFTs, stabilization of the highly ordered smectic phases, which exhibit high carrier mobility, by photopolymerization may be desirable. Kreouzis et al. studied the carrier transport properties of photopolymerizable phenylnaphthalene, diphenylbithiophene, and quaterthiophene derivatives having an oxetane moiety or 1,4-pentadien-3-yloxy in their alkyl side chain (Fig. 21) [107, 108].

Thin films of the photoreactive liquid crystals containing 0.5 wt % of initiator (10-biphenyl-4-yl-2-isopropyl-9-oxo-9*H*-thioxanthen-10-ium hexafluorphosphate) were polymerized in the smectic phases by irradiation of blue semiconductor laser ($\lambda = 405$ nm). Polymerization of the oxetane moiety proceeded via cationic intermediates. The carrier transport characteristics of the polymerized thin films were studied by the time-of-flight technique.

Dialkylphenylbithiophene derivative **24** exhibits a smectic G phase between 140 °C and 225 °C. In the smectic G phase, high electron mobility of up to 0.07 $cm^2\ V^{-1}\ s^{-1}$ as well as a high hole mobility of 0.044 $cm^2\ V^{-1}\ s^{-1}$ is observed using the time-of-flight method [107]. Kreouzis and coworkers

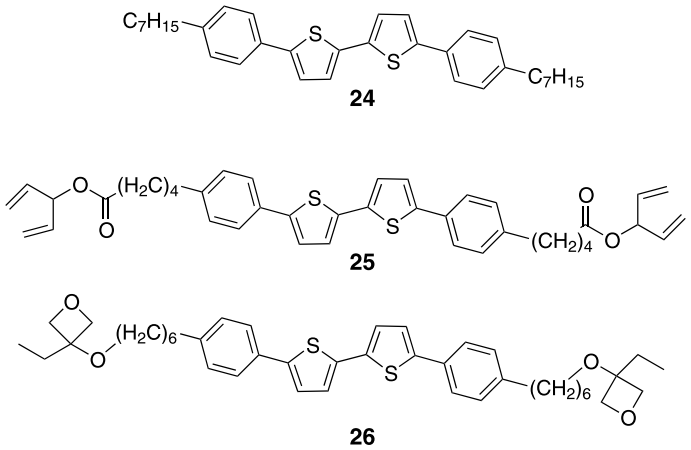

Fig. 21 LC semiconductor containing an oxetane moiety, which retains highly ordered smectic phase around room temperature

synthesized diphenylbithiophene derivatives containing a polymerizable 1,4-pentadien-3-yloxy (**25**) or oxetane (**26**) group at the extremity of the alkyl chains. Monomeric and polymerized diphenylbithiophene with an oxetane moiety **26** and quaterthiophene with an oxetane moiety exhibited ambipolar carrier transport in the ordered smectic phases. It was surprising that the diphenylbithiophene derivative having the oxetane moiety in its side chains exhibited quite high ambipolar carrier mobility (on the order of 10^{-2} cm^2 V^{-1} s^{-1}) even in polymerized films. In this case, excellent carrier transport properties (ambipolar and high mobility) were retained after photopolymerization to stabilize the liquid-crystalline thin films. In addition, the hole and electron mobility were independent of temperature and electric field, which is characteristic for ordered smectic phases of liquid crystals with low molecular weight. These results suggest that molecular ordering was not perturbed during the polymerization process in the smectic phases. Photopolymerization in the isotropic phase produces thin films that do not exhibit excellent carrier transport properties [108].

The carrier transport characteristics were analyzed using Bässler's disorder formalism and Holstein's small polaron theory; however, the temperature range in which the carrier mobility was measured precisely was not so wide that the transport mechanism could be determined clearly [108].

Polymerization of reactive monomeric liquid crystals is one method for stabilizing the liquid-crystalline thin films. Another approach is to form chemical gels of liquid crystal molecules with low molecular weight by construction of a polymer network. This method has been investigated for the stabilization of ferroelectric liquid crystal displays. Guymon et al. reported that a polymer network produced by photochemical cross-linking accumu-

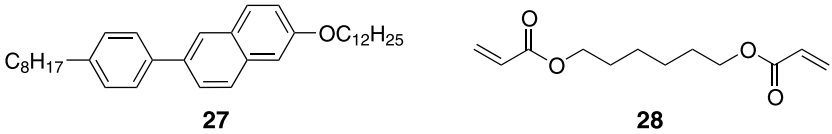

27 28

Fig. 22 Molecular structures of LC 2-phenylnaphthalene derivative and hexanediol diacryalte

lated between smectic layers, resulting in the stabilization of the smectic thin films [109]. Yoshimoto et al. reported stabilization of the smectic A and B phases of 2-phenylnaphthalene derivative **27** doped by hexanediol diacrylate **28** with photopolymerization (Fig. 22). In this study, carrier mobility was maintained in the smectic A and B phases when photopolymerization was carried out in the smectic phases; however, carrier mobility decreased when the photopolymerization was done in the isotropic phase. In this case, microscopic segregation of the polymer network formed during the photopolymerization process should play important role [110, 111].

Enhanced photoconductive properties were reported for physical gels of a liquid-crystalline triphenylene derivative [112].

3.5 Miscellaneous Systems and Related Compounds

Conjugated polymers have become very important materials in organic electronics since the discovery of electrical conductivity in doped polyacetylenes [113]. In a single chain of conjugated polymers, 1D band structure should be formed under an ideal state. Here, each π-conjugated chain extends linearly and is planar without defects, resulting in fast carrier transport along the single chain. However, in actual systems, the single chain is bent or twisted and carriers have to migrate between many chains and segments when they drift between electrodes. Therefore, the carrier transport process in bulk or in thin films of conjugated polymers is mainly controlled by interchain or inter-segment hopping of charge carriers rather than fast carrier transport within single chains [114].

Comparing with conventional amorphous organic semiconductors [16], it is characteristic that conjugated polymer films consist of crystal-like domains, in which π-conjugated chains are stacked closely, and an amorphous domain, in which polymer chains are disordered [115]. In crystal-like domains, band-like carrier transport that is similar to that of molecular crystals should be possible. However, hopping transport influenced by structural disorder is the dominant process in the amorphous domains. The total carrier transport process is dominated mainly by that in amorphous domains, resulting in bulk carrier transport characteristics similar to those of amorphous organic semiconductors.

In field-effect transistors based on the thin films of poly(3-alkyl)thiophene derivatives, high field-effect mobility has been observed because of the formation of crystal-like grains [116]. The mobility depends strongly upon the crystallinity of the thin films. Introduction of liquid crystallinity into conjugated polymers is expected to be effective for enhancing microscopic crystallization of conjugated polymers to increase their carrier mobilities. It can also cause anisotropy in various physical properties if macroscopic molecular alignment is achieved.

Conjugated polymers having mesogenic groups in their side chains have been synthesized by the Akagi group [117]. In particular, polyacetylenes having mesogenic side chains exhibited a high anisotropy in electrical conductivity. In polyacetylenes bearing cyclohexylphenyl groups in the side chains, macroscopically aligned film can be fabricated under application of a magnetic field. In the iodine-doped aligned film, conductivity along the main chain was 1.5×10^{-6} S cm^{-1} while that perpendicular to the main chains was 1.4×10^{-11} S cm^{-1} [118].

Poly(9,9-dialkylfluorene) exhibits a nematic phase above 160 °C and a uniaxially aligned nematic film can be fabricated on a rubbed substrate. This uniaxally aligned nematic state can be quenched by cooling it below 75 °C [119]. The hole mobility was determined to be 9×10^{-3} cm^2 V^{-1} s^{-1} at room temperature by the time-of-flight method, while it was on the order of 10^{-5} cm^2 V^{-1} s^{-1} in the isotropic film fabricated by the spin-coating method [119]. Carrier transport is remarkably enhanced by nematic ordering of polyfluorene chains. Amplified spontaneous emission from this polymer and the related compounds are now being studied [120].

The liquid crystallinity of poly(3-alkylthiophene) has been pointed out [121]. Enhancement of crystallinity by molecular alignment in a liquid crystal phase is prominent in poly(2,5-bis(3-alkylthiophen-2-yl)thieno[3,2-b]thiophene) exhibiting a lamellar mesophase. When a thin film of the polymer fabricated by the spin-coating method is annealed at 100 °C, domain size remarkably extends from several tens of nanometers to a several micrometers, maintaining molecular alignment within domains because of the thermal motion of the polymer chains. The hole mobility of the thin film transistors based on this polymer reached 0.7 cm^2 V^{-1} s^{-1} [122].

4 Conclusion

Liquid-crystalline nanostructures formed by polymeric materials have great potential to be applied for ion- and electron-conducting materials because efficient and low-dimensional conduction can be achieved in nano-segregated LC phases. Recent progress in supramolecular chemistry and nanotechnology enables the design of new materials for ion conductors. Nematic LC poly-

meric semiconductors that are very promising for the application to polarized electroluminescence devices have been fabricated as well as smectic materials. Stabilization of ordered smectic and columnar phases has been displayed by aligned functional monomers with in-situ photopolymerization. Optimization of photoreactive groups and polymerization conditions will be necessary.

References

1. Richardson TH (2000) Functional organic and polymeric materials. Wiley, Chichester
2. Gray GW (1987) Thermotropic liquid crystals. Wiley, Chichester
3. Demus D, Goodby JW, Gray GW, Spiess HW, Vill V (1998) Handbook of liquid crystals. Wiley-VCH, Weinheim
4. Kato T (2002) Science 295:2414
5. Kato T, Mizoshita N, Kishimoto K (2006) Angew Chem Int Ed 45:38
6. Simpson CD, Wu JS, Watson MD, Müllen K (2004) J Mater Chem 14:494
7. Ten Brinke G, Ikkala O (2004) Chem Rec 4:219
8. Goodby JW, Mehl GH, Saez IM, Tuffin RP, Mackenzie G, Auzely-Velty R, Benvegnu T, Plusquellec D (1998) Chem Commun, p 2057
9. Gin DL, Lu X, Nemade PR, Pecinovsky CS, Xu Y, Zhou M (2006) Adv Funct Mater 16:865
10. O'Neill M, Kelly SM (2003) Adv Mater 15:1135
11. Meyer WH (1998) Adv Mater 10:439
12. Shahinpoor M (2003) Electrochim Acta 48:2343
13. Singh TB, Sariciftci NS (2006) Annu Rev Mater Res 36:199
14. Dodabalapur A (2006) Mater Today 9(4):24
15. Thomas SW, Joly GD, Swager TM (2007) Chem Rev 107:1339
16. Bässler H (1993) Phys Status Solidi B 175:15
17. Salaneck WR, Seki K, Kahn A, Pireaux J-J (2001) Conjugated polymer and molecular interfaces. Dekker, New York
18. Lehn J-M (1995) Supramolecular chemistry: concepts and perspectives. VCH, Weinheim
19. Ciferri A (2005) Supramolecular polymers, 2nd edn. Taylor and Francis, London
20. Lehn J-M (2005) In: Ciferri A (ed) Supramolecular polymers, 2nd edn. Taylor and Francis, London, p 3
21. Kato T (2005) In: Ciferri A (ed) Supramolecular polymers, 2nd edn. Taylor and Francis, London, p 131
22. Kato T, Mizoshita N, Kanie K (2001) Macromol Rapid Commun 22:797
23. Stupp SI, LeBonheur V, Walker K, Li LS, Huggins KE, Keser M, Amstutz A (1997) Science 276:384
24. Saez IM, Goodby JW (2005) J Mater Chem 15:26
25. Guillon D, Deschenaux R (2002) Curr Opin Solid State Mater Sci 6:515
26. Lee M, Cho BK, Zin WC (2001) Chem Rev 101:3869
27. Fischer H, Poser S (1996) Acta Polym 47:413
28. Thünemann AF, Kubowicz S, Burger C, Watson MD, Tchebotareva N, Müllen K (2003) J Am Chem Soc 125:352
29. Hoeben FJM, Jonkheijm P, Meijer EW, Schenning A (2005) Chem Rev 105:1491

30. Tschierske C (2001) J Mater Chem 11:2647
31. Ishikawa M, Morita M, Asao M, Matsuda Y (1994) J Electrochem Soc 141:1105
32. Bruce PG, Vincent CA (1993) J Chem Soc Faraday Trans 89:3187
33. Meyer WH (1998) Adv Mater 10:439
34. Scrosati B (2000) Electrochim Acta 45:2461
35. Wright PV (2002) MRS Bull 27:597
36. Stephan AM, Nahm KS (2006) Polymer 47:5952
37. Wright PV (1975) Br Polym J 7:319
38. Nishimoto A, Watanabe M, Ikeda Y, Kohjiya S (1998) Electrochim Acta 43:1177
39. Rogers RD, Seddon KR (2003) Science 302:792
40. Wasserscheid P, Keim W (2000) Angew Chem Int Ed 39:3772
41. Ohno H (2005) Electrochemical aspects of ionic liquids. Wiley, New Jersey
42. Yoshizawa M, Hirao M, Ito-Akita K, Ohno H (2001) J Mater Chem 11:1057
43. Ogihara W, Washiro S, Nakajima H, Ohno H (2006) Electrochim Acta 51:2614
44. Ohtake T, Ito K, Nishina N, Kihara H, Ohno H, Kato T (1999) Polymer J 31:1155
45. Ohtake T, Ogasawara M, Ito-Akita K, Nishina N, Ujiie S, Ohno H, Kato T (2000) Chem Mater 12:782
46. Ohtake T, Takamitsu Y, Ito-Akita K, Kanie K, Yoshizawa M, Mukai T, Ohno H, Kato T (2000) Macromolecules 33:8109
47. Hoshino K, Kanie K, Ohtake T, Mukai T, Yoshizawa M, Ujiie S, Ohno H, Kato T (2002) Macromol Chem Phys 203:1547
48. Iinuma Y, Kishimoto K, Sagara Y, Yoshio M, Mukai T, Kobayashi I, Ohno H, Kato T (2007) Macromolecules 40:4874
49. Kato T, Yoshio M (2005) In: Ohno H (ed) Electrochemical aspects of ionic liquids. Wiley, New Jersey, p 307
50. Yoshio M, Mukai T, Kanie K, Yoshizawa M, Ohno H, Kato T (2002) Adv Mater 14:351
51. Yoshio M, Kato T, Mukai T, Yoshizawa M, Ohno H (2004) Mol Cryst Liq Cryst 413:2235
52. Yoshio M, Mukai T, Kanie K, Yoshizawa M, Ohno H, Kato T (2002) Chem Lett 31:320
53. Mukai T, Yoshio M, Kato T, Ohno H (2004) Chem Lett 33:1630
54. Mukai T, Yoshio M, Kato T, Ohno H (2005) Chem Lett 34:442
55. Mukai T, Yoshio M, Kato T, Yoshizawa M, Ohno H (2005) Chem Commun, p 1333
56. Yoshio M, Mukai T, Ohno H, Kato T (2004) J Am Chem Soc 126:994
57. Lehn JM, Malthête J, Levelut AM (1985) J Chem Soc Chem Commun, p 1794
58. van Nostrum CF, Picken SJ, Nolte RJM (1994) Angew Chem Int Ed Engl 33:2173
59. Percec V, Johansson G, Heck JA, Ungar G, Batty SV (1993) J Chem Soc Perkin Trans 1:1411
60. Brunsveld L, Vekemans J, Janssen HM, Meijer EW (1999) Mol Cryst Liq Cryst Sci Technol, Sect A 331:2309
61. Hsieh CJ, Hsiue GH, Hsu CS (1990) Macromol Chem 191:2195
62. Percec V, Tomazos D (1993) J Mater Chem 3:643
63. Lauter U, Meyer WH, Wegner G (1997) Macromolecules 30:2092
64. Zheng YG, Chia FS, Ungar G, Wright PV (2000) Chem Commun, p 1459
65. Zheng YG, Lui JG, Ungar G, Wright PV (2004) Chem Rec 4:176
66. Dias FB, Batty SV, Ungar G, Voss JP, Wright PV (1996) J Chem Soc Faraday Trans 92:2599
67. Kishimoto K, Yoshio M, Mukai T, Yoshizawa M, Ohno H, Kato T (2003) J Am Chem Soc 125:3196
68. Kishimoto K, Suzawa T, Yokota T, Mukai T, Ohno H, Kato T (2005) J Am Chem Soc 127:15618

69. Hoshino K, Yoshio M, Mukai T, Kishimoto K, Ohno H, Kato T (2003) J Polym Sci, Part A: Polym Chem 41:3486
70. Yoshio M, Kagata T, Hoshino K, Mukai T, Ohno H, Kato T (2006) J Am Chem Soc 128:5570
71. Kosonen H, Valkama S, Hartikainen J, Eerikäinen H, Torkkeli M, Jokela K, Serimaa R, Sundholm F, ten Brinke G, Ikkala O (2002) Macromolecules 35:10149
72. Ikkala O, ten Brinke G (2004) Chem Commun, p 2131
73. Ruokolainen J, Mäkinen R, Torkkeli M, Mäkelä T, Serimaa R, ten Brinke G, Ikkala O (1998) Science 280:557
74. Mäki-Ontto R, de Moel K, Polushkin E, van Ekenstein GA, ten Brinke G, Ikkala O (2002) Adv Mater 14:357
75. Cho BK, Jain A, Gruner SM, Wiesner U (2004) Science 305:1598
76. Cho BK, Jain A, Mahajan S, Ow H, Gruner SM, Wiesner U (2004) J Am Chem Soc 126:4070
77. Cho BK, Jain A, Nieberle J, Mahajan S, Wiesner U, Gruner SM, Türk S, Rader HJ (2004) Macromolecules 37:4227
78. Borsenberger PM, Weiss DS (1993) Organic photoreceptors for imaging systems. Dekker, New York
79. Boden N, Bushby RJ, Clements J, Jesudason MV, Knowles PF, Williams G (1988) Chem Phys Lett 152:94
80. Adam D, Closs F, Frey T, Funhoff D, Haarer D, Ringsdorf H, Schuhmacher P, Siemensmeyer K (1993) Phys Rev Lett 70:457
81. van de Craats AM, Warman JM, Fechtenkötter A, Brand JD, Harbison MA, Müllen K (1999) Adv Mater 11:1469
82. Kastler M, Laquai F, Müllen K, Wegner G (2006) Appl Phys Lett 89:252103
83. Funahashi M, Hanna J (1997) Phys Rev Lett 78:2184
84. Funahashi M, Hanna J (1996) Jpn J Appl Phys, Part 2 35:L703
85. Funahashi M, Hanna J (1997) Appl Phys Lett 71:602
86. Shimizu Y, Shigeta K, Kusabayashi S (1986) Mol Cryst Liq Cryst 140:105
87. Murakami S, Naito H, Okuda M, Sugimura A (1995) J Appl Phys 78:4533
88. Funahashi M, Tamaoki N (2006) ChemPhysChem 7:1193
89. Woon KL, Aldred MP, Vlachos P, Mehl GH, Stirner T, Kelly SM, O'Neill M (2006) Chem Mater 18:2311
90. Funahashi M, Tamaoki N (2007) Chem Mater 19:608
91. Funahashi M, Hanna J (2001) Mol Cryst Liq Cryst 368:4071
92. Simmerer J, Glüsen B, Paulus W, Kettner A, Schuhmacher P, Adam D, Etzbach KH, Siemensmeyer K, Wendorff JH, Ringsdorf H, Haarer D (1996) Adv Mater 8:815
93. Kreouzis T, Donovan KJ, Boden N, Bushby RJ, Lozman OR, Liu Q (2001) J Chem Phys 114:1797
94. Mallia VA, Tamaoki N (2004) Chem Soc Rev 33:76
95. Ikeda T, Mochizuki H, Hayashi Y, Sisido M, Sasakawa T (1991) J Appl Phys 70:3689
96. Ikeda T, Mochizuki H, Hayashi Y, Sisido M, Sasakawa T (1991) J Appl Phys 70:3696
97. Adam D, Schuhmacher P, Simmerer J, Häußling L, Paulus W, Siemensmeyer K, Etzbach KH, Ringsdorf H, Haarer D (1995) Adv Mater 7:276
98. Bleyl I, Erdelen C, Schmidt HW, Haarer D (1999) Philos Mag B 79:463
99. Bleyl I, Erdelen C, Etzbach KH, Paulus W, Schmidt HW, Siemensmeyer K, Haarer D (1997) Mol Cryst Liq Cryst Sci Technol, Sect A 299:149
100. Bacher A, Bleyl I, Erdelen CH, Haarer D, Paulus W, Schmidt HW (1997) Adv Mater 9:1031
101. Walzer K, Maennig B, Pfeiffer M, Leo K (2007) Chem Rev 107:1233

102. Collings PJ (1990) Liquid crystals: Nature's delicate phase of matter. Princeton University Press, New Jersey
103. Aldred MP, Contoret AEA, Farrar SR, Kelly SM, Mathieson D, O'Neill M, Chung-Tsoi W, Vlachos P (2005) Adv Mater 17:1368
104. Farrar SR, Contoret AEA, O'Neill M, Nicholls JE, Richards GJ, Kelly SM (2002) Phys Rev B 66:125107
105. Contoret AEA, Farrar SR, Jackson PO, Khan SM, May L, O'Neill M, Nicholls JE, Kelly SM, Richards GJ (2000) Adv Mater 12:971
106. Aldred MP, Vlachos P, Contoret AEA, Farrar SR, Chung-Tsoi W, Mansoor B, Woon KL, Hudson R, Kelly SM, O'Neill M (2005) J Mater Chem 15:3208
107. Kreouzis T, Baldwin RJ, Shkunov M, McCulloch I, Heeney M, Zhang W (2005) Appl Phys Lett 87:172110
108. Baldwin RJ, Kreouzis T, Shkunov M, Heeney M, Zhang W, McCulloch I (2007) J Appl Phys 101:023713
109. Guymon CA, Hoggan EN, Clark NA, Rieker TP, Walba DM, Bowman CN (1997) Science 275:57
110. Yoshimoto N, Hanna J (2002) Adv Mater 14:988
111. Yoshimoto N, Hanna J (2003) J Mater Chem 13:1004
112. Mizoshita N, Monobe H, Inoue M, Ukon M, Watanabe T, Shimizu Y, Hanabusa K, Kato T (2002) Chem Commun, p 428
113. Shirakawa H (2001) Angew Chem Int Ed 40:2574
114. Hadziioannou G, van Hutten PF (2000) Semiconducting polymers. Wiley-VCH, Weinheim
115. Street RA, Northrup JE, Salleo A (2005) Phys Rev B 71:165202
116. Sirringhaus H, Brown PJ, Friend RH, Nielsen MM, Bechgaard K, Langeveld-Voss BMW, Spiering AJH, Janssen RAJ, Meijer EW, Herwig P, de Leeuw DM (1999) Nature 401:685
117. Akagi K (2007) Bull Chem Soc Jpn 80:649
118. Akagi K, Shirakawa H (1993) Synth Met 60:85
119. Redecker M, Bradley DDC, Inbasekaran M, Woo EP (1999) Appl Phys Lett 74:1400
120. Heliotis G, Choulis SA, Itskos G, Xia R, Murray R, Stavrinou PN, Bradley DDC (2006) Appl Phys Lett 88:081104
121. Tashiro K, Ono K, Minagawa Y, Kobayashi M, Kawai T, Yoshino K (1991) J Polym Sci, Part B: Polym Phys 29:1223
122. McCulloch I, Heeney M, Bailey C, Genevicius K, Macdonald I, Shkunov M, Sparrowe D, Tierney S, Wagner R, Zhang WM, Chabinyc ML, Kline RJ, McGehee MD, Toney MF (2006) Nat Mater 5:328

Struct Bond (2008) 128: 181–222
DOI 10.1007/430_2007_064

Published online: 8 September 2007

Functional Lyotropic Liquid Crystal Materials

Douglas L. Gin[1,2] (✉) · Cory S. Pecinovsky[1] · Jason E. Bara[2] · Robert L. Kerr[1]

[1]Department of Chemistry and Biochemistry, University of Colorado, Boulder, Colorado 80309, USA
gin@spot.colorado.edu

[2]Department of Chemical and Biological Engineering, University of Colorado, Boulder, Colorado 80309, USA

Abstract Lyotropic liquid crystals (LLCs) are amphiphilic molecules that have the ability to self-organize into highly ordered yet fluid, phase-segregated assemblies in the presence of an added polar liquid such as water. The resulting ordered assemblies, called LLC phases, have specific nanometer-scale geometries with periodic hydrophilic and hydrophobic features ranging in structure from bilayer lamellae to extended and interconnected channel systems. Because of their highly uniform, porous nanoscale structures, LLC phases and LLC-based materials have been proposed for use in a number of materials applications. However, only during the last two decades have LLC materials with functional properties and demonstrated applications of LLC systems been realized. This work provides an overview of functional LLC materials and the areas of application where they have made an impact. As new functional properties and capabilities are realized in LLC materials, it is almost certain that they will play more prevalent roles in nanoscience and nanotechnology in the near future.

Keywords Functional · Lyotropic · Liquid crystal · Materials · Polymers · Self-assembly · Surfactant

1 Introduction

Liquid crystals (LCs) are molecules that have the ability to self-assemble into organized mesophases with properties intermediate between those of crystalline solids and isotropic liquids [1, 2]. In LC phases, the molecules are dynamic and collectively behave as a viscous liquid but retain *on average* a degree of organization reminiscent of an ordered, crystalline solid. Consequently, they can be considered ordered fluids, as a more accurate definition. LCs can be subdivided into two general classes—thermotropic LCs and lyotropic LCs—depending on the environmental and molecular factors that govern how they form ordered fluid phases.

By definition, *thermotropic LCs* are molecules that form ordered fluid phases in which the degree of average order depends primarily on the temperature of the material [1, 2]. Unlike conventional materials which undergo a melting transition from a crystalline solid directly to an isotropic liquid, thermotropic LCs lose their order incrementally by adopting a number of ordered yet progressively more fluid states with increasing temperature. In terms of their molecular structure, thermotropic LCs are molecules with an anisotropic shape (e.g., typically rod- or disk-shaped) containing a relatively rigid core and a number of flexible peripheral alkyl tails. The rigid cores of these molecules encourage ordered packing while the flexible tails tend to disorder the system until a compromise is met to produce an ordered fluid state.

In contrast, *lyotropic LCs* (*LLCs*) are molecules that form ordered fluid phases that are *phase-separated mixtures* in which the degree of order depends on the proportion of LC mesogen relative to an added immiscible solvent such as water [3, 4]. In addition to morphology dependence on system composition, LLC phases are also sensitive to other external parameters

such as temperature and pressure. In terms of molecular structure, LLCs are very different from thermotropic LCs in that LLCs are flexible amphiphilic molecules (i.e., surfactants) that contain both a hydrophobic organic tail section and a hydrophilic headgroup. The shape and amphiphilic character of these molecules encourage them to self-organize into highly ordered, phase-separated matrices in the presence of a polar solvent such as water. The flexible aliphatic tails of the amphiphiles aggregate into fused hydrophobic regions while the hydrophilic headgroups (ionic or neutral) encapsulate extended aqueous regions. Depending on the molecular shape/packing preferences of the LLC molecules [5] and interfacial curvature energy considerations [6], LLC phases can be formed with aqueous domains ranging from planar bilayer lamellae to extended, cylindrical channels to 3-D interconnected channels and manifolds. These LLC phases are termed lamellar (L), hexagonal (H), bicontinuous cubic [Q (or V)], and discontinuous cubic (I) phases, based on their symmetry [3, 4]. They are also subdivided into type I (or type 1) and type II (or type 2) phases depending whether they are on the water-excessive (type I) or water-deficient (type II) side of the phase diagram relative to the central L phase. The L phase is considered to have no intrinsic curvature and often viewed as the midpoint of an ideal, symmetrical LLC phase progression (Fig. 1) [3–6]. Type I or II LLC phases are indicated with subscripts after the principal phase label designation. In addition to these more classical LLC phase architectures, there are also a number of less common LLC phases such as "intermediate" (e.g., ribbon or mesh) LLC phases [7]; and lyotropic nematic phases [8]. Intermediate ribbon and mesh-type LLC phases are sometimes called rhombohedral, monoclinic, or tetrahedral LLC phases based on their observed symmetries. These phases are believed to have ribbon-like or porous mesh-like continuous or bicontinuous structures [7], but their structures are not well characterized (Fig. 2). These intermediate phases can also be type I or type II structures. Lyotropic nematic phases are believed to be composed of collections of discrete disk-shaped or rod-shaped micellar aggregates that have a common average orientation direction (i.e. a director) due to their anisotropic shapes and close packing considerations (Fig. 3) [8, 9]. These other LLC phases usually appear between the classical LLC phase architectures shown in Fig. 1.

It should be noted that LLC phases are different from the ubiquitous *individual*, phase-separated aggregate structures commonly formed by amphiphilic molecules or surfactants, such as micelles, reverse micelles, vesicles, and lipid microtubules. These *discrete* aggregate structures formed from amphiphiles lack periodic order, and are not condensed-phase materials—two defining characteristics of LLC phases. *For the purposes of this review, LLC phases will be defined as fluid, condensed-phase materials composed of amphiphilic molecules that have periodic order and are formed via phase separation of the amphiphiles around an added solvent as a secondary component (i.e., mixtures).* Consequently, functional normal micelle, reverse micelle,

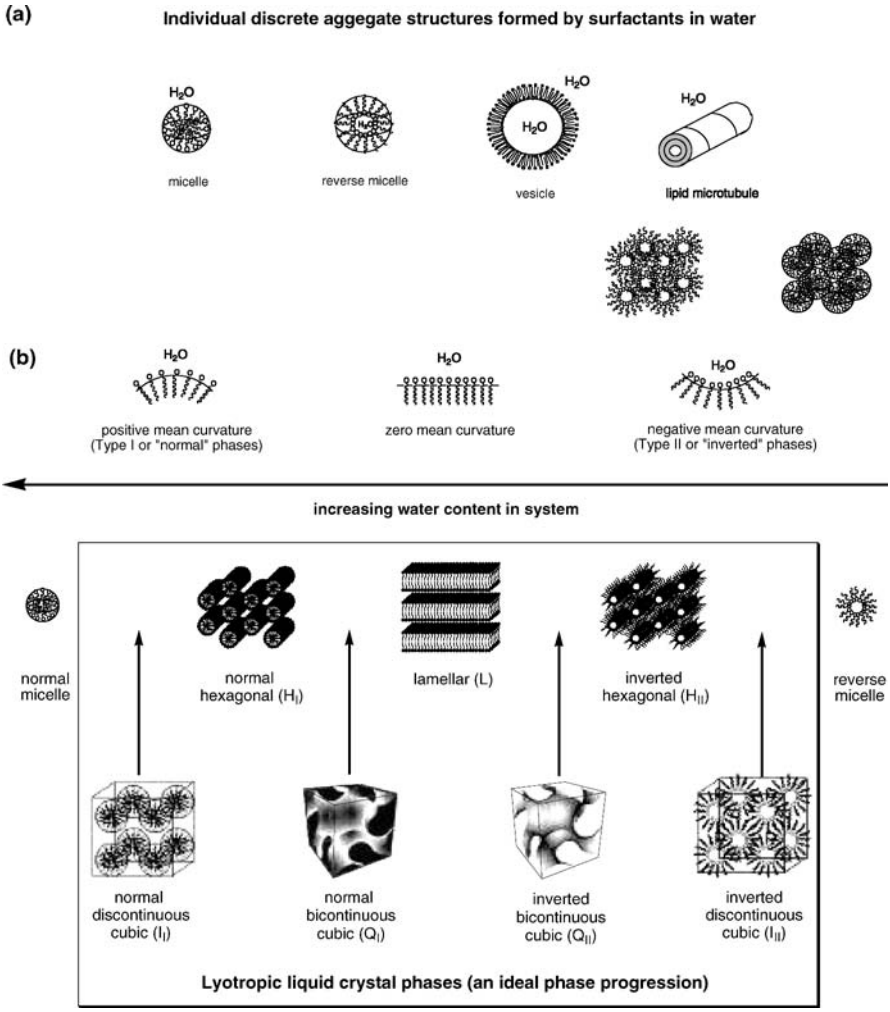

Fig. 1 Schematic representations of **a** individual aggregate structures commonly formed by amphiphiles in water; and **b** common LLC phases formed by amphiphiles in water. A small element in Fig. 1b is partially reproduced with permission from [176]. © 1997 by the American Chemical Society

Langmuir–Blodgett films, vesicle, and lipid microtubule systems (Fig. 1a) will not be covered in this review, even though micelle and microemulsion systems have historically been assigned phase designations (e.g., L_1 and L_2, respectively) despite the fact that such systems do not have periodic order [2–4].

There is also a small family of LCs called lyotropic chromonic LCs that are in-between traditional thermotropic LCs and LLCs [10]. Lyotropic chromonic

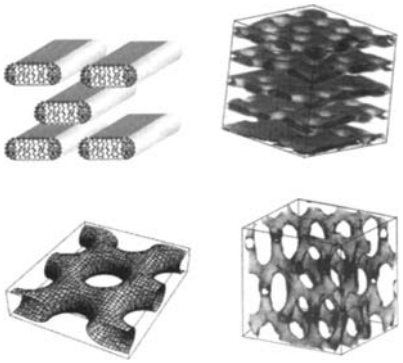

Fig. 2 Proposed structures of some "intermediate" LLC phases. Reproduced with permission from [7]. © 2005 by Taylor and Francis

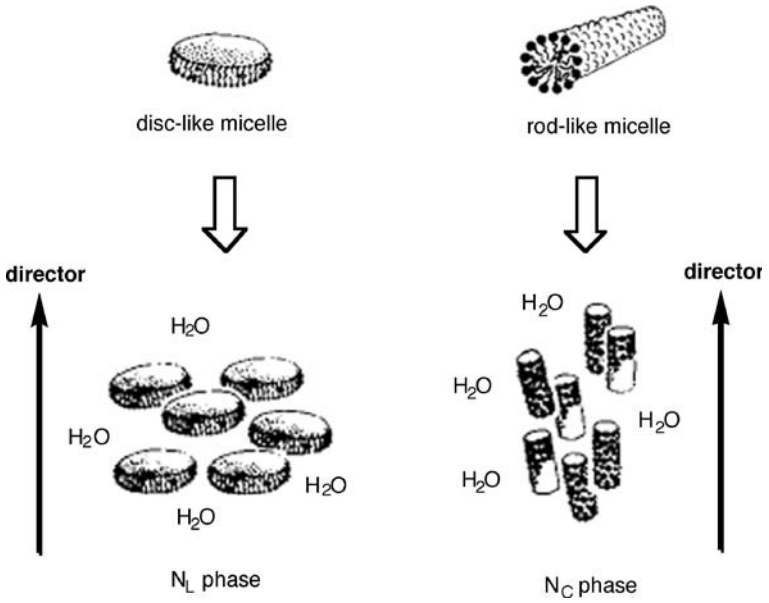

Fig. 3 Schematic representation of lyotropic nematic phases with disk-like (N_L) and rod-like (N_C) micellar aggregates. Partially reproduced with permission from [9]. © 1988 by Wiley-VCH

LCs typically have an aromatic organic core with ionic groups lining the periphery, giving them a disk- or plank-like shape (e.g., ionic organic dye molecules). They are technically classified as LLCs because they can self-assemble into ordered phases in the presence of water. However, unlike traditional amphiphiles, lyotropic chromonic LCs are rigid rather than flexible, and their hydrophobic components are based on aromatic units rather than aliphatic chains. Unlike traditional amphiphilic LCs, they self-organize in so-

lution into columns via stacking of their rigid cores, rather than forming traditional micellar-based structures (Fig. 4). They also do not exhibit a critical micelle concentration or a Krafft temperature like traditional flexible amphiphiles in water. In many respects, lyotropic chromonic LCs are closer to thermotropic LCs than conventional LLCs, in terms of their structure and LC behavior. Consequently, lyotropic chromonic LCs will be not discussed in this review. Proposed applications of functional lyotropic chromonic LCs include switchable display materials, optical gratings, polarizers, biosensors, light-emitting diodes, organic transistors, and even drug delivery materials. Their structures, LC behavior, and emerging applications can be found in two recent review articles [10, 11].

Traditional LLC phases formed by flexible amphiphilic mesogens [which are the focus of this review article (Fig. 1b)], have many characteristics that make them ideal for use as advanced materials, or for potential applications [12, 13]. First, their highly regular, nanoporous architectures can be used to incorporate or encapsulate hydrophobic as well as hydrophilic reagents in separate compartments with nanoscale precision. Second, the amphiphilic LLC self-assembly process localizes the hydrophilic headgroups of the LLC mesogens exclusively at the hydrophilic/hydrophobic interface. This arrangement allows one to engineer the environments in those regions for specific applications via choice of LLC headgroup and solvent. Third, LLC mesogens offer excellent control over parameters such as phase geometry and symmetry on the 1–5 nanometer scale via molecular design. This control can be extended to the macroscopic scale through appropriate alignment and processing of the fluid assemblies. Finally, because LLC phases are inherently fluid, their ordered structures can be disrupted by physical or chemical changes as desired for specific applications such as controlled release. Alternatively, LLC phase architectures can be stabilized by polymerization or cross-linking for robustness, if polymerizable analogues of the LLC molecules are employed in the phase preparation [9, 12–14].

Conventional thermotropic LCs are currently used in a number of technological and functional applications, including electro-optic displays, non-

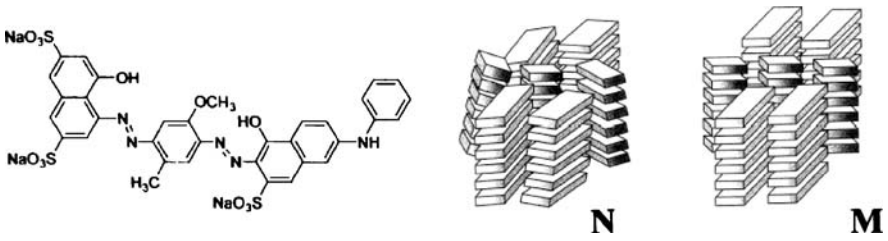

Fig. 4 Structure of a typical lyotropic chromonic LC, and schematic representations of two lyotropic chromonic LC phases. Reproduced with permission from [10]. © 2004 by Elsevier

linear optical materials, and optical gating systems [1, 2]. They are also commonly used as ordering elements in high-strength polymers (i.e., main-chain and side-chain LC polymers) [2, 15]. Non-functionalized thermotropic LCs have also been explored for use as anisotropic solvents for chemical reactions [16], and for delivery systems in the pharmaceutical industry [17]. Many examples of thermotropic LC systems with new or additional functional properties also exist in the literature [18–22]. However, functional versions of LLCs and demonstrated applications of LLC materials are much less developed. Only within the last two decades have examples of functional LLC mesogens and functional materials based on LLC assemblies been realized.

The goal of this article is to provide an overview of the major research areas and activities in the area of functional LLC materials over the last 10–20 years, and also describe some emerging new directions for this field of materials research. In addition to limiting this review to LLC systems as defined above, we will also restrict the scope of this review in several other ways for focus. This review will also be restricted to LLC systems containing *small-molecule or oligomeric* amphiphiles that self-assemble into ordered systems in the presence of an added solvent. Ordered, phase-separated block copolymer assemblies are similar in geometry and structure to LLC phases [23], but they will not be included in this review as true LLC phases. This is because block copolymers can self-organize in the absence of an added solvent, and amphiphilic polymer systems have periodic features that are 1–2 orders of magnitude larger in size than those found in typical LLC phases. Recent reviews on applications of functional amphiphilic block copolymer materials are available [24, 25]. Additionally, this review will be focused solely on the discussion of *functional* LLC materials. By the term "*functional*", we mean LLC-based systems (as defined structurally and compositionally above) in which (1) the LLC mesogens themselves have *additional properties of potential utility* in addition to their intrinsic self-organization behavior; (2) the mesogens *perform a specific function for generating useful materials*; and/or (3) the collective material has a *demonstrated* application or useful function. Whether such LLC materials are organic or hybrid, monomeric or polymerized, or formed around water or a different polar solvent, does not matter.

This review is divided into sections according to the type of functional properties or areas of application that have been identified or demonstrated for LLC materials.

2
LLC-templated Materials and Composites

While LLCs have the intrinsic ability to self-organize in an added solvent, an additional function frequently made use of is their ability to organize extrinsic molecules, macromolecules, or materials into that LC structure. LLCs,

having hydrophilic and hydrophobic domains, can segregate guest molecules into the domain these guests most prefer. Once the guests are localized into the domain of preference, they can be chemically manipulated (e.g., polymerized, solidified) within the confines of the nano-environment that the LLC phase provides. Thus, materials with no intrinsic self-assembling properties can be organized into nanostructures that are often an exact replica of the LLC phase template. These guests can be inorganic or organic molecules, and are usually materials whose bulk properties benefit from being nanostructured (e.g., semiconductors, conductors, catalysts) but are unable to organize themselves. Also, it has been proposed that these templated nanostructured and nanocomposite materials may have unique and enhanced properties over either of the individual components.

2.1 Direct Templating of Nanostructure in Inorganic Materials

Surfactant-templated formation of mesostructures in silica and other inorganic materials is a rapidly growing field, and has been recently reviewed [26–31]. Low surfactant concentrations (e.g., 0.1 M) lead to phases where micelles and microemulsions dominate, from which the inorganic materials are templated via a co-assembly process. The surfactants by themselves, at those low concentrations, do not form LLC mesophases. Typically, there are noncovalent interactions between the surfactant and inorganic precursor that result in the ordered co-assembly. On the other hand, high surfactant concentrations (e.g., 50 wt %) lead to LLC phases without the co-assembly, which is the focus of this review and this section. This method is often called "the direct templating method" or "nanocasting" because the replica is often a close-to-perfect copy of the template (Fig. 5) [32]. It has the advantage of yielding mesostructures with predicable geometry and pore size. This is typically accomplished by starting from a LLC phase, and then the liquid continuous phase is simply solidified by some chemical or electrochemical reaction. One can tailor the pore size by changing the tail length of the amphiphile, or tailor the architecture by changing the LLC phase (e.g., L, H, I, and Q phases). Thus, this method offers enormous potential for control over the geometries of these nanostructures. In the majority of the literature in this area, the function of the LLC phase is to direct or template the organization of another material. Often this second material introduces additional useful properties into the system, rather than the LLC system having additional functional properties. After solidification of this secondary material, the LLC component is typically removed to allow access to the interior of these mesoporous structures.

The first example of this method was reported in 1995, where silica mesostructures were produced as a near-exact negative copy of the LLC (H_I phase) template [33]. As an indication of the versatility of this method,

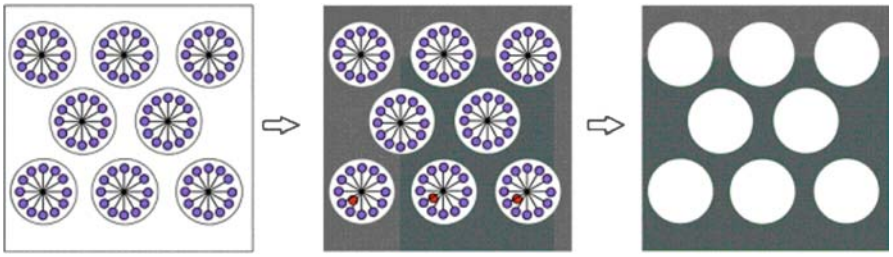

Fig. 5 The three-step process of "nanocasting". First, a condensed LLC phase is formed, with the inorganic precursors occupying the liquid (aqueous) phase. Second, the inorganic molecules are solidified by some chemical or electrochemical means. Third, the LLC template is removed, leaving a mesoporous structure. Partially reproduced with permission from [32]. © 2002 by the Royal Society of Chemistry

it has since been applied to other inorganic materials with functional properties, including metals and semiconductors, using a variety of surfactants and LLC phases, including polymerized LLC phases [34–48].

Bulk semiconductor nanostructured networks of CdS have been prepared in L and H_I phases [33, 34]. The L phase was formed by a polyol amphiphile shown in Fig. 6. This LLC phase was doped with Cd^{2+} ions and then CdS was precipitated by diffusion of H_2S into the gel. This nanocomposite was found to incorporate the amphiphile and metal in alternating layers (Fig. 6), closely resembling the structure of biominerals (e.g., mother of pearl). Similarly, H_I phases were prepared from an oligo(ethylene oxide) oleyl ether amphiphile (Fig. 7) mixed with a solution of Cd^{2+}. Again, H_2S was added to precipitate CdS and the resulting composite preserved the hexagonal symmetry (Fig. 7).

Thin films of nanostructured metals and semiconductors (e.g., Pt, Sn, CdTe) can be prepared by electrodeposition of the metal ions doped into the H_I LLC phase [40, 47, 48]. Similar to the precipitation of CdS, these films can retain the symmetry of the LLC template during the deposition. These materials allow one to combine well-defined porous nanostructures, high specific surface areas, electrical connectivity, fast electrolyte diffusion, and good mechanical and electrochemical stability. With this approach, hexagonally structured semiconductor films of uniform thickness can be prepared. Nanostructured thin films of this type are proposed to have relevance in catalysis, batteries, fuel cells, capacitors, and sensors.

A recent example of a templated thin film is shown in Fig. 8 [48]. Initial experiments showed that the templated CdTe film generated a higher closed-circuit current and open-circuit voltage than the non-templated film, although the reasons for this were not entirely clear. Also, the role of the surfactant, beyond simply aiding in organization, is not clear. However, the surfactant used in templating the semiconductor is of special interest (Fig. 8), given the phase stability required to retain the nanoscale features and orientation of the replica. While oligo(ethylene oxide)-based surfactants undergo

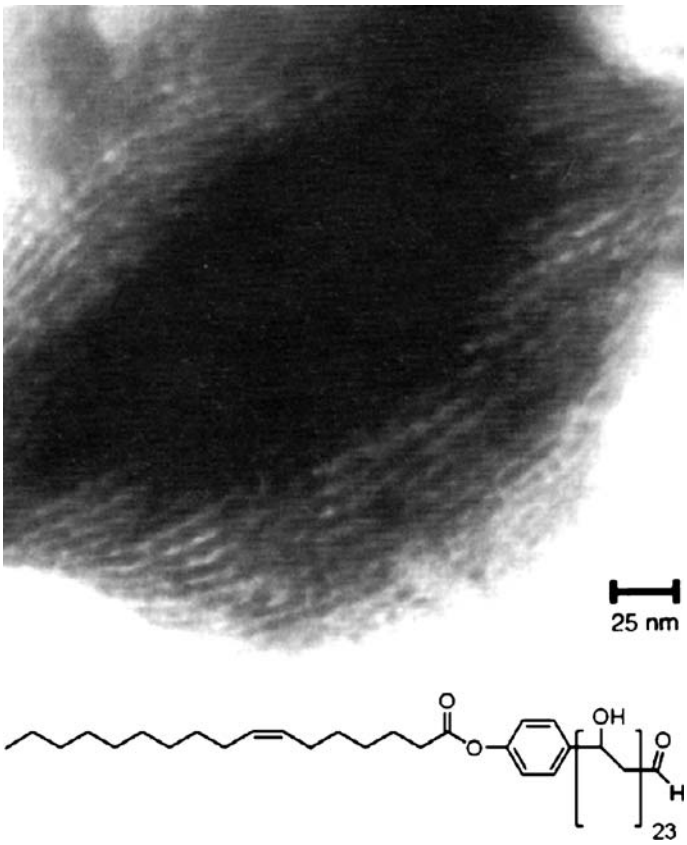

Fig. 6 TEM image showing the nanocomposite L phase of a polyol amphiphile (*inset*) and CdS precipitated by diffusion H_2S into the LLC doped with Cd^{2+} ions. Partially reproduced with permission from [36]. © 1996 by Wiley-VCH

an isotropic phase transition at ~ 60 °C, the hexagonal phase formed by this hydrogen-bonded oligo(vinyl alcohol) is stable up to the boiling point of water. As a result, surfactants of this type are likely broadly applicable as templating agents.

In some cases, it can be useful to leave the LLC phase template incorporated into the lattice. Often, the resulting organic/inorganic nanocomposite materials can have properties that neither the template nor the inorganic lattice have separately. For example, the incorporation of organic molecules into an inorganic lattice can strengthen an otherwise fragile material, increase thermal stability, enhance the separation or catalytic properties, or be used to tune the electronic properties [38]. From this standpoint, the technique is used not only to pattern, but also to anchor organic molecules in inorganic materials for improved functionality.

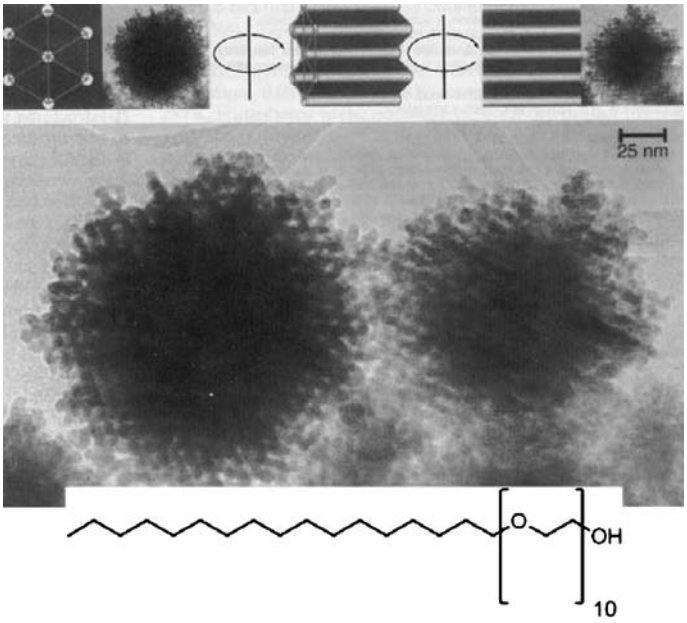

Fig. 7 TEM image showing the CdS replica of the H_I phase of an oligo(ethylene oxide) oleyl ether amphiphile (*inset*). Reproduced with permission from [34]. © 1996 by the Nature Publishing Group

The possibility of enhancing the properties of the composites by functionalizing the organic component has been proposed, but to our knowledge this has yet to be realized [43]. In our opinion, this is an important area for future work, given the promise of enhanced functionality and materials properties that they hold.

2.2 Templated Nanowire Synthesis

In addition to porous nanostructures and nanocomposites, nanowires can also be formed by templating with LLCs [49–51]. As opposed to H_I phases, which compartmentalize the LLCs into the "channels", these nanowires are generally formed from H_{II} phases. Here, the metal ions are confined to the channels, and the confinement can be preserved when electrodeposition takes place. As an example, the surfactant, sodium bis(2-ethylhexyl)sulfosuccinate (AOT), which forms a H_{II} mesophase, has been used to template Ag^+ ions which were electrodeposited to form Ag nanowires tens of nanometers long and 20–30 nm in diameter (Fig. 9). Interestingly, the wires also had orientational order, being organized perpendicular to the cathode surface. This suggests that the high electric field during electrodeposition may enhance

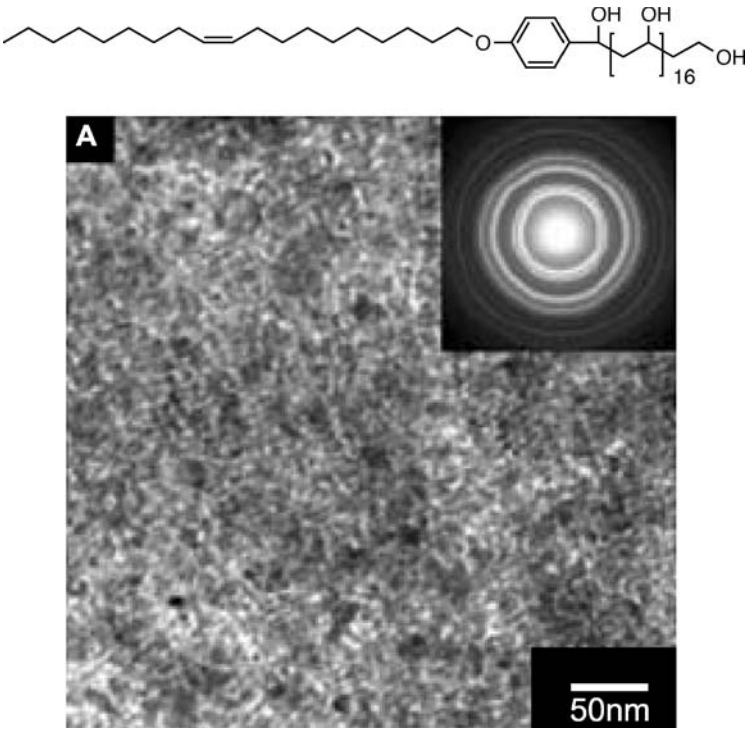

Fig. 8 Oligo(vinyl alcohol)-based surfactant (*top*) used in templating CdTe semiconducting films (TEM, *bottom*) by electrodeposition from an H_I LLC phase. Reproduced with permission from [48]. © 2005 by Wiley-VCH

the alignment of the LLC template. In the absence of AOT, only micrometer-sized Ag particles were observed. Similarly, AOT in the reverse hexagonal phase was used to template Cu^{2+} ions from which Cu_2O nanowires were electrodeposited [51]. In both cases, there is some question as to the templating mechanism, since the rods are larger than the aqueous domains formed by the LLC phase.

2.3 Templated Nanoparticle Synthesis

Similarly, LLCs can aid in the control of nanoparticle synthesis. The majority of this literature involves dilute, microemulsion surfactant conditions (see review, [52]). However, there are still numerous examples of these particles synthesized in the condensed phases of LLCs. When LLCs are employed, analogous to the formation of metal nanowires and lattices, the inorganic precursors (e.g., M^{n+} ions) are reduced and solidified. The LLC network provides nano-confinement and nano-control over the diffusion of ions. There are two

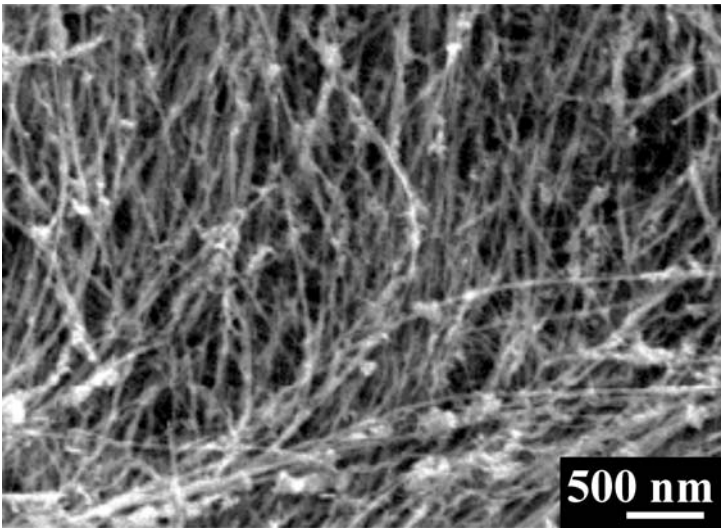

Fig. 9 TEM image of Ag nanowires electrodeposited from the H_{II} mesophase of AOT. Reproduced with permission from [50]. © 2002 by Wiley-VCH

general methods used to synthesize nanoparticles: using intrinsic or extrinsic reducing agents [53–57].

Using intrinsic reducing agents, where the LLC has the reactant incorporated into its structure, Pd and Ag nanoparticles have been synthesized in Q and L phases, respectively [53, 54]. When the Q phase was employed, Pd nanoparticles that matched the diameter of the aqueous domains were produced. Increasing the water content (i.e., swelling the LLC phase) produced correspondingly larger particles.

Extrinsic reducing agents (e.g., H_2, H_2S) have been diffused into the LLC matrix with similar results [55–57]. Pd nanoparticle/polymer composites have been synthesized by diffusing H_2 gas into an initial cross-linked H_{II} phase with Pd^{2+} in the water channels [55]. The Q_{II} phase of AOT containing $Pb(NO_3)_2$ was used to synthesize semiconducting PbS nanoparticles of very narrow size distribution by three-dimensional diffusion of Na_2S [56]. An oligo(ethylene oxide) oleyl ether amphiphile capable of forming H_I, L, and H_{II} mesophases was used to synthesize Bi and PbS nanoparticles. The size of the nanoparticles had a clear dependence on the morphology of the LLC phase, showing the trend: $H_I > L > H_{II}$ [57].

2.4 Templated Polymerization

While the templating of inorganic materials in LLC mesophases has been very successful, replicating the template by polymerizing organic monomers

within these phases presents some additional challenges. These difficulties revolve around preserving the order of the surfactant molecules during polymerization. The enthalpic penalties associated with the polymer trying to stay solvated within the surfactant, and the entropic penalties due to loss of conformational freedom within the confinement of the mesophase most often result in phase separation [58]. In these cases the replica (polymer) does not copy the template (LLC phase) perfectly, but interestingly the replica often still possesses a degree of order [59–64]. Instead of nanometer-sized features, however, they are often orders of magnitude larger. In one example, AOT is used to form the H_{II} and L phases [61]. Polymerization of styrene and divinylbenzene is carried out in the hydrophobic domains. In the case of the H_{II} phase, strings of polymer beads ~ 100 nm in diameter resulted after the re-

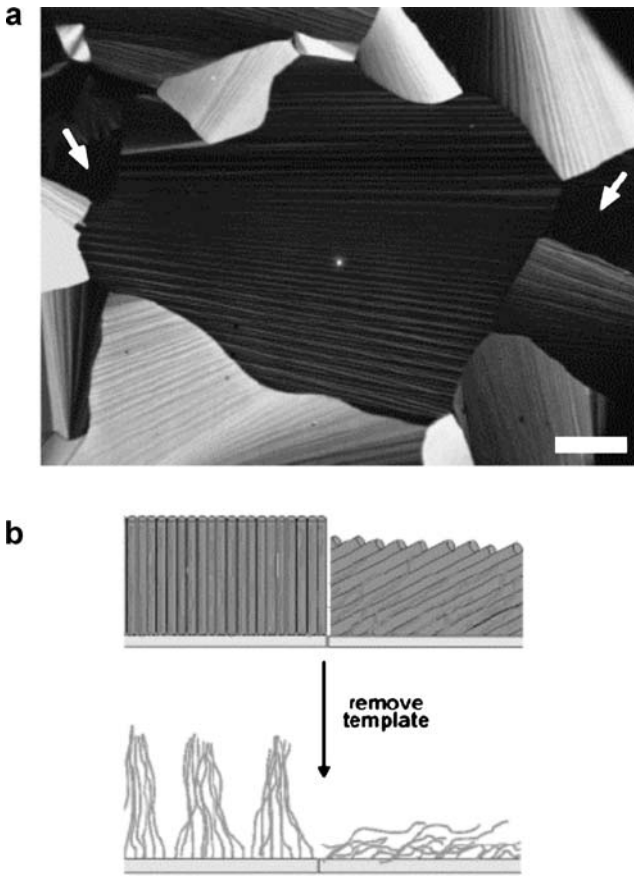

Fig. 10 **a** PLM image of thiophene conducting polymer after template is removed (scale bar = 100 μm). **b** Methodology for creating polymer "molecular wires". Reproduced with permission from [69]. © 2003 by Wiley-VCH

moval of the template. Polymerization in the L phase yielded beads with no long-range order. Even when the LLC template is not preserved, it still has an influence on the polymer replica.

In exceptional cases, the order of the LLC phase is reported to be templated directly during polymerization [62, 63]. When the L, H_{II}, and Q phases of AOT are mixed with acrylamide and methylenebis(acrylamide), the resulting polymer composite had nearly identical order. However, the order (and lattice shrinkage) shown by XRD could have been due to only the LLC component of mixture, since the polymer was characterized with the template remaining. Also, the robustness of the replica was questionable, since once it was washed in acetone, it dissolved readily in water [62]. Similarly, cetyltrimethylammonium bromide (CTAB) can be used to form L and H mesophases which dissolve a mixture of phenol and aqueous formaldehyde in the hydrophilic regions. After polymerization, XRD measurements showed an increase in disorder. However, TEM images showed that while some long-range order was lost, the H and L phases (disordered) were still preserved as long as the template was not removed. Most importantly, the scale of the features was nearly identical to what a perfect replica should be. Unfortunately, the replica lost the nanostructure upon removal of the template [63].

An interesting application of templated growth of polymers, is in using LLC phases to control the ordering of conducting polymers [64–69]. A problem in conducting polymer synthesis is that with some conducting polymers, disorder decreases the bulk conductivity. Using an H_{II} phase to template the growth of "nanowires" has been demonstrated by several groups [64–69]. A recent example involves using the hexagonal phase of a poly(oxyethylene)-alkyl mixed with a thiophene monomer and supporting electrolyte [69]. The thiophene monomer segregates to the hydrophobic domains of the liquid crystal, where it can then be electropolymerized. The template can be removed to yield a replica that closely matches its structure (Fig. 10).

2.5 Carbon Nanotube Disaggregation and Alignment

It has recently been reported that surfactant molecules can associate with carbon nanotubes (CNTs) to form supramolecular assemblies [70, 71]. In the two models that have been proposed, the hydrophobic portion of the surfactants associate with the nanotube to form either a uniformly covered cylindrical supermolecule, or a "beads-on-a-string" assembly of disks encapsulating the nanotube (Fig. 11). As such, amphiphiles are frequently used in the disaggregation of CNTs into discreet nanotubes in aqueous solution [72].

When concentrated surfactants are used, single-wall carbon nanotubes (SWNTs) are thought to be partitioned into the hydrophobic domains. Thus, in lyotropic mesophases, the possibility of dispersion *combined with* alignment exists [73, 74]. In this effort, the H_I phase of Triton X-100 has been used

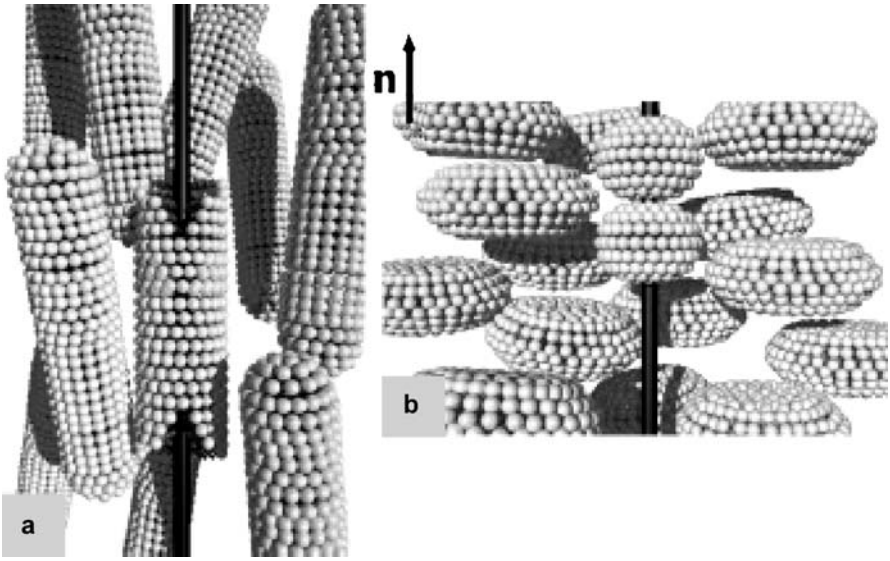

Fig. 11 Two proposed models for the supramolecular assembly of surfactants with CNTs: **a** cylindrical assembly, and **b** beads-on-a-string assembly. Reproduced with permission from [74]. © 2007 by Wiley-VCH

to disperse SWNTs. These nanotubes are believed to line up in the hydrophobic channels [73]. This was supported by a change in macroscopic properties (viscosity), as well as X-ray diffraction (XRD) measurements (d-spacing increase with addition of SWNTs). Therefore, the LLC matrix seems to impose a certain degree of alignment upon the SWNTs along the director. Another example involves the lyotropic nematic phase of SDS, which was used to disperse SWNTs (Fig. 11). In this case, alignment along the director was achieved by application of a magnetic field, and unambiguously proved by Raman spectroscopy [74]. Given the unique materials properties that CNTs possess (e.g. tensile strength, thermal and electrical conductivity), these ordered, composite materials hold great promise in expanding the function of LLCs.

3 LLC-based Conducting Materials

LLC systems have also recently been investigated as conductive materials. LLC research in this area addresses the growing need for new ion-conductive [75], proton-conductive [76], and electrically conductive materials [77] for generating and storing energy to help offset fossil fuel consumption for energy production. As alternative sources of energy and method for storing energy

are scrutinized for potential replacement of fossil fuels, new conductive materials have come to the forefront of this research area.

Solid-state materials with high conductivity for ions such as Li^+ are essential for the development of more efficient Li ion batteries with higher energy densities. The solid electrolytes [e.g., poly(ethylene oxide), (PEO)] that transport Li^+ in the current generation of Li batteries arguably play the most crucial role in dictating overall battery performance. In a similar vane, materials with high proton conductivity are essential for the development of high efficiency fuel cells for electrical power generation [76]. Additionally, the development of more efficient electrical storage devices with higher energy density, lower overall mass, and higher amperage output is the current focus of ion-conductive materials research [75]. Furthermore, the miniaturization of electronic devices to smaller and smaller dimensions requires specialized electrically conductive materials to meet new high performance requirements.

Nanostructured LLC systems offer potential advantages over conventional non-ordered, ion-conducting materials such as amorphous non-charged PEO polymers, and non-coordinating charged polymers such as Nafion. LLC systems made from surfactant molecules containing the same types of ion-transporting units, as found in PEO and Nafion, have uniform nanoscale domains that run through the bulk materials which can be interconnected or continuous in 1, 2, or 3 dimensions depending on the LLC phase. This unique feature of LLC phases can potentially afford superior transport of ions and better bulk ionic conductivity, compared to amorphous polymers, so long as the solvent, used in LLC formation, is conducive to good ion transport and stability. Similarly, if the ordered LLC domains contain electrically conducting materials such as metals, semiconductors, or conjugated polymers, then new composite materials, with anisotropic and perhaps enhanced bulk electrical conductivity may be obtained. Functional LLC systems have already made an impact in the design of new ion- and electrically conductive organic materials.

3.1
LLC Phases as Ion Conductors

Although a substantial number of functionalized thermotropic LC systems have been designed and investigated as anisotropic ion-conducting materials [18, 19, 21, 78–80], interest in solvent-based LLC systems as ion conductors has only recently emerged. The bulk of the research into the ionic conductivity of LLC materials has only been investigated within the last decade. Somewhat unique approaches to testing the bulk conductivity of these materials are required due to the concentration dependent ordering of the LLC systems as well as the solvent(s) utilized (water, methanol, etc.) in phase formation. Methods have recently been developed to measure the ionic conductivity of these materials in their respective LLC phases.

Utilizing these methods, the ionic conductivity of a number of aqueous LLC systems based on commercially available amphiphiles has been measured. For example, the "inverse" L phase of the sodium dodecylsulfate/pentanol/water system has been studied under shear conditions and found to exhibit anisotropic conductivity, resulting in a material with a conductivity range of approximately 1 to 2.5×10^{-3} S cm^{-1} [81]. The ionic conductivities of the L and micellar phases of the potassium laurate/decanol/D_2O system [82], and the lithium triflate-loaded regular H_I phase of an oligo(EO) surfactant-templated silicate nanocomposite have also been measured [83] resulting in conductivities that range from 3 to 6×10^{-2} S cm^{-1} and 10^{-4} to 10^{-7} S cm^{-1}, respectively. It has also been determined that the ionic conductivity of an L phase is dependent on its thickness [82, 84].

Recently, non-water-based LLC materials have taken the forefront of LLC-based ion conducting materials. Instead of using water as the polar solvent to form ordered LLC phases, room-temperature ionic liquids (RTILs) have emerged as the solvent of choice for improved composition stability in forming LLC assemblies (i.e., no evaporative solvent loss), and also for improving ion conductivity in the LLC polar domains. RTILs are polar, molten organic salts under ambient conditions that are typically based on substituted imidazolium, phosphonium, ammonium, and related organic cations, which are complemented by a relatively non-basic and non-nucleophilic large anion [85]. RTILs possess negligible vapor pressures; and as such, offer a new non-volatile solvent medium for organization of LLCs. As RTILs are very different from solvents like water, fundamental work has been concerned with understanding how small-molecule surfactants organize around and in RTILs [86, 87]. A number of RTIL-based LLC systems have already been specifically designed to serve as anisotropic, ion-conducting nanocomposite materials. For example,

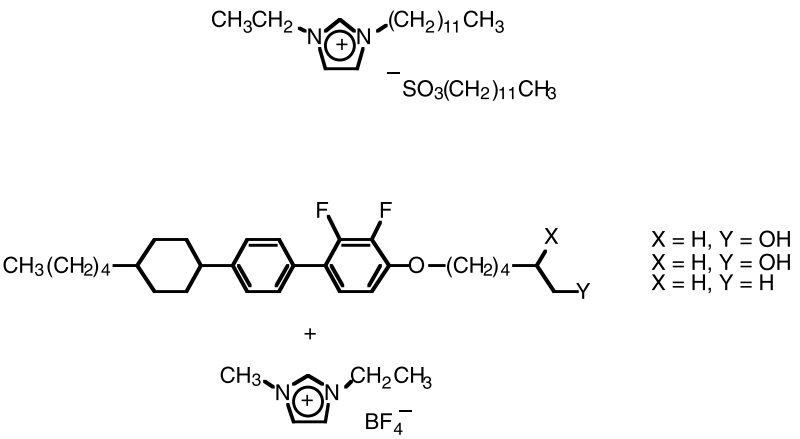

Fig. 12 Examples of ion-conductive LLC systems that form L phases with imidazolium-based RTILs as the polar liquid phase [89, 90]

L phase materials formed by combining a conventional RTIL with an amphiphilic LC mesogen has been found to have ca. three orders of magnitude higher ionic conductivity parallel vs. perpendicular to the lamellae [88]. Similar anisotropic ion conductivity results have also been obtained with L phases of imidazolium-based amphiphiles and also hydroxyl-terminated fluorinated surfactants formed by mixing with imidazolium-based RTILs (Fig. 12) [89, 90].

3.2 Electrically Conducting LLC Materials

LLC systems incorporating materials that conduct electrons instead of salt ions or protons have been investigated for electrically conducting materials. As described previously in Sect. 2 of this review, LLC phases in non-polymerized and polymerized form have been used as nanostructured organic templates to define the growth of electrically conducting materials such as metals, semiconductors, and conducting organic polymers in the hydrophilic domains [40–51, 64–69]. This approach affords both structural replicas and LLC nanocomposites containing electrically conductive nanowires and nanoparticles as functional fillers. However, although functional properties such as optical and catalytic properties have been measured for these materials, the bulk electrical conductivity of only a few of these materials has been measured.

In addition to templated electrical conductor formation, LLCs have been used in another way to make nanostructured electrically conductive materials. Several acidic surfactant molecules have been used to dope, encapsulate, and order the conducting polymer, polyaniline, to form nanostructured LLC-conducting polymer nanocomposites. Recently, a bicontinuous cubic phase was utilized as a templated scaffolding for the in situ polymerization of an acidified, monomeric solution of aniline [91]. The cubic phase was comprised of 55% surfactant of $(EO)_{10}$ nonyl phenol ether, 22% octane, and 23% of aqueous solution with monomer and initiator. The material was successfully polymerized and formed the emeraldine salt, although no conductivity testing was completed. Furthermore, materials such as dodecylbenzenesulfonic acid (DBSA) [92, 93], 1,2-benzenedicarboxylic acid, 4-sulfo, 1,2-di(2-ethylhexyl)ester [94], *n*-octyl- and *n*-hexyl phosphonic acid [95], 3-pentadecylphenylphophonic acid [96], and 3,4,5-tris(dodecyloxy)phenylmethylphosphonic acid [97] have all been used to protonate polyaniline into its electrically conducting form and simultaneously generate L phases via the resulting LLC-polyaniline salt complexes (Fig. 13). In these systems, only DBSA and 3,4,5-tris(dodecyloxy)phenylmethylphosphonic acid have intrinsic LLC properties on their own. The rest of the systems could only form LLC phases after salt formation with polyaniline. The measured bulk electrical conductivities of these LLC-polyaniline complexes were found to range from 10^{1} S cm^{-1} for the DBSA complexes to ca. 10^{-5} S cm^{-1} for the 3,4,5-tris(dodecyloxy)phenylmethylphosphonic acid complex.

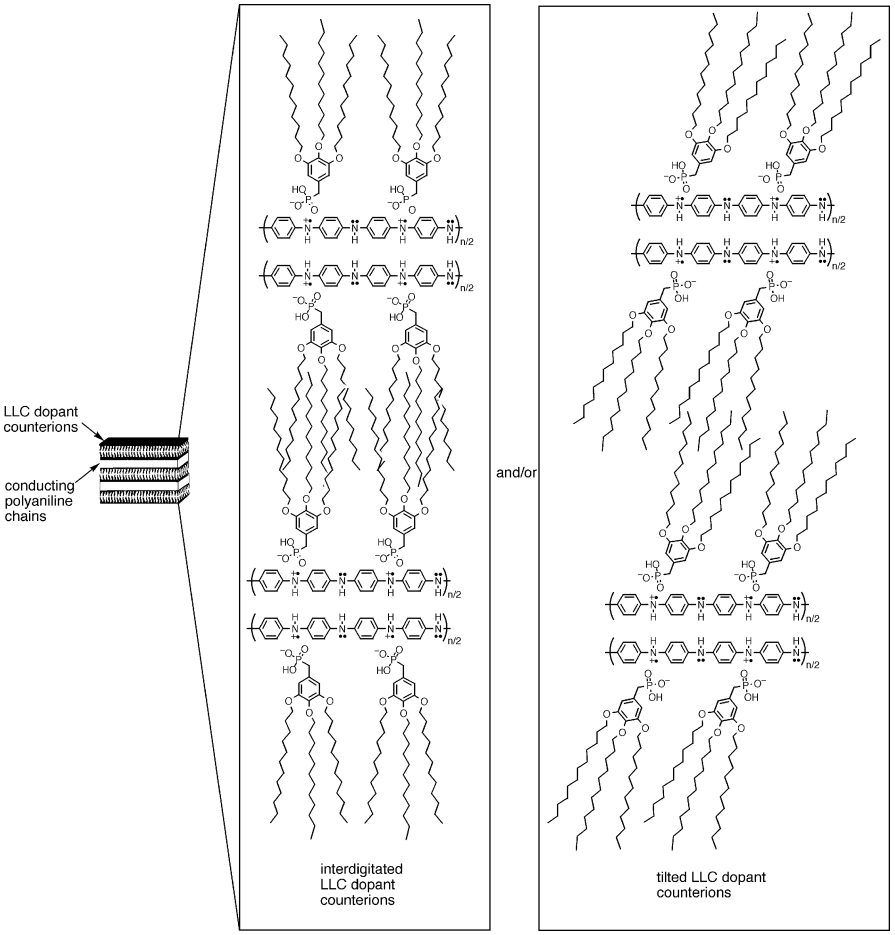

Fig. 13 Example of an electrically conducting LLC acid-doped polyaniline salt complex that forms an L phase. Reproduced with permission from [97]. © 2002 by Taylor and Francis

4 LLC Materials for Catalysis

In addition to forming functional nanocomposites and optical materials, LLC systems also have value in the area of catalysis. LLC phases have a number of features that make them amenable for accelerating chemical reaction rates. For example, LLC phases have regular nanometer-scale water- or polar solvent-filled cavities and hydrophobic domains of uniform size that are close in size to typical small molecule substrates. These domains can afford confined environments to encapsulate reactants and catalytic entities, thereby increasing their local concentration and the probability of productive colli-

sions. In addition, the hydrophilic polar headgroups of the LLC mesogens are localized exclusively and densely in the walls of LLC cavities via the amphiphilic self-assembly process. This arrangement can lead to electrostatic, hydrophobic, electrophilic, and/or nucleophilic interactions that can cause a change in free energy activation for the overall process and affect reaction rate. This is similar to what is believed to occur during catalysis in micelle systems [98–100]. The open domains in LLC phases may impose dimensional constraints that allow reactants with certain sizes or shapes to enter more easily than others, or favor the formation of certain transition state configurations over others, to give rise to enhanced reaction selectivity. These effects would be similar to how inorganic zeolites and molecular sieves operate as selective heterogeneous catalysts [101]. If the hydrophilic headgroups in the LLC pore domains were made to be catalytically active, the resulting LLC phases could afford a much higher local density of catalytic groups in the pores for reactions to occur than is typically possible in normal solution or heterogeneous catalysis environments.

The past 10–15 years have seen major advances in the development and realization of LLC materials for catalytic applications. These advances range from the use of non-catalytically functionalized LLC phases as a means of accelerating reactions via confinement, to the design of polymerized LLC materials containing discrete catalytic groups that act like organic analogues to catalytic molecular sieves.

4.1 LLC Phases as Reaction Media

The earliest examples demonstrating the promise of LLC materials for accelerating chemical reactions involved the use of LLC phases of commercially available ionic or non-charged surfactants in water as nanoscale reaction media. In these systems, the surfactants and resulting LLC phases were not functionalized with any catalytic or reactive groups. All the reactants and catalytic entities were from external sources and solubilized in the LLC domains during reaction. Consequently, the rate acceleration effects observed in these systems can be attributed to the same types of confinement, solubilization, and electronic interactions found in micellar catalysis systems [98–100].

4.1.1 Catalysis of Small Molecule Transformations

One of the first examples of catalysis inside non-functionalized LLC phases involved the type I LLC phases of the cationic surfactant, cetyl trimethylammonium bromide (CTAB), and its longer analogs [102]. These LLC phases were able to accelerate the deprotonation of (*p*-nitrophenoxy)propiophenone by *n*-decyl-N(O^-)-Bz acting as a base. The rate of this base-catalyzed reac-

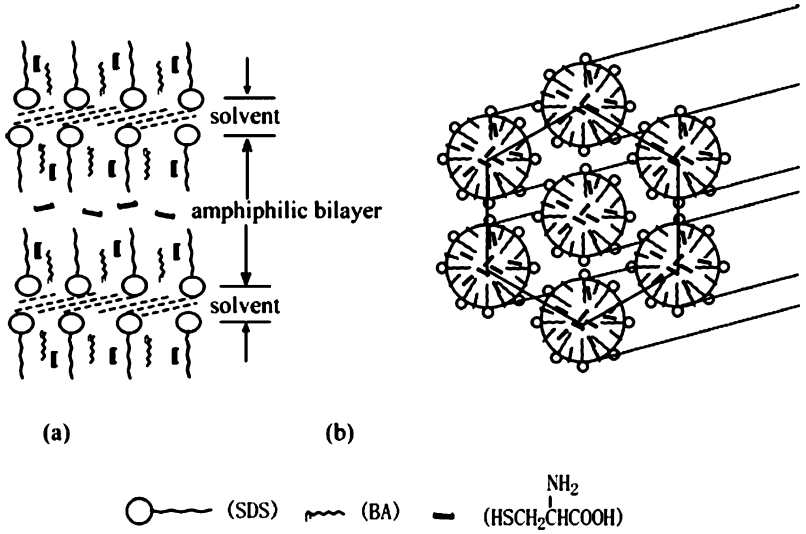

Fig. 14 Location of L-cysteine during electrochemical oxidation in the LLC phases of the dodecylsulfate/benzyl alcohol/water (SDS/BA/H_2O) system: **a** L phase and **b** H_I phase. Reproduced with permission from [106]. © 2004 by Springer

tion was enhanced 100–4000-fold in the hydrophobic domains of the LLC phases compared to that in solution [101]. Similarly, the lyotropic nematic and H_I phases of myrystyltrimethylammonium bromide in 1-decanol, ammonium bromide, and water have been found to be able to increase the rate of *o*-iodosobenzoic acid-catalyzed hydrolysis of two organophosphinate esters by a factor of over 100 compared to a simple micelle system [103, 104]. Similarly, the micellar and L phases of commercial *n*-decylammonium chloride in *n*-decylamine and water were found to accelerate the dealkylation of *p*-nitrophenyl dimethyl thiophosphate, with the L phase having a much more pronounced effect than the micellar phase [105]. More recently, the L and H_I phases of the ternary sodium dodecylsulfate/benzyl alcohol/water system have been found to increase the rate of electrochemical oxidation of L-cysteine, with increasing benzyl alcohol content in the LLC system causing the largest increase in reaction rate (Fig. 14) [106].

4.1.2 Biocatalysis

LLC phases as reaction media have also been explored for biocatalysis. The LLC phases of commercial surfactants have been used to successfully stabilize enzymes and cofactors for reaction in non-aqueous solvent environments. In addition to significant stabilization of the enzyme biocatalyst in the biphasic LLC system, product recovery has also been found to be facilitated [107].

Examples of LLC phases for enzyme stabilization and biocatalysis include the micellar and LLC phases water (or glucose in water)/octanol/octyl-β-D-glucoside LLC system for accelerating β-D-glucosidase-catalyzed hydrolysis of octyl-β-D-glucoside to form glucose and octanol [108]; and the use of LLC phases of numerous commercial surfactants to accelerate the (*S*)-hydroxynitrile lyase-catalyzed synthesis of (*S*)-mandelonitrile [109].

4.1.3
Catalysis of Polymerization Reactions

In addition to catalysis of small molecule transformations and biocatalysis, non-functionalized LLC phases used as reaction media have also been found to accelerate polymerization reactions as well. For example, the L and H_I phases of the sodium dodecylsulfate/*n*-pentanol/sulfuric acid system have been found to lower the electric potential needed to electropolymerize aniline to form the conducting polymer, polyaniline [110]. In this system, it was also found that the catalytic efficiency of the L phase was superior to that of the H_I phase. In addition to this work, the I_I, H_I, Q_I, and L phases of non-charged Brij surfactants (i.e., oligo(ethylene oxide)-alkyl ether surfactants) have been observed to accelerate the rate of photo-initiated radical polymerization of acrylate monomers dissolved in the hydrophobic domains [111, 112]. The extent of polymerization rate acceleration was found to depend on the geometry of the LLC phase in these systems. Collectively, this body of work on catalysis with *non-functionalized* LLC phases indicates that LLC phase geometry and system composition have a large influence on reaction rate.

4.2
Cross-linked LLC Phases as Heterogeneous Catalysts

Cross-linked or polymerized LLC phases containing catalytic headgroups have recently been explored as robust, heterogeneous catalyst systems. By chemically cross-linking these *functionalized* LLC systems, rigid, solid-state, nanoporous materials containing a high local density of catalytic groups in the LLC pores are produced. These LLC networks can be considered organic "analogues" to inorganic molecular and mesoporous sieve catalysts [113].

The first example of a catalytic LLC polymer network involved the cross-linked H_{II} phase of a styrene-substituted sodium carboxylate LLC monomer and added divinylbenzene cross-linker (Fig. 15).

This material was able to act as a solid Brønsted base catalyst and accelerated the Knoevenagel condensation of ethyl cyanoacetate with benzaldehyde better than basic forms of mesoporous sieves and zeolite catalysts. It was found that this carboxylate-functionalized LLC material exhibited enhanced basicity due to the ordered nanostructure, and that the LLC pores were capable of substrate molecular size exclusion [114].

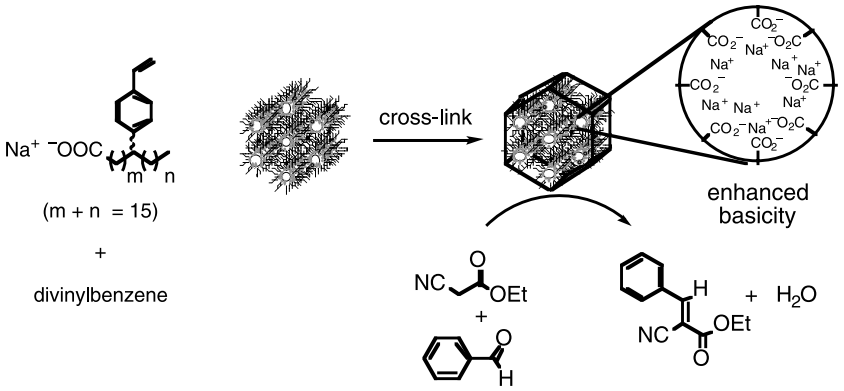

Fig. 15 Heterogeneous Brønsted base catalysis of the Knoevenagel condensation of ethyl cyanoacetate with benzaldehyde using a cross-linked H_{II} assembly

LLC networks containing catalytic headgroups have also been shown to be useful for heterogeneous Lewis acid catalysis. The Sc(III)-exchanged cross-linked H_{II} phase of a taper-shaped sulfonate-functionalized LLC monomer has been shown to be able to catalyze the Mukaiyama aldol and Mannich reactions [115] with enhanced diastereoselectivity. This Sc(III)-functionalized H_{II} network affords condensation products with syn-to-anti diastereoselectivity ratios of 2-to-1, whereas Sc(III) catalysts in solution or supported on amorphous polymers show no reaction diastereoselectivity at all.

More recently, cross-linked LLC phases containing strong Brønsted acid groups have been shown to catalyze heterogeneous esterification reactions with higher product selectivity than non-ordered acid resins containing the same catalytic acid groups. The cross-linked H_{II} phase of a 5 : 1 (mol/mol) blend of a sulfonic acid-functionalized LLC monomer and an L-analine-functionalized LLC monomer was found to catalyze the esterification of 1-hexanoic acid and benzyl alcohol with higher product selectivity than commercial, non-ordered sulfonic acid resin catalysts (e.g., Amberlyst, Nafion) under the same conditions (Fig. 16) [116].

This LLC acid resin displayed more than an order of magnitude higher selectivity for the desired ester product over dibenzyl ether side-product compared to amorphous Amberlyst-15, Nafion NR-50, and also an isotropic analog of the LLC acid resin. Control experiments revealed that a large component of the enhanced selectivity is due to the regular nanostructure present in the LLC acid resin, which is believed to afford a much more uniform local acid microenvironment for reactions to occur. This same LLC acid resin was subsequently found to catalyze the synthesis of dioctyl phthalate (DOP) from phthalic anhydride and 2-ethyl-1-hexanol in toluene with a slightly higher overall yield of DOP than amorphous Amberlyst-15 [117]. Experiments revealed that the LLC acid resin is a much better catalyst for the

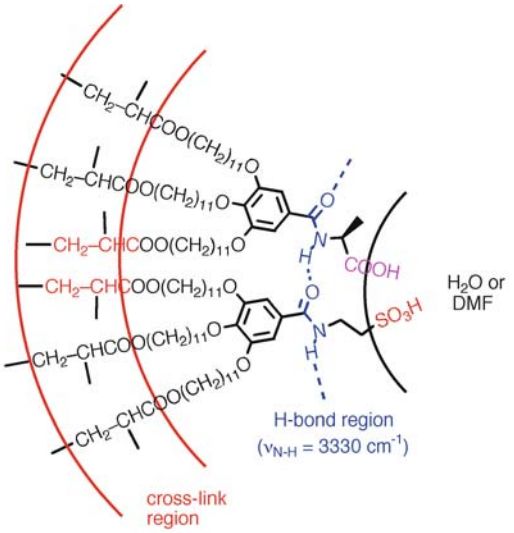

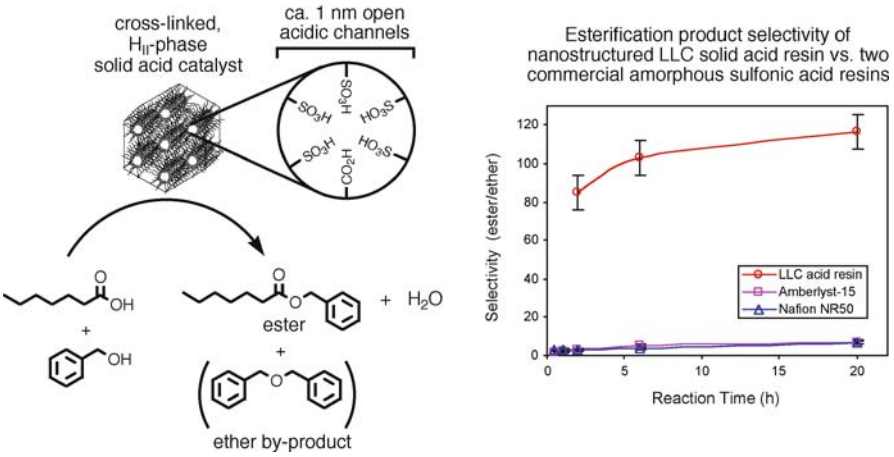

Fig. 16 Heterogeneous catalysis of the esterification of benzyl alcohol with 1-hexanoic acid using a cross-linked H_{II}-phase sulfonic acid resin formed by amide H-bond-assisted LLC phase formation

formation of DOP from the mono-octyl phthalate (MOP) reaction intermediate than Amberlyst-15, resulting in a ca. 38% increase in the initial rate of DOP production from MOP [117].

One of the unique chemical aspects of this LLC acid catalyst work is the use of an LLC structure-directing agent (the L-analine-functionalized LLC monomer) to induce H_{II}-phase formation of the sulfonic acid-functionalized

LLC monomer via complementary shape-packing and amide H-bonding near the pore interface (Fig. 16). The sulfonic acid monomer is only able to form a mixture of L and H_{II} phases on its own because the sulfonic acid headgroup is not conducive to good H_{II}-phase formation [118]. This LLC blending/H-bond templating approach may be a general method for inducing highly functionalized LLC mesogens that do not exhibit good LLC behavior, into well-defined LLC phases [119].

Enantioselective catalysis with cross-linked LLC materials has also recently been demonstrated. The crossed-linked H_{II} phase of a taper-shaped LLC monomer containing a chiral imidazolinone headgroup has been shown

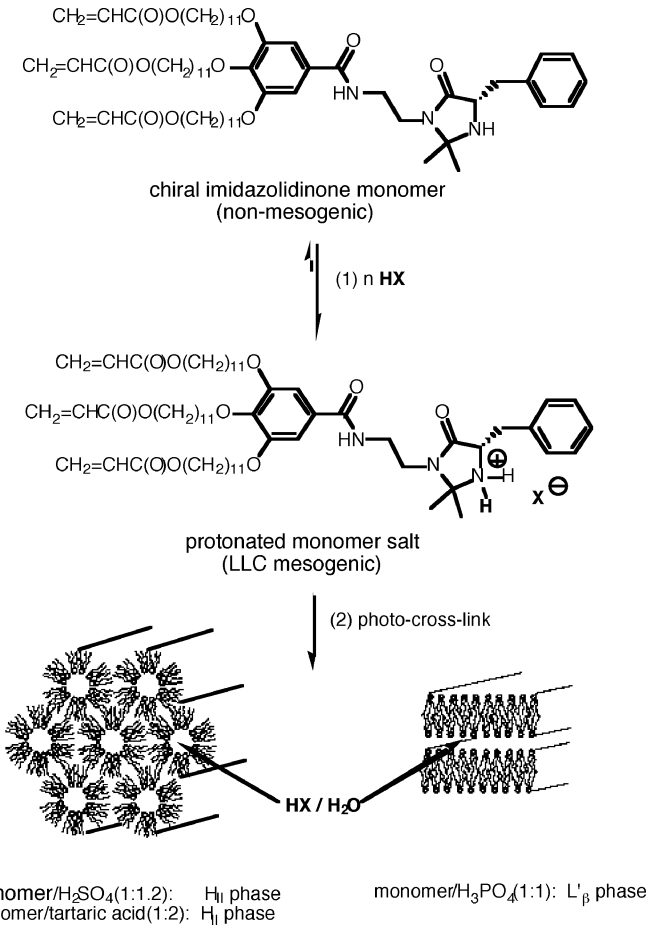

Fig. 17 Brønsted acid-induced LLC phase formation of a chiral imidazolinone monomer as means of generating nanoporous, solid-state, chiral Diels–Alder catalysts. Partially reproduced with permission from [120]. © 2005 by the American Chemical Society

to catalyze the enantioselective Diels–Alder reaction of cyclopentadiene and crotonaldehyde (Fig. 17), with ee and de values identical to those of the parent chiral imiazolinone catalyst in solution [120]. In this system, the initial chiral imidazolinone monomer did not display any LLC properties; but upon protonation to the active catalyst salt form, different LLC phases were obtained depending on the nature and amount of acid used. Transient salt formation via protonation with Brønsted acids may be another general method for inducing highly functionalized monomers with weak or no mesogenic properties in their pristine state, to form well-defined LLC phases [119].

5
LLC-based Drug Delivery Systems

The use of delivery systems for the sustained release of drugs at optimum therapeutic ranges is extremely important not only for maintaining drug efficacy, but also for reducing the number of applications or injections needed for therapy [121]. Matrices for drug delivery for intravenous, oral, or dermal application must meet certain criteria, such as non-toxicity, compatibility with the drug to be delivered, good chemical stability under physiological conditions, and eventual biodegradability/excretion from the body [122]. A number of hydrophilic polymer systems and surfactant systems that form vesicles and micelles meet these above criteria, and have been employed as drug delivery vehicles [123, 124].

Over the last two decades, it has been recognized in the drug delivery community that water-based LLC phases can also be used as viable matrices for the sustained and controlled release of drugs. The fact that many LLC phases have periodic nanometer-scale pores allows for a high and uniform loading of drugs, as well as good controlled diffusion out of the pores [121]. In addition, the ability of unpolymerized LLC assemblies to be dispersed by eventual or purposely triggered changes in solvent concentration or temperature, allows for easy removal of the delivery matrix at a desired point in time after its job has been accomplished. For the most part, only certain LLC phases containing open water channels or pores (i.e., the L and inverted (type II) LLC phases) have been explored for drug delivery because most drugs are hydrophilic or water-soluble molecules [121]. As such, LLC phases containing water compartments are required for initially encapsulating these drugs and then performing controlled and sustained release.

Only a few surfactant systems and their derivatives have been explored as LLC-based drug delivery systems because of the chemical and physiological compatibility requirements listed above, and because of cost and availability issues. These LLCs include commercially available non-ionic surfactants such as esters of oleic acid and related fatty acids [e.g., glyceryl monooleate (GMO) (aka, monoolein)], and oligo(ethylene oxide)-alkyl ether surfactants (e.g.,

Brij surfactants) (Fig. 18). Additionally, LLC phases of commercially available ionic surfactants such as metal salts of alkylsulfonic and alkylcarboxylic acids [e.g., dioctyl sodium sulfosuccinate (aka, Aerosol OT)] and long-chain ammonium salts have also been explored (Fig. 19). Some of these surfactants are even U.S. Food and Drug Administration (FDA)-approved because of their prior utility in other food or medication-related formulations.

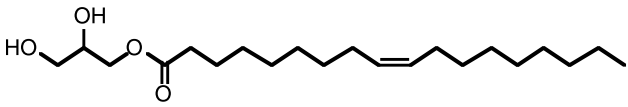

Glyceryl monooleate (GMO) (aka, monoolein)

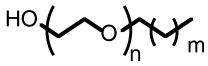

Oligo(ethylene oxide)-alkyl ether surfactants

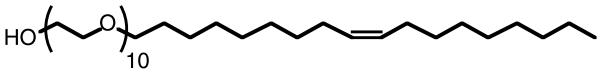

Brij-96: $(\text{ethylene oxide})_{10}$ oleyl ether surfactant

Fig. 18 Structures of some neutral LLCs commonly used for drug delivery

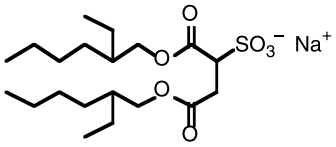

Aerosol OT (AOT)

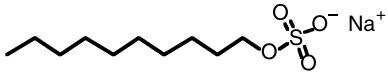

sodium decyl sulfate

potassium laurate

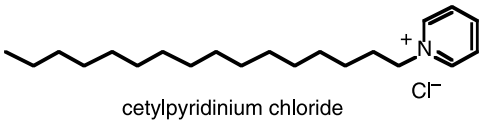

cetylpyridinium chloride

decylammonium chloride

Fig. 19 Structures of some ionic LLCs used for drug delivery

The earliest reports describing the use of LLC phases as matrices for drug delivery appeared in ca. 1988 [125, 126]. These initial reports focused on exploring the basic concept and viability of using LLC phases for controlled release of drugs. Since that time, work in the field can be categorized according to the type of LLC molecule or type of LLC matrix formulation used for drug delivery studies.

5.1 Drug Delivery Using LLC Phases Based on GMO

The bulk of the work in the LLC-based drug delivery area over the last 15 years has been focused on exploring the LLC phases formed from GMO (aka, monoolein) (Fig. 18) in water [127–129]. GMO is an FDA-approved food additive that is known to form sequential L, Q_{II}, and H_{II} LLC phases in the presence of water (Fig. 20) [130]. This system is also able to incorporate water-soluble molecules without disruption of the LLC phase microstructure. GMO or monoolein can be obtained commercially as a mixture of the glyceride esters of oleic and other fatty acids (consisting mainly of the monooleate) under the tradenames Myverol™ and Rylo™.

The release characteristics of the L, Q_{II}, and H_{II} LLC phases of GMO and water have been studied for the controlled release of large numbers of drug molecules. These drugs include common analgesics (aspirin [129, 130]); vitamins (vitamin E [133]); antiviral drugs (1-aminoadamantane hydrochloride [132], acyclovir [134]); anionic drugs (sodium diclofenac [133, 135]); met-

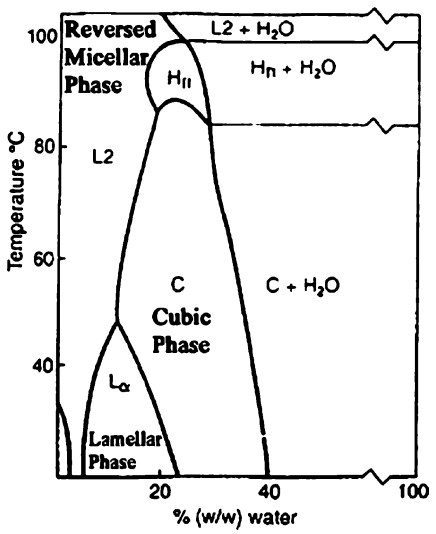

Fig. 20 Phase diagram of GMO in water. Reproduced with permission from [130]. © 2004 by Elsevier

alloenzymes (serratiopeptidase [136]); prodrugs for photodynamic therapy (5-aminolevulinic acid derivatives, meso-tetra(hydroxyphenyl)chlorin [137]); peptides ([D-Ala_2, D-Leu_5]enkephalin [138–141]); and even antimuscarinic drugs (propanetheline bromide and oxybutynin hydrochloride [142]). Other bioactive molecules such as nicotine [143], caffeine [12], salbutamol sulfate [143], chlorpheniramine, and diazapam [130] have also been studied as substrates for delivery from GMO-water LLC phases. The release conditions for these drugs have varied from oral ingestion to dermal application to in vitro cavity insertion. In addition to these drug molecules, the various water-based LLC phases of GMO have also been studied for the controlled release of a number of model hydrophobic and hydrophilic drugs, such as paclitaxel, irinotecan, glucose, histidine, octreotide [120], and furosemide [144].

In the area of GMO-based LLC phase drug delivery, there have been several innovative research directions of note: One new direction has been the incorporation of co-surfactants with molecular recognition units into the LLC matrices as a means of directing or targeting drug delivery to specific areas of the body [133]. Another new direction has been the use of hydrophobic inorganic additives such as magnesium trisilicate as a means of more quickly inducing GMO LLC phase formation and controlling pH microenvironment for the drug during delivery into gastric environments [136]. A third new direction has been the incorporation of amphiphilic permeation enhancers such as poly(ethylene glycol)s (i.e., PEGs) in combination with fatty acids [130, 141] or modified glycerol lipids [132] to aid in the transport and release of small-molecule drugs and large peptide drugs from LLC phases. Finally, new derivatives of oleic acid and other fatty acids with structures similar to GMO have recently been synthesized that show excellent promise for LLC phase-based drug release [122].

5.2 Drug Delivery Using LLC Phases Based on Oligo(ethylene oxide)-Alkyl Ether Surfactants

Drug delivery from LLC phases of oligo(ethylene oxide)-alkyl ether (i.e., $(EO)_n$-O-alkyl) surfactants have also been explored but to a much lesser extent than GMO. For example, the L, Q_{II}, and H_{II} phases of commercial Brij-96 surfactant (i.e., $(EO)_{10}$-O-oleyl) (Fig. 18) formed with water and other additives, have been explored for release of ephedrine hydrochloride, tenoxicam [145], and topical dermal delivery of benzocaine [146]. Work in this area has found that the amount of water swelling the hydrophilic domains of the LLC phase increases drug diffusion and release [145]. In addition to this work, the L phase of the $(EO)_{21}$-O-stearyl/oil/water system has been explored for dermal delivery of itraconazole [147]; and the L and H_I phases of the $(EO)_7$-O-$C_{13–15}$ (i.e., Symperonic A7)/water system have been explored for the release of the model drug chlorhexidine diacetate [148].

5.3
Drug Delivery Using LLC Phases Based on Ionic Surfactants

In contrast to the LLC phases of GMO and $(EO)_n$-O-alkyl surfactants, only a handful of reports on the study of LLC phases of ionic surfactants for drug delivery are available. For example, the L, Q_{II}, and H_{II} phases of the water/octanol/dioctyl sodium sulfosuccinate system have been studied for the transport of water and glucose across human skin [149]. Also, Q_{II} phases of mixed ionic and uncharged phospholipids in water have been explored for the sustained in vitro release of timolol maleate, a drug for treatment of glaucoma [150].

5.4
Drug Delivery via LLC Nanoparticles

There is also a large body of work in the LLC-based drug delivery area that is based on the use of specific preparation forms or formulations of LLC phases, rather than on a specific chemical type of surfactant molecule. That is, there has been a great deal of research into the use of LLC nanoparticles (LLCNPs). LLCNPs are dispersed submicron-sized particles of LLC phases suspended in a solvent, that allow for extremely convenient drug delivery applications upon dispersion or solubilization. Typically, LLCNPs are formed by introducing a liquid formulation of the LLC, cosurfactants, and solvent into water to form the dispersion. However, LLCNPs often have difficulties with respect to fabrication, formulation, and stabilization with current methods, so a great deal of research has been devoted to these areas. The majority of drug delivery research with LLCNPs has been focused on the use of LLCNPs of Q_{II} phases, commonly called "cubosomes" [151–154]. This is because Q_{II} phases have the potential for high drug loading and good release of hydrophilic drug molecules as a result of their 3-D interconnected water nanopore structures. The majority of the cubosome systems studied have been based on GMO because of the prevalence of a Q_{II} phase in its phase diagram. One of the newest innovations in the LLCNP drug delivery area involves preparation of dry powder precursors of cubosomes [136, 155]. Q-phase LLCNPs have been studied for a wide range of drug molecules [151–154], including the drug propofol, an anesthetic currently used in clinical practice in the form of a stable emulsion [156].

5.5
New Directions for LLC Phases in Drug Delivery and Medical Therapy

One very new direction for potential drug or medical therapy with LLC phases is using them to aid in antibody recognition and binding to functionalized surfaces. A number of commercially available non-charged and charged surfactants have recently been explored for this purpose [157]. An-

other new direction for LLC phases that might generate new avenues for medical therapies, is the use of cationic amphiphiles or lipids to complex with DNA to form surfactant-DNA complexes that exhibit LLC phases [158]. L and H_{II}-type phases have been observed in such systems. It is believed that understanding the aggregation and LLC phase formation of these cationic surfactant-DNA complexes may lead to the development of better gene delivery therapies.

6 LLC Materials for Membrane Separations

Membrane separations are of rapidly growing importance as world energy demands are projected to continually increase and more stringent guidelines are placed on the cleanup of waste streams [159]. Membranes potentially offer many less energy intensive alternatives to traditional separation technologies [159]. Proper design considerations are needed to engineer high-performance membranes that selectively segregate specific components from mixtures based on affinity, shape, size, charge or other chemical and physical properties [159]. However, a great deal of research is still needed in order for membranes to be economically viable and displace older technologies [159].

Traditional membranes are either porous or dense materials. Porous membranes operate via size discrimination and dense membranes by the solution-diffusion mechanism [160]. Porous membranes can be highly ordered materials such as zeolites [161] or materials such as polymers, processed to create specific types of voids within their structure. Dense membranes are typically rubbery or glassy polymers that lack voids and pinholes. Each class of material lends itself to different applications yet has its own limitations. Zeolites are capable of molecular sieving of gases and other small molecules, but are difficult to process into uniform films of large surface area [161]. Porous polymers can be used in applications such as aqueous nanofiltration (NF), but the processes that produce them result in the lack of a uniform structure within the film [162]. These materials are thus unable to perform precise molecular sieving [162]. Dense polymers are easily processed and can be used for a variety of applications, such as reverse osmosis (RO) for water desalination [163], gas separations [164], and barrier films [165], but the solution-diffusion mechanism dictates that all solutes will penetrate the membrane, making complete molecular sieving virtually impossible [160].

The need to overcome the disadvantages of each class of membrane drives research for novel, composite materials that combine the advantageous properties of each class [159]. LLCs have potential to offer desirable hybrids of these two types of materials, as they allow for the incorporation of a porous, ordered nanostructure within an otherwise dense film. LLC membranes capable of performing several different applications, such as

aqueous NF [119, 166], gas separations [167, 168], and selective vapor rejection [169, 170], have recently been realized.

6.1 Aqueous Nanofiltration

The first example of a functional LLC membrane separation was reported in 2005 [166]. A three-tailed, wedge-shaped, photopolymerizable LLC exhibiting the H_{II} structure was employed to selectively filter anionic dye molecules from aqueous solution when supported as a thin film on a commercial ultraporous polysulfone (PSf) membrane support (Fig. 21). For increasingly larger solutes, the rejection of the dyes through the LLC pores became quantitative as the molecular diameter approached that of the cylindrical nanochannels. Furthermore, neutral, monodisperse PEG chains could be filtered with the same trends in rejection. These LLC membranes outperformed a commercially available NF membrane in rejection of the charged dyes, and significantly outperformed the same NF membrane in rejection

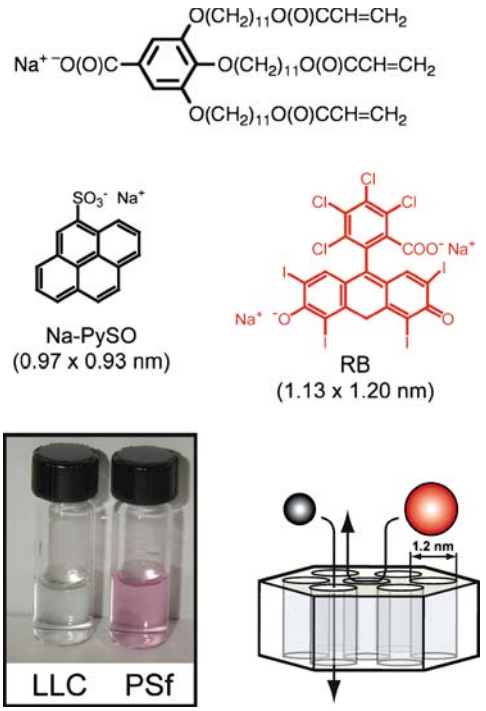

Fig. 21 Molecular size-selective aqueous NF using a supported LLC membrane with a cross-linked H_{II} phase top-layer. Partially reproduced with permission from [166]. © 2005 by Wiley-VCH

of the neutral solutes [119]. However, these H_{II}-phase LLC membranes suffered from markedly lower water flux than the commercially available NF membrane [166]. The limitations on water throughput appear to be related to the processing of the films, and not as a material shortcoming. Only a small percentage of the aqueous channels were oriented normal to the membrane surface and were accessible for filtration [166]. Nonetheless, this work represents a shift in the rationale of polymer membrane design.

Expanding upon the successes of aqueous NF with an LLC membrane, promising preliminary results were obtained with the same H_{II} networks of the three-tailed LLC monomer (Fig. 21) in water desalination applications [119]. These systems were only capable of removing a small percentage of metal ions from aqueous solution because the effective nanopore size was significantly larger than the diameter of the hydrated small metal salt ions [119]. As the hydrated ionic diameters of the metal ions increased (Rb^+, Na^+, Mg^{2+}, and Nd^{3+}), the amount rejected also increased. The H_{II} membranes were unable to compete with the current commercially available RO membranes in either rejection or water flux. However, preliminary results showed that these polymerized LLC membranes have superior hypochlorite (ClO^-) resistance properties when compared to polymers typically used in RO [119]. ClO^- degradation is a significant problem for current RO membranes. Research in this field will proceed further. LLC systems with smaller pores as well as those exhibiting more hydrophilic Q phases have been speculated to be better candidates for RO applications than H_{II} materials.

6.2 Gas Separations

The cross-linked H_{II} phase of the triacrylate LLC monomer shown in Fig. 21 has also been studied as a gas separation membrane material [167, 168]. In the first report of the fabrication and use of large area, freestanding, photo-cross-linked LLC film for gas separations [167], the transport properties of five light gases (CO_2, N_2, O_2, CH_4 and H_2) were determined in both polymerized H_{II} membranes and disordered films with the same chemical composition. The presence of an H_{II}-phase nanostructure was found to have significant effects on CO_2 transport when compared to an isotropic analogue. The periodic, aqueous nanochannels in the H_{II} membrane impeded diffusion of all gases, and as such, higher fluxes for all gases were observed in the disordered material. It was proposed that "non-interacting" gases (N_2, O_2, CH_4, and H_2) must circumvent the open, polar nanochannels, as they are repelled from those regions. Thus, a longer path length through the membrane must be taken (Fig. 22). The behavior of CO_2 in the H_{II} system is exceptionally different. CO_2 exhibited strong non-covalent interactions with the ordered, ionic nanochannels present in the membrane, and its diffusion was slowed more than the other four gases tested. However,

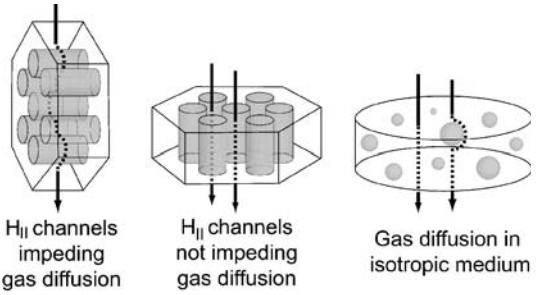

Fig. 22 Model for light gas separations in H_{II}-phase LLC polymer membranes. Reproduced with permission from [167]. © 2007 by Elsevier

the localized polarity in the H_{II} nanochannels served to increase solubility of CO_2 in the material by $\sim 35\%$. Such interactions were not as prevalent in the isotropic analogue. This is because the polar headgroups are rearranged and hidden inside of closed micelles, which were much less accessible to CO_2. As a result, H_{II} membranes could achieve enhanced CO_2/N_2 and CO_2/CH_4 ideal separation factors than disordered membranes of the same composition. Other separations relevant to industry not involving CO_2, such as O_2/N_2, are largely unaffected by the presence of nanostructure. These first-generation LLC membranes fall close to the "upper bound" of the Robeson Plot for CO_2/N_2 separation. Thus, further research into LLCs as materials for gas separations appears warranted.

6.3 Selective Vapor Barrier Materials

Among its many uses, cross-linked butyl rubber (BR) is widely used as a protective garment against harmful chemical vapors. However, as it is largely impermeable to all vapors, those wearing BR suits often experience discomfort, as their perspiration cannot escape. In a major step to overcome this issue, selectively "breathable" composites can be made by copolymerizing LLC monomers with BR. Initial work focused on incorporating the H_{II} phase formed by the aforementioned LLC monomer into BR [169]. The addition of H_{II} domains into BR was found to increase the water vapor transport through the composite by over four orders of magnitude compared to pure cross-linked BR. In contrast, the permeability of a chemical warfare simulant, chloroethyl ethyl sulfide (CEES), increased only by a factor of 75%. Pure cross-linked BR was observed to have a water/CEES molar transport selectivity of 0.25, while the composite material exhibited a selectivity of 23. The inclusion of hydrophilic, nanostructured water channels through the polymer allowed water vapor to readily pass through the material and resulted in an drastic improvement in selectivity between pure BR and the composite.

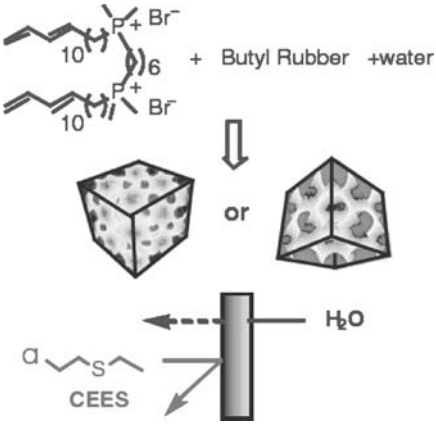

Fig. 23 Selective vapor transport with a cross-linked Q_I-phase LLC-BR membrane (*gray areas* = hydrophobic organic domains; *white areas* = aqueous domains). Reproduced with permission from [170]. © 2006 by Wiley-VCH

A follow-up study demonstrated that Q_I phases further enhance the performance of LLC-BR composite membranes in both water transport and harmful chemical vapor rejection [170]. A cross-linkable, gemini phosphonium amphiphile (Fig. 23) was blended with BR and cross-linked to form films exhibiting a Q_I-phase nanostructure. Materials with a Q_I-phase showed 300 times greater water vapor permeability and 500 times greater permeability selectivity for water/CEES than pure cross-linked BR. Furthermore, these Q_I-phase composite films were far superior to their H_{II} and L analogues in both water vapor permeability and water/CEES transport selectivity. Further studies were planned to process thinner films as well as test their rejection properties against other types of chemical agents.

The use of LLC-based membrane systems is still in its infancy. Promising early results indicate that research in this field will be expanded. The applications outlined here are just a few where functional LLC materials might be implemented. More challenging separation materials, such as water desalination membranes, selective proton-conducting membranes for fuel cells, catalytic membranes, chromatography, and chiral separation media are perhaps future candidates for new LLC membrane materials.

7 Summary and Future Directions

Functional LLC systems offer great promise to revolutionize materials science. The applications outlined herein have thus far received the most attention from researchers. The future of LLCs and LLC-based materials will not be

limited solely to these functions [119, 171]. New ideas for the use of LLCs are being conceived regularly, necessitating a need for a "bottom-up" approach to materials design. Novel materials and chemistry are needed for LLCs to meet application-specific demands. In particular, three areas of opportunity have presented themselves, which may drastically alter and expand the functional capabilities of LLC materials. These include (i) the further development of Q phase LLC materials; (ii) the incorporation of functional groups into LLC mesogens other than catalytic moieties; and (iii) the use of RTILs to form LLC phases instead of water. These three areas of research offer gateways for radically new designs and applications for LLC-based materials

Q phases are already one of the most promising, research-intensive LLC-based drug delivery systems because of the superior diffusion and access characteristics afforded by their 3-D interconnected nanopore systems [129, 151–154]. Initial results have also shown that Q-phase LLC materials also possess superior transport and access properties in membrane applications compared to L and H_{II} phases [170]. This phenomenon could translate into the design of superior LLC-based heterogeneous catalysts or bulk sorbents, as the interconnected nanochannels may provide more open pathways for better accessibility and selective molecular and/or ion diffusion. However, designing functional amphiphiles that can readily form useful Q-phase materials is not a straightforward task. To date, less than a handful of LLC monomers are known in the literature that can be polymerized in Q phases [172–175].

The ability to design LLC mesogens containing functional units other than catalytic moieties has the potential for extending the use of functionalized LLC phases and LLC polymer materials beyond catalysis. For example, the incorporation of other types of functional, task-specific chemical units onto LLC starting materials could lead to NF membranes that could perform molecular level separations using mechanisms other than simple size exclusion. Similarly, such materials could broaden the use of nanoporous LLC systems into as of yet unimagined application areas.

Ion conduction has been the only application examined thus far for RTIL-based LLC materials. However, given the seemingly exponential expansion of research into RTILs as new reaction solvents, new gas sorption media, and new ion-conductive materials [85, 88–90], it appears to be only a matter of time before RTILs make a significant impact on the design of functional LLC materials. RTILs promise to open the door to new applications for LLC materials.

References

1. Collins PJ (1990) Liquid crystals: nature's delicate state of matter. Princeton University Press, Princeton
2. Stegemeyer H (ed) (1994) Liquid crystals. Springer, New York
3. Tiddy GJT (1980) Phys Rep 57:1

4. Seddon JM (1990) Biochim Biophys Acta 1031:1
5. Israelachvili JN (1985) In: Intermolecular and surface forces with applications to colloidal and biological systems. Academic, London, pp 249–257
6. Gruner SM (1989) J Chem Phys 93:7562
7. Holmes MC, Leaver MS (2006) Intermediate phases. In: Lynch ML, Spicer PT (eds) Bicontinuous liquid crystals. Surfactant science series, vol 127, Taylor and Francis, Boca Raton, pp 15–40
8. Forrest BJ, Reeves LW (1981) Chem Rev 81:1
9. Ringsdorf H, Schlarb B, Venzmer J (1988) Angew Chem Int Ed Engl 27:113
10. Lydon J (2004) Curr Opin Colloid Interface Sci 8:480
11. Tortora L, Park H-S, Antion D, Finotello D, Lavrentovich OD (2007) In: Chien LC (ed) Proceedings of SPIE-The International Society for Optical Engineering, 6487 (Emerging liquid crystal technologies II). SPIE-The International Society for Optical Engineering, pp 64870I-1–64870I-15
12. Gin DL, Gray DH, Smith RC (1999) Synlett 10:1509
13. Miller SA, Ding JH, Gin DL (1999) Curr Opin Colloid Interface Sci 4:338
14. Mueller A, O'Brien DF (2002) Chem Rev 102:727
15. Yoon HN, Charbonneau LF, Calundann GW (1992) Adv Mater 4:206
16. Patrick DL, Wilkinson FS, Fegurgur TL (2005) In: Proceedings of SPIE-The International Society for Optical Engineering, 5936 (Liquid Crystals IX). SPIE-The International Society for Optical Engineering, pp 59360A/1-59360A/8
17. Muller-Goymann CC (1998) PZ Prisma 5:129
18. Kato T, Mizoshita N, Kishimoto K (2006) Angew Chem Int Ed 45:38
19. Yoshio M, Kagata T, Hoshino K, Mukai T, Ohno H, Kato T (2006) J Am Chem Soc 128:5570
20. Kamikawa Y, Kato T (2006) Org Lett 8:2463
21. Kato T, Yoshio M (2005) In: Ohno H (ed) Electrochemical aspects of ionic liquids. Wiley, Hoboken, NJ, Chapter 25, pp 307–320
22. Kato T (2000) Struct Bond 96:95
23. Lohse DJ, Hadjichristidis N (1997) Curr Opin Colloid Interface Sci 2:171
24. Hayakawa T (2005) In: Naga N (ed) Novel strategies for fundamental innovation in polymer science. Research Signpost, Trivandrum, India, pp 39–57
25. Yuan ZY, Su BL (2006) J Mater Chem 16:663
26. Holmberg K (2004) J Colloid Interface Sci 274:355
27. Palmqvist AEC (2003) Curr Opin Colloid Interface Sci 8:145
28. Antonietti M (2001) Curr Opin Colloid Interface Sci 6:244
29. Ying JYMCP, Wong MS (1999) Angew Chem Int Ed 38:56
30. Patarin J, Lebeau B, Zana R (2002) Curr Opin Colloid Interface Sci 7:107
31. Berggren A, Palmqvist A, Holmberg K (2005) Soft Matter 1:219
32. Polarz S, Antonietti M (2002) Chem Commun 2593
33. Attard GS, Glyde JC, Göltner GC (1995) Nature 378:366
34. Yang H, Kuperman A, Coombs N, Mamiche-Afara S, Ozin GA (1996) Nature 379:703
35. Braun V, Osenar P, Stupp SI (1996) Nature 380:325
36. Osenar P, Braun PV, Stupp SI (1996) Adv Mater 8:1022
37. Tohver V, Braun PV, Pralle MU, Stupp SI (1997) Chem Mater 9:1495
38. Stupp SI, Braun PV (1997) Science 277:1242
39. Lu Y, Ganguli R, Drewien CA, Anderson MT, Brinker CJ, Gong W, Guo Y, Soyez H, Dunn B, Huang MH, Zink JI (1997) Nature 389:364
40. Attard GS, Bartlett PN, Coleman NRB, Elliott JM, Owen JR, Wang JH (1997) Science 278:838

41. Attard GS, Goltner CG, Corker JM, Henke S, Templer RH (1997) Angew Chem Int Ed Engl 36:1315
42. Gray DH, Gin DL (1998) Chem Mater 10:1827
43. Braun PV, Stupp SI (1999) MRS Bull 34:463
44. Braun PV, Osenar P, Tohver V, Kennedy SB, Stupp SI (1999) J Am Chem Soc 121:7302
45. Nandhakumar I, Elliott JM, Attard GS (2001) Chem Mater 13:3840
46. Gabriel T, Nandhakumar IS, Attard GS (2002) Electrochem Commun 4:610
47. Nandhakumar IS, Gabriel T, Li X, Attard GS, Markham M, Smith DC, Baumberg JJ (2004) Chem Commun 1374
48. Braun PV, Osenar P, Twardowski M, Tew GN, Stupp SI (2005) Adv Funct Mater 15:1745
49. Jiang XC, Xie Y, Lu J, Zhu L, He W, Qian Y (1993) Chem Mater 13:1213
50. Huang L, Wang H, Wang Z, Mitra A, Bozhilov KN, Yan Y (2002) Adv Mater 14:61
51. Huang L, Wang H, Wang Z, Mitra A, Zhao D, Yan Y (2002) Chem Mater 14:876
52. Cushing BL, Kolesnichenko VL, O'Connor CJ (2004) Chem Rev 104:3893
53. Puvvada S, Baral S, Chow GM, Qadri SB, Ratna BR (1994) J Am Chem Soc 116:2135
54. Qi L, Gao Y, Ma J (1999) Colloids Surf A 157:285
55. Ding JH, Gin DL (2000) Chem Mater 12:22
56. Yang JP, Qaqri SB, Ratna BR (1996) J Phys Chem 100:17255
57. Dellinger TM, Braun PV (2004) Chem Mater 16:2201
58. DeGennes PG (1979) Scaling concepts in polymer physics. Cornell University Press, Ithaca, NY, p 49
59. Antonietti M, Göltner C, Hentze HP (1998) Langmuir 14:2670
60. Antonietti M, Caruso RA, Göltner CG, Weissenberger MC (1999) Macromolecules 32:1383
61. Hentze HP, Kaler EW (2003) Chem Mater 15:708
62. Laversanne R (1992) Macromolecules 25:489
63. Moriguchi I, Ozono A, Mikuriya K, Teraoka Y, Kagawa S, Kodama M (1999) Chem Lett 1171
64. Nguyen TQ, Wu JJ, Doan V, Schwartz BJ, Tolbert SH (2000) Science 288:652
65. Wu JJ, Gross AF, Tolbert SH (1999) J Phys Chem B 103:2374
66. Gin DL, Smith R, Deng H, Leising G (1999) Synth Met 101:52
67. Huang LM, Wang ZB, Wang HT, Cheng XL, Mitra A, Yan YX (2002) J Mater Chem 12:388
68. Li XH, Zhang XG, Li HL (2001) J Appl Polym Sci 81:3002
69. Hulvat J, Stupp SI (2003) Angew Chem Int Ed 42:778
70. O'Connell M, Bachilo SM, Huffman C, Moore V, Strano MS, Haroz E, Rialon KL, Boul P, Noon W, Kittrell C, Ma J, Hauge R, Weisman R, Smalley R (2002) Science 297:593
71. Richard C, Balavoine F, Schultz P, Ebbesen TW, Mioskowski C (2003) Science 300:775
72. Islam MF, Rojas E, Bergey DM, Johnson AT, Yodh AG (2003) Nano Lett 3:269
73. Weiss V, Thiruvengadathan R, Regev O (2006) Langmuir 22:854
74. Lagerwall J, Scalia G, Haluska M, Dettlaff-Weglikowska U, Roth S, Giesselmann F (2007) Adv Mater 19:359
75. Tarascon J, Armand M (2001) Nature 414:359
76. Wang C (2004) Chem Rev 104:4727
77. McCullough RD (1998) Adv Mater 10:93
78. Beginn U, Zipp G, Möller M (2000) Adv Mater 12:510
79. Beginn U, Zipp G, Mourran A, Walther P, Möller M (2000) Adv Mater 12:513
80. Kishimoto K, suzawa T, Yokota T, Mukai T, Ohno H, Kato T (2005) J Am Chem Soc 127:15618

81. Panniza P (2001) Phys Rev E 64:021502-1
82. Photinos P (1998) Phase transitions in complex Fluids. World Scientific, Singapore, pp 173–175
83. Nesrullaev A (1992) Mol Cryst Liq Cryst: Sci Tech, Sect A 215:303
84. Dag O, Verma A, Ozin G, Kresge CT (1999) J Mater Chem 9:1475
85. Welton T (1999) Chem Rev 99:2071
86. Greaves TL, Weerawardena A, Fong C, Drummond CJ (2007) Langmuir 23:402
87. Wang Z, Liu F, Gao Y, Zhuang W, Xu L, Han B, Li G, Zhang G (2005) Langmuir 21:4931
88. Yoshio M, Kato T, Mukai T, Yoshizawa M, Ohno H (2004) Mol Cryst Liq Cryst 413:2235
89. Mukai T, Yoshio M, Kato T, Yoshizawa M, Ohno H (2005) Chem Commun 10:1333
90. Yoshio M, Mukai T, Kanie K, Yoshizawa M, Ohno H, Kato T (2002) Adv Mater 14:351
91. Khiew PS, Radiman S, Huang NM, Kan CS, Ahmad MS (2004) Colloids Surf A 247:35
92. Cao Y, Smith P (1993) Polymer 34:3139
93. Levon K, Ho KH, Zheng WY, Laasko J, Kärnä T, Taka T, Österholm JE (1995) Polymer 36:2733
94. Olinga TE, Fraysse J, Travers JP, Dufresne A, Pron A (2000) Macromolecules 33:2107
95. Paul RK, Vijayanathan V, Pillai CKS (1999) Synth Met 104:189
96. Klose G, Petrov A, Volke F, Meyer HW, Foerester G, Rettig W (1982) Mol Cryst Liq Cryst 88:109
97. Hammond SR, Zhou WJ, Gin DL, Avlyanov JK (2002) Liq Cryst 29:1151
98. Rathman JF (1996) Curr Opin Colloid Interface Sci 1:514
99. Romsted LS, Bunton CA, Yao J (1997) Curr Opin Colloid Interface Sci 2:622
100. Fendler JH (1987) Chem Rev 87:877
101. Corma A (1997) Chem Rev 97:2373
102. Okahata Y, Tanamachi S, Kunitake T (1980) Nippon Kagaku Kaishi 442
103. Ramesh V, Labes MM (1988) J Am Chem Soc 110:738
104. Ramesh V, Labes MM (1988) J Chem Soc, Chem Commun 891
105. Bakeeva RF, Tartykova LY, Kudryavtseva LA, Bel'skii VE, Usol'tseva NV, Ivanov BE (1992) Izvestiya Akademi Nauk, Seriya Khimicheskaya 1042
106. Guo R, Li Z, Liu T (2004) Colloid Polym Sci 283:243
107. Miethe P, Gruber R, Voss H (1989) Biotechnol Lett 11:449
108. Chopineau J, Thomas D, Legoy MD (1989) Eur J Biochem 183:459
109. Boy M, Voss H (1998) J Mol Catal B: Enzymatic 5:355
110. Guo R, Li ZC, Liu TQ (2006) J Polym Sci A: Polym Chem 44:2388
111. DePierro MA, Olson AJ, Guymon CA (2005) Polymer 46:335
112. DePierro MA, Guymon CA (2006) Macromolecules 39:617
113. Gin DL, Gu W (2001) Adv Mater 13:1407
114. Miller SA, Kim E, Gray DH, Gin DL (1999) Angew Chem Int Ed 38:3022
115. Gu W, Zhou WJ, Gin DL (2001) Chem Mater 13(6):1949
116. Xu Y, Gu W, Gin DL (2004) J Am Chem Soc 126:1616
117. Xu Y, Gin DL, Elliott BJ (2006) AIChE J 52:418
118. Zhou WJ, Gu W, Xu Y, Pecinovsky CS, Gin DL (2003) Langmuir 19:6346
119. Gin DL, Lu X, Nemade PR, Pecinovsky CS, Xu Y, Zhou M (2006) Adv Funct Mater 16:86
120. Pecinovsky CS, Nicodemus GD, Gin DL (2005) Chem Mater 17:4889
121. Drummond CJ, Fong C (2000) Curr Opin Colloid Interface Sci 4:449
122. Boyd BJ, Whittaker DV, Khoo S-M, Davey G (2006) Int J Pharm 309:218
123. Malmsten M (2006) Soft Matter 2:760

124. Lawrence MJ (1994) Chem Soc Rev 417
125. Engström S, Larsson K, Lindman B (1988) In: Liquid crystalline phases as delivery systems for drugs. I. Basic principles (Proc Int Symp Control Rel Bioactive Mater). Controlled Release Society, Lincolnshire, IL, 15:105
126. Ericsson B, Loander S, Ohlin M (1988) In: Liquid crystalline phases as delivery systems for drugs. III. In vivo (Proc Int Symp Control Rel Bioactive Mater). Controlled Release Society, Lincolnshire, IL, 15:382
127. Chang CM, Bodmeier R (2005) In: Surfactant science series 127(Bicontinuous liquid crystals). CRC Press, Baton-Rouge, p 321
128. Lee J, Kellaway IW (2003) In: Drugs and the pharmaceutic sciences 126 (Modified-release drug delivery technology). Marcel-Dekker, New York, p 447
129. Sagalowicz L, Leser ME, Watzke HJ, Michel M (2006) Trends Food Sci Technol 17:204
130. Kumar KM, Shah MH, Ketkar A, Mahadik KR, Paradkar A (2004) Int J Pharm 272:151
131. Wyatt DM, Dorschel D (1992) Pharm Technol 16:116
132. Liu SJ, Wang LC, Zhang J, Zhao XY, Shen Q, Zheng LQ (2005) Shandong Daxue Xuebao, Lixueban 40:95
133. Angius R, Murgia S, Berti D, Baglioni P, Monduzzi M (2006) J Phys: Condensed Mater 18:S2203
134. Helledi LS, Schubert L (2001) Drug Develop Ind Pharm 27:1073
135. Fitzpatrick D, Corish J (2005) Int J Pharm 301:226
136. Shah MH, Paradkar A (2005) Int J Pharm 294:161
137. Turchiello RF, Vena FCB, Maillard P, Souza CS, Bentley MVBL, Tedesco AC (2003) J Photochem Photobiol B: Biol 70:1
138. Lee J, Kellaway IW (2002) Drug Develop Ind Pharm 28:1155
139. Lee J, Kellaway IW (2000) Int J Pharm 195:35
140. Lee J, Kellaway IW (2000) Int J Pharm 195:29
141. Lee J, Kellaway IW (2000) Int J Pharm 204:137
142. Geraghty PB, Attwood D, Collett JH, Dandiker Y (1996) Pharm Res 13:1265
143. Carr MG, Corish J, Corrigan OI (1997) Int J Pharm 157:35
144. Sallam AS, Khalil E, Ibrahim H, Freij I (2002) Eur J Pharm Biopharm 53:343
145. Makai M, Csanyi E, Nemeth Z, Palinkas J, Eros I (2003) Int J Pharm 256:95
146. Tiemessen HLGM, Bodde HE, Van Mourik C, Junginger HE (1988) Prog Colloid Polym Sci 77:131
147. Nesseem DI (2001) J Pharm Biomed Anal 26:387
148. Farkas E, Zelkó R, Németh Z, Pálinkás J, Marton S, Rácz I (2000) Int J Pharm 193:239
149. Osborne DW, Ward AJI (1995) Int J Pharm Adv 1:38
150. Lindell K, Engblom J, Jonstroemer M, Carlsson A, Engstroem S (1998) Prog Colloid Polym Sci 108:111
151. Spicer P (2005) Chem Eng Res Design 83:1283
152. Chung H, Jeong SY, Kwon IC (2005) In: Surfactant science series 127 (Bicontinuous liquid crystals). CRC Press, Baton Rouge, p 353
153. Boyd BJ (2005) In: Surfactant science series 127 (Bicontinuous liquid crystals). CRC Press, Baton Rouge, p 285
154. Puvvada S, Ratna BR (1996) In: Lasic DD, Barenholz Y (eds) Handbook of nonmedical applications of liposomes, vol 3. CRC Press, Baton Rouge, p 225
155. Spicer PT, Small WB II, Lynch ML, Burns JL (2002) J Nanoparticle Res 4:297
156. Johnsson M, Barauskas J, Norlin A, Tiberg F (2006) J Nanosci Nanotechnol 6:3017
157. Luk YY, Jang CH, Cheng LL, Israel BA, Abbott NL (2005) Chem Mater 17:4774
158. Safinya CR (2001) Curr Opin Struct Biol 11:440

159. Noble RD, Agrawal R (2005) Ind Eng Chem Res 44:2887
160. Wijmans JG, Baker RW (1995) J Membr Sci 107:1
161. Caro J, Noack M, Kolsch P, Schafer R (2000) Micropor Mater 38:3
162. Matsuura T (1993) Synthetic membranes and membrane separation processes. CRC Press, Boca Raton, FL
163. Bhattacharya A, Ghosh P (2004) Rev Chem Eng 20:111
164. Baker RW (2002) Ind Eng Chem Res 41:1393
165. Cussler EL, Hughes SE, Ward III WJ, Aris R (1998) J Membr Sci 38:161
166. Zhou M, Kidd TJ, Noble RD, Gin DL (2005) Adv Mater 17:1850
167. Bara JE, Kaminski AK, Noble RD, Gin DL (2007) J Membr Sci 288:13
168. Noble RD (2006) Maku 31:91
169. Jin J, Nguyen V, Gu W, Lu X, Elliott BJ, Gin DL (2005) Chem Mater 17:224
170. Lu X, Nguyen V, Zhou M, Zeng X, Jin J, Elliott BJ, Gin DL (2006) Adv Mater 18:3294
171. Gin DL, Gu W, Pindzola BA (2001) Acc Chem Res 34:973
172. Lee YS, Yang JZ, Sisson TM, Frankel DA, Gleeson JT, Aksay E, Keller SL, Gruner SM, O'Brien DF (1995) J Am Chem Soc 117:5573
173. Srisiri W, Benedicto A, O'Brien DF, Trouard TP (1998) Langmuir 14:1921
174. Yang D, O'Brien DF, Marder SR (2002) J Am Chem Soc 124:13388
175. Pindzola BA, Jin J, Gin DL (2003) J Am Chem Soc 125:2940
176. Benedicto AD, O'Brien DF (1997) Macromolecules 30:3395

Author Index Volumes 101–128

Author Index Vols. 1–100 see Vol. 100

The volume numbers are printed in italics

Subject Index